TECHNISCHE UNIVERSITÄT MÜNCHEN
Ingenieurfakultät Bau Geo Umwelt
Lehrstuhl für Siedlungswasserwirtschaft

“Integrating energy recovery concepts into potable water reuse schemes”

Nils Horstmeyer

Vollständiger Abdruck der von der Ingenieurfakultät Bau Geo Umwelt der Technischen Universität München zur Erlangung des akademischen Grades eines

Doktor-Ingenieurs (Dr.-Ing.)

genehmigten Dissertation.

Vorsitzende:	apl. Prof. Dr. rer. nat. habil. Brigitte Helmreich
Prüfer der Dissertation:	1. Prof. Dr.-Ing. Jörg E. Drewes
	2. Prof. Dr.-Ing. Joachim Hansen
	3. Prof. Dr. Stuart Khan

Die Dissertation wurde am 29.11.2018 bei der Technischen Universität München eingereicht und durch die Ingenieurfakultät Bau Geo Umwelt am 14.02.2019 angenommen.

Water is the driving force of all nature
(Leonardo da Vinci)

Abstract

Establishing sustainable water supply is a major challenge in the 21st century and one of the 17 sustainable development goals of the United Nations (UN). Worldwide water quantity and quality issues are becoming more and more severe. Potable water reuse applications have the potential to provide sustainable water supplies while offering a viable alternative to conventional freshwater resources. Many regions around the world have already established or are considering potable water reuse. Traditionally, these schemes utilize conventional wastewater treatment including aerobic biological treatment followed by advanced water treatment processes (e.g., reverse osmosis (RO), advanced oxidation processes (AOPs), biologically-active carbon (BAC) filtration). While meeting a high product water quality, these treatment schemes are characterized by rather high specific energy demands.

The core research objectives of this dissertation in a conceptual phase were addressing (i) the evaluation of existing potable water reuse schemes regarding their energy demand and product water quality and (ii) the design of a more energy-efficient potable water reuse scheme that integrate water, energy, and nutrient recovery strategies. Based on the findings of the conceptual phase, the subsequent research objectives were focussed on the evaluation of the operational performance of membrane treatment as a core element of the novel treatment approach, including fouling mitigation strategies and their optimization using state-of-the-art methods. Therefore, a pilot-scale hollow-fibre ultrafiltration (UF) membrane reactor was conceived, designed, built, and continuously operated with raw municipal wastewater. A fluidized bed reactor with granular activated carbon (GAC) was employed as a strategy to mitigate membrane fouling. In order to study the performance of subsequent downstream water treatment processes, flat-sheet (laboratory-scale) nanofiltration (NF) and RO membrane treatment was employed. Beside the evaluation of membrane fouling behaviour during operation, different fouling mitigation strategies were analyzed (e.g., hydraulic flushing pulses, optimized spacer geometries, membrane vibration). To better understand the hydrodynamic and solute transport mechanisms of membrane modules in detail, an X-ray computed tomography (CT) scan method coupled with a modelling approach by use of COMSOL Multiphysics, was applied.

The results of this dissertation revealed that the concept of energy recovery can be integrated into potable water reuse schemes. Overall, the energy consumption of conventional potable reuse schemes could be reduced up to 29% (for the overall energy balance up to 80%) compared to current reuse schemes, resulting in an overall net energy demand balance of 0.22 kWh/m³. This can mainly be achieved by (i) a lower energy input, (ii) physical separation of carbon and nitrogen removal, (iii) an increased biogas yield from carbon, and (iv) implementation of the coupled aerobic-anoxic nitrous decomposition operation (CANDO) process for nitrogen removal for later energy recovery from nitrous oxide.

The operational performance of UF treatment was monitored over a period of 576 days. A GAC fluidized bed reactor proofed to be a suitable fouling mitigation strategy and fouling was reduced by 51–97% compared to operation with no fouling mitigation strategy. The energy demand could be reduced by 38% due to a hydraulically optimized tailored impact plate resulting in less required recirculation flow velocity. Chemical cleaning was applied approximately every 6 weeks. The operation of the pilot-scale UF reactor successfully revealed that UF treatment is capable to efficiently reject colloidal and dissolved matter by separating these two fractions from raw sewage. Thereby the total organic carbon (TOC) concentration was reduced by approximately 50%, while maintaining total nitrogen (TN) in its predominant form as ammonia nitrogen (NH_4-N).

Downstream water treatment with NF and RO treatment showed comparable performance for both membrane types. In total 16 fouling tests were performed with a DOW NF-270 nanofiltration and Toray TMG10 reverse osmosis membrane. The average permeate flux decline for both membrane types was below 30% during short-term experiments (90–120 h), with an average flux decline of 18% for NF treatment and 26% for RO, respectively. Shear stress enhancement via hydrodynamic optimization (e.g., fluid dynamics, spacer geometries) or vibration (via electroactive polymers (EAPs)) could be key strategies for fouling mitigation. The application of EAPs indicated to be a very promising approach to develop induced vibrating anti-fouling membranes.

Beside the fouling measurements, the permeate water quality was analyzed regarding dissolved organic carbon (DOC) and nitrogen species. Results indicate that both membrane types show a high DOC removal of approximately 90%. However, the NH_4-N rejection capability of both membrane types differed strongly, approximately 30% for the NF and 97% for the RO, respectively. Thus, RO is considered more suitable to concentrate NH_4-N in the reject stream, which is subsequently used for energetic utilization via the CANDO process.

Within this dissertation the product water quality was evaluated on a conceptual level. The efficacy of multiple barriers for the wide range of naturally occurring and anthropogenic trace organic and inorganic contaminants, residual nutrients, total dissolved solids, residual heavy metals and pathogens was considered. Within this treatment train, the UF-RO hybrid membrane systems represented the core membrane treatment stage. The overall log-removal for pathogens for the novel treatment train was similar or above of existing potable water reuse schemes and thus fulfilled the minimum log reduction values (LRVs) for microbial contaminants for potable water reuse projects by the World Health Organization (WHO) and the State of California (CA), USA.

Future research should focus on the operational validation of the proposed alternative potable water reuse scheme, in particular on the performance of downstream water treatment (e.g., BAC filtration, AOP, disinfection) and validation of the final product water quality. Additionally, the long-term behaviour of RO membrane treatment (e.g. biofouling) and upscaling effects need to be considered prior to full-scale application. Overall, by rethinking conventional potable water reuse schemes and optimizing existing treatment technologies, this dissertation

proposed a novel concept, which could result in a significant lower energy balance of state-of-the-art potable reuse schemes.

Keywords: Sustainable water treatment; water scarcity; potable water reuse; energy-efficiency; membrane treatment; membrane fouling; fouling mitigation.

Zusammenfassung

Die nachhaltige Verfügbarkeit von sauberem (Trink-)Wasser ist eine der wichtigsten Herausforderungen des 21. Jahrhunderts, definiert als eines der 17 globalen Ziele für nachhaltige Entwicklung der Vereinten Nationen (United Nations, UN). Weltweit werden die Wasserknappheits- und Wasserqualitätsherausforderungen immer schärfer. Die Wiederverwendung kommunaler Abwässer zur Stützung der Trinkwasserversorgung ist bereits weltweit in zahlreichen Regionen etabliert oder wird für zukünftige Projekte berücksichtigt. Traditionell werden in diesen Wasserrecyclingprojekten Prozessvarianten bestehend aus der konventionellen Abwasserbehandlung (inklusiver aerober biologischer Behandlung mit Nährstoffelimination) gefolgt von weitergehenden Wasserreinigungsprozessen (z.B. Umkehrosmose (UO), weitergehende Oxidationsverfahren (Advances Oxidation Processes, AOP´s), biologische Aktivkohlefilter (Biologically-Active Carbon (BAC)) verwendet. Neben der Bereitstellung von gereinigtem Wasser ist ein signifikanter Nachteil der Prozessvarianten der vergleichsweise hohe Energiebedarf.

Der Hauptfokus dieser Dissertation lag in einer konzeptionellen Phase auf: (1) der Untersuchung bestehender Wasserrecyclingprozessvarianten mit dem Ziel der Trinkwasseraufbereitung bezüglich ihres Energiebedarfs und der generierten Wasserqualität, sowie (2) der Entwicklung energieeffizienterer Wasserrecyclingprozessvarianten mit dem Ziel der Trinkwasseraufbereitung unter Einbeziehung von Wasser-, Energie- und Nährstoffaufbereitungsaspekten. Basierend auf den Ergebnissen der konzeptionellen Phase lag der Schwerpunkt der nachfolgenden Forschungsgebiete auf der Untersuchung der Betriebsleistung der Membranbehandlungsstufen. Dies beinhaltete die Untersuchung des Membranfoulings sowie der Membranfoulingminimierungsstrategien und deren Optimierung. Hierzu wurde ein Membranreaktor bestehend aus Hohlfaser-Ultrafiltrationsmembranen (UF) im Pilotmaßstab konzipiert, entworfen, erstellt und im Dauerbetrieb mit kommunalem Rohabwasser betrieben. Granulierte Aktivkohle (GAK) in einer Wirbelschicht fungierte dabei als Membranfoulingminimierungsstrategie. Die nachgeschaltete Behandlung des Wassers mit Nanofiltrationsmembranen (NF) und UO-Membranen wurde unter Verwendung eines Flachmembranteststandes im Labormaßstab untersucht. Neben der Untersuchung des Membranfoulings während des Betriebs wurden Membranfoulingminimierungsstrategien für die NF und RO Membranen analysiert (z.B. hydraulische Pulsstöße, optimierte Spacergeometrien, Membranvibrationen). Eine röntgenstrahlenbasierte Computertomographie (CT) Aufnahmemethode gekoppelt mit einem Modellierungsansatz unter Verwendung von COMSOL Multiphysics wurde zur genaueren Abbildung und zum besseren Verständnis der hydrodynamischen- und Stofftransportmechanismen entwickelt und angewendet.

Die Ergebnisse dieser Arbeit zeigen, dass Energierückgewinnungskonzepte erfolgreich in Wasserrecyclingprozessvarianten mit dem Ziel der Stützung der Trinkwasserversorgung eingebunden werden können. Insgesamt konnte der Energiebedarf von

Wasserrecyclingprozessvarianten zur Trinkwasseraufbereitung im Vergleich zu derzeit angewendeten Prozessvarianten bis zu 29 % gesenkt werden. Dabei wurde die Gesamtenergiebilanz bis zu 80 % reduziert. Die Gesamtnettoenergiebilanz betrug 0,22 kWh/m³. Hauptsächlich kann dieses durch folgende Punkte erreicht werden: (1) geringerer Energiebedarf, (2) Trennung der Kohlenstoff- und Stickstoffentfernung durch vorherige physikalisch Trennung, (3) gesteigerter Biogasertrag aus Kohlenstoff und (4) Implementierung des sogenannten gekoppelten aeroben-anoxischen Stickstoffabbau-Prozesses (Coupled Aerobic-anoxic Nitrous Decomposition Operation, CANDO) zur Stickstoffentfernung und späteren energetischen Rückgewinnung aus Lachgas.

Die Betriebsleistung der UF Behandlungsstufe wurde über einen Zeitraum von 576 Tagen untersucht. Eine Wirbelschicht bestehend aus GAK bestätigte sich als erfolgreiche Membranfoulingminimierungsstrategie mit einem geringeren Membranfouling von 51–97 % gegenüber dem Betrieb ohne Membranfoulingminimierungsstrategie. Der Energiebedarf konnte durch hydraulische Optimierungen mit Hilfe einer entwickelten Prallplatte und dadurch verursachten geringeren notwendigen Rezirkulationsflüssen um 38 % gesenkt werden. Eine chemische Reinigung der UF Membranen wurde ca. alle 6 Wochen angewendet. Durch den Betrieb des UF-Reaktors im Pilotmaßstab konnte erfolgreich nachgewiesen werden, dass die UF-Behandlung in der Lage ist die kolloiden und gelösten Bestandteile wirksam voneinander zu trennen. Dadurch wurde der Gesamtkohlenstoffanteil (Total Organic Carbon, TOC) um ca. 50 % reduziert, während der Gesamtstickstoffanteil (Total Nitrogen, TN) in seiner überwiegend vorliegenden Form als Ammoniumstickstoff (NH_4-N) beibehalten wurde.

Die nachgeschalteten Wasserbehandlungsstufen beinhalteten NF- und UO- Behandlung. Diese Behandlungsstufen zeigten eine vergleichbare Betriebsleistung gegenüber dem Membranfoulingverhalten. Insgesamt wurden 16 Membranfoulingtests mit einer DOW NF-270 Nanofiltrationsmembran und Toray TMG10 Umkehrosmosemembran durchgeführt. Die durchschnittliche Permeatflussreduzierung für beide Membranen während Kurzzeittests (90–120 Stunden) war unter 30 %. Dabei lag die durchschnittliche Permeatflussreduzierung der NF-Membran bei 18 %, während die RO-Membran eine durchschnittliche Permeatflussreduzierung von 26 % aufwies. Scherkraftserhöhungen durch hydrodynamische Optimierungen (z.B. Strömungsmechanik, Spacergeometrien) oder Vibration (durch elektroaktive Polymere (EAPs)) stellen potentielle Membranfoulingminimierungsstrategien dar. Insbesondere die Anwendung von EAPs deutete im Abschluss der Arbeit sehr vielversprechende Ergebnisse an, um zukünftig vibrierende Anti-fouling Membranen zu entwickeln.

Neben den Membranfoulinguntersuchungen wurde die Permeatwasserqualität in Form von gesamt gelöstem Kohlenstoff (Dissolved Organic Carbon, DOC) sowie der Stickstoffvarianten analysiert. Die Ergebnisse zeigen, dass beide Membranen hohe DOC-Rückhalteraten von ca. 90 % aufweisen. Allerdings unterscheiden sich beide Membranen bezüglich ihrer NH_4-N Rückhaltefähigkeit sehr. Die NF-Membran konnte ca. 30 % des NH_4-N zurückhalten, während die RO-Membran ca. 97 % zurückhalten konnte. Somit wird die RO-Membran als geeigneter

für das Gesamtkonzept betrachtet, da die Konzentrierung des NH_4-N und spätere energetische Verwertung des Konzentratstroms im CANDO Prozess so ermöglicht wird.

In der vorliegenden Arbeit wurde die Wasserqualität des generierten Wassers überwiegend konzeptionell betrachtet. Die Wirksamkeit mehrfacher Barrieren für die große Anzahl von natürlich und anthropogen aufkommenden Spurenstoffe, inorganischer Verunreinigungen, Nährstoffe, gelöster Feststoffe, Schwermetallen und Pathogenen wurde hierbei berücksichtigt. Hierbei spielt die Kopplung der UF- und RO-Behandlung als Hybridsystem eine entscheidende Rolle. Der log-Rückhalt für Pathogene lag für die untersuchte neue Prozessvariante mindestens auf vergleichbarem Niveau im Vergleich zu existierenden Wasserrecyclingprozessvarianten. Somit erfüllt diese Prozessvariante die Mindestanforderungen für die log-Reduzierungswerte für mikrobielle Verunreinigungen für Wasserrecyclingprojekte zur Trinkwasseraufbereitung der Weltgesundheitsorganisation (World Health Organization, WHO) und des Staates Kalifornien der Vereinigten Staaten von Amerika (USA).

Zukünftige Forschungsschwerpunkte sollten sich auf Betriebsvalidierung der vorgeschlagenen neuen Prozessvariante fokussieren. Insbesondere die Betriebsleistung der nachgeschalteten Wasserbehandlung (z.B. BAC-Filter, AOP, Desinfektion) und die Validierung der finalen Wasserqualität spielen dabei eine wichtige Rolle. Des Weiteren müssen die Langzeitstabilität der RO-Membranbehandlung (z.B. Biofouling) und Skalierungseffekte für den Vollbetrieb berücksichtigt werden. Insgesamt lässt sich mit dieser Arbeit und dem Vorschlag einer neuen Prozessvariante feststellen, dass durch Überdenken der bestehenden Wasserrecyclingprozessvarianten mit dem Ziel der Trinkwasseraufbereitung und der Optimierung von einzelnen Prozess- und Behandlungsschritten die Energierückgewinnung sich erfolgreich integrieren lässt. Hierdurch werden signifikant geringere Energiebilanzen für bestehende Wasserrecyclingprojekte ermöglicht.

Schlagwörter: Nachhaltige Wasserversorgung; Wasserknappheit; Trinkwasserrecycling; Energieeffizienz; Membranbehandlung; Membranfouling; Foulingminimierung.

Affidavit

I hereby confirm that the dissertation titled *Integrating energy recovery concepts into potable water reuse schemes* prepared under the guidance and supervision of Professor Jörg E. Drewes at the Chair of Urban Water Systems Engineering at the Technical University of Munich and submitted to the degree-awarding institution of: Civil, Geo and Environmental Engineering of TUM is my own, original undertaken in partial fulfillment of the requirements for the doctoral degree. I have made no use of sources, materials or assistance other than those specified.

This thesis has not yet been submitted as part of another examination process neither in identical nor similar form.

Munich, ____ of _____ 2018.

Nils Horstmeyer

Acknowledgements

This work would never have been possible without the support and help of many people. At first, I want to thank my supervisor, Prof. Jörg E. Drewes, for his support and help over the last years. Thank you for giving me the opportunity to work in this research area.

I thank the whole team and colleagues at the Chair of Urban Water Systems Engineering / Technical University of Munich for the support and working atmosphere. I am very grateful to everyone who contributed to my work. Thank you Claus Lindenblatt for practical help and always be available with technical issues, thank you Dr. Konrad Koch and Dr. Uwe Hübner for having me in your research groups. Thank you Dr. Bastian Herzog for the support with laboratory or biologiocal questions and legendery soccer games. In addition, thank you to all the other PhD people at the chair for the great time. Thomas Lippert, Philipp Michel, Johann Müller, Karin Hellauer, Dietmar Strübing and many more. Thank you for fruitful discussions and exchange. Especially, I would like to thank Dr. Max Weißbach as my office roommate for the topic related and private support and help over the last years.

Next, I would like to thank Prof. Stuart Khan and Prof. Joachim Hansen for joining the PhD committee and their contributions to the project.

It is very important for me to highlight the importance of the excellent work of all the students that were part of the project during the last years. Jonas Aniol, Philipp Sperle, Cornelius Thies, Jan Schmitz, Maximilian Wunderlich, Maximilian Stahlschmidt, David Schön, Felizitas Schlederer, Rosiane Caetano, and many more.

Furthermore, I thank Dr. Cristian Picioreanu for the excellent collaboration in the area of membrane modeling. Also I thank Dr. Klaus Achterhold for the possibility and support of using the CT scanner. In addition, I would like to thank Prof. Stefan Seelecke, Dr. Steffen Hau and Sophie Nalbach for the collaboration and support in the field of vibration measurements.

For the planning and construction of the electronical control cabinets I would like to thank Josef Jell. Also I would like to thank Hubert Moosrainer for the technical support in the laboratory-hall and Susanne Wießler for all the organizational support from the secretariat.

A very big thank you goes to my mentor, Prof. Wolfgang Osswald, for the continuous support. Also Prof. Brigitte Helmreich is thanked to open the door to the water research area during my diploma thesis and continuous support over the last years.

The Oswald Schulze Foundation, TUM-GS and BayChina are thanked for financial support.

Last but not least I thank all the people in my private life. During the last years it was not always easy to give you the time and importance you deserve. I thank my parents to give me the opportunity, education, support and love to have the freedom to choose my way. And of course I thank you, Mirjam Hotho, for everything you did to support me.

Research papers, author contributions, topic related publications and additional scientific contributions

This cumulative doctoral thesis is based on the following peer-reviewed research papers and bookchapters, which are presented with editorial changes and supplements in chapters 3, 4, 7 and 9:

Publication #1 (Chapter 3):

- Drewes, J.E., Horstmeyer, N. (2016) **Recent developments in potable water reuse**. Fatta-Kassinos, D. et al. (eds.) Advanced Treatment Technologies for Urban Wastewater Reuse. The Handbook of Environmental Chemistry. Springer 45, 269–290.
- Author contributions: Nils Horstmeyer prepared the manuscript, wrote section 4 and 5 about design principles of potable water reuse and energy requirements. Jörg E. Drewes initiated the manuscript and provided his knowledge to all sections.

Publication #2 (Chapter 3):

- Drewes, J.E., Horstmeyer, N., Michel, P., Khan, S.J. (2017) **Producing high-quality recycled water**. Lema, J., Suarez Martinez, S. (eds.) Innovative Wastewater Treatment & Resource Recovery Technologies: Impacts on Energy, Economy and Environment, Chapter 13, 285–296, IWA Publishing.
- Author contributions: Nils Horstmeyer conducted the literature research and drafted major parts of the manuscript. In particular, section 13.3, 13.4 and 13.5 about treatment schemes for potable reuse, energy-efficiency of potable water reuse schemes and design requirements of potable water reuse schemes / energy potential are based on his work. Jörg E. Drewes initiated the manuscript and provided his knowledge to all sections. Philipp Michel supported the preparation of the manuscript. Stuart J. Khan reviewed the manuscript and supported the work with constructive comments and discussions.

Publication #3 (Chapter 3):

- Drewes, J.E., Horstmeyer, N. (2016) **Strategien und Potenziale zur Energieoptimierung bei der Wasserwiederverwendung (in German). Strategies and opportunities for energy optimization in recycling water**. Österreichische Wasser- und Abfallwirtschaft, 68, 99–107.
- Author contributions: Nils Horstmeyer prepared the manuscript, wrote section 1, 4 and 5. Jörg E. Drewes initiated the manuscript and provided his knowledge to all sections.

Publication #4 (Chapter 4):

- Horstmeyer, N., Weißbach, M., Koch, K., Drewes, J.E. (2018) **A novel concept to integrate energy recovery into potable water reuse treatment schemes**. *Journal of Water Reuse and Desalination*, 8(4), 455–467.

- Author contributions: Nils Horstmeyer conducted the literature research, developed the concept, conducted the energy and mass balances and prepared the manuscript. Max Weißbach supported the paper with knowledge about the nitrogen removal part. Konrad Koch and Jörg E. Drewes supervised this study and reviewed the manuscript.

Publication #5 (Chapter 7.1):

- Horstmeyer, N., Thies, C., Lippert, T., Drewes, J.E. (submitted) **A hydraulically optimized fluidized bed UF membrane reactor (FB-UF-MR) for direct treatment of raw municipal wastewater to enable potable water reuse with integrated energy recovery**. *Separation and Purification Technology*.
- Author contributions: Nils Horstmeyer was responsible for the research plan, designed and constructed the membrane reactor, was responsible for the execution of the experimental plan and operation of the experiments, data evaluation and preparation of the manuscript. Cornelius Thies supported the study with laboratory measurements, operation of the membrane reactor and data evaluation. Thomas Lippert supported the hydrodynamic simulations of the membrane reactor. Jörg E. Drewes supervised this study and reviewed the manuscript.

Publication #6 (Chapter 9):

- Horstmeyer, N., Lippert, T., Schön, D., Schlederer, F., Picioreanu, C., Achterhold, K., Pfeiffer, F., Drewes, J.E. (2018) **CT scanning of membrane feed spacers – Impact of spacer model accuracy on hydrodynamic and solute transport modeling in membrane feed channels**. *Journal of Membrane Science*, 564, 133–145.
- Author contributions: Nils Horstmeyer was responsible for the research plan and prepared the manuscript. Hydrodynamic and solute transport simulations were conducted by Thomas Lippert, Felizitas Schlederer, David Schön and Nils Horstmeyer. Particle simulations were conducted by Thomas Lippert and Nils Horstmeyer. Experimental measurements of pressure drop were applied by Cristian Picioreanu. Experimental measurements of particle distribution were conducted by Nils Horstmeyer. CT scan measurements and data converting were conducted by Klaus Achterhold, Nils Horstmeyer and Thomas Lippert. Jörg E. Drewes supervised this study and reviewed the manuscript. Franz Pfeiffer reviewed the manuscript.

In addition to the published data and experiments, supporting literature reviews, experiments and analyzes were conducted and serve as additional information in chapter 5-9. These results are not published, in preparation for publishing or serve as basis for future research proposals.

The following topic related publications have also been prepared and published during this PhD study. However, they are not presented as entire manuscript in this dissertation, but serve as supplemental information.

Topic related German publications:

- Koch, K., Weißbach, M., Leix, C., Horstmeyer, N., Drewes, J.E. (2015) **Gezielte Erzeugung von Lachgas als alternative Behandlung stickstoffreicher Abwasserteilströme einschließlich einer Energierückgewinnung** (in German). Umwelttechnologie Bayern, 62-65.

Topic related invention disclosures:

- Horstmeyer, N., Michel, P., Drewes, J.E. (2018) **Verfahren zur gezielten Induktion von Vibrationskräften auf permeable Luft- oder Wassermembranen durch elektroaktive Polymere** (in German). Invention disclosure 2018-05E07 to the Technical University of Munich.

In the following topic related presentations, conference proceedings and posters are listed.

Presentations / Conference Proceedings:

- Drewes, J.E., Horstmeyer, N., Magalhaes, N.C. (2017) **Keynote: Novel membrane applications for energy-efficient potable water reuse**. 8th IWA Membrane Technology Conference & Exhibition for Water and Wastewater Treatment and Reuse, Singapore, 5.-9.09.2017.
- Horstmeyer, N., Drewes, J.E. (2017) **A novel concept to integrate energy-recovery into potable water reuse treatment schemes**. IWA 11th International Conference on Water Reclamation and Reuse, Long Beach, CA, USA, 23.-27.07.2017.
- Horstmeyer, N., Drewes J.E. (2016) **An alternative energy-efficient treatment scheme for water reuse**. TUM DeSal, Young Scientist Colloquium, Networking event for young scientists with research focus water & desalination in Germany, 17.06.2016.
- Horstmeyer, N., Drewes, J.E. (2016) **An ultrafiltration membrane reactor with fluidized bed as a building block of a novel water reuse scheme**. IFAT, Munich. Hochschulforum – Marktplatz der Universitäten. University Forum – Universities´ presentations – Education and Research in the Water and Waste Sector, 31.05.2016.
- Drewes, J.E., Horstmeyer, N., Hübner U. (2015) **Spurenstoffelimination mit Membranen, AOP und Bodenpassagen – Erfahrungen aus den USA**. DWA Seminar „Spurenstoffelimination auf Kläranlagen“, Berlin, 17.11.2015.
- Horstmeyer, N., Weißbach, M., Koch, K., Drewes, J.E. (2015) **Coupling water reuse with energy recovery strategies**. Research Workshop Tsinghua University – Technical University of Munich. Garching, Germany. 18.09.2015 (Presentation / Workshop).
- Horstmeyer, N., Drewes, J.E. (2015) **Alternative energy-efficient treatment schemes for potable water reuse**. Evides Industriewater WWTP Harnaschpolder, Delft, Netherlands (RINEW Project Rotterdam). 26.08.2015 (Presentation / Workshop).

- Horstmeyer, N., Vatankhah H., Drewes, J.E. (2015) **Alternative energy-efficient treatment schemes for potable water reuse**. IWA 10th International Conference on Water Reclamation and Reuse, Harbin, China, 05.-09.07.2015.
- Horstmeyer, N., Stahlschmidt, M., Regnery, J., Drewes, J.E. (2015) **3D-fluorescence excitation-emission spectroscopy for water and wastewater samples**, FluoroFest 2015, Starnberg, Germany, 29.06.-01.07.2015.
- Drewes, J.E., Horstmeyer, N., Weißbach, M., Koch, K. (2015) **Potable water reuse – Towards an energy-neutral treatment scheme**. TUM-UQ Research Symposium on Water, Environment & Sustainability, Munich, Germany, 11.-12.06.2015.
- Drewes, J.E., Horstmeyer, N., Müller, J., Müller, E., Hübner, U. (2015) **Alternative energy-efficient treatment approaches to augment drinking water supplies with recycled water**. TUM Institute of Advanced Study „Remediating the Human Water Footprint“, Garching, Germany, 22.-23.01.2015.
- Drewes, J.E., Horstmeyer, N., Hübner, U. (2015) **Advances in water reclamation technologies and reuse**. 3rd IWA Water Research Conference, Shenzhen; China, 11.-14.01.2015.
- Horstmeyer, N., Drewes, J.E. (2014) **Potable reuse – Novel energy efficient treatment schemes for drinking water augmentation**. IWA 6th Eastern European Young Water Professionals Conference “East meets West”, Istanbul, Turkey, 28.-30.05.2014.

Poster:

- Horstmeyer, N., Michel, P., Drewes, J.E. (2015) **Potable water reuse – Novel treatment schemes for drinking water augmentation**. Doctoral Candidates Day (FGC-BGU). 08.01.2015.
- Horstmeyer, N., Stahlschmidt, M., Regnery, J., Drewes, J.E. (2015) **3D-fluorescence excitation-emission spectroscopy for water and wastewater samples**. FluoroFest 2015. Starnberg, Germany. 29.06.-01.07.2015.

Other topic related achievements, projects, proposals and inventions can be found in appendix A (Additional achievements) and Appendix B (Curriculum vitae).

Abbreviations

2D	Two dimensional	CEC	Contaminants of emerging concern
3D	Three dimensional	CFD	Computational fluid dynamics
3D-EEM	3D-fluorescence excitation-emission matrix	CFV	Cross-flow velocity
ABS	Acrylonitrile butadiene	CHP	Combined heat and power
AD	Anaerobic digestion	CL	Cake layer
ADI	Acceptable daily intake	CO	Colorado
AnMBR	Anaerobic membrane bioreactor	CO_2-e	CO_2-equivalent
AOP	Advanced oxidation processes	COD	Chemical oxygen demand
AOX	Adsorbable organic halides	CP	Concentration polarization
AWT	Advanced water treatment	CPU	Central processing unit
AZ	Arizona	CSM	Colorado School of Mines
BAC	Biologically-active carbon	CT	Computed tomography
BAF	Biological aerated filtration	Da	Dalton
BCA	Bicinchoninic acid	DAF	Dissolved air flotation
bCOD	Biodegradable COD	DALY	Disability adjusted life years
BNR	Biological nutrient removal	DBP	Disinfection by-products
BSA	Bovine serum albumin	dCOD	dissolved COD
C	Carbon	DE	Dielectric elastomers
CA	California	DEET	N,N-Diethyltoluamide
CA	Cellulose acetate	DI	Deionized
CAD	Computer-aided design	DICOM	Digital imaging and communications in medicine
CANDO	Coupled anaerobic-anoxic nitrous decomposition operation	DNS	Direct numerical simulation
CAS	Conventional activated sludge	DOC	Dissolved organic carbon
CDPH	California Department of Public Health	DOM	Dissolved organic matter

DPR	Direct potable water reuse	LRV	Log reduction values
EAP	Electroactive polymer	MAX	Maximizing
EC	Electrical conductivity	MBR	Membrane bioreactor
Em	Emission	MCL	Maximum contaminant level
EPHC	Environmental Protection and Heritage Council	MF	Microfiltration
EPS	Extracellular polymeric substances	MIN	Minimizing
EU	European Union	MW	Molecular weight
Ex	Excitation	N	Nitrogen
FB-UF-MR	Fluidized bed ultrafiltration membrane reactor	N/DN	Nitrification/Denitrification
FL	Florida	NASA	National Aeronautics and Space Administration
FS	Flat-sheet	nbCOD	non-biodegradable COD
GAC	Granular activated carbon	NDMA	N-Nitrosodimethylamine
GDWQ	Guidelines for Drinking-water Quality	NF	Nanofiltration
GHG	Greenhouse gases	NRC	National Research Council
GHz	Gigahertz	NOM	Natural organic matter
GWRS	Groundwater Replenishment System	O_3	Ozonation
HAA	Haloacetic acid	O&M	Operational and maintenance
HF	Hollow fibre	OM	Organic matter
iCOD	Inorganic (non-biodegradable) COD	OP	Osmotic pressure
IMS	Integrated membrane system	OSD	Object to scintillator distance
IPR	Indirect potable water reuse	PA	Polyamide
LC-OCD	Liquid chromatographie-organic carbon detection	PAC	Powdered activated carbon
LMH	L/m² hour	PARAFAC	Parallel factor (analysis)
LMWC	Low molecular weight compounds	pCOD	particulate COD

PE	Population-equivalent	SUVA	Specific UV absorbance
PESU	Polyether sulfone	SW	Spiral-wound
PFOA	Perfluorooctanoic acid	SWRCB	State Water Resources Control Board
PFOS	Perfluorooctane sulfonic acid	TBL	Triple bottom line
PIV	Particle image velocimetry	TCEP	Tris(2-chloroethyl)phosphate
PN/A	Partial nitritation/Anammox	THM	Trihalomethane
PNEC	Predicted no-effect concentration	TMP	Transmembrane pressure
POM	Particulate organic matter	TN	Total nitrogen
PP	Polypropylene	TOC	Total organic carbon
PSU	Polysulfone	TSS	Total suspended solids
PVC	Polyvinyl chloride	TT	Treatment train
PVDF	Polyvinylidene fluoride	TTC	Thresholds of toxicological concern
R	Rejection	TUM	Technical University of Munich
RAM	Random access memory	TX	Texas
RBAL	Risk-based action level	UF	Ultrafiltration
RBF	Riverbank filtration	UK	United Kingdom
Re	Reynolds number	UN	United Nations
RfD	Reference dose	UncFactor	Uncertainty factor
RO	Reverse osmosis	UNESCO	United Nations Educational, Scientific and Cultural Organization
ROI	Region of interest	USA	United States of America
R.U.	Raman units	USEPA	United States Environmental Protection Agency
SAT	Soil-aquifer treatment	UV	Ultraviolet light
SEM	Scanning electron microscopy	UVA_{254}	UV absorbance at 254 nm
SMP	Soluble microbial products	WHO	World Health Organization
SMR	Surface mesh refinements	WSI	Water stress indicator
SOD	Source to object distance	WTP	Water treatment plant
spp.	species pluralis	WWTP	Wastewater treatment plant
SRT	Solids retention time		
STL	Stereo lithography		

Chemicals

CH_4	Methane
Cl_2	Chlorine
CO_2	Carbon dioxide
H_2O_2	Hydrogen peroxide
N_2	Nitrogen gas
N_2O	Nitrous oxide
NaCl	Sodium chloride
NaOH	Sodium hydroxide
NaOCl	Sodium hypochloride
NH_4^+	Ammonia
NH_4-N	Ammonia nitrogen
NO_2^-	Nitrite
NO_3^-	Nitrate
O_2	Oxygen
O_3	Ozone

Figures

Content

1 Introduction

1.1 Water – Resources, Demands, Scarcity

Water is an essential resource of all life on planet earth. All organisms contain 50–90% water, some aquatic organsims even 99% (Lozán et al. 2007). From an outer space perspective, 75% of earth´s surface is covered by water (Marcinek and Rosenkranz 1996). In addition, water has many functions regarding the regulation of the climate. Physically water exists on planet earth in three states – solid ice, liquid water and water vapor. Hereby the water is continously going through a hydrological cycle (water cycle). In this process, the mean residence times of one water molecule in the water reservoires are in the range from days (atmospheric water), weeks (rivers) up to hundreds and thousands of years (e.g., groundwater aquifers, oceans) (Oki 2005). However, the amount of water on planet earth is constant, if considering a geological time scale (Oki 2005). Most of the global water (~1,386 million km³) is located as saline water in oceans (~96.5%), while about 2.5% remain as freshwater (considering ~1% as saline groundwaters or lakes). Over 68% of the freshwater is captured in solid form in glaciers and ice caps. Thus, only approximately 31% of the freshwater is present in liquid form (corresponding to ~0.76% of the gloal water resources) (Shiklomanov 1993, Charette 2010).

Human beings use water for agriculture, industrial, domestic (including drinking water) purposes. Agriculture accounts for approximately 70% of the global water demand, while industrial use of water is responsible for approximately 20% of the global water demand (~75% for energy production and ~25% for industrial manufacturing). Domestic use of water accounts for approximately 10% of the global water demands (UNESCO 2014, 2018). Each human drinks approximately 2 litres of water per day (Lozán et al. 2007). Beside the water quantity also water quality is important. When used, water changes the quality in terms of purity, heat content and potential energy (Oki 2005). Conventional utilized freshwater resources are (i) surface water supplies (river and lakes), (ii) groundwater supplies, (iii) seawater desalination, or (iv) imported water from other watersheds. The utilization of these options depends on the local availability and other site-specific factors. Over the past 100 years the global water demand has increased by a factor of 8–9 from approximately 500 to 4,000–4,600 km³/year (Wada et al. 2016, Burek et al. 2016). The global water demand will continue to grow over the next two decades significantly by a factor of about 1% per year (UNESCO 2018). Thus, by 2050 the demand for water is expected to increase by nearly one-third to 5,500–6,000 km³/year (Burek et al. 2016).

Natural impacts always changed the distribution and local availability of water. There is no global water scarcity as such (global water amount constant, considering a geologic time scale). Unless a certain development and growth of civilization there was a balance between human needs and natural resources. However, anthropogenic factors (i.e., population growth, industrialization, demographic changes, urbanization, climate change) combined with natural factors (i.e. limited and uneven freshwater distribution) changed this situation of available local

freshwater supplies. A 15-year survey from the National Aeronautics and Space Administration (NASA) revealed that freshwater supplies changed due to natural and anthropogenic factors (NASA 2018). Thus, single regions or countries already are faced with a severe water shortage or drinking water becomes scarce. In addition, water scarcity and water quality issues are becoming more and more pressing worldwide in the future. A common expression of water scarcity is the water stress indicator (WSI), showing regions with higher withdrawal of water than can be replenished from local watersheds (physical water scarcity) (Figure 1) (UNESCO 2018). Hereby, regions are facing different levels of water scarcities from low, moderate, significant up to severe. Nowadays, estimated 3.6–4.3 billion people (~50–70% of the global population) live in areas that are potentially water-scarce at least one month per year (moderate to severe water scarcity, WSI>1.0), this could be increased to 4.8–5.7 billion by 2050 (UNESCO 2018, Mekonnen and Hoekstra 2016). At a worldwide level, most people in India and China are facing severe water scarcity (1.0 billion India, 0.9 billion China) (Mekonnen and Hoekstra 2016). However, water scarcity doesn´t have boarders and effects people worldwide, including more industrialized countries like the United States of America (USA), where most people in the western and southern states (such as California (CA), Arizona (AZ), Texas (TX) and Florida (FL)) are experiencing severe water scarcity issues. The same trends become evident in Australia, Singapore or the European Union (EU). A survey of 500 cities revealed that under the 20 most likely cities running out of water are cities all over the world, including Tokyo (Japan), Delhi (India), Mexico City (Mexico), Shanghai and Beijing (China), Los Angeles (CA, USA), Rio de Janeiro (Brazil), Moscow (Russia), Istanbul (Turkey), Lima (Peru), or London (United Kingdom (UK) (McDonald et al. 2014, Noiva et al. 2016).

Figure 1. Physical water scarcity in 2010 (UNESCO 2018, Burek et al. 2016).

At the same time, the global developments are intensifying the water scarcity in the future, in particular in regions of Africa, Asia, central and south America (UNESCO 2018). The main drivers for water scarcity are (i) water cycle intensification due to climate change effects, (ii) population growth, and (iii) urbanization. The world population is expected to increase from 7.7

billion in 2017 to 9.4–10.2 billion by 2050, two thirds living in cities (UNESCO 2018). Hence, the water challenge is one of the most urgent challenges of the 21st century, recently defined as one of the 17 UN sustainibilty goals to reach by 2050 (Goal 6: Clean water and sanitation) (UN 2018).

1.2 Water treatment – Technologies, Energy, Water quality

Beside the described challenges and issues, there is enough evidence that suggest that solutions may be closer than we think. Technically, it is possible to treat water from each level of contamination for human consumption (drinking water quality) and close the water cycle on a local or regional scale. The very nature of water constrain that water reuse is an ongoing process on planet earth. Surface replenishment and groundwater recharge occurs naturally through the hydrological water cycle (e.g., natural drainage, infiltration of irrigation water, storm water runoff) (Oki and Kanae 2006). Water reuse for non-potable applicartions started over 5,000 years ago (Angelakis and Gikas 2014). Potable reuse applications, where highly treated wastewater effluents is utilized for drinking water augmentation, is practiced since the 1960s (WHO 2017a). Thus, potable water reuse is included in the natural water reuse cycle as one (additional) element for water supply.

In general, water treatment requires energy and resources (water-energy nexus), depending on the (i) source water characteristic, (ii) applied treatment technology and treatment train configuration, (iii) and product water quality. Current wastewater treatment technologies applied for potable water reuse applications consist of physical, chemical and biological processes to remove and/or degrade the wide range of particulate and dissolved contaminants present in municipal wastewater. Key treatment technologies are (i) preliminary treatment, (ii) primary treatment, (iii) secondary treatment, (iv) advanced water treatment (AWT), (v) disinfection, and (vi) engineered natural processes.

From a health perspective, water quality is inevitably linked to water usage, particularly if considering potable water purposes. First and foremost, the main treatment goal of drinking water supply is the provision of an adequate, safe and reliable treatment of source waters to drinking water standards. Even under energy-efficiency considerations of water treatment applications, this is an imperative. However, potable water reuse applications with wastewater as source water usually have not been considered in national or international drinking water regulations (Drewes and Horstmeyer 2016). In 2017, the World Health Organization (WHO) published the first international guidance for potable reuse, with the purpose to describe how to apply appropriate management systems to the production of safe drinking water from municipal wastewater. In this context, the latest health-based water quality targets (Guidelines for Drinking-water Quality = GDWQ) includes a comprehensive discussion of microbial, chemical and radiological public health hazards to assess disease burdens (WHO 2017b, Annex 1). The highest risk to the safety of potable water reuse represents enteric pathogens, as they are at potential high concentration in wastewater (WHO 2017a). In addition, a broad array of chemical hazards can be present in wastewater (industrial, commercial and dometic).

The very nature of potable water reuse applications is that a wide range of substances and contaminants can be potentially present in the source and in the product water. To manage the health risk in potable water reuse schemes, appropriate treatment barriers and monitoring strategies are required to minimize exposure to a wide range of contaminants of emerging concern (CECs) that may be harmful to human health (Drewes et al. 2018). The potable water reuse schemes must be reliable, meaning that multiple and independent (redundance) treatment barriers must exist. (Olivieri et al. 2016). In addition, a frequent monitoring of surrogate parameters is required (Olivieri et al. 2016). This includes a system assessment and operational monitoring of control measures and verification of product water quality (microbiological and chemical) (UNESCO 2018).

Membrane treatment is a key water treatment technology for potable water reuse applications due to the very high removal efficiency of contaminants. The size exclusion of membranes depends primarily on the effective pore size of the implemented membrane. Pore sizes can be distinguished by macropores (> 50 nm), mesopores (2 to 50 nm), and micropores (< 2 nm), respectively (Figure 2) (Tchobanoglous et al. 2014).

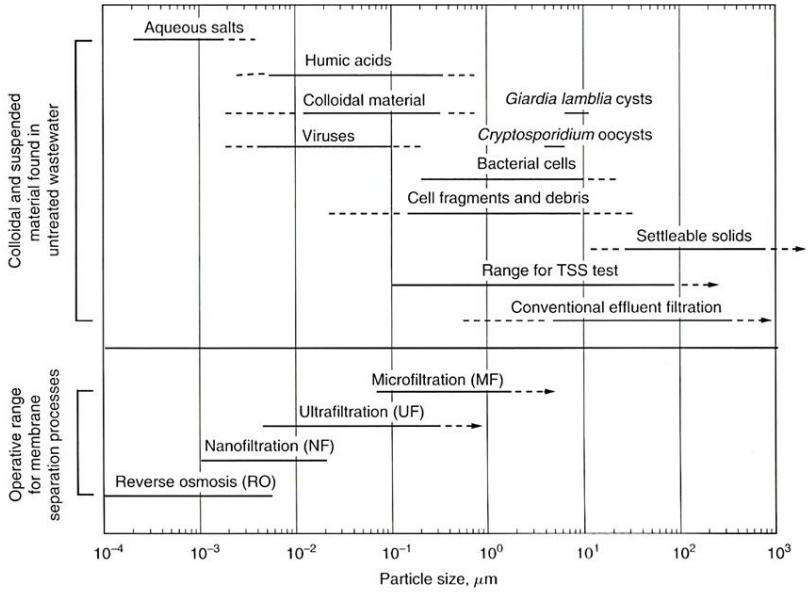

Figure 2. Partical separation ranges of various membrane types (Tchobanoglous et al. 2014).

However, the main disadvantage of high-pressure membrane systems is the high energy demand and membrane fouling (see chapter 5). Since natural resources are limited, energy-efficiency becomes also a key element for design and operation of integrated membrane systems. Furthermore, there is an ongoing paradigm change to consider wastewater not only as disposal stream, but as a resource, including nutrients, energy, heat and water (McCarty et al. 2011, Hering et al. 2013, Gao et al. 2014). Thus, this rethinking enables to ensure adequate quantities and qualities of water for human and nature to balance human needs with the future

of our planet. With this spirit, this thesis may contribute to a more sustainable water world and offer new ways and thinking for solutions of the future. We need to view this as a challenge, but at the same time also an unique opportunity to make water treatment much more sustainable. Water is essential for all life and cannot be replaced by any other substance.

2 Research significance

The provision of sustainable freshwater supply is a major challenge worldwide. This chapter describes the research significance of this thesis and research objectives with corresponding research hypotheses. The thesis is designed as a cumulative thesis, thus, research objectives and hypotheses are addressed in peer-reviewed publications (see chapter 2.2, Figure 5). Three key elements for a sustainable water treatment and supply are defined as core research pillars in this thesis (Figure 3). Sustainable water treatment and supply depends on (i) energy efficient treatment, (ii) operational/economic feasibility (operational performance), and (iii) final product water quality, explained in more detail in the following sections. All three research pillars have an equal impact as a basis for sustainable water treatment and supply.

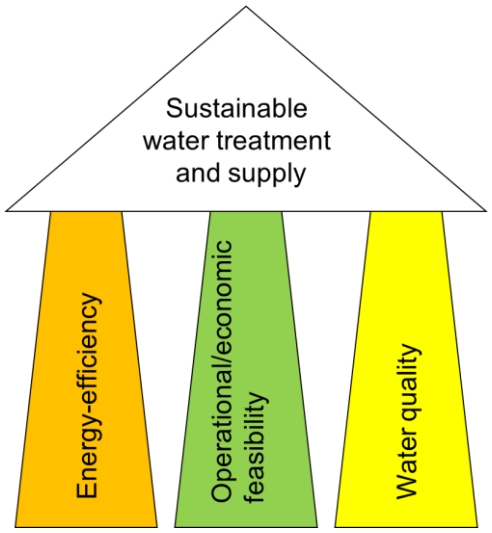

Figure 3. Defined research pillars as a basis for sustainable water treatment.

Energy-efficient treatment:

The technical ability to treat wastewater to a quality suitable for potable reuse has been achieved through multiple treatment train configurations (Khan 2015). However, proper treatment requires energy and resources (such as greenhouse footprint, capital, operational and maintenance costs). Membrane treatment is a key element of potable water reuse schemes due to its high removal efficiencies of contaminants. Since high energy demand is the main hurdle for membrane treatment applications, energy-efficiency becomes a core element for future potable water reuse applications. An improved energy-efficiency will simultaneously lead to more and more water reuse applications worldwide.

In particular, if considering the energy content of wastewater, it is difficult to understand why energy-efficiency is still not widely incorporated into potable water reuse applications. In the past, strategies for energy-efficiency were established (e.g. biogas yield increase with co-

substrate utilization), however, this extends the system boundaries. In contrast, the overall consideration of the terminology energy-efficiency needs to be understand broader. Energy-efficiency does not just mean to increase energy-efficiency by more efficient treatment and improvements (which is indispensable), it means also to look to the present potential resources and energy flows as a whole integrated concept. Simplified, a more energy-efficient potable water reuse concept could also integrate energy recovery into potable water reuse schemes by utilizing the present potential energy in wastewater. Wastewater contains energy in form of (i) kinetic energy, (ii) potential energy, (iii) thermic energy, and (iv) chemically-bound energy. The latter is considered a viable and transportable energy source.

Operational/economic feasibility (Operational performance):

Core design principles of potable water reuse schemes are (i) reliability, (ii) robustness, and (iii) resilience. Thus, the operational performance of new or improved treatment technologies and schemes are of major importance for sustainable water treatment. As described above, membrane treatment is a key element of potable water reuse schemes. Thus, it becomes a core element of investigation of the operational performance within this thesis. The membrane treatment stages of alternative and potential more energy-efficient potable water reuse schemes needs to be analyzed regarding their assessment and feasibility. Fouling during operation of membrane is one of the main limitations of membrane treatment. These phenomena cannot be entirely prevented but mitigation strategies need to be applied and further improved. In particular, when the conceptional approach of maximizing the overall energy-efficiency of potable water reuse schemes is considered, which results in (i) more anaerobic treatment and (ii) higher concentration factors of the membrane stages to concentrate carbon (C) and nitrogen (N). Both factors can lead to a severe fouling of the membrane stages. Thus, this thesis is focusing on the operational performance of membrane treatment applications with respect to improved membrane fouling mitigation strategies. Therefore, laboratory- and pilot-scale systems will be designed, constructed and operated to assess the operational performance and to analyze and develop fouling mitigation strategies.

Water quality:

The product water quality is indispensable linked to the design and operation of potable water reuse schemes. To manage the health risk of potable water reuse schemes a multiple-barrier concept is applied. Generally, it is not possible to monitor all contaminants potentially present in wastewater (Khan 2015). Thus, analytical and monitoring aspects become key elements of future research projects. Within this thesis the product water quality has been considered at a conceptual level by designing a potable water reuse scheme. Detailed investigations of the water quality assessment of novel potable wate reuse schemes are part of another dissertation.

2.1 Research objectives and hypotheses

Based on the above described core research pillars of this thesis, namely energy-efficiency and operational performance, the thesis is structured in two core sections (see chapter 2.2, Figure 5). In a first conceptual section, the research objectives are:

- Evaluate existing state-of-the-art potable water reuse schemes regarding their energy demand and product water quality.
- Define a specific potable water reuse scheme as benchmark.
- Design more energy-efficient potable water reuse schemes that integrate water, energy and nutrient recovery strategies.
- Evaluate state-of-the-art methods to analyze the operational performance of membrane treatment, in detail membrane fouling, including existing fouling mitigation strategies.
- Design, construct and operate membrane treatment systems facilitating potable water resue applications, while monitoring the assessment of the operational performance. This includes membrane fouling mitigation strategies and their optimization.
- Evaluate the assessment and feasibility of downstream high-pressure membrane treatment stages. This includes membrane fouling mitigation strategies, their investigation and potential optimization.

The general conceptual approach of an alternative more energy-efficient potable reuse treatment within this thesis follows the idea of minimizing (MIN) energy demands/input (optimized alternative treatment schemes) while maximizing (MAX) energy recovery/output (by improved utilization of C and N). Figure 4 illustrates this MIN/MAX concept by considering the energetic flows of corresponding energy recovery platforms and the removal stages for contaminants (multiple-barrier concept). By considering the theoretical energy content of municipal wastewater, the potential highest energy-efficiency can be calculated. C and N are considered as potential energy sources. Thus, the energetic utilization of these compounds is a key focus of investigation (orange circle in Figure 4). The separation and concentration of these compounds are the main treatment goals of the membrane stages beside the removal of contaminants and load reductions for subsequent treatment stages. While anaerobic treatment and the utilization of C to methane (CH_4) is current state-of-the-art technology, it is worth to consider alternative N removal strategies. Current N removal strategies like nitrification/denitrification (N/DN) require high oxygen demands and carbon sources. Instead, the so-called coupled aerobic-anoxic nitrous decomposition operation (CANDO) process allows for a more energy-efficient N removal (Scherson et al. 2013, 2014). The process is a double-stage biological treatment train (aerobic and anoxic) for the intended production of nitrous oxide (N_2O) and subsequent energetic recovery (52 kJ/mol) (Weißbach 2018). Additionally, the process allows for a tight emission control compared to other N removal strategies with uncontrolled N_2O emissions. Anthropogenic N_2O emissions account for a third of the total N_2O flux into the atmosphere (Gruber and Galloway 2008). With a carbon dioxide (CO_2) equivalent of 300 this leads to a contribution of approximately 6% to the global greenhouse gas effect (Ravishankara et al. 2009).

In fact, each membrane stage of the proposed treatment scheme is facing a severe membrane fouling risk. Thus, the operational performance and improved anti-fouling strategies are necessary for ultrafiltration (UF) and nanofiltration (NF) / reverse osmosis (RO) membrane applications (green circle in Figure 4). These strategies can involve shear stress enhancement via hydrodynamic optimization (e.g., fluid dynamics, spacer geometries) or vibration. Thereby, a detail understanding of the hydrodynamic and solute transport mechanism is essential. Therefore, a X-ray computed tomography (CT) scan approach is proposed as method to model the hydrodynamic and solute transport mechanisms in membrane modules. This offers the possibility to improve spacer geometries with optimized anti-fouling behavior. Another possibility is the inducement of vibration directly onto the membrane surface. The integration of electroactive polymers (EAPs) could be a suitable approach to develop tailored vibrating anti-fouling membranes.

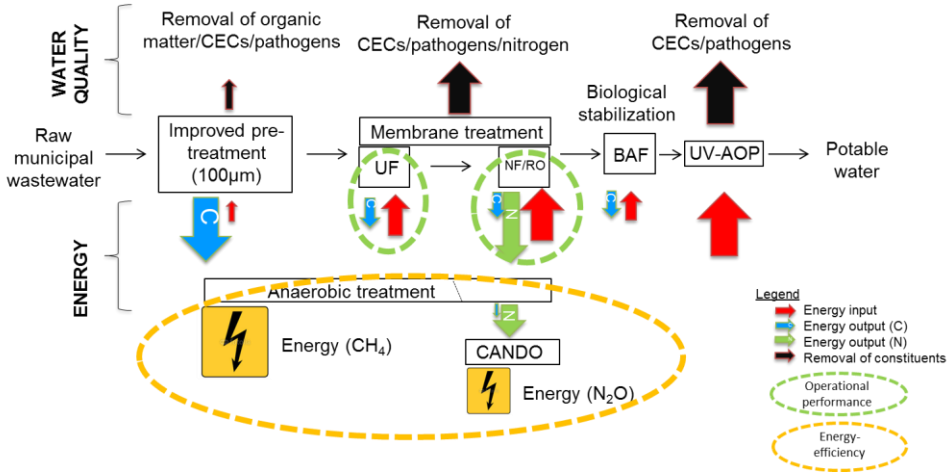

Figure 4. Conceptual design of alternative more energy-efficient potable water reuse schemes. The concept considers the energetic flows with corresponding energy-recovery platforms and removal stages for contaminants (multiple-barrier concept). The yellow marked circle indicates the link to energy-recovery platforms for improved energy-efficiency, while the circle marked in green indicates the membrane treatment stages as core element of investigation of the operational performance.

The described research objectives concluded in corresponding research hypotheses. These hypotheses were tested and finally assessed within each corresponding chapter (see chapter 2.2, Figure 5). The following research hypotheses have been tested in this thesis:

Hypothesis #1 (Overarching dissertation hypothesis):

> *"An alternative potable reuse treatment design can treat municipal wastewater with a lower energy demand (< 1.0 kWh/m³) compared to a potable reuse benchmark (CAS, MF, RO, UV/H_2O_2) by generating an equivalent water quality. The alternative potable reuse*

treatment design consists of the following core processes: sedimentation & microsieving, UF, NF/RO, BAF, and UV/H_2O_2."

The overall dissertation hypothesis was tested and assessed in chapter 4 (Publication #4).

Hypotheses #2:

Hypothesis #2 is targeting the design, construction and analysis of the first proposed membrane processes (UF) within the postulated novel treatment scheme. These hypotheses include membrane fouling issues and mitigation strategies against higher fouling risk. Stated as:

"A fluidized bed UF reactor is able to treat reliably (regarding membrane fouling, cleaning intervals and generated water quality) pretreated raw municipal wastewater and generate a permeate quality which is suitable for subsequent NF or RO treatment."

Hypothesis #2 was tested and asessed in chapter 7.

Hypothesis #3:

The downstream water treatment of UF pretreated wastewater is considered in hypothesis #3.

"NF/RO membrane treatment downstream of a fluidized bed UF reactor can be sustained while generating a suitable water quality for downstream BAF, UV-AOP with the purpose to generate potable water quality."

Hypothesis #3 was tested and assessed in chapter 8.

Hypothesis #4:

The modeling approach of the hydrodynamic and solute transport of spacer geometries within spiral-wound modules of NF/RO membranes is considered in hypothesis #4. The aim is to develop novel spacer designs with improved fouling propensities.

"A new spacer design can be developed for NF/RO membranes which can significantly reduce pressure drop and concentration polarization. An altered shape and orientation of the filaments can generate an unsteady flow regime, conventional spacers are not able to produce. The unsteadiness will further enhance depolarization and hence reduce the fouling potential."

Hypothesis #4 was tested and assessed in chapter 9 (Publication #6).

2.2 Thesis structure

The presented work and research was conducted at the Chair of Urban Water Systems Engineering at the Technical University of Munich (TUM). The project was part of the Membrane Filtration (Prof. Drewes), Advanced Water Treatment (Dr. Hübner), and Energy-Efficient Wastewater Treatment (Dr. Koch) research groups. The project was funded by seed funds of the Chair of Urban Water Systems Engineering and the Oswald-Schulze Foundation.

The project started in October 2013 with a research stay at the Colorado School of Mines (CSM), Golden, Colorado (CO), USA. At CSM, the first conceptual designs and assembling of the first flat-sheet test-skid (NF/RO) was conducted. In October 2015, the research objectives were summarized in a research proposal submitted to the scientific committee.

The thesis is structured based on the previous context in a state-of-the-art chapter of water reuse applications (chapter 3) with three corresponding publications (Figure 5). Chapter 4 is targeting the overall research hypothesis #1, published as publication #4. The following section is focusing on the operational performance and feasibility of the proposed novel concept. Chapter 5 provides a state-of-the-art review of membrane treatment and membrane fouling. Hypothesis #2 and #3 were subsequently tested and published as publications #5 and #6, including additional results, experiments and information (not published).

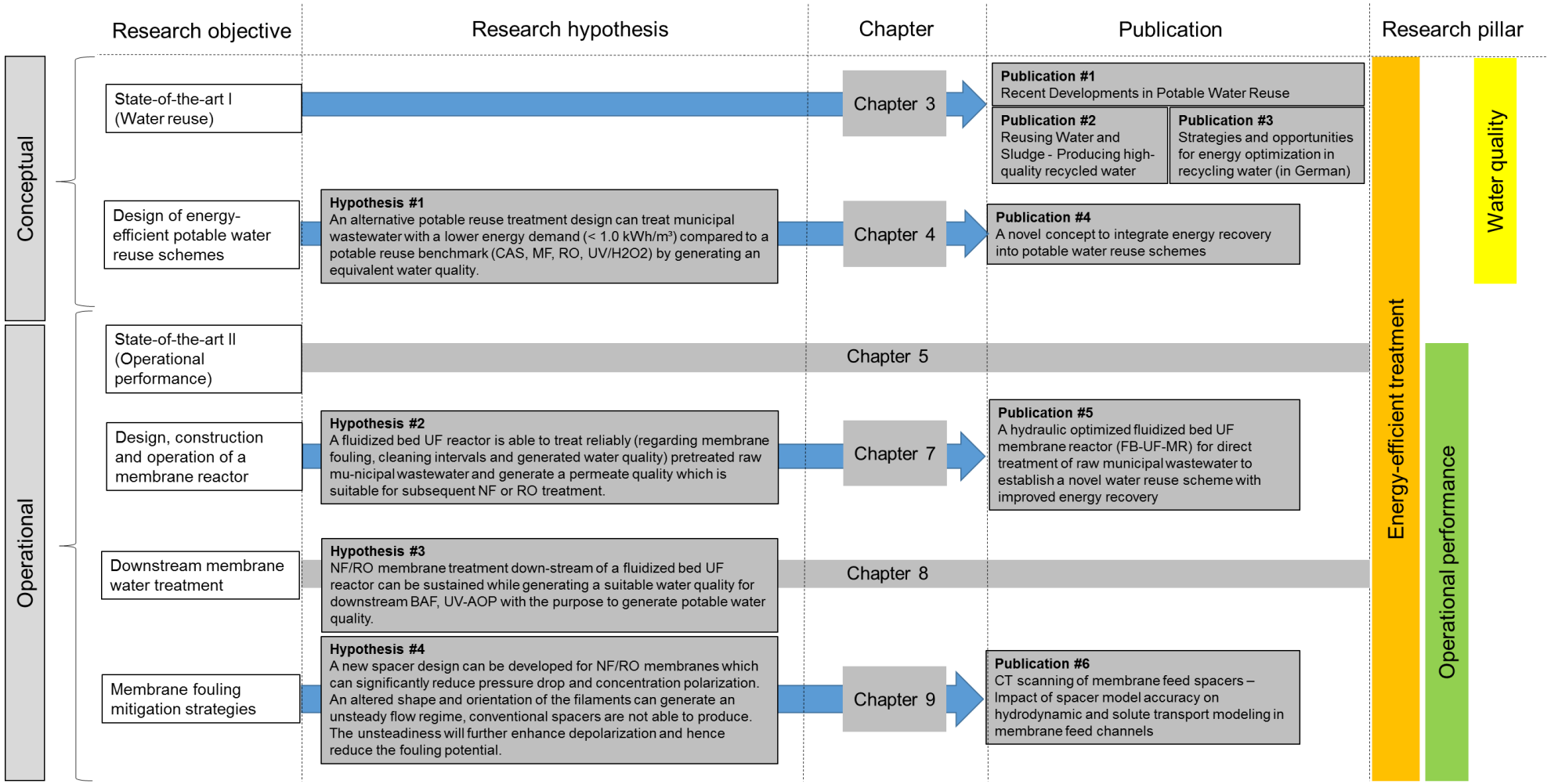

Figure 5. Overview of the tested hypotheses/objectives, publications and chapters of this dissertation with the three defined research pillars of (i) energy effieciency, (ii) operational performance, and (iii) product water quality.

Publication #1:

- Drewes, J.E., Horstmeyer, N. (2016) **Recent developments in potable water reuse**. Fatta-Kassinos, D. et al. (eds.) Advanced Treatment Technologies for Urban Wastewater Reuse. The Handbook of Environmental Chemistry. Springer 45, 269–290.

Publication #2:

- Drewes, J.E., Horstmeyer, N., Michel, P., Khan, S.J. (2017) **Producing high-quality recycled water**. Lema, J., Suarez Martinez, S. (eds.) Innovative Wastewater Treatment & Resource Recovery Technologies: Impacts on Energy, Economy and Environment, Chapter 13, 285–296, IWA Publishing.

Publication #3:

- Drewes, J.E., Horstmeyer, N. (2016) **Strategien und Potenziale zur Energieoptimierung bei der Wasserwiederverwendung (in German). Strategies and opportunities for energy optimization in recycling water**. Österreichische Wasser- und Abfallwirtschaft, 68, 99–107 (in German).

Publication #4:

- Horstmeyer, N., Weißbach, M., Koch, K., Drewes, J.E. (2018) **A novel concept to integrate energy recovery into potable water reuse treatment schemes**. *Journal of Water Reuse and Desalination*, 8(4), 455–467.

Publication #5:

- Horstmeyer, N., Thies, C., Lippert, T., Drewes, J.E. (submitted) **A hydraulically optimized fluidized bed UF membrane reactor (FB-UF-MR) for direct treatment of raw municipal wastewater to enable potable water reuse with integrated energy recovery**. *Separation and Purification Technology*.

Publication #6:

- Horstmeyer, N., Lippert, T., Schön, D., Schlederer, F., Picioreanu, C., Achterhold, K., Pfeiffer, F., Drewes, J.E. (2018) **CT scanning of membrane feed spacers – Impact of spacer model accuracy on hydrodynamic and solute transport modeling in membrane feed channels**. *Journal of Membrane Science*, 564, 133–145.

3 State-of-the-art I (Water reuse)

This chapter describes the state-of-the-art of water reuse. In detail, the development and evolution of potable water reuse schemes over 50 years, the current state-of-the-art, evaluation of existing schemes, environmental and health risks, design principles, water quality constituents, monitoring approches and requirements, regulatory requirements and energy requirements are presented. This chapter is based on three publications (Publications #1–#3), which serve as basis for chapter 3.

Publication #1 provides information about (i) the evolution of treatment schemes over 50 years, (ii) state-of-the-art of present treatment approaches, (iii) environmental and human health risks, (iv) design principles (i.e., monitoring, source water, reliability, storage and blending), and (v) energy requirements.

Publication #2 provides information about (i) water quality constituents of concern and regulatory requirements, (ii) treatment schemes, (iii) design requirements and energy potential, and (iv) state-of-the-art water quality monitoring approaches.

Publication #3 provides information about (i) water reuse concepts, (ii) water quality and operational aspects, (iii), health risk associated with microbial and chemical constituents, (iv) design principals, and (v) energy-efficiency.

3.1 Publication #1 (Abstract)

Recent developments in potable water reuse

Jörg E. Drewes[a] and Nils Horstmeyer[a]

[a]Chair of Urban Water Systems Engineering, Technical University of Munich, Am Coulombwall 3, 85748 Garching/München, Germany.

The following publication was published 2016 with editorial changes in:

Drewes, J.E., Horstmeyer, N. (2016). Recent developments in potable reuse. Fatta-Kassinos, D. et al. (eds.) Advanced Treatment Technologies for Urban Wastewater Reuse, The Handdook of Environmental Chemistry. Springer, 45, 269–290.

Abstract

Potable water reuse through the use of treated wastewater effluents has been practiced for more than 50 years. The majority of projects worldwide are characterized as indirect potable water reuse, where an environmental buffer (groundwater aquifer or surface water reservoir) provided retention, additional attenuation and blending prior to use as drinking water. In order to protect public health, these projects have utilized different treatment processes and combinations to establish multiple barriers against microbial and chemical contaminants. Due to the advancements in environmental analytical chemistry and the recognition of

contaminants of emerging concern (CEC) occurring in reclaimed water that might exhibit adverse health effects, additional advanced treatment processes (including ozone, advanced oxidation, activated carbon) were implemented. With increasing reliability of advanced water treatment processes and operational experience over several decades, the role of the environmental buffer to provide treatment and retention time has been revisited in projects that came online during the last 10 years. Recent trends are favoring direct potable water reuse applications in particular in the USA and Southern Africa that might evolve as the new paradigm for drinking water augmentation using impaired source water. However, questions remain regarding proper protection of public health, reliability and degree of treatment, appropriateness and design of monitoring strategies, maintenance requirements, and cost.

Keywords: Potable water reuse; multiple barriers; contaminants of emerging concern; environmental buffer; pathogens

3.2 Publication #2 (Abstract)

Re-using water and sludge / Producing high-quality recycled water

Jörg E. Drewes[a], Nils Horstmeyer[a], Philipp Michel[a] and Stuart Khan[b]

[a]Chair of Urban Water Systems Engineering, Technical University of Munich, Am Coulombwall 3, 85748 Garching/München, Germany.

[b]Water Research Centre, School of Civil and Environmental Engineering, The University of New South Wales, Sydney 2052, Australia.

The following publication was published 2017 with editorial changes in:

Drewes, J.E., Horstmeyer, N., Michel, P., Khan, S.J. (2017) Producing high-quality recycled water. Lema, J., Suarez Martinez, S. (eds.) Innovative Wastewater Treatment & Resource Recovery Technologies: Impacts on Energy, Economy and Environment, Chapter 13, IWA Publishing, 285-296.

Abstract

An increasing number of regions worldwide have suffered from water scarcity in the recent past. This has resulted in a growing interest in utilizing unconventional water resources to augment drinking water supplies (Drewes and Khan 2015, Drewes and Horstmeyer 2016). Water reuse is increasingly being recognized as an effort to re-use water as part of a 3R concept in contemporary urban water systems design (Hering et al. 2013). This chapter will discuss options to produce high-quality recycled water for potable reuse applications through reuse of municipal wastewater effluents. In addition, the role of an environmental buffer will be discussed in particular in lieu of recent developments to transition from indirect to direct potable reuse. The key water quality issues will be addressed as well as current and potentially future regulatory requirements, which will determine treatment scheme design. Different treatment scheme approaches to potable water reuse will be compared regarding water quality but also

regarding their specific energy requirements. The chapter will also touch upon recent developments to combine water reuse and energy recovery concepts driving innovation in contemporary design of water reclamation and reuse schemes.

Keywords: Energy requirements; high-quality water; micropollutants; potable water reuse; water reclamation and reuse

3.3 Publication #3 (Abstract)

Strategies and opportunities for energy optimization in recycling water (in German)

Jörg E. Drewes[a] and Nils Horstmeyer[a]

[a]Chair of Urban Water Systems Engineering, Technical University of Munich, Am Coulombwall 3, 85748 Garching/München, Germany.

The following publication was published 2016 with editorial changes in:

Drewes, J.E., Horstmeyer, N. (2016). Strategien und Potenziale zur Energieoptimierung bei der Wasserwiederverwendung (in German) Strategies and opportunities for energy optimization in recycling water. *Österreichische Wasser- und Abfallwirtschaft,* 68, 99–107 (in German).

Abstract

The energy and materials derived from treating sewage are becoming increasingly important worldwide and are thus progressively considered resources rather than a disposal problem. This is also apparent in the growing interest in recycling water from municipal wastewater for both non-potable and potable purpose, supplementing the drinking water supply in the latter case. However, the energy consumption of about 0.9–1.8 kWh/m³, required to recycle drinking water, is not insignificant. Due to the lack of national as well as international standardized regulatory specifications for recycled water quality, very different technical solutions for potable water reuse have been deployed worldwide. Therefore, energy-saving measures often can only be applied to internal operational optimizations and the achievable savings are rather limited. Strategies for integrated energy recovery, the increased use of anaerobic biological processes and combined heat and power (CHP) for water recycling are hence very promising. These provide opportunities for internal power provision and therefore options to reduce the specific energy requirements for potable water reuse to well below 1 kWh/m³, despite the necessary treatment processes. However, the greatest potential for energy-efficient water recycling is at the regional planning level. Recycling water is only attractive where local freshwater resources are insufficient or there is a dependency on imported water, and it is the significantly more cost-effective option than the treatment of brackish or sea water.

3.4 Introduction

Reuse of municipal wastewater - untreated or treated - has been practiced for less than two centuries with the objective of diverting human waste outside of urban settlements (Sedlak 2014). However, water reuse as a *planned* activity started about one century ago with the use of treated effluent to irrigate Golden Gate Park in San Francisco, California in 1912 (Hyde 1937). Non-potable water reuse applications have grown substantially since then from urban landscape irrigation to irrigation of food crops, cooling water, car wash facilities, fire fighting, public fountains, stream flow augmentation to seawater intrusion barriers (Asano et al. 2007). With better effluent qualities and scarcity of locally available freshwater supplies, water reuse using treated municipal wastewater effluents has also been considered to augment drinking water supplies as early as the 1960s with pioneering applications in the USA and Namibia. Today, planned potable water reuse is recognized worldwide as an increasingly important component of regional water resource management with a growing number of established projects (WHO 2017a, Hering et al. 2013, Drewes and Khan 2011).

Planned potable water reuse projects are characterized as indirect or direct (Figure 6). Indirect potable water reuse (IPR) is referred to as the purposeful addition of highly treated wastewater (i.e. reclaimed or recycled water) via an environmental buffer that is subsequently used to augment a drinking water supply (Drewes and Khan 2011). The environmental buffers can comprise a groundwater aquifer or a surface water reservoir with the intent to provide retention, additional attenuation of contaminants and blending prior to use as drinking water. Direct potable water reuse (DPR) is defined as the immediate addition of reclaimed water to a drinking water distribution system or the raw water supply directly upstream of a drinking water treatment facility. In order to provide time to react to any process upset conditions in DPR projects, an engineered storage facility can provide the desired retention time prior to release of the treated water into a distribution system.

Indirect potable water reuse (IPR)

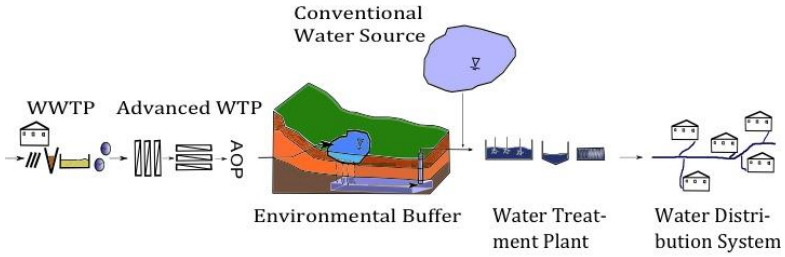

Direct potable water reuse (DPR)

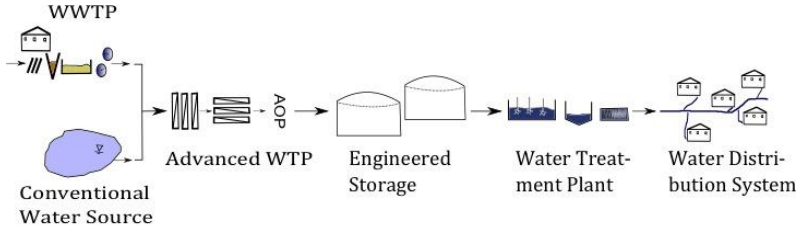

Figure 6. Conceptual design of indirect and direct potable water reuse applications (IPR/DPR).

In particular during the last 10 years, there is increasing interest worldwide in establishing drinking water augmentation projects using reclaimed water. These initiatives in potable water reuse are driven by population growth, lack of conventional freshwater supplies, competing environmental, industrial and agricultural needs for water, more frequent and severe drought conditions stressing the availability of conventional freshwater resources, and a higher level of confidence in the efficiency of treatment processes involved.

3.5 The current state of potable water reuse applications

3.5.1 The evolution of indirect potable water reuse

Indirect potable water reuse has been practiced in the USA for more than 50 years. In 1962, the pioneering IPR project was established in the Montebello Forebay in Southern California to augment local groundwater supplies with a blend of reclaimed water, stormwater and imported surface water via surface spreading operation. Severe water scarcity and a lack of alternatives led to the establishment of the first direct potable water reuse project by the City of Windhoek in 1968, which has been replaced by the new Goreangab Water Reclamation Plant in 2002.

In 1976, the Orange County Water District, California, established the Water Factory 21, which was the first IPR facility employing advanced water treatment processes including integrated membrane systems (microfiltration (MF) / RO) for direct injection projects. Further process evolutions and program expansions in Orange County have resulted in the Groundwater Replenishment System established in 2008, which after completion of a plant expansion in 2015 represents the largest IPR project worldwide with a capacity of 348,000 m^3/day. Potable water reuse projects located in coastal areas in the USA, Singapore and Australia have favored the use of integrated membrane systems (IMS), in same cases coupled with advanced oxidation processes using ultraviolet light irradiation with hydrogen peroxide (UV / H_2O_2) addition. For inland projects, however, high-pressure membrane filtration is favored less due to the lack of suitable and cost-effective waste stream disposal options. Instead, IPR projects in these locations have employed various combinations of low-pressure membranes (e.g. UF), granular activated carbon (GAC) filtration, chemical oxidation (e.g. ozone), and natural treatment systems (e.g., soil-aquifer treatment (SAT), riverbank filtration (RBF), wetland treatment) (Drewes and Khan 2011, Khan 2013). Table 1 summarizes established potable water reuse projects worldwide.

Table 1. Established potable water reuse projects worldwide (adopted from Drewes and Khan 2011, WHO 2017a, Water Corporation 2018).

Year	Project	Capacity (m^3/d)	Country	Advanced treatment sequence	Potable Water Reuse Type
1962	Montebello Forebay Spreading Grounds, Los Angeles County Sanitation Districts/Water Replenishment District, California	165,000	USA	Media filtration-SAT	IPR/groundwater recharge
1968	(Old) Goreangab Water Reclamation Plant, Windhoek	7,000	Namibia	DAF-media filtration-GAC	DPR
1976	Water Factory 21, Orange County Water District, California	60,000	USA	Lime clarification-air stripping-RO-UV/AOP	IPR/seawater intrusion barrier
1978	Upper Occoquan Service Authority, Virginia	204,000	USA	Lime clarification-media filtration-GAC-ion exchange	IPR/surface water augmentation
1985	Hueco Bolson Recharge Project, El Paso, Texas	38,000	USA	Lime clarification-media filtration-Ozone-GAC-Ozone	IPR/groundwater recharge
1985	Clayton County, Georgia	66,000	USA	UV-Wetland	IPR/surface water augmentation
1993	West Basin Water Recycling Plant, California	47,000	USA	MF-RO-UV/AOP	IPR/seawater intrusion barrier
1999	Gwinnett County, Georgia	227,000	USA	UF-Ozone-GAC	IPR/surface water augmentation
1999	Scottsdale Water Campus, Arizona	53,000	USA	Media filtration-MF-RO-UV/AOP	IPR/groundwater recharge
2002	New Goreangab Water Reclamation Plant, Windhoek	21,000	Namibia	Ozone-clarification-DAF-media filtration-Ozone-BAC/GAC-UF	DPR
2002	Toreele Reuse Plant	7,000	Belgium	UF-RO-UV	IPR/groundwater recharge
2003	NeWater Bedok	86,000	Singapore	UF-RO-UV	IPR/surface water augmentation
2003	NeWater Kranji	55,000	Singapore	UF-RO-UV	IPR/surface water augmentation
2005	Alimitos Barrier, California	10,000	USA	UF-RO-UV	IPR/seawater intrusion barrier
2007	Chino Basin Recharge Project, California	69,000	USA	Media filtration-SAT	IPR/groundwater recharge

2008	Groundwater Replenishment Project, California	265,000	USA	MF-RO-UV/AOP	IPR/groundwater recharge/seawater intrusion barrier
2008	Western Corridor Project, Southeast Queensland	232,000	Australia	MF-RO-UV/AOP	IPR/surface water augmentation (not operational)
2008	Loudon County, Virginia	42,000	USA	MF-GAC	IPR/surface water augmentation
2009	Arapahoe/Cottonwood, Colorado	34,000	USA	Riverbank filtration-RO-UV/AOP	IPR/groundwater recharge
2010	NeWater, Changi	230,000	Singapore	UF-RO-UV	IPR/surface water augmentation
2010	Prairie Waters Project, Colorado	190,000	USA	Riverbank filtration-softening-UV/AOP-BAC-GAC	IPR/groundwater recharge
2010	Groundwater Replenishment Trial, Perth, Western Australia	5,000	Australia	UF-RO-UV	IPR/groundwater recharge
2011	Cloudcroft, New Mexico	100	USA	MF-RO-UV/AOP-UF-GAC	DPR (not operational)
2012	Dominguez Gap Barrier	10,000	USA	MF-RO	IPR/groundwater recharge
2012	Beaufort West	1,000	South Africa	Media filtration-UF-RO-UV/AOP	DPR
2013	Raw Water Production Facility, Big Springs, Texas	7,000	USA	MF-RO-UV/AOP	DPR
2014	Groundwater Replenishment Project, California (expansion)	348,000	USA	MF-RO-UV/AOP	IPR/groundwater recharge/seawater intrusion barrier
2016	Beenyup Groundwater Replenishment Scheme, Perth	72,000	Australia	UF-RO-UV	IPR/groundwater recharge

IPR: Indirect potable water reuse; DPR: direct potable water reuse; DAF: dissolved air flotation; RO: reverse osmosis; GAC: granular activated carbon; BAC: biologically-active carbon; AOP: advanced oxidation processes; UV: ultraviolet light; SAT: soil-aquifer treatment; MF: Microfiltration; UF Ultrafiltration.

A portfolio of multiple treatment options and combinations exist, including engineered and natural treatment processes, to design IPR schemes. While these schemes are unified in the goal to lower the risk from microbial and chemical constituents of concern, their individual process treatment efficiency for various contaminants and reliability can vary widely. A similar degree of variability exists regarding the functions of the environmental buffer, including (1) the provision of time to respond to process upsets, (2) attenuation of contaminants, and (3) blending or dilution. While there is ample evidence that an environmental buffer such as soil-aquifer treatment can be very effective regarding these three functions (Regnery et al. 2013, Alidina et al. 2014), in cases where advanced treatment such as RO is employed, additional water quality improvements in a subsequent environmental buffer are marginal at best (Snyder et al. 2014). Previous studies could not demonstrate that natural barriers provide any public health protection that is not also available by other engineered (above-ground) processes. Thus, the National Research Council (NRC) of the USA concluded that environmental buffers are not essential elements to achieve quality assurance in water reuse projects (NRC 2012). As a consequence, the NRC suggested that the classification of potable water reuse projects as indirect (i.e. includes an environmental buffer) and direct (i.e. does not include an environmental buffer) is not meaningful from a technical perspective because the terms are not linked to product water quality (NRC 2012).

3.5.2 Trends towards direct potable water reuse

Significant technological improvements, operational experience over many decades and advancements in microbiology, chemistry, and toxicology have resulted in a high degree of confidence in the practice of drinking water augmentation using reclaimed water in the USA (Drewes and Khan 2011). In the early 2010th, this confidence level along with the impacts from severe droughts, rising energy prices, and requirements for environmental restoration have resulted in a number of initiatives to explore the viability of DPR (Leverenz et al. 2011). While some smaller scale DPR projects were recently established in South Africa and the USA primarily driven by severe drought conditions and a lack of alternative supplies (see Table 1), a large initiative was launched in 2010 to advance DPR as a future water supply option for California (Khan 2013, Tchobanoglous et al. 2011). In September 2010, reflecting the increased interest in DPR, the Governor of the State of California signed into law Senate Bill 918. This bill mandated the California Department of Public Health (CDPH) to investigate the feasibility of developing regulatory criteria for DPR and to provide a final report on that investigation to the legislature by the end of 2016.

California's Water Recycling Policy has set ambitious goals to increase the total amount of recycled water of currently 802 million m^3/year by a factor of four by 2030. However, especially in Southern California it has been recognized that further growth of non-potable water reuse in urban settings has reached its limit in many locations and the goal to significantly grow water recycling in the state cannot be met by non-potable water reuse activities. The main limitations of non-potable water reuse are the cost-prohibitive expansion of dedicated dual-distribution

systems in built-out urban environments and the lack of additional large customers that could be served for non-potable water reuse applications (i.e., public parks, golf courses). Southern California has also relied on imported water from the Colorado River and the State Water Project, which availability has been significantly reduced due to competing environmental needs and declining supplies as a consequence of climate change impacts. Thus, DPR has been recognized in California as a locally sourced, sustainable water supply for the future since it does not require a dedicated dual distribution system and provides cost savings compared to the development and importation of conventional supplies (Leverenz et al. 2011, Tchobanoglous et al. 2011). Nevertheless, there is still a significant gap of knowledge regarding requirements of a fail-safe operation, real-time monitoring, appropriateness of treatment barriers against new contaminants and transformation products, blending options with conventional supplies, and regulatory and public acceptance before DPR can be implemented at a large scale (Tchobanoglous et al. 2011).

These trends and developments point to the need to develop better guidance and standardization for the design and operation of potable water reuse schemes including best management practices that can assist the regulatory community and water industry in developing high confidence in fail-safe potable water reuse applications that are protective of public health.

3.6 Managing health risks in potable water reuse

Health risks in potable water reuse applications are associated with microbial and chemical contaminants that can have adverse effects on human health (Drewes and Khan 2011). In addition, aesthetic issues related to taste and odor are also an important consideration for public acceptance of potable water reuse projects (Agus et al. 2011). While conventional wastewater treatment in many countries provides an effluent quality that is suitable to be discharged to surface water, treated effluents are still composed of a wide range of naturally occurring and anthropogenic trace organic and inorganic contaminants residual nutrients, total dissolved solids, residual heavy metals, and pathogens (Drewes and Khan 2011). Microbial contaminants including bacteria, viruses and protozoan parasites are acknowledged as the most critical constituent in reclaimed water due to potential acute human health impacts in public water supplies. Chemical contaminants, of which a large number can still be present in reclaimed water, can be of concern due to potential adverse acute and chronic health effects (NRC 2012).

In the USA, there are no federal water quality standards for potable water reuse that go beyond drinking water standards under the Safe Drinking Water Act. Four states have developed state-specific regulations or guidelines specifically pertaining to IPR, which differ widely (USEPA 2012). The State Water Resources Control Board (SWRCB) published in 2018 the latest update with a list of CECs and other monitoring parameters (SWRCB 2018). In 2008, Australia has published as the first country national guidelines for the augmentation of drinking water supplies with recycled water, which follow a risk-based approach individual states and

territories can adopt (EPHC 2008). In 2017, the WHO published the first international guidance for potable reuse (WHO 2017a).

In the EU, the basis for European water policy is the Water Framework Directive 2000/60/EC (EU 2000). The Directive divides chemical contaminants into priority substances (significant risk to or via aquatic environment) and priority hazardous substances (subset of priority substances, considered to be extremely harmful). While no specific guidelines for potable water reuse currently exist in the EU, water quality standards will likely consider requirements set forth in the Drinking Water Directive (1998/83/EC) (EU 1998), the Groundwater Directive (2006/118/EC) (EU 2006), and the Environmental Quality Standards Directive (2008/105/EC) (EU 2008). Environmental quality standards are currently identified for 45 priority (hazardous) substances with the aim to achieve good chemical status of groundwater and surface waters (EU 2008, EU 2013). In 2018, the European Commission published a proposal for specifying minimal requirements for non-potable reuse for agricultural irrigation which might be expanded to include groundwater recharge in the future (EU 2018).

As a baseline requirement in any country practicing potable water reuse using reclaimed water, the water quality has to meet drinking water standards. In Europe and the USA maximum quality standards for drinking water can be used as performance standards for treatment trains, however, they currently only cover less than 100 contaminants potentially also present in reclaimed water. While these include a range of pesticides and industrial contaminants, they do not comprise contaminants that are typically associated with discharges from municipal wastewater effluents, including pharmaceutical residues, personal care products, household chemicals, hormones, or emerging disinfection by-products. Thus, given the origin of reclaimed water, additional water quality requirements acknowledging the impaired quality of the source should be defined where potable water reuse is practiced.

3.6.1 Setting water quality performance requirements in potable water reuse

In order to quantify the potential for human health effects as a result of exposure to microbial and chemical contaminants, regulatory agencies have adopted the concept of a ‘tolerable level of risk’ to assist in setting water quality guidelines or standards. In the regulatory realm, *de minimis* risk, which is defined as a level of risk characterized by the risk being virtually non-existent to describe risks that are “below regulatory concerns”. Traditionally, for drinking water supplies, *de minimis* risk levels are related to health criteria (i.e., toxicity of the constituent; characteristics of the population; exposure). Different risk levels are commonly used, depending on the specific situation and type of contaminant. The United States Environmental Protection Agency (USEPA), Office of Drinking Water, uses a “regulatory window” of 10^{-6} to 10^{-4} for evaluation of risk where 10^{-4} is the baseline risk for all regulations and 10^{-6} is the *de minimis* risk level (USEPA 1992). Microbial contaminants are regulated at a *de minimis* level of 10^{-4} (where 10^{-4} is the annual individual risk of infection by a given pathogen).

In order to mitigate the acute risk from microbial contaminants, the Australian Water Recycling Guidelines have adopted a numerical definition of safety using disability adjusted life years

(DALYs) to convert the likelihood of infection or illness into burdens of disease, setting a tolerable risk as 10^{-6} DALYs per person per year (Khan 2013). Considering a concentration of selected pathogens in raw sewage and an average daily consumption of two liters per person per year, the log reduction required to achieve compliance with 10^{-6} DALYs per person per year can be calculated using equation 1. Removal criteria for pathogenic microorganisms are listed in Table 2.

Log reduction = Log((source concentration x 2 L x 365 days)/DALYd) (1)

Where DALYd (the dose equivalent to 10^{-6} DALYs) for Cryptosporidium is 1.6×10^{-2}, for enteric viruses is 2.5×10^{-3}, and for Campylobacter is 3.8×10^{-2} (Khan 2013).

Performance goals for potable water reuse projects in California have been proposed that are based on a low tolerable or *de minimis* risk level of 10^{-4} annual risk of infection and occurrence data of pathogens in raw wastewater (NWRI 2013).

Table 2. Removal criteria for pathogenic microorganisms for the evaluation of potable water reuse schemes (adopted from (Khan 2013, NWRI 2013)).

Microbial Group	Criterion (Log_{10} Removal) California	Criterion (Log_{10} Removal) Australia	Possible Surrogates	Notes
Enteric Virus	12	9.4	MS-2 bacteriophage	
Cryptosporidium spp.	10	8	Inactivated Cryptosporidium oocysts, aerobic spores	Addresses also Giardia and other protozoa
Total Coliform Bacteria	10	NA	NA	Addresses also enteric pathogenic bacteria
Campylobacter	NA	8.1		

In order to meet these requirements, a given potable water reuse treatment train has to demonstrate that the additive removal efficiencies for microbial contaminants provided by individual treatment processes can meet the desired overall log removal criteria. Meeting this goal would ensure that the reclaimed water is free of pathogenic microorganisms with a large margin of safety and could be safely used for potable purposes. The reason for this rather high degree of conservatism is the lack of comprehensive occurrence data for pathogenic microorganisms in raw sewage.

For the evaluation of potable water reuse treatment schemes regarding chemical contaminants the following factors need to be considered:

- The contaminant chosen to assess treatment performance must occur frequently enough and at a concentration significantly above the analytical method detection limit.
- Appropriate and commercially available analytical methods exist for the quantification of target contaminants in reclaimed water.
- Targeted contaminants for monitoring programs should be broadly representative of both the varying types of contaminants of health concern ("indicator contaminants with health relevance") and the wide range of physicochemical and biological properties that affect their removal of various unit processes within a potable water reuse treatment train ("performance indicator contaminants to assess treatment efficacy").
- The establishment of multiple treatment barriers with different removal mechanisms (i.e., chemical oxidation, biological treatment, physical separation) provides robustness against a wide range of currently not yet identified contaminants.

Performance goals for chemical contaminants for a proposed potable water reuse scheme will include contaminants of recognized health concern that have published guideline values or standards. These include regulated contaminants with an acceptable health risk specified for example as drinking water standards in the EU Water Framework Directive, the USEPA maximum contaminant levels (MCLs) in the USA, chemical guideline values in the Australian Water Recycling Guidelines, WHO Drinking Water Goals or USEPA health advisories or health reference levels. For unregulated contaminants with known toxicological information, the *de minimis* risk approach can be used. In order to specify *de minimis* benchmarks for these contaminants, a reference dose (RfD), acceptable daily intake (ADI) or predicted no-effect concentration (PNEC) information expressing their toxicological relevance can be adopted (Khan 2013, Schwab et al. 2005, Snyder et al. 2008, Bull et al. 2011). These benchmarks are considered in a risk-based action level (RBAL) following a framework proposed by the WHO (van den Berg et al. 2006) and the USA NRC (NRC 2012) for chemical exposure via drinking water (considering a relative source contribution of 0.2):

$$RBAL, \mu g/L = \frac{\left(Benchmark, \frac{\mu g}{kg \cdot d} \right) \cdot 60 kg \cdot 0.2}{2 L/d \cdot UncFactor} \quad (2)$$

Where neither existing guideline values nor relevant toxicological data to develop benchmark values are available, a quantitative structure-activity relationship approach can be used as a method for deriving thresholds of toxicological concern (TTCs) (Khan 2013). The TTC approach is based upon the statistical evaluation of a large group of chemicals with similar

structure and functional groups. It allows to identify a 95-percent lower confidence level for chronic no adverse effect level and then applying uncertainty factors similar to non-cancer risk assessments. The use of TTCs is well established internationally and has been used by the USA Food and Drug Administration and the WHO for setting guidelines for minor contaminants. A similar approach has been proposed by the German Environmental Protection Agency (Umweltbundesamt) to derive public health advisory values and precautionary values for contaminants of emerging concern (UBA 2011). Precautionary values for unregulated contaminants with insufficient toxicological data usually are assigned a blanket value of 0.01 $\mu g L^{-1}$.

Given the large number of contaminants, deviations in published RfD or PNEC values for individual contaminants, and differences in expert opinion regarding appropriate uncertainty factors (UncFactor) for carcinogenic contaminants, a uniform list of contaminants that should be monitored in potable water reuse schemes does not yet exist. Nevertheless, several scientific groups and panels have proposed contaminants with human health relevance to be used in monitoring programs of potable water reuse projects (NWRI 2013, Drewes et al. 2013, SWRCB 2013, 2018). Table 3 lists a selection of proposed health-based indicator contaminants for potable water reuse projects. An updated list of CECs can be found in SWRCB (2018).

Table 3. Health-based indicator contaminants proposed for monitoring programs of potable water reuse projects (adopted from (NWRI 2013, Drewes et al. 2013, SWRCB 2013, 2018)).

Chemical	Criterion	Note
N-Nitrosodimethylamine (NDMA)	10 ng/L	CA reporting level
Bromate	10 µg/L	USEPA; EU
Chlorate	210 µg/L	USEPA
Perfluorooctanoic acid (PFOA)	0.07 µg/L	CA reporting level
Perfluorooctanesulfonic acid (PFOS)	0.07 µg/L	CA reporting level
Perchlorate	15 µg/L	USEPA
1,4-Dioxane	1 µg/L	CA notification level
2,4-Dichlorophenoxyacetic acid	70 µg/L	USEPA

Performance validation and verification of established and alternative treatment trains can occur through direct measurements of indicator contaminants representing a variety of structures and physicochemical properties that correlate with the core removal mechanisms (i.e., biotransformation, adsorption, size exclusion, chemical oxidation) of individual unit processes (Drewes et al. 2008, Dickenson et al. 2009, 2011). In addition, the removal of

specific performance-based indicator contaminants or families of contaminants with closely related properties may be correlated with the removal of other routinely measured compounds or operational parameters that can be monitored continuously as a surrogate parameter (e.g., electrical conductivity, UV absorbance) (Drewes et al. 2008, Wert et al. 2009, Drewes et al. 2010). These approaches have the advantage that they can be established as real-time monitoring strategies where a high-resolution of system performance control is desired. Table 4 summarizes proposed maximum concentrations of performance-based indicator contaminants and expected removal percentages for monitoring of treatment train efficacy of potable water reuse projects.

Table 4. Performance-based indicator contaminants proposed for monitoring programs of potable water reuse projects (adopted from (NWRI 2013, SWRCB 2013, 2018, Bull et al. 2011)).

Chemical	Criterion (max. concentration or minimum percent removal)	Note
Atenolol	4 µg/L	Bull et al. 2011
Carbamazepine	100 µg/L	Bull et al. 2011
N,N-diethyltoluamide (NN-diethyl-3-methylbenzaide (DEET)	250 µg/L	SWRCB 2018
	90%	Removal by SAT or RO/AOP treatment (SWRCB 2013)
Phenytoin (Dilantin)	50 µg/L	Bull et al. 2011
Gemfibrozil	90%	Removal by SAT (SWRCB 2013)
Iopromide	90%	Removal by SAT (SWRCB 2013)
Meprobramate	200 µg/L	Bull et al. 2011
Primidone	375 µg/L	Bull et al. 2011
Sucralose	none	Approved for use as a sweetener in food
	25%	Removal by SAT (SWRCB 2013)
	90%	Removal by RO/AOP treatment (SWRCB 2013)
Tris(2-chloroethyl)phosphate (TCEP)	5 µg/L	Monitoring trigger level; State of Minnesota guidance value (SWRCB 2013, Bull et al. 2011)

3.7 State-of-the-art water quality monitoring approaches for high-quality recycled water

Currently, regulatory strategies for monitoring programs where high-quality product water is desired offer different approaches to ensure a consistent water quality. The most common approach is to define threshold values of the target contaminants in the final product water. These threshold values are commonly based on health-effect studies, which estimate the acute and chronic risk to human health (or the environment) providing an exposure risk. These defined thresholds are embedded into a monitoring and control concept of treatment schemes designed to provide high-quality water. While these schemes can differ among countries, the threshold values for certain contaminants, since they are based on scientific evidence, usually are similar.

Water quality management of projects delivering high-quality product water depends on many factors and variables and represents a complex dynamic system. The major elements of that dynamic system are the source water (i.e., variable flow conditions, dilution processes, industrial and commercial discharger), the treatment system (i.e., dynamic contaminant load and inherent system variability), and other holistic parameters, which can influence the natural degradation of several contaminants in the environmental buffer (e.g. variably sun irradiation triggering photolytic degradation processes). In traditional water quality schemes these dynamic changes are rarely considered and the different forms of dynamics are compensated by buffer values or safety factors added to the threshold. This is assumed to address the variability of complex dynamic systems, but there is no anticipation when these systems will occur and what the overall variability might be. Generally, anticipation of water quality changes needs four core elements:

1. Continuous monitoring and a reliable prediction of expected water qualities.
2. Dynamic system operation.
3. Scientific model.
4. A cost-benefit approach.

The last point might not be of primary focus in potable reuse projects where protection of public health is concerned, but it has been demonstrated that systems operating by a cost-benefit incentive are more likely to be implemented in today's world of tight economic budgets. For traditional contaminants (e.g., nitrate, phosphorous), advanced dynamic water quality scheme might not be needed due to cost intense monitoring. However, for contaminants with acute and chronic risk (e.g., pathogens, certain trace organic chemicals) monitoring of water quality variability might be more appropriate. Based on a literature review, three typical monitoring approaches dealing with system dynamics have been identified:

- Static regulatory standards but dynamic treatment approaches to meet the target concentrations.

- Static regulatory standards extended by integrated seasonal dilution factor in order to account for variability.
- Regulatory authorities accept a dynamic treatment goal (e.g., different seasons, different reuse applications) and adapt the regulatory thresholds to different dynamic resolutions (e.g., minutes, hours day months or seasons). This can be again combined with treatment strategies offering dynamic characteristics.

In this context the usage of advanced stochastically simulation and predictions should be emphasized. Although research is able to provide a diverse range of such predictive programs to simulate contaminant faith, no real world example can be found where these simulations are accepted and integrated into a regulatory real-time water quality scheme. However, a dynamic real-time water quality scheme strongly increased monitoring complexity and eventually increased cost. Conventional treatment targets in the past have been met using static thresholds, where the main purpose was to discharge to the aquatic environment. The requirements for treatment efficiency in these conventional treatment plants did not justify a new thinking in terms of advanced anticipation to different system dynamics. However, in providing high-quality recycled water different approaches are needed when dealing with complex contaminant occurrence and mixtures including emerging trace organic chemicals or pathogens. Being able to adapt to those challenges will make the difference in term of cost efficiency and more appropriately optimizing removal of critical contaminants.

Advanced wastewater treatment technologies (e.g., ozonation (O_3), UV/H_2O_2, activated carbon adsorption, and membrane technologies) have been proposed to reduce contaminants in potable reuse schemes. However, these advanced treatment technologies are energy-intensive, operationally complex and expensive. As such, the investment of implementing advanced treatment should be balanced against reliably meeting public health goals versus environmental impacts and financial costs. The relationships between these benefits and costs will vary between locations and also over time, for instance as a function of seasonal or even daily variations. In balancing the benefits and costs of advanced water treatment, there are potential opportunities to establish more flexible modes of operation, for instance by incorporating a dynamic load-dependent dosing regime (e.g. for O_3) or a dynamic hydraulic flux adjustment (e.g. for membrane systems). However, the ability to apply these flexible and potentially more ideal operational modes will depend upon our ability to dynamically assess and respond to a range of diverse factors affecting treatment process performance and its desired outcome. These aspects may include considering variable concentrations of contaminants in raw wastewater, the inherent treatment process performance, environmental dilution, natural attenuation capability, variable exposure factors as well as energy costs and energy sources.

As mentioned previously, static thresholds respectively standards have been stated as the central elements regulatory authorities use for water quality management. Stepping into responsibility for the upcoming treatment challenges this won’t be sufficient. In a general scheme the treatment objectives can be visualized in Figure 7.

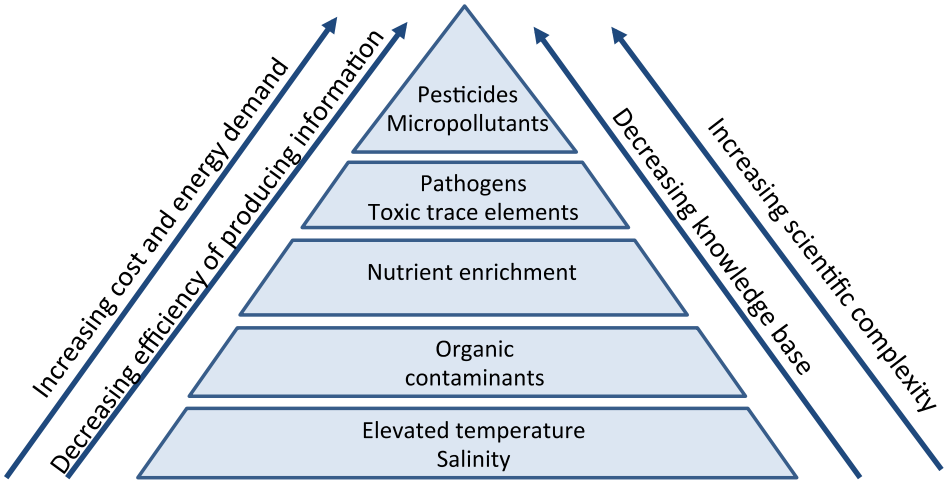

Figure 7. Hierarchical complexity of wastewater treatment objectives in producing high-quality water.

Figure 7 illustrates that advanced treatment in particular of emerging contaminants achieves limits in the following 4 criteria.

- Scientific complexity
- Limited knowledge base
- Highest treatment cost
- Most limited information about the contaminant

This position raises the question whether the traditionally used static threshold approach is comprehensive enough to fulfill the various requirements for treatment process design. For emerging micropollutants the scientific complexity limits direct or strongly simplified monitoring concepts. Therefore, only very advanced simulations techniques appear to be capable to make realistic predictions about real-time contaminant concentrations. These predictive models make use of advanced stochastic simulations and allow probabilistic predictions. Once a threshold based on probabilities is accepted it is the next step to optimize the prediction by knowing as much as possible about surrogate and system parameters. This knowledge is likely to be triggered by holistic and treatment plant specific parameters. Eventually the system and schematic real-time knowledge will be increasingly advanced. This allows for a dynamic operation of the treatment plant to reduce the high treatment costs associated with the removal of these contaminants as illustrated Figure 7.

Nevertheless, this is not the only way to optimize the cost-benefit ratio between treatment cost and target removal. There are natural processes such as an environmental buffer of IPR schemes, which decrease the contaminant concentration immediately or in an acceptable time

scale. This might include dilution and natural attenuation processes in a reservoir or groundwater aquifer. They can cause a tremendous reduction of the contaminant concentration and are provided at low or no cost. The only price is the real-time knowledge and management of those additional processes. Those advanced dynamic treatment schemes and scenarios require a dynamic threshold management and it is necessary that this can be transparently displayed. There will be a fundamental change in designing monitoring programs for facilities producing high-quality recycled water. Benchmarking approaches of water reclamation facilities will be combined with regulatory targets. This will accelerate the demand for smart monitoring technologies and push shared data and also big data processing in a reuse scheme designed to deliver high-quality water. The traditional static way of dealing with contaminations is not impossible or unlikely, but cost pressure will favor intelligent and dynamic treatment approaches.

3.8 Design principles of potable water reuse

The core design elements of potable water reuse treatment trains involve a thorough understanding of source water characteristics, the establishment of reliable treatment systems, storage and blending considerations, and an overarching monitoring program for performance and compliance (Figure 8). These elements are further discussed in the sections below.

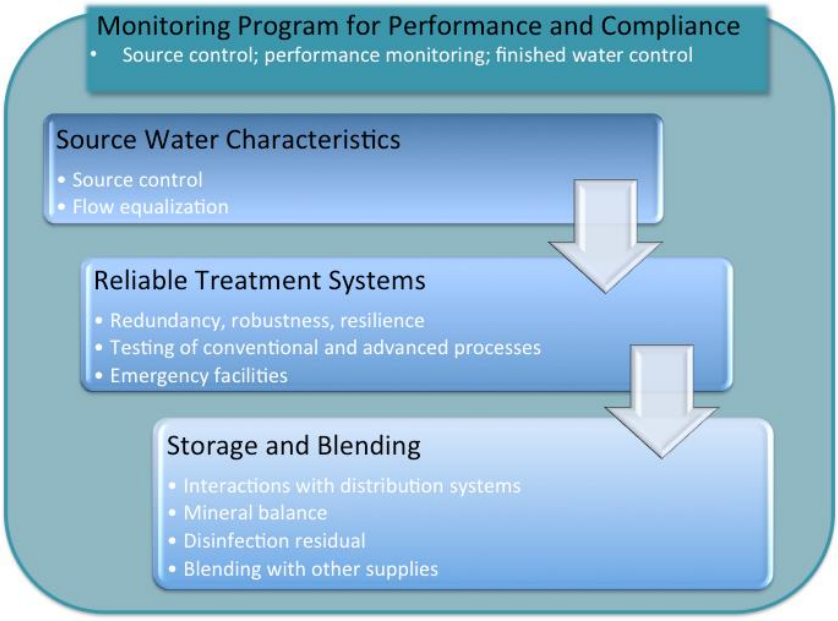

Figure 8. Key design elements of potable water reuse schemes.

Monitoring program for performance and compliance

Monitoring programs for potable water reuse projects need to be considered and designed to address source control, treatment performance assessments, and assuring that specified

finished water quality criteria are met. Assessing treatment train performance and compliance and finished water quality criteria have been discussed in previous sections. Source control requirements are being addressed in the next section. Additional information can be found in Drewes and Khan (2011).

Source water characteristics

Understanding the variability of source water quality is a pre-requisite to properly design efficient processes for a potable water reuse treatment train. Beside treatment processes, flow equalization measures can be effective in mitigating and eliminating significant differences in source water quality and quantity. In particular for DPR project, flow equalization is an important design feature that can result in both a more consistent source water quality and a more homogeneous load to downstream treatment processes, in general contributing to a more consistent finished water quality.

In addition, source control through monitoring and compliance assessments of point discharges to the sewer system is a critical element to maintain a consistent reclaimed water quality (Drewes and Khan 2011, Khan 2013). These programs are conducted with the goal of reducing treatment costs, targeting inorganic and organic contaminants of concern that are not primarily removed during conventional wastewater treatment (i.e., heavy metals, trace organic contaminants) and therefore improving the reliability of the final water quality.

Reliable treatment systems

Any potable water reuse scheme should be designed to reliably supply a finished water quality that is safe for human consumption at all times. System reliability of a potable water reuse project is defined as the probability of adequate performance for a specified period of time under predefined conditions. Reliability in potable water reuse systems can be achieved by a number of supporting concepts including redundancy, robustness, and resilience.

The concept of redundancy describes the use of multiple barriers to control acute risks. Robustness is defined as the capacity to remove a wide range of particular chemical contaminants. In addition, potable water reuse facilities must also be resilient to ensure reliability even under rare failure events. A resilient system in this respect is not a system that never fails, but a system that fails safely, meaning that failures are mitigated through well-designed response plans including the prevention of distributing water that does not meet specified requirements. System reliability requirements may include standby power supplies, provisions for alarms, readily available replacement equipment, online monitoring of system performance and water quality, redundant process components that are critical for the protection of public health, flexible piping and pumping configurations, trained personnel, and emergency storage or disposal options.

Combining water treatment processes that are capable of providing effective, reliable, and redundant barriers to pathogens and contaminants are referred to as the *multiple-barrier approach* to water treatment. For potable water reuse projects, although the multiple barriers do tend to be relied on to provide cumulative steps toward the achievement of overall treatment

goals, there is generally an expectation that they will accommodate a degree of treatment redundancy for pathogens. That is, the protection of public safety will be maintained even if a single treatment barrier fails. The independence of multiple barriers is a key aspect of system reliability and safety. In order to mitigate the acute risk from microbial contaminants and to meet overall removal criteria as discussed earlier (see Table 2), various unit processes can be combined in a meaningful fashion considering conservative expected log-removal efficiency of individual unit processes for pathogenic microorganisms as specified in Table 5 (Trussel 2014).

Table 5. Log-removal efficiencies of various unit processes to remove target microbial contaminants (adopted from Trussel 2014)).

Unit Process	Enteric Viruses	Cryptosporidium	Total Coliform Bacteria
Conventional activated sludge (CAS)	1	0	2
Microfiltration (MF)	0	4	4
Ultrafiltration (UF)	1	4	4
Reverse osmosis (RO)	2	2	2
Ozonation (O_3)	6	1	4
Biologically-active carbon (BAC)	0	0	0
Ultraviolet light (UV)	6	6	6
UV light with hydrogen peroxide (UV-AOP)	6	6	6
Free chlorine (Cl_2)	6	0	4

For an IPR scheme typically designed for direct injection into a potable aquifer, accumulative virus log-removal efficiencies for enteric viruses would total 22 (Figure 9). An IPR treatment train with very short retention in an environmental buffer consisting of biofiltration via subsurface treatment, advanced oxidation and activated carbon treatment followed by final disinfection prior to blending with conventional supply would achieve an overall virus log removal efficiency of 12 (Figure 10). Both treatment combinations would also exceed the required log removal criteria for cryptosporidium and total coliform bacteria (data not shown). Given that the proposed log removal criteria are already very conservative (see Table 2), the margin of safety that potable water reuse projects utilizing treatment combinations as illustrated in Figure Figure 9 and Figure 10 can provide against pathogenic contaminants will likely exceed conventional drinking water supplies that are using source water receiving small amounts of wastewater discharge (exceeding a contribution of 5%) by several orders of magnitude (NRC 2012).

Figure 9. Virus log-removal efficiency by a potable water reuse treatment train consisting of integrated membrane systems followed by advanced oxidation processes and an environmental buffer.

Figure 10. Virus log-removal efficiency by a potable water reuse treatment train consisting of biofiltration via subsurface treatment, advanced oxidation and activated carbon treatment followed by final disinfection prior to blending with conventional supply.

Given the wide range of different contaminants present in reclaimed water, robust multiple barriers should be designed to consider a sequence of diverse processes that are capable of targeting the wide range of physicochemical properties represented by various classes of contaminants. The requirement for redundancy normally associated with pathogen removal is not applied to multiple barriers for chemicals. This is because exposure to chemicals is more of a chronic risk, relating to long-term exposure, as compared with the acute risks associated with pathogens, for which even short-term exposure may have significant impacts on human health. Thus, for removal of chemical contaminants diversity in treatment rather than redundancy can result in highly efficient overall removal of trace organic contaminants generating a finished water quality that is indistinguishable to conventional supplies (Figure 11).

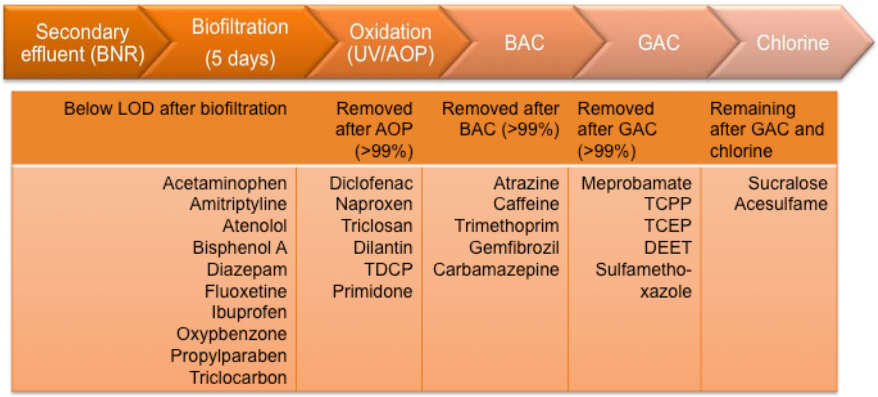

Figure 11. CEC removal efficiency by a potable water reuse treatment train consisting of biofiltration via subsurface treatment, advanced oxidation and activated carbon treatment followed by final disinfection prior to blending with conventional supply (Note: concentrations for the artificial sweetener

sucralose and acesulfame in the finished where in the elevated ng/L range were well below any health relevance level).

Storage and blending

The water quality after advanced treatment requires adjustments in particular where different source waters are blended regarding compatibility with the drinking water distribution system (i.e., saturation index, corrosivity) and aesthetics (i.e., mineral balance, color). In IPR systems, storage and blending can occur by passing water through an environmental buffer. In many potable water reuse systems, however, the primary benefit of environmental buffers is to provide time to respond to an inadequate water quality associated with inappropriate treatment or other factors (Drewes and Khan 2011). Thus, in the context of DPR projects an engineered storage unit or adequate (real-time) monitoring systems (or both) might be able to fulfill the function of the environmental buffer. However, additional research is needed to develop specific storage and blending requirements for DPR projects.

3.9 Energy-efficiency of potable water reuse schemes

Potential conventional process combinations of water reuse schemes (Figure 12) usually utilize secondary or tertiary treated effluents from conventional biological wastewater treatment. Advanced water treatment (AWT) is applied worldwide in different scenarios to generate high-quality effluent for potable reuse. For example, common treatment combinations for AWT are: 1) MF, RO and advanced oxidation processes (UV/H_2O_2) (Orange County, USA); 2) UF, BAC filtration, O_3, UV disinfection (Gwinnett County, USA); or 3) O_3, BAC, Chlorine (Cl_2) UV disinfection (Melbourne, Australia). The AWT processes commonly utilized in potable reuse schemes do increase the energy footprint significantly. The total energy footprint of potable water reuse schemes using AWT can vary between 0.9 and 1.8 kWh/m³.

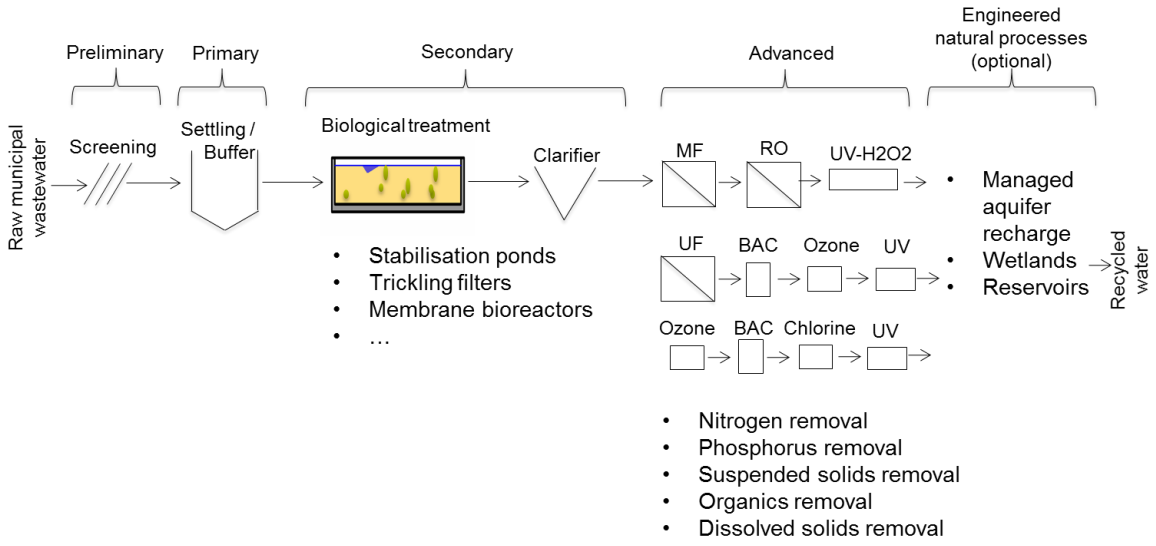

Figure 12. Process combinations of water reuse schemes using advanced treatment process to produce high-quality water.

The energy requirements and associated carbon footprint of selected treatment processes for conventional drinking water facilities, conventional biological wastewater treatment, and advanced treatment processes representing barriers to pathogens and chemical constituents are listed in Table 6.

Table 6. Average energy requirements and CO_2-Footprint of conventional drinking water augmentation, wastewater treatment, and water reuse processes (Tchobanoglous et al. 2015, Lazarova et al. 2012, Bolle and Pinnekamp 2015).

Process	Energy demand		CO_2-Footprint
	Range [kWh/m³]	Typical [kWh/m³]	[kg CO_2/m³]
Conventional drinking water treatment	0.1 – 1.13	0.1	0.05
Conventional biological wastewater treatment without nutrient removal	0.37 – 1.0	0.33	0.17
Conventional biological wastewater treatment without nutrient removal and subsequent filtration	0.29 – 1.22	0.49	0.25
MF – RO – UV/H_2O_2 – Stabilization – Chlorination	0.86 – 1.06	0.95	0.48
O_3	0.04 – 0.17	0.05	0.06 – 0.13
PAC	0.03 – 0.04	0.03	0.15 – 0.24
MF, UF	0.06 – 0.1	0.07	-
NF	0.16 – 0.25	0.2	-

Brackish water desalination	0.82 – 1.64	1.55	0.6
Seawater desalination	2.51 – 3.9	3.17	1.59

MF=Microfiltration, RO=Reverse osmosis, UV=Ultraviolet light treatment, H_2O_2=Hydrogen peroxide, O_3=Ozonation, PAC=Powdered activated carbon, UF=Ultrafiltration, NF=Nanofiltration.

Energy optimizations and additional savings of individual unit operations and processes employed in water reuse schemes have either already been implemented or have limited potential. However, integrating energy and heat recovery concepts into water reuse schemes might have a significantly larger savings potential. This could be accomplished by implementing anaerobic biological processes and subsequent energy utilization with combined heat and power (CHP) units.

3.10 Conclusions

The practice of potable water reuse has evolved over the last 50 years into a viable option for an integrated water resource management to safely augment drinking water supplies with recycled water. Today, potable water reuse is also practiced in locations that are not characterized by arid or semi-arid climate conditions, but regions that experience seasonal water shortage or have a desire to diversify their water resource portfolio for future climate change impacts.

While there is also increasing recognition that unplanned or *de facto* potable water reuse is occurring where treated wastewater effluents are discharged to surface water that subsequently serves as a source of drinking water, proper safeguards to mitigate the risks associated with microbial and chemical contaminants is not always appropriately addressed (NRC 2012, Rice et al. 2013). Thus, best management practices and risk management frameworks developed for potable water reuse projects as described in this chapter might also provide guidance for *de facto* potable water reuse situations.

4 A novel concept to integrate energy recovery into potable water reuse treatment schemes (Publication #4)

Based on the review of current state-of-the-art potable water reuse schemes (including their energy demands) in chapter 3, in this chapter the overall dissertation hypothesis is tested and assessed. Expressed as hypothesis #1:

> *"An alternative potable reuse treatment design can treat municipal wastewater with a lower energy demand (< 1.0 kWh/m³) compared to a potable reuse benchmark (CAS, MF, RO, UV/H_2O_2) by generating an equivalent water quality. The alternative potable reuse treatment design consists of the following core processes: sedimentation & microsieving, UF, NF/RO, BAF, and UV/H_2O_2."*

Thus, this chapter, published as publication #4, focusses on the systematically evaluation of existing potable water reuse applications, the determination of the energy potential within wastewater and the identification of energy recovery opportunities. Finally, it was possible to design three alternative more energy-efficient potable water reuse schemes. Hence, hypothesis #1 was confirmed.

Publication #4:

Nils Horstmeyer[a], Max Weißbach[a], Konrad Koch[a], and Jörg E. Drewes[a]

[a]Chair of Urban Water Systems Engineering, Technical University of Munich, Am Coulombwall 3, 85748 Garching/München, Germany.

The following publication was published with editorial changes in:

Horstmeyer, N., Weissbach, M., Koch, K., Drewes, J.E. (2018) A novel concept to integrate energy recovery into potable water reuse treatment schemes. *Journal of Water Reuse and Desalination* **8**(4), 455-467.

Abstract: Potable water reuse applications can provide a safe and sustainable water supply where conventional freshwater resources are limited. The objectives of this study were fourfold: (i) to analyze existing potable water reuse applications regarding operational characteristics and energy demands, (ii) to determine the theoretical energy potential of wastewater and identify opportunities for energy recovery, (iii) to define design requirements for potable water reuse schemes that integrate energy recovery, (iv) to propose strategies for more energy efficient potable water reuse schemes. Existing potable water reuse schemes commonly utilize conventional wastewater treatment processes including biological nutrient removal followed by advanced water treatment processes. While meeting a high product water quality, these treatment schemes are characterized by relatively high specific energy demands (1.18 kWh/m³). Given that the theoretical energy potential of municipal wastewater is

approximately 2 times higher (2.52 kWh/m³), opportunities exist to integrate energy recovery strategies. We propose three alternative potable water reuse schemes that integrate energy recovery from carbon via methane and nitrogen via either the coupled aerobic-anoxic nitrous decomposition operation process or partial nitritation/anammox. Compared to conventional potable water reuse schemes, the energy requirements of these schemes can be reduced by 7–29%, the overall energy balance by 38–80%.

Keywords: Energy-efficiency; energy recovery; potable water reuse; resource recovery; water reclamation

4.1.1 Introduction

Population growth and demographic shifts, climate change impacts, uneven distribution of freshwater resources, water scarcity, and emerging water quality issues are becoming more and more pressing worldwide (UN 2017; Mekonnen and Hoekstra 2016). Various options exist to provide sufficient water supplies locally. These options depend on their local availability and other site-specific factors and range from conventional surface water supplies (from rivers and lakes) or groundwater to brackish water or seawater desalination and imported water from other watersheds. Depending on the type of water source the required energy demands for treatment (no water conveyance and distribution included) typically range from 0.05–0.37 kWh/m³ for conventional water supply from surface water, 0.19–0.58 kWh/m³ for conventional water supply from groundwater, 0.26–2.6 kWh/m³ for brackish water desalination, and up 3.7–4.4 kWh/m³ for seawater desalination (Schimmoller and Kealy 2014, Arzbaecher et al. 2013, Cooley and Wilkinson 2012, Appelbaum 2002). Importing water from other regions is a unique solution for certain regions and depends mainly on transport distance and elevation difference (Arzbaecher et al. 2013). The State Water Project in California, USA requires about 0.79 kWh/m³ only for water conveyance, excluding energy requirements for water treatment (Cooley and Wilkinson 2012).

Many regions around the world have already established potable water reuse applications (Drewes and Khan 2011, NRC 2012) or are considering it as a future water supply option. The required energy demands of existing potable water reuse schemes employing advanced treatment processes vary in the range of 1.15–2.00 kWh/m³ (Cooley and Wilkinson 2012, NRC 2012, Tchobanoglous et al. 2011). However, these potable water reuse schemes represent a more cost-efficient option to augment local water supplies than brackish water or seawater desalination. Nevertheless, compared to conventional water supplies their specific energy demands are still significant.

Potable water reuse is being practiced for more than 50 years while providing a reliable and safe drinking water quality. Significant improvements in individual treatment processes and improved water quality monitoring have resulted in an increased confidence in potable water reuse practices worldwide (Schimmoller et al. 2015, Drewes and Khan 2015).

However, the widespread implementation of potable water reuse schemes is hindered by the lack of public confidence and regulatory uncertainty, but also high energy consumption and subsequent high operational and maintenance (O&M) costs. With increasingly more stringent water quality requirements, it is expected that additional treatment steps for the removal of emerging microbial and chemical contaminants will be required that will further increase the energy demand of water treatment systems in the future.

In the past, significant process optimizations have resulted in improved energy-efficiency of the overall treatment scheme (mainly by improved aeration systems for activated sludge processes; employment of energy recovery devices for high-pressure membranes, and by utilizing anaerobic treatment processes). However, the current design philosophy of water reclamation facilities is still focused on initial biological carbon and nutrient removal followed by advanced treatment with little attention to simultaneous energy recovery. A new paradigm has emerged that is shifting the perception of wastewater as a disposal issue to an opportunity to continuously recover resources including nutrients, energy, heat, and water (McCarty et al. 2011, Gao et al. 2014, Hering et al. 2013). Verstraete et al. (2009), Remy et al. (2014), and Batstone et al. (2015) have proposed physical and biological treatment technologies to integrate improved energy and nutrient recovery in water reuse concepts. Schaum et al. (2015) analyzed the water cycle (water flows and energy demands) of metropolitan areas.

It is worth making a note that untreated municipal wastewater contains potential, thermal and chemical bound energy. The potential energy (E_{pot}) of wastewater is proportional to its elevation and can be calculated with:

$$E_{pot}=m*g*h \text{ (J)} \quad (3)$$

where m is the water quantity/mass (kg), g the gravitational acceleration of the earth (9.81 m/s^2), and h the elevation (m). In theory, potential energy can be utilized in the sewer system or wastewater treatment plants (WWTPs) influent and/or effluent. In many settings, this energy is not considered a significant energy source due to gravity-driven conveyance systems and dependency on the local topography.

The amount of recoverable thermal energy (E_{therm}) can be calculated by:

$$E_{therm}=c_p*\Delta T_m*m \text{ (kJ)} \quad (4)$$

where c_p is the specific heat capacity of water (4.18 kJ/(kg*K)), ΔT_m the temperature gradient (K), and m the water quantity/mass (kg). Typical temperature ranges in wastewater streams vary from 10 to 20°C (Dürrenmatt and Wanner 2014). In colder areas heat recovery can be a viable option for heat generation (McCarty et al. 2011). However, the maximum recoverable thermal energy depends strongly on the point of heat recovery e.g., most feasible in sewer system and potential heat consumers. Additionally, studies already indicated the negative side-effect of heat recovery in the sewer system on downstream biological processes of WWTP, in particular nitrification efficiency (Wanner et al. 2005). Due to these drawbacks, the thermal energy will not be considered a viable on-site energy source in this study.

Beside thermal energy, electrical energy can be generated from the chemical energy potential. Thus, it is the preferable option in terms of subsequent energy utilization as it is more versatile and can be transported almost without losses. The chemical energy potential of waste streams is commonly assessed by the chemical oxygen demand (COD). The energy content per g COD can be determined using the overall enthalpy (ΔH of products – ΔH of reactants) expressed in the following reaction, assuming CH_4 as the organic substrate:

$$CH_4 + 2\ O_2 \rightarrow CO_2 + 2\ H_2O\ (1\ mol\ CH_4 = 64\ g\ COD) \quad (5)$$

with $\Delta H\ (CH_4)$ = -74.87 kJ/mol, $\Delta H\ (O_2)$ = 0 kJ/mol, $\Delta H\ (CO_2)$ = -393.50 kJ/mol, and $\Delta H\ (H_2O)$ = -285.83 kJ/mol. The overall enthalpy results in ΔH = -890.29 kJ/mol or -13.91 kJ/g COD, which equals 3.86 kWh/kg COD.

Municipal raw wastewater contains typically COD concentration in the range from 250–950 mg/L (Tchobanoglous et al. 2014, Remy et al. 2014). Thus, the considered energy potential of wastewater depends on the assumed COD load and usually varies in the range of 1.66–1.93 kWh/m³ (COD = 430–500 mg/L) (Scherson and Criddle 2014, McCarty et al. 2011) up to 3.09–3.86 kWh/m³ (COD = 800–1,000 mg/L) (Remy et al. 2014, Batstone et al. 2015). For comparison, the energy requirements of a CAS process with nitrification is in the range of 0.35–0.80 kWh/m³ (Appelbaum 2002, Fricke et al. 2015). Thus, it is noteworthy investigating treatment alternatives that can further reduce the energy demand to make potable water reuse not only a technically feasible, but also a more energy efficient solution and to integrate resource recovery as a cornerstone of integrated water management concepts.

The objective of this study were to (i) analyze systematically existing potable water reuse applications regarding operational characteristics and energy demands, (ii) to determine the theoretical energy potential of wastewater and identify opportunities for energy recovery, (iii) to define design requirements for potable water reuse schemes that integrate energy recovery, and (iv) to propose strategies for more energy efficient potable water reuse schemes. Hence, we designed three alternative potable water reuse schemes that integrate energy recovery from carbon and nitrogen. The alternative potable water reuse schemes are compared among each other and to a benchmark regarding (i) overall energy balance, (ii) greenhouse gas potential, (iii) effluent water quality, and (iv) process stability. Finally, necessary investigations which needs to be addresses in the future are proposed.

4.1.2 Existing potable water reuse schemes

Potable water reuse is being practiced worldwide using a broad variety of treatment process configurations. This variety is due to a wide range of possible treatment options and different regulatory requirements. The trend to meet more stringent water quality criteria over the last 20 years has resulted in incremental improvements of unit processes in potable water reuse treatment train design.

4.1.2.1 Treatment train (TT) characteristics

Existing potable water reuse schemes can be classified into membrane-based or non-membrane-based treatment trains, and treatment schemes with or without an environmental buffer (Figure 13). Membrane applications are a robust process for organic carbon removal and an effective barrier to pathogens and trace organic contaminants. High-pressure membrane applications (e.g. RO) have become the backbone of many potable water reuse schemes worldwide (Drewes and Khan 2011, Gerrity et al. 2013). The efficient removal of dissolved solids, pathogens, and trace organic compounds result in the fact that more than half of the existing potable water reuse schemes worldwide and 80% of the schemes in California, USA, utilize RO as a key treatment process (Drewes and Khan 2011, Drewes and Horstmeyer 2016). In particular, potable water reuse schemes located in coastal areas are favouring RO and in California and Australia are also combined with AOPs (e.g. UV-H_2O_2 (Gerrity et al. 2013). The Orange County Water District in Southern California established Water Factory 21 in 1976, which was later replaced by the Groundwater Replenishment System (GWRS) representing the largest potable water reuse project worldwide with a capacity of 348,400 m³/d (Drewes and Horstmeyer 2016). The GWRS treatment scheme consists of the core processes MF/RO/AOP (UV-H_2O_2). Due to the lack of brine disposal options, inland potable reuse projects are considering low-pressure membrane filtration (e.g. UF), GAC adsorption, chemical oxidation (e.g. O_3), and natural treatment systems (e.g., SAT, RBF, wetland treatment) (Drewes and Horstmeyer 2016). Managed aquifer recharge options are only applicable if the geological conditions are suitable. Advanced processes like GAC or RO (with the exception of suitable brine disposal options) can be employed practically everywhere. Non-membrane based reuse schemes consider activated carbon as a robust barrier for organic contaminants. If GAC is applied, usually RO is not considered. Many locations utilize GAC for the removal of bulk and trace organic compounds, other treatment schemes consider BAC filtration in combination with O_3 (Gerrity et al. 2013, Drewes and Khan 2015).

Certain technologies have been employed over the past few decades (e.g. O_3), while other technologies have become more and more economically feasible in the recent past (e.g., RO, UV-AOP) (Gerrity et al. 2013). As a result, a number of ozone-based alternatives (e.g. ozone/BAC) are increasing in popularity throughout the world (Gerrity et al. 2013). It is expected that the attention to a broader spectrum of contaminants will increase the diversity and/or the treatment complexity of treatment units of potable water reuse applications. Recently, more attention has been given to schemes that facilitate DPR without the use of an environmental buffer (Drewes and Khan 2015, Lahnsteiner et al. 2017).

Several decades of operational experiences with potable water reuse applications demonstrated the reliability and robustness of existing treatment schemes.

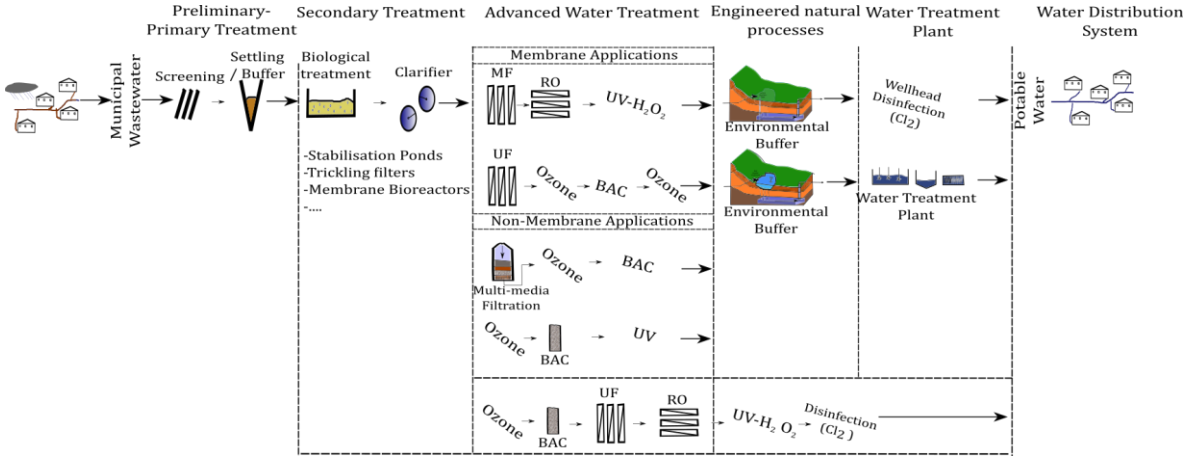

Figure 13. Design of selected potable water reuse schemes worldwide. MF=Microfiltration, RO=Reverse osmosis, UV=Ultraviolet light, H2O2=Hydrogen peroxide, Cl2=Chlorine, UF=Ultrafiltration, BAC=Biologically-active carbon.

4.1.2.2 Energy demand, greenhouse gases (GHG) and carbon footprint

Augmentation, distribution and (waste)water treatment require energy at all stages. The reported energy demands within this study are only for the (waste)water treatment. Water collection, transport and distribution are not included in the reported energy demands. These factors depend mainly on the distance and net elevation (Cooley and Wilkinson 2012). Depending on the specific treatment configuration, degree of treatment (wastewater characteristic, effluent criteria), regional and site-specific factors, and the facility's capacity, existing potable water reuse schemes require between 1.15–2.0 kWh/m³, while the energy demand of CAS (with nitrification) can vary between 0.35–0.80 kWh/m³ (Appelbaum 2002, Fricke et al. 2015), and the AWT can vary between 0.85–1.2 kWh/m³ (Cooley and Wilkinson 2012, NRC 2012, Tchobanoglous et al. 2011). The GWRS treatment scheme represents a characteristic membrane-based treatment configuration (including MF/RO/UV-H_2O_2) and is considered as a benchmark for comparison of alternative potable water reuse schemes as the largest potable water reuse project worldwide. The average energy demand of this scheme is 1.18 kWh/m³ (Figure 14). With 0.70 kWh/m³, the use of the integrated membrane system (MF/RO) consumes more than 90% of the AWT energy demand (Holloway et al. 2016). While these membrane processes provide very efficient treatment barriers in potable water reuse, they are characterized by high energy requirements (Schimmoller and Kealy 2014). As a result, the entire AWT process train is representing 181% to the CAS energy demand. The energy demand for AWT can vary between 0.85–1.20 kWh/m³ (Schimmoller and Kealy 2014, Cooley and Wilkinson 2012).

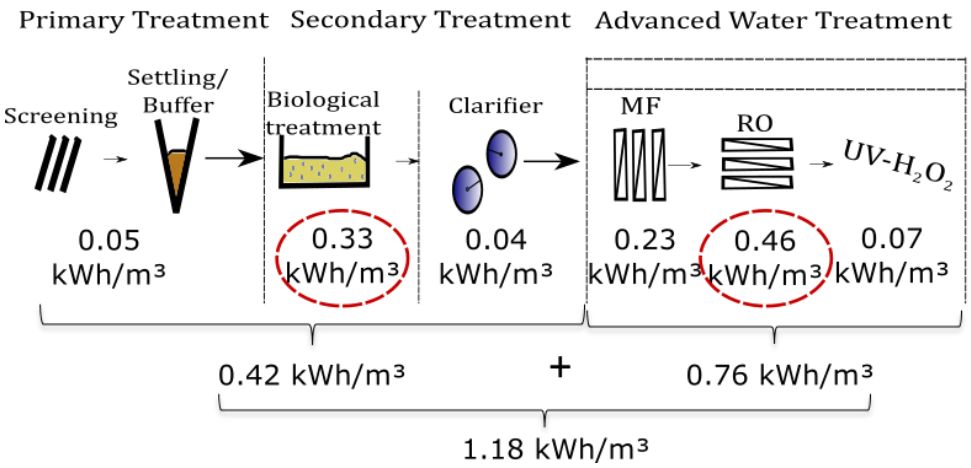

Figure 14. Energy demand of the characteristic benchmark Groundwater Replenishment System (GWRS) example. Main energy sinks of the primary- secondary treatment and AWT are marked with red circles. MF=Microfiltration, RO=Reverse osmosis, UV=Ultraviolet light, H2O2=Hydrogen peroxide, AWT=Advanced water treatment (Holloway et al. 2016, Fricke et al. 2015, Arzbaecher et al. 2013).

Beside the direct energy demand of single treatment processes and total treatment scheme configuration, the generation of greenhouse gases (GHG) and the resulting overall carbon footprint needs to be considered. The main contributor to GHG emissions is undisputable the energy demand (Cornejo et al. 2014, Schimmoller and Kealy 2014). The carbon footprint for CAS treatment with biological nutrient removal (BNR) is ranging from 0.13–0.69 kg CO_2-equivalent (CO_2e)/m³ (Lazarova et al. 2012, Cornejo et al. 2014, Remy et al. 2014). Membrane-based potable water reuse schemes are in the range from 0.60–2.40 kg CO_2e/m³ (Cornejo et al. 2014, Vince et al. 2008, Stokes and Horvath 2009, Kalbar et al. 2013, Niero et al. 2014). Holloway et al. (2016) analyzed the GWRS benchmark showing that the GHG emissions range between 1.15–1.50 CO_2e kg/m³, depending on the RO concentrate disposal pressure (ocean disposal or deep well injection with 69 bar). The direct and accurate comparison of different GHGs calculations is challenging due to the variability in location, technologies, life-cycle stages and considered parameters (Cornejo et al. 2014). Another approach to consider the full financial, environmental, and social elements of a potable water reuse project is the triple bottom line (TBL) framework (Schimmoller and Kealy 2014, Schimmoller et al. 2015).

Additionally, CAS systems have been recognized for direct emissions of GHGs. Beside CO_2 and CH_4, N_2O has come to the forefront in the last decade (Kampschreur et al. 2008, 2009, Daelman et al. 2013, Desloover et al. 2011). With a CO_2e of 300 (Ravishankara et al. 2009), the contribution of N_2O to the operational carbon footprint of CAS systems is estimated to be on average 0.40 kg CO_2e/m³ (minimum 0.02 kg CO_2e/m³, maximum 1.18 kg CO_2e/m³) (assumption 0.081 kg N_2O/(population-equivalent (PE)*a) (Daelman et al. 2013) and potentially increases the total carbon footprint in the range of 0.15 to 1.87 kg CO_2e/m³.

Presently, considerable additional nitrogen loads are released to the system by ammonification of organic nitrogen during anaerobic digestion (AD). Applying main-stream treatment of reject

water imposes additional ammonia loads to the nitrification/denitrification (N/DN) process elevating aeration energy demand for nitrification and COD demand for denitrification. Eventually, a lack of organic reducing power by intensive use of AD potentially leads to anoxic nitrous denitritation (Weißbach et al. 2018) and ultimately to higher N_2O emissions than during conventional treatment without AD.

To mitigate this drawback on main-stream nitrogen removal, the partial nitritation/anammox (PN/A) process was developed, because it facilitates complete autotrophic nitrogen removal (and thus higher process efficiency). However, considerable N_2O emissions need to be accounted for in GHGs calculations. Kampschreur et al. (2008) and Desloover et al. (2012) quantified conversion of 2.3–3.8% of the reactor nitrogen load to N_2O. The unintended production of N_2O and associated CO_2e emissions possibly compromises the benefit of higher process efficiency.

4.1.3 Municipal wastewater as energy and nutrient source

Municipal raw wastewater contains a considerable chemical energy potential (see chapter 4.1.1). Thus, the energy and nutrient content of municipal raw wastewater was characterized through weekly measurements during a period of one year at the WWTP Garching, Germany. Wastewater influent was collected after a 4 mm drum screen. Average values were determined as follows: flowrate 4,644 ±724 m³/d, temperature 15.3 ±2.4°C, pH value 8.24 ±0.06, and electrical conductivity (EC) 1,438 ±241 µS). The theoretical energy potential has been determined to vary between 1.90 and 3.14 kWh/m³ (with a mean of 2.52 kWh/m³) (Figure 15 and Table SM1 in supplementary material, Appendix C).

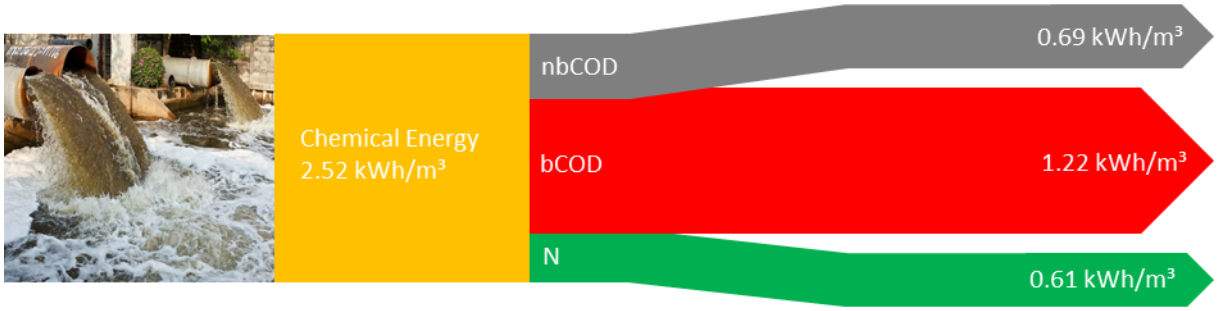

Figure 15. Chemical bound energy potential of raw municipal wastewater (COD=496 mg/L, TN=81 mg/L, nbCOD=179 mg/L, bCOD=317 mg/L). Based on complete COD oxidation and 3.86 kWh/kg COD and on the (higher) heating value for ammonia nitrogen. bCOD=biodegradable COD, iCOD=inorganic (non-biodegradable) COD.

4.1.4 Energy recovery platforms (from carbon and nitrogen)

Raw wastewater represents a high theoretical energy potential (2.52 kWh/m³). Common options of transforming chemical energy into electrical usage via energy recovery platforms are CHP units, for instance combustion of biogas harvested from anaerobic treatment.

Anaerobic main-stream treatment results in approximately twice the methane yield compared to main-stream CAS (100 L/m³ via main-stream anaerobic digestion compared to 50 L/m³ via AD of waste activated sludge) (McCarty et al. 2011). Additionally, less waste sludge is produced in anaerobic treatment compared to aerobic treatment (1.2 L/m³ compared to 2.6 L/m³) (McCarty et al. 2011). Considering accumulated losses of e.g., waste heat, friction and kinetics during energy conversion, the total yield of electrical energy is approximately 6–11% (0.15–0.28 kWh/m³) (Lazarova et al. 2012, Remy et al. 2016). This yield represents approximately 67% of the required energy demand of a CAS system and only 24% of CAS system including AWT processes. Puchongkawarin et al. (2015) estimate that approximately only 25–50% of the CAS system energy demand and only 11–22% of CAS system including downstream AWT can be recovered. Hence, the limitations of presently existing schemes are evident in terms of achieving neutral net energy operation.

Temperature is a key factor for efficient AD. Anaerobic processes are most effective in mesophilic (28–40°C) and thermophilic (50–57°C) conditions. Nevertheless, full-stream anaerobic treatment plants operate also commonly under psychrophilic conditions (>20°C) (Petropoulos et al. 2017, Martinez-Sosa et al. 2011) and with high strength wastewater. Inoculated reactors with cold-adapted biomass from low temperatures regions over evolutionary time-scales (e.g. from the high arctic or alpine lakes) showed promising results to establish anaerobic treatment also for low temperature ranges (10–30°C) and low-strength wastewater (Petropoulos et al. 2017, Tauseef et al. 2013). Other challenges associated with anaerobic treatment are (i) corrosion by sulfuric acid, (ii) nitrogen removal, and (iii) capturing residual methane in effluents (25 times CO_2e). Particularly low temperatures increase the solubility of methane and as a consequence result in higher GHG emissions (Tauseef et al. 2013, Crone et al. 2016). Up to 6.9% of dissolved methane losses are possible (Crone et al. 2016).

For nitrogen removal, N/DN is still the most established and traditional process in CAS (Lackner et al. 2014). Nitrification describes the two-step process where ammonia (NH_4^+) is oxidized to nitrite (NO_2^-) and nitrite is oxidized to nitrate (NO_3^-). Stoichiometrically expressed as (Schmidt et al. 2003):

$$NH_4^+ + 1.5\ O_2 \rightarrow NO_2^- + 2H^+ + H_2O \quad (6)$$

$$NO_2^- \rightarrow 0.5\ O_2 \rightarrow NO_3^- \quad (7)$$

$$\text{Total reaction: } NH_4^+ + 2\ O_2 \rightarrow NO_3^- + 2\ H^+ + H_2O \quad (8)$$

Considering the energy demand, 4.67 kg O_2/kg NH_4-N are necessary for nitrification resulting in an aeration energy demand of 2.38 kWh/kg NH_4-N (Sobieszuk and Szewczyk 2006). To

mitigate the significant aeration energy demand for nitrification, technologies and strategies have been applied to increase oxygen mass transfer into the mixed liquor and prevent excess aeration. However, similar to the PN/A process, oxygen limitation can trigger aerobic nitrous denitritation resulting in increased N_2O emissions. Beside the energy demand of nitrification, 7.60 kg COD/(kg N) are necessary for complete denitrification (Sobieszuk and Szewczyk 2006). Hence, a considerable amount of the energy potential of COD is lost by applying conventional nitrogen removal. Enabling more efficient nitrogen removal, novel processes have been proposed focusing on short-cuts in the microbial metabolism or completely alternative microbial pathways. These processes e.g., N/DN, PN/A and the CANDO process, potentially facilitate more efficient nitrogen removal, because they combine both lower oxygen and COD demand (Table 7). Considering oxygen demand, PN/A is theoretically most efficient, because only 37.5% oxygen are required compared to N/DN (50% of NH_4^+ is oxidized to NO_2^- with 25% less oxygen demand). Furthermore, the process is completely autotrophic saving theoretically 7.60 kg COD/kg N for additional 10.9 kWh/kg N removed with PN/A (64% biodegradable COD (bCOD) and 2.25 kWh/kg COD based on data from the WWTP Garching, see Table SM2 in supplementary material, Appendix C).

In contrast, the CANDO process (Scherson et al. 2014) enables energy recovery from nitrogen. It is a two-stage biological treatment train for intentional N_2O production, harvesting and subsequent energetic utilization as co-oxidant during biogas combustion. The oxygen demand represents 75% of the N/DN oxygen demand. Weißbach et al. (2018) could demonstrate a conversion of 63% of NH_4-N to N_2O-N under real feed-stream conditions treating digester effluent. The partially heterotrophic process was operated at a COD/N ratio of 4.0 kg COD/kg N (Weißbach et al. 2018). The degradability of 64% resulted in a considerably lower bCOD demand of 2.60 kg COD/kg N compared to CAS (7.60 kg COD/kg N) (Table 7). As a result, 5.0 kg COD/kg N removed are available for biogas production (7.20 kWh/kg N, based on 64% bCOD and 2.25 kWh/kg COD) and 0.53 kWh/kg N (0.083 kg N/m³, 82.3 kJ/mol N_2O, conversion efficiency NH_4-N to N_2O-N 63%, 23.2 mol N_2O/kg N), resulting in additional 7.73 kWh/kg N that can potentially be generated.

Table 7. Comparison of N/DN, PN/A and CANDO processes. N/DN=Nitrification/Denitrification, PN/A=Partial nitritation/anammox, CANDO=Coupled aerobic-anoxic nitrous decomposition operation.

Process	O_2 demand (kg O_2/kg N)	COD demand (kg COD/kg N)	Energy demand (kWh/kg N)	Energy potential from COD (kWh/kg N)*	Energy potential from N (kWh/kg N)	Overall balance (kWh/kg N)
CAS N/DN	4.67	7.60	2.38	-	-	2.38
PN/A	1.75	-	0.90	10.9	-	-10.0
CANDO	3.50	2.60	1.80	7.20	0.53	-5.93

4.1.5 Alternative potable water reuse schemes

This chapter provides the design requirements that integrate energy recovery and the explanation and comparison of the alternative treatment trains (TTs) among each other and with the defined benchmark for potable water reuse schemes. Thereby, the overall energy balance, the greenhouse gas potential, the effluent water quality, and the process stability are considered.

4.1.5.1 Design requirements

The design of alternative potable water reuse schemes requires a thorough understanding of (i) source water characteristics, (ii) regulatory and water quality requirements, (iii) maintaining proper performance of treatment processes and their combinations, and (iv) storage and blending requirements. Maintaining system reliability (by establishing redundancy, robustness, and resilience) is a very important design element for potable water reuse schemes and is defined as the probability of providing adequate performance for defined time periods while meeting predefined water quality conditions (Drewes and Horstmeyer 2016). System reliability can be achieved by various combinations of treatment processes considering expected log-removal efficiencies of single unit operations for pathogenic microorganisms as well as chemicals of concern. However, an overtreating of the final water quality should be avoided (Schimmoller and Kealy 2014).

So far, the concept of process optimization to increase energy-efficiency in potable water reuse schemes has primarily targeted savings of individual unit operations and processes. However, integrating energy recovery platforms into potable water reuse schemes offer opportunities for a significant savings potential but might also result in a reinvention of the design of current potable water reuse schemes. These novel approaches embrace the concept of lowering the energy requirements while increasing energy recovery. The substitution of energy intensive CAS treatment by coupling biological, chemical and physical treatment processes could reduce the overall energy demand while providing more organic material present in primary effluent for intensified biogas production and more energy efficient nitrogen removal via concepts like CANDO or PN/A.

4.1.5.2 Alternative treatment trains (TT)

Three alternative TTs for potable reuse schemes are proposed (Figure 16). TT I consists of an improved pretreatment with coagulation, flocculation, and microsieving (100 µm) to increase carbon removal during primary sludge removal. The primary sludge is diverted to an anaerobic digester to convert C to CH_4. The primary effluent is subject to downstream physical treatment including UF prior to subsequent RO treatment as an additional membrane separation step. The RO also severs as a concentration step for residual dissolved organic constituents and

ammonia. The UF retentate and RO concentrate is diverted to the anaerobic digester to utilize as much as possible from the dissolved organic C for CH_4 production. The concentrated ammonia is transferred after the anaerobic treatment (via the digester centrate) to the CANDO process as a second energy recovery platform. The CANDO process converts the ammonia in a double-stage biological treatment train to N_2O. Methane and N_2O are subsequent energetically utilized in a CHP. The RO permeate is further treated by a biological aerated carbon filter (BAF) to remove remaining low molecular organic carbon and nutrients (<100 Dalton (Da)). Subsequent water treatment is applied as pathogen barriers and for any residual trace organic chemicals in two chemical processes via an advanced oxidation process (UV-H_2O_2) and final chlorine disinfection.

Treatment trains II and III (TT II and III) are based on anaerobic treatment with intensified biogas production via an anaerobic membrane bioreactor (AnMBR). Raw municipal wastewater is directly fed into the AnMBR after a fine screen (4 mm) to remove coarse particulate matter. The AnMBR represents the first energy recovery platform for CH_4 production from C. The MBR filtrate is diverted to downstream RO treatment followed by BAF and UV/AOP and final disinfection like TT I. In TT II, the RO concentrate (elevated in ammonia) is utilized in the CANDO process (intentional N_2O production for subsequent co-combustion with CH_4. In TT III, the RO concentrate is subject to PN/A treatment to convert ammonia to N_2 with final release into the atmosphere. CANDO and PN/A were chosen for nitrogen removal due to the better overall energetic balance compared to conventional N/DN (N/DN: 2.38 kWh/kg N; CANDO: -5.93 kWh/kg N; PN/A: -10.0 kWh/kg N, see Table 7). The comparison of TT II and TT III will provide an assessment whether the approximately 2 times better energetic balance of PN/A compared to the CANDO process influence the overall energetic balance.

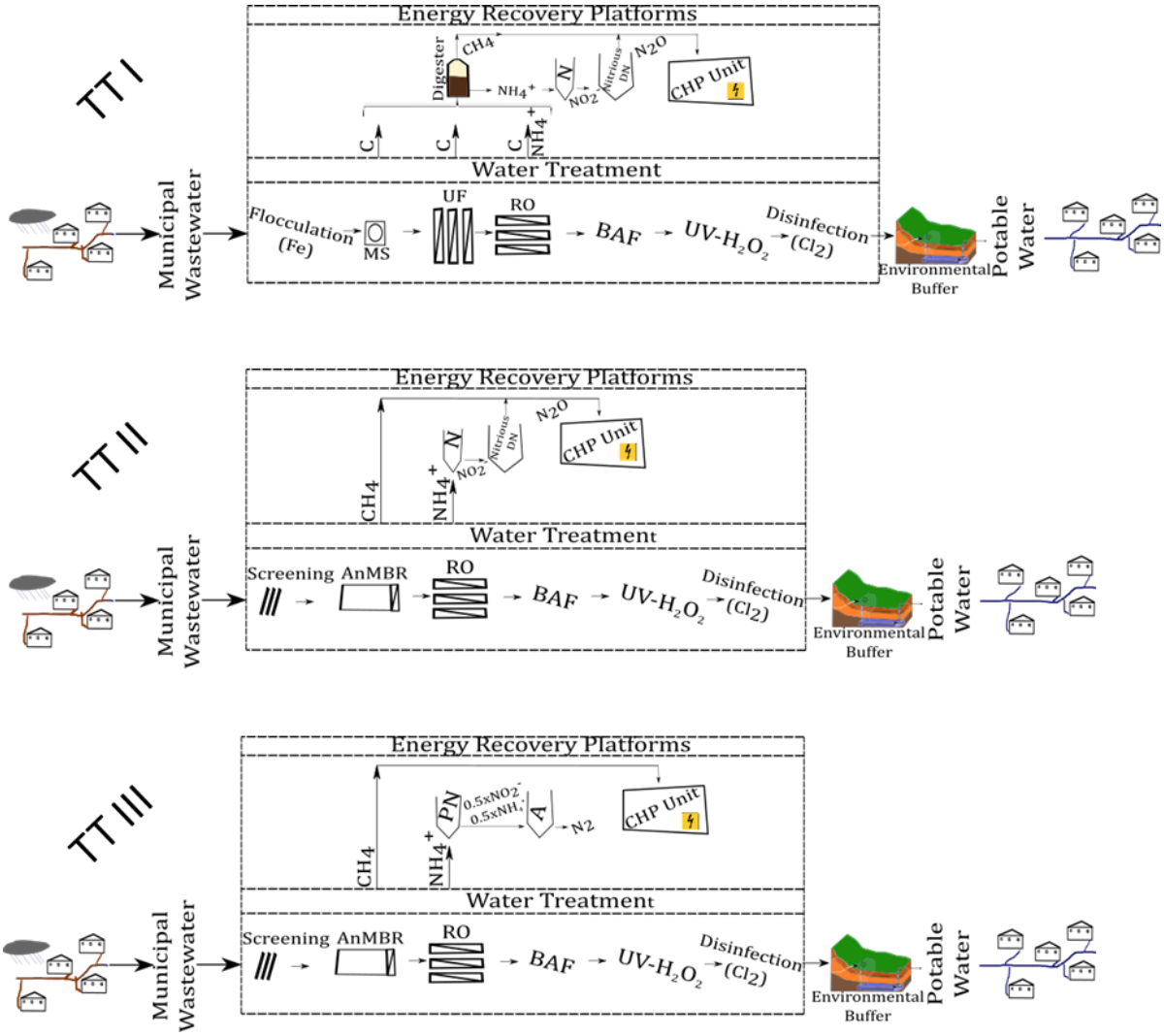

Figure 16. Alternative potable water reuse schemes (TT I, II and III). TT=Treatment train, N=Nitrification, DN=Denitrification, C=Carbon, CHP=Combined heat and power plant, Fe=Ferrous iron, MS=Microsieve, UF=Ultrafiltration, RO=Reverse osmosis, BAF=Biological aerated carbon filtration, UV-H2O2=Ultraviolet light-Hydrogen peroxide, Cl2=Chlorine, AnMBR=Anaerobic membrane bioreactor, PN=Partial nitritation, A=Anammox.

Previous studies have demonstrated the viability of microsieving at pilot-scale to remove particulate matter (Remy et al. 2014). Combined with coagulation/flocculation, this solids separation process removed more than 95% of suspended solids. Moreover, the microsieve removed 70–85% of organic matter (COD). Nearly 95% of particulate COD (pCOD) and 20% of the dissolved COD (dCOD) from raw wastewater was removed (Remy et al. 2014). This increased primary sludge removal can result in a higher CH_4 yield and with up to 40% a higher energy recovery compared to CAS treatment (Remy et al. 2014). Additionally, the organic load on the subsequent purification steps is reduced (95% total suspended solids (TSS) removal). However, downstream UF treatment of the microsieved pretreated raw wastewater as proposed for TT I is still challenging due to the remaining high organic carbon load and

associated high fouling propensity of the UF membrane. Advanced fouling mitigation strategies are required to maintain a sustainable UF operation. Kim et al. (2011) analyzed a new fouling mitigation strategy by using fluidized GAC in a two-stage anaerobic system with the second stage operating as AnMBR. The system was operated continuously over 120 days at laboratory scale at 35°C with synthetic wastewater (average COD = 513 mg/L) while achieving a permeate flux of 10 L/m² hour (LMH). The total energy demand for both stages was 0.06 kWh/m³. The approach was also successfully established at pilot scale by Shin et al. (2014).

The energetic comparison of the three proposed alternative treatment trains (TTs I–III) against the benchmark potable water reuse scheme (CAS+AWT) reveals that the energy requirements can be decreased by 7% (TT I) and 29% (TT II and III), respectively (Figure 17A, detailed data see Table SM3 in supplementary material, Appendix C). TT II and III consists of an AnMBR which lowers the overall energy requirements for wastewater treatment to 0.84 kWh/m³. The calculation of the overall net energy balance even results in higher energy efficiencies for TTs I–III (Figure 17A). The chosen nitrogen removal strategy is the main contributor to achieving an overall more energy efficient potable water reuse schemes. PN/A and the CANDO process can increase the energy production via additional CH_4 production by 0.22 and 0.34 kWh/m³ (64% bCOD, 2.28 kWh/kg COD and η_{el}=38%), respectively. Additional N_2O utilization via the CANDO process (0.04 kWh/m³) results in a more energy efficient balance for TT I and II. TT III with PN/A has the best overall energy balance with 0.22 kWh/m³. However, process stability and considerable N_2O emissions are of concern, especially aiming for complex and varying wastewater compositions or full-stream applications (Laureni et al. 2016). Kampschreur et al. (2008) and Desloover et al. (2012) quantified N_2O emissions of a full-scale PN/A process with 2.3–3.8% of the reactor nitrogen load. While the CANDO process captures all N_2O emissions and converts it to energy, the additional GHG from a PN/A process due to N_2O emissions to the atmosphere account for 0.92 kg CO_2e/m³ (0.081 kg/m³ N, N_2O CO_2e=300) (Figure 17B). Considering both energy recovery and GHG emissions, TT II is the most sustainable potable water reuse scheme with a net energy balance of 0.32 kWh/m³ and 0.45 kg CO_2e/kWh based on the assumptions of this analysis. However, additional research is needed to demonstrate feasibility, reliability and water quality of the proposed alternative water treatment as well as the CANDO implementation in a main-stream application.

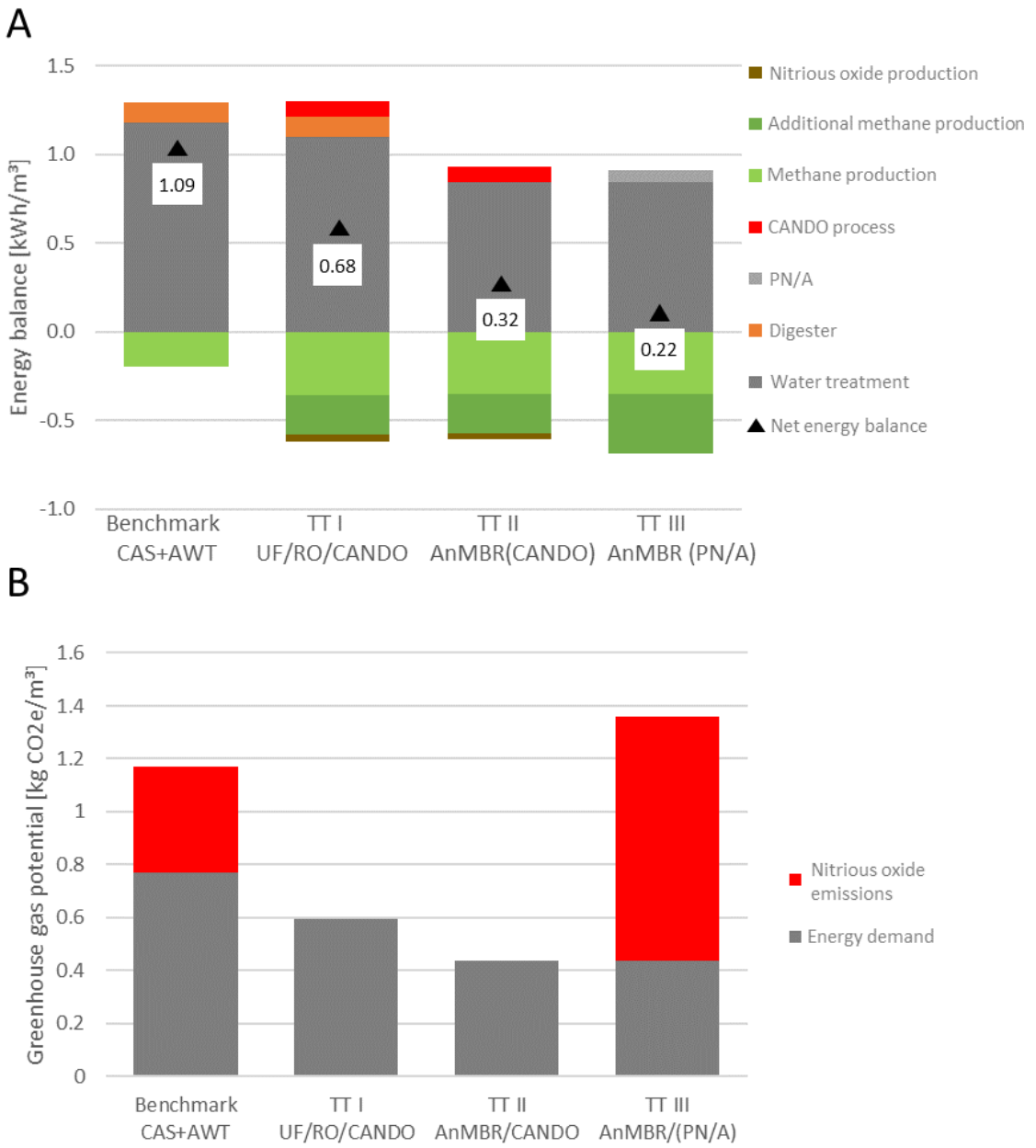

Figure 17 (A). Energy balance of benchmark and treatment trains (TT) I, II and III; **(B).** Nitrous oxide emissions and energy demand as greenhouse gas potential of benchmark and treatment trains (TT) I, II, III based on 0.40–0.92 kg CO_2e/m^3 for N_2O emissions and an energy demand equivalent of 0.54 kg CO_2e/kWh. CAS=Conventional activated sludge, AWT=Advanced water treatment, UF=Ultrafiltration, RO=Reverse osmosis, AnMBR=Anaerobic membrane bioreactor, CANDO= Coupled aerobic-anoxic nitrous decomposition operation, PN/A=Partial nitritation/Anammox.

The main requirement of all potable water reuse schemes is the reliable and continuous generation of high-quality water in compliance with drinking water regulations. A wide range of naturally occurring and anthropogenic trace organic and inorganic contaminants, residual nutrients, total dissolved solids, residual heavy metals, and pathogens needs to be properly

removed by individual treatment units. Each alternative potable water reuse scheme fulfills the minimum removal requirements for microbial contaminants (9-log removal for total coliform bacteria, 12-log removal for enteric viruses and 10-log removal for protozoa (*Cryptosporidium*)) for potable reuse projects in California, USA (SWRCB 2013, Trussell et al. 2017) (Table 8).

Table 8. Log-removals efficiencies of treatment trains (TT) I, II and III compared to the benchmark (CAS+AWT). CAS=Conventional activated sludge, AWT=Advanced water treatment.

	Benchmark*	**TT I****	**TT II and III****
Enteric virus log-removal	14.0	18.0	18.0
Cryptosporidium	12.0	12.5	12.5
Total coliform bacteria log-removal	18.5	21.0	21.0

Log-removal efficiencies of treatment steps according to the Treatment Train Toolbox from Trussell et al. (2017). *Assuming CAS with SRT of 7 days, UV dose of 300 mJ/cm², Cl_2 of 450 mg-min/L and a contact time of 90 min with an initial Cl_2 demand of 0 mg/L. **Assuming UV dose of 300 mJ/cm², Cl_2 of 450 mg-min/L and a contact time of 90 min with an initial Cl_2 demand of 0.0 mg/L and additional log-removal for UF treatment. TT=Treatment train, CAS=Conventional activated sludge, SRT=Solids retention time, UF=Ultrafiltration.

4.1.6 Conclusions

Environmental sustainability is one of the most critical challenges in contemporary water and wastewater management. The aim of technologies employed to treat water and wastewater should not only be to remove relevant contaminants, but also to gain high energy-efficiency by recovering useful resources from wastewater. The theoretical energy content in raw wastewater is 2.52 kWh/m³. Conventional potable water reuse schemes (CAS+AWT) currently require an average of 1.18 kWh/m³. Integrating anaerobic treatment (e.g. AnMBR) and the CANDO process offers the opportunity to establish more energy efficient potable water reuse schemes with significant lower GHG emissions. However, more detailed investigations of these alternative treatment schemes are needed including a detailed technical feasibility study. In particular, the feasibility of the proposed physical treatment processes (microsieving, UF and RO) coupled with subsequent biological (BAF) and disinfection processes require detailed research to overcome operational issues, proof long-term operation and guarantee final water quality for drinking water purposes.

4.1.7 Acknowledgements

This work was supported by the German Science Foundation (DFG) and the Technical University of Munich (TUM) in the framework of the Open Access Publishing Program.

5 State-of-the-art II (Operational performance)

Membrane treatment is a key element of advanced water treatment processes. The fundamentals of membrane filtration are provided in chapter 5.1. However, full-scale membrane applications are mainly hindered by membrane fouling. This phenomenon is the key focus of the second part of this thesis. Thus, chapter 5.2 provides background information about membrane fouling, its mechanisms and foulants, and potential membrane fouling mitigation strategies.

5.1 Membrane filtration

Membrane filtration is a pressure-driven process in which a membrane is used as a physical barrier to selectively separate compounds in a defined matrix, e.g. water (Singh 2015). The membranes are classified based on their characteristics according to pore size, feed pressure and membrane rejection capacity (Table 9). Thus, four pressure-driven membrane processes are distinguished: (i) MF, (ii) UF, (iii) NF, and (iv) RO. The pore size can be defined either in terms of the effective equivalent pore diameter (e.g. µm) or the equivalent mass of the smallest molecule in Dalton (Da) the membrane is capable of rejecting (Judd and Judd 2011). A basic classification can be made between low-pressure membranes (MF/UF) and high-pressure membranes (NF/RO). Further classification is based on their separation principle. The rejection in MF and UF is based on size exclusion, meaning that particles larger than the membrane pores are rejected by the membrane. In NF and RO processes, separation is based on both, size exclusion and diffusion through the membrane. In fact, diffusion of solutes e.g. salts or low molecular weight compounds (LMWC) is lower compared to water, resulting in a rejection of those compounds by NF and RO membranes.

Table 9. Classification of membrane processes (adapted from Peinemann and Nunes (2010), Singh (2015)).

Process	Pore size range	Feed pressure (bar)	Purpose and application
Microfiltration (MF)	0.05-10 µm	1-2 bar	Removal of suspended and colloidal substances and microorganisms
Ultrafiltration (UF)	0.001-0.05 µm	2-5 bar	Removal of suspended and colloidal substances and microorganisms
Nanofiltration (NF)	< 2.0 nm	5-15 bar	Removal of hardness, sulfate, color, natural organic matter (NOM) and organic micropollutants

Reverse Osmosis (RO)	~0.6 nm, non-porous	15-100 bar	Water reclamation, brackish or seawater desalination

The majority of membranes utilized in potable water reuse schemes is manufactured from various classes of polymers as there are cellulose acetate (CA), polypropylene (PP), polyvinylidene fluoride (PVDF), polysulfone (PSU), polyether sulfone (PESU) and polyamide (PA) (Singh 2015). The polymers can be formed into membrane materials with sprecific physical properties. This includes properties such as hydrophobicity and hydrophilicity as well as surface charge. Hydrophobicity is the tendency of a membrane to repel water, whereas hydrophilicity describes the tendency to attract water. Those properties influence the membrane performance and on the other hand their interaction with the feed matrix and as a result of that, their susceptibility towards membrane fouling. The general consensus is that hydrophobic membranes are more prone towards membrane fouling by natural organic matter (NOM) (Hong and Elimelech 1997, Fan et al. 2001).

To utilize the membranes in a technical application, the membranes need to be configurated in specific membrane configuration. The configuration of the membrane, i.e., its geometry and the way it is oriented to the flow of water, is crucial in determing the overall process performance (Judd and Judd 2011). There are five principal configurations of membrane applications: (i) plate and frame / flat-sheet (FS), (ii) hollow fibre (HF), (iii) tubular (e.g. multi-tubular or capillary), (iv) pleated filter cartridge, and (v) spiral-wound (SW).

The membrane process operation relates to the influence of the following parameters on the overall permeate flux: (i) the membrane resistance, (ii) the operational driving force, (iii) the hydrodynamic conditions, and (iv) the fouling of the membrane. Thereby, it can be distinguished between dead-end and cross-flow operation. In dead-end systems the water flows perpendicular to the membrane, and bulk (organic) matter is flushed along with the effluent or with a small side stream of retentate (concentrate). In contrary, in cross-flow systems, the feed water flows parallel to the membrane surface, which reduces the risk of membrane fouling due to the rinsing effects and shear forces of the cross flow.

5.2 Membrane fouling

Membrane fouling describes the coverage of the membrane pores and/or surface by chemical and biological deposits with a subsequent loss in permeability (Drews 2010) depending on a combination of physical, chemical and biological processes (Le-Clech et al. 2006, Tchobanoglous et al. 2014). Thus, it is not an individual process, but rather a combination of specific mechanisms and types. Fouling mechansims can be categorized into three main types: (i) (complete) pore

blocking, (ii), (intermediate/standard) pore constriction, and (iii) cake layer (CL) formation (Figure 18).

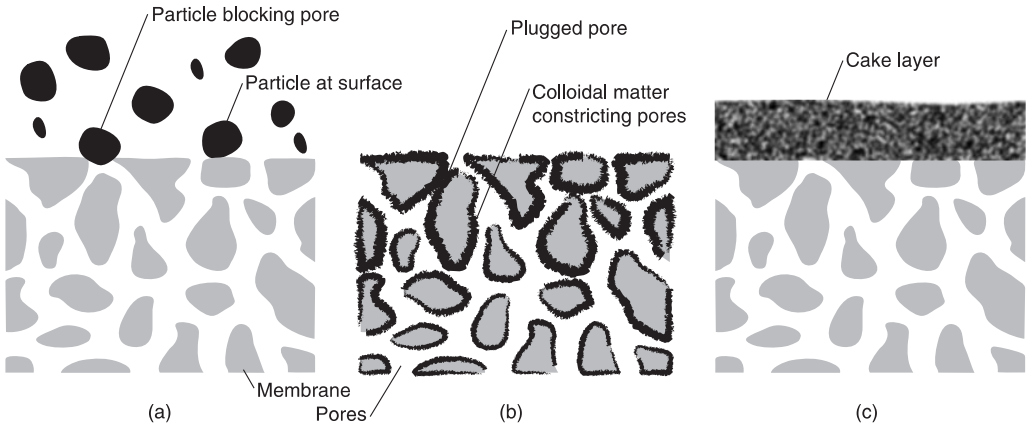

Figure 18. Types of membrane fouling **(a)** (complete) pore blocking, **(b)** (intermediate/standard) pore constriction, **(c)** cake layer (CL) formation (Crittenden 2012).

In the following, the distinct mechanisms are descripted. It is noteworthy that in most of the relevant cases and especially in environments with complex feed matrices (i.e. municipal wastewater) several types of fouling can be encountered in a membrane process referred to as combined fouling.

Concentration polarization (CP):

CP is considered as build-up of solutes, which are retained by the membrane nearby its surface. Consequently, this results in a higher concentration of the solutes at the membrane surface than in the bulk solution, so that it is critical for both fouling and retention of the membrane. CP itself cannot be considered as stand-alone fouling mechanism, but it is often the first step towards fouling. The concentration polarization phenomenon forms rapidly after start-up, in particular at later stages of a multi-stage membrane system.

Osmotic pressure (OP):

OP is the pressure which forms by water moving across the membrane surface due to osmosis (motion of water from an area of low solute concentration to an area of higher solute concentration). As the CP at the membrane surface occurs also the OP increases leading to a reduced transmembrane pressure (TMP) and membrane flux. Like CP, OP can also not be considered as an individual fouling mechanism, but it may also contribute to fouling.

Adsorption:

Regarding to membrane filtration, adsorption can be defined as the adhesion of particulate or colloidal matter and/or dissolved organic matter (DOM) on the membrane surface.

Pore blogging:

Pore blogging occurs when either particles of similar size to the membrane pores penetrate into the pores and block them completely (complete pore blogging) or adhere at the wall of the membrane pores and block them partially (internal pore blogging). It is mostly determined by the size of the organic molecules and the pore size of the membrane. As a result, particles smaller than the membrane pores most likely tend to penetrate into the membrane pores.

Cake layer formation:

Cake layers are formed when particles bigger than the pores remain at the membrane surface. This general phenomenon also applies for the formation of gel layers, so that cake layers might be hard to differentiate from gel layers.

Gel layer formation:

Gel layer formation can be considered as the precipitation of organic matter (OM) on the membrane surface. When the concentration of OM nearby the membrane surface exceeds their solubility due to CP, gel layer formation usually occurs. Precipitation of OM is favoured in the presence of salts (flocculation of OM) or at neutral charge conditions. Gel layer formation is linked to organic membrane fouling, but does not necessarily result in an irreversible flux decline.

Membrane fouling can be also classified in reversible and irreversible fouling (Figure 19). At constant flux operation, the increase of the TMP during filtration can be used as indicator for fouling.

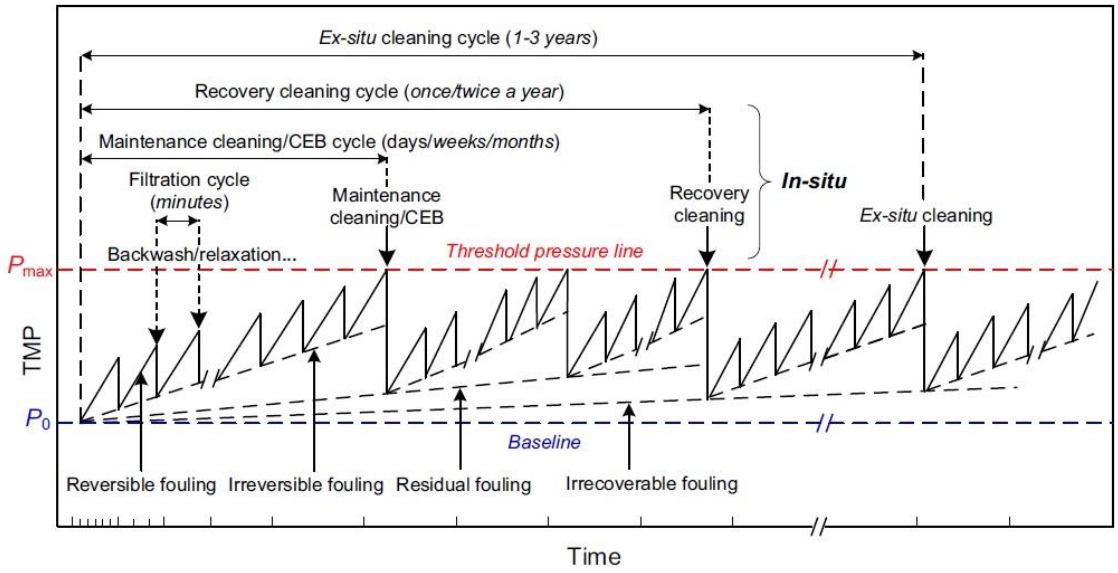

Figure 19. Fouling rates during long-term membrane operation (Wang et al. 2014).

5.2.1 Factors affecting membrane fouling

The fouling rate of a membrane depends on (i) characteristics of the feed solution, (ii) characteristics and properties of the membrane, and (iii) operational / hydrodynamic conditions.

Characteristic of feed solution:

The characteristics of the feed matrix can strongly contribute towards membrane fouling. Their composition and characteristics are known to play a major role in fouling formation. The type and concentration of the foulants as well as the water pH, ionic strength and the presence of (divalent) ions such as calcium (Ca^{2+}) can increase the likelihood of fouling (Hong and Elimelech 1997, Al-Amoudi 2010). Membrane fouling is caused by complex physical and chemical interactions between these foulants in the matrix and the membrane surface (Guo et al. 2012). The OM in municipal wastewater contributes mainly to membrane fouling due to organic fouling. Natural organic matter (NOM) has been identified as the most important foulant and is commonly composed of two major fractions: Non-dissolved and dissolved organic matter (DOM), operationally defined by the isolation technique using filters. DOM is the fraction of organic substances which is able to pass through a 0.45 µm filter. Colloidal and particulate organic matter (POM) remains on the filter (Metsämuuronen et al. 2014, Sillanpää 2015). NOM is a heterogeneous mixture of undefined organic compounds originating from animals, plants and microorganisms as well as their waste and metabolic products consisting of components with varying properties and molecular sizes. Therefore, NOM is omnipresent in all natural water bodies. The factors that determine the composition and amount of NOM are location dependent and

include the origin of OM, the water chemistry, temperature, pH and the biological processes which occur in the water matrix. Thus, the amount and makeup of NOM varies with source and seasonal variations such as e.g. heavy rains, drain seasons or algal blooming (Metsämuuronen et al. 2014).

NOM consist of hydrophobic, hydrophilic and transphilic fractions. In natural waters, hydrophobic acids with larger molecular weight (MW) are the largest fraction of NOM making up approximately 50% of the total organic carbon (TOC), which can be related to humic acids, fulvic acids and to a minor extent humins (Thurman 1985). The hydrophilic fraction refers more to carbohydrates, sugars and amino acids including aromatic carbon, phenolic structures and conjugated double bonds (Sillanpää 2015). A detailed classification of NOM in water sources is illustrated in Figure 20.

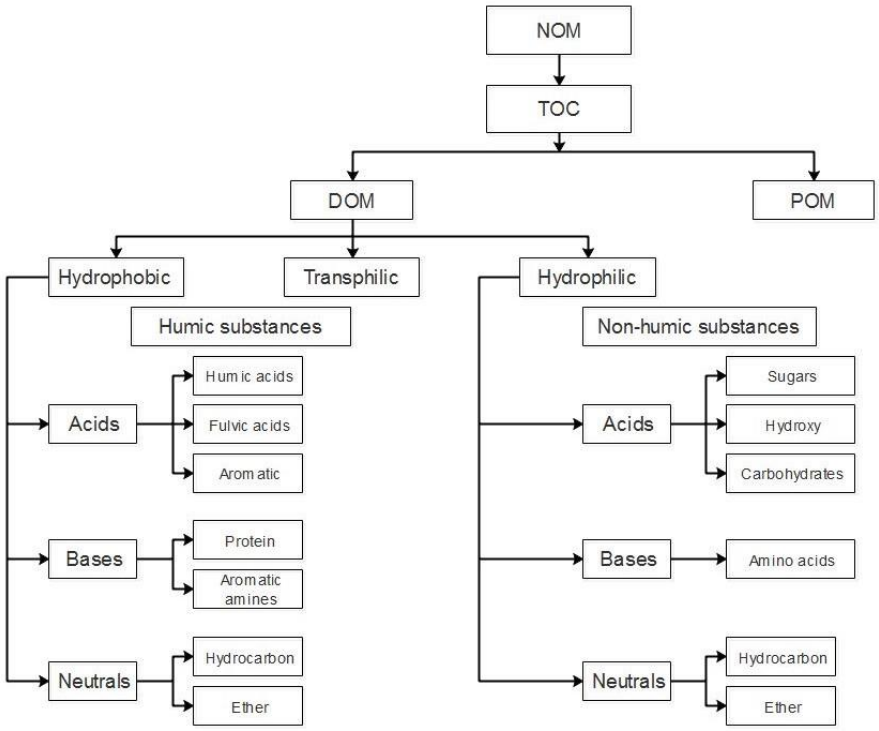

Figure 20. Classification of natural organic matter (NOM) in water. Relationship between certain NOM fractions and its chemical groups (adopted from Ibrahim and Aziz (2014)).

In water treatment and drinking water applications, NOM causes serious concerns such as color, taste and odor and can bind to potential harmful contaminants. The DOM fraction, which is biodegradable, can furthermore cause biological growth and biofilm formation in (drinking) water distribution systems. Applying chemical treatment for disinfection purposes, NOM can react with

the chemical treatment agents leading to the formation of disinfection by-products (DBP), which are known to have harmful effect on humans and animals (Krasner et al. 2006).

Characteristics and properties of the membrane:

When considering specific membrane-foulant interactions, the characteristics of the membrane determine fouling formation. Regarding membrane fouling, the materials affinity to water considerably influences the propensity of water constituents to stick on the membrane surface or not. Many polymeric membranes are hydrophobic, and therefore especially organic matter tends to attach to the material (Iorhemen et al. 2016; van der Marel et al. 2010). To improve hydrophobic membrane properties, these can be coated or modified (Rana and Matsuura 2010). Also, the surface quality impacts the development of fouling, where rough membrane surfaces are more prone to fouling. Another influential membrane characteristic is the pore size. From a morphologic point of view, smaller pore sizes are less likely to suffer from fouling than larger pores because particulate and colloidal matter do not enter the small membrane pores, and therefore their deposition can be removed or controlled by turbulent conditions (Baker 2012). However contrary observations have been made, and the pore size effect seems to differ for distinct membrane materials (Miyoshi et al. 2015). The morphology of the membrane e.g. a low surface roughness can also limit the fouling propensity (Al-Amoudi 2010).

Operational / Hydrodynamic conditions:

The operational conditions encompass the operational flux, recovery rate, temperature, potential fouling control strategies (e.g., backwashing, cleaning intervals), and mode of operation (e.g. cycle length). Membrane separation is based on the balance between the mass transported towards the membrane and the mass transported back into the bulk solution. Hence membrane fouling is substantially influenced by the applied flux rate (assuming constant flux operation). In practical applications, the flux has to be set to meet a compromise between an acceptable fouling rate and the operational and economic expenditure for its alleviation. The recovery rate, defined as the ratio of produced permeate to feed volume, determines the concentration of foulants on the feed side of the membrane. Thus, the recovery rate is an important design parameter regarding membrane fouling. The operating temperature changes important reactor medium properties like its viscosity, fluid turbulence, as well as water constituents' diffusion. All these three properties decrease with decreasing temperature and therefore worsen the fouling conditions (Crittenden 2012).

The hydrodynamic conditions of membrane applications are influenced by design parameters (e.g., membrane/module configuration, reactor design, packing density of membranes) and operational conditions. These parameters include the operational mode (e.g., external or submerged membeane, death-end or cross-flow) and potential additional hydrodynamic measures (e.g., recirculation flow rate, spacers).

5.2.2 Membrane fouling mitigation strategies

The complex composition of municipal wastewater depicts a high fouling risk, which has to be managed with appropriate fouling mitigation strategies. In order to limit and control membrane fouling, the previous mentioned parameters (i.e., feed solution composition, membrane characteristic, operational/hydrodynamic conditions) need to be well balanced. In general fouling mitigation strategies can be separated based on (i) strategies to prevent fouling by removing the relevant foulants of the matrix (pretreatment) or (i) strategies to limit fouling to an acceptable level by specific conditions and/or additional treatment strategies. It is important to consider that fouling cannot be limited completely, due to the fundamental principle of membrane treatment. Depending on the membrane type different mitigation strategies are conceivable. One common approach are mechanical cleaning approaches through shear stress enhancement on the membrane surface. Mechanical cleaning generally encompasses approaches like the addition of particles and carriers, membrane induced vibrations, rotation of membranes, or ultrasonic cleaning (Wang et al. 2014). For UF and MF membranes in MBRs also air scouring is a common approach to increase the shear forces on the membrane surface. Beside these mechanical cleaning approaches also the hydrodynamic regime and its optimization to increase turbulences on the membrane surface are currently applied fouling mitigation strategies.

During operation the fouling phenomenon can be limited by hydrodynamic (e.g. backwashing) and/or chemical cleaning approaches. Chemical cleaning is carried out as maintenance and recovery cleaning. The choice of a sufficient detergent depends on the fouling matter and the manufacturer's instructions. Inorganic foulants like precipitated salts can be dissolved with pH-lowering agents. Citric and hydrochloric acids are common in wastewater treatment processes. Oxidative agents like sodium hypochlorite (NaOCl) or hydrogen peroxide (H_2O_2) are very efficient and are therefore used as primary cleaning reagents. NaOCl is very powerful and acts as an oxidation agent to remove organic matter, but also serves as a disinfectant to eliminate biofouling. Sometimes the oxidative purification is enhanced by the addition of a base or is supported by an alkaline pretreatment (Wang et al. 2014). Chemical cleaning is an efficient way to maintain an appropriate membrane permeability and ensure a long service life. However, obvious disadvantages like expenses for chemicals, chemical storage, and safety considerations, come along with interruptions of filtration, additional membrane degradation, as well as environmental concerns due to the formation of adsorbable organic halides (AOX) by-products (Wang et al. 2014).

6 Materials and methods

The first part of this thesis is focused on the conceptual design of potable water reuse schemes. All relevant material and methods are published in publication #4. The second part of this thesis is focusing on the feasibility and operational performance of membrane treatment applications. This includes the detailed monitoring of membrane treatment and investigation regarding mitigation of membrane fouling. Therefore, different membrane test-skids were designed and constructed. In detail an UF-pilot-scale, an UF-laboratory-scale and NF/RO-laboratory-scale test-skid were designed and constructed. The material and methods of the second part of this thesis are presented in the corresponding publications (publications #5 and #6) and in this chapter 6.

6.1 Test-skids

6.1.1 Laboratory flat-sheet test-skid (NF/RO)

NF and RO membrane fouling experiments were performed using an automated laboratory-scale cross-flow flat-sheet membrane test-skid (Figure 21).

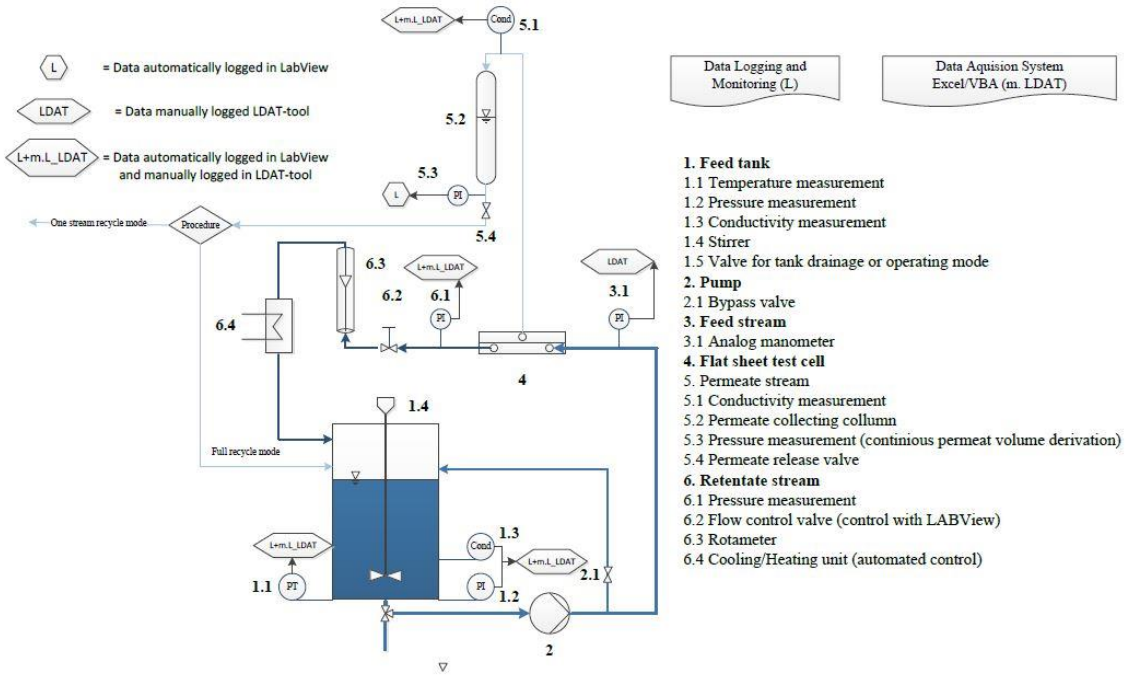

Figure 21. Schematic of the laboratory-scale cross-flow flat-sheet NF/RO membrane test-skid.

It was comprised of 6 main parts: (1) a feed tank (60 L), (2) a feed pump (Piston diaphragm pump, Verder), (3) the feed stream, (4) the flat-sheet test cell (Sepa II, Osmonics, surface area 139 cm^2), (5) the NF/RO permeate stream, and (6) the retentate stream. The system was monitored and controlled using LabVIEW™ software. A visualization of the test-skid is presented in Figure SM1, supplementary material, Appendix D.

NF and RO membranes

Cut flat-sheet samples of two different membranes were selected for this study. A polyamide (PA) thin-film composite NF membrane, the NF-270 (DOW FilmTec™, Minneapolis, USA) and a RO membrane, the Toray Romembra® TMG10 (Toray Industries., Inc., Tokyo, Japan). The specific membrane properties are summarized in Table 10.

Table 10. Specific properties of the DOW NF-270 and Toray TMG10 RO membrane according to the manufacturer (Toray 2004, DOW n.d.).

	DOW NF-270	**Toray TMG10**
Membrane type	Polyamide thin-film composite	Fully aromatic crosslinked polyamide composite
Nominal permeate flux (LMH)	52	/
Max. pressure tolerance (bar)	41 (~600 psi)	25 (365 psi)
Molecular weight cut-off (Da)	200	/
pH range for continuous operation	2-11	2-11
Salt rejection (NaCl)	> 97 %	99.5 %

Membrane fouling experiments

Recirculation mode fouling experiments were carried out to investigate organic membrane fouling. To avoid accumulation of organic chemicals in the system, both retentate and the permeate were recirculated back to the feed tank. New membrane specimens and feed spacer were used for each fouling experiment. The permeate spacer was not changed for the experiments.

Prior to each experiment the membrane setup was flushed with deionized (DI) water for approximately 3 h by applying a high cross-flow velocity (CFV) (> 0.65 m/s). Here, no membrane and spacers were installed and the connection to the permeate column was always closed in order to avoid cross contamination of the permeate side. Thereafter, a cut piece of a membrane was checked visually for damages, placed in the flat-sheet test cell, and rinsed with DI water. A new feed spacer and the permeate spacer were placed as well.

Due to the temperature correction of the membrane flux for a target temperature of 20.7 °C, the NF/RO feed matrix required a minimal temperature of 17 °C for the experiment in order to avoid flux uncertainties because of the higher viscosity of water at lower temperatures. If the NF/RO feed matrix was stored in the fridge, it was equilibrated to room temperature until the experiment was started.

For experiments, the NF/RO membranes were first equilibrated for 2-3 h with DI water to allow sufficient membrane compaction, optimal rejection and in order to ensure reproducible flux curves during subsequent fouling experiments. Equilibration was always conducted at slightly higher fluxes than the corresponding fouling experiment (Table 11). As soon as a stable flux was achieved, a “membrane rejection test” was conducted to roughly exclude membrane damages, which were not visible during the visual inspection. For that, 10 L of normal tap water were added to the feed tank just to increase the conductivity of the DI water. As soon as conductivity values of the feed (σ_F) and permeate (σ_P) increased and stabilized, the percent membrane rejection (R) was calculated:

$$\mathrm{R}\,[\%] = \left(1 - {}^{\sigma_\mathrm{F}}/_{\sigma_\mathrm{P}}\right) \cdot 100\,\% \qquad (9)$$

Where σ_F and σ_P are given in the unit (µS/cm). The following threshold values for membrane conductivity rejection were defined as limited values for optimal operation: $\mathrm{R} \geq 85\,\%$ for the NF-270 membrane and $\mathrm{R} \geq 98\,\%$ for the Toray TMG10 RO membrane.

After discharging the DI water for equilibration, the feed tank was refilled with the corresponding NF/RO feed matrix for the fouling experiment. The initial feed pressure was kept constant for all fouling experiments at ~2.8 bar for NF membrane operation and ~5.5 bar for RO membrane operation. This corresponds to a permeate flux of ~20 LMH, which is common for full-scale NF/RO designs using reclaimed water (Bellona et al. 2010a). The CFV was also kept constant between 0.07 and 0.08 m/s during the experiments. A stirring unit in the feed tank was used to ensure a constant homogenous distribution of the feed. Basic operational parameters for NF and RO operation are summarized in Table 11.

Table 11. General operational parameters for membrane equilibration and fouling experiments.

	Membrane equilibration			Fouling experiment		
	Pressure (bar)	**CFV (m/s)**	**Permeate flux (LMH)**	**Pressure (bar)**	**CFV (m/s)**	**Permeate flux (LMH)**
NF membrane	3.4 (50 psi)	0.18-0.22	~35-37	2.8 (40 psi)	0.18-0.22	19-21
RO membrane	6.9 (100 psi)	0.18-0.22	~34-36	5.5 (80 psi)	0.18-0.22	19-21

In order to constantly monitor system operation throughout the experiment R was calculated each day after 24 h according to equation 9. In addition, the percentage dissolved organic carbon (DOC) rejection ($\mathrm{DOC_R}$) was calculated based on the values obtained by the DOC measurements:

$$\mathrm{DOC_R} = \left(1 - {}^{c_F}/_{c_P}\right) \cdot 100\ \% \qquad (10)$$

Where:

$\mathrm{DOC_R}$ Percentage DOC rejection of the NF/RO membrane (%)

c_F DOC concentration (mg/L) of the NF/RO feed at time t

c_P DOC concentration (mg/L) of the NF/RO permeate at time t

Sampling

Samples for the DOC measurement were taken from the permeate line and also directly from the feed tank at predetermined times of 0 h, 48 h, and the end of each experiment. Initial DOC concentrations of the NF/RO feed matrices were not adjusted equally in order to investigate the effect of varying concentrations on membrane fouling. Each, feed and permeate were analyzed according to DOC, UV absorbance at 254 nm (UVA_{254}), specific UV absorbance (SUVA) and 3D-fluorescence excitation-emission matrix (3D-EEM) measurements. For that, approximately 100 mL of both feed and permeate was collected in 150 mL amber glass bottles and stored in the fridge at 4 °C. The DOC of the feed and permeate was measured directly. UVA_{254} and 3D-EEM measurements were measured within 2 weeks after sampling together with other collected samples. Besides, the feed was analyzed for its protein and carbohydrate content. For that, 10 mL of the feed were collected in 15 mL plastic centrifuge tubes and frozen until measurement.

Exposition of the membranes

To compare the experiments with different operation times, the exposition per hour (E_h) and the total exposition over the whole operation time (E_T) of the membranes was calculated. For that, following assumptions and simplifications were made:

- Flux decline proceeds linear (average flux between the initial flux and the flux of the end of the experiment was calculated).
- No steady-state flux is reached so that DOC accumulation onto the membrane is not "completed".
- Initial DOC, protein and carbohydrate concentrations of the feed matrices (c_{Feed}) are constant throughout the experiment.

$$E_h = J_A \cdot A_m \cdot c_{Feed} \quad (11)$$

Where:

E_h	DOC, protein or carbohydrate exposition of the membrane per hour (mg/h)]
J_A	Average membrane flux over the whole operation time (LMH)
A_m	Membrane area [m^2], here 0.0139 m^2
c_{Feed}	Initial DOC, protein or carbohydrate concentration of the feed matrix (mg/L)

$$E_T = E_h \cdot t \quad (12)$$

Where:

E_T	Total DOC, protein or carbohydrate exposition of the membrane over the whole operation time (mg)
t	Operating time of the experiment (h), (Table 12)

6.1.2 UF laboratory-scale test skid

The UF test skid consists of two identical UF membrane bench reactors designed as smaller models (~ 1:10) of an existing UF pilot system (see chapter 7.1/publication #5). A schematic illustration of the test-skid and its components specifications is presented in Figure 22. The bodies of the reactors (R1) consist of two acryl glass columns with 90 mm inner diameter and a height of 1,065 mm, together with fixed enlargements (280 mm in diameter and 360 mm high) at the top. The total volume of one test column was around 25 L. By installing the overflow outlet at the beginning of the enlargement (at the edge of the funnel area) the operation volume was reduced to 7 L. The membrane modules (M1) were particularly designed and assembled for this study and consisted of 25 *PURON*® hollow fibre membranes, with an individual fibre length of 246 mm and a filtration area of 0.05 m^2 each. In contrast to the pilot system, the membrane fibres were

positioned upside down, with the loose fibre ends directed downwards. The spacing between fibre ends and the reactor bottom was 5 cm. A compilation of the *PURON*® membrane characteristics can be found in Table 12.

The feed matrix was provided from a 50 L tank. It contained a stirrer (X1) to prevent particulate and colloidal matter from settling and kept the feed matrix homogeneous. For temperature control, two cooling elements (H1, U-shaped, stainless steel pipes) were immersed into each reactor from the top and supplied with cool water of 10 °C from the general laboratory cooling system. A pair of universal online probes (S4) recorded the temperature during experiments. Two online pressure transducers (S2) measured the TMP. Each transducer was located at the same height as the overflow outlet, which ensured the direct measurement of the exact TMP (plus the low and negligible hydraulic losses in the permeate tubes). Additionally, pressure gauges (S1) were installed to check the operational pressure (TMP) and to calibrate the electronic sensors. Fluid flow rates had to be measured in the recirculation cycle as well as in the permeate line. For the recirculation, flow meters (S3) were used. In contrast, the relatively small volume flow rates of filtration and backwashing had to be measured by hand. Two glass columns (T1, T2) with scales helped to capture the time required to fill a certain volume.

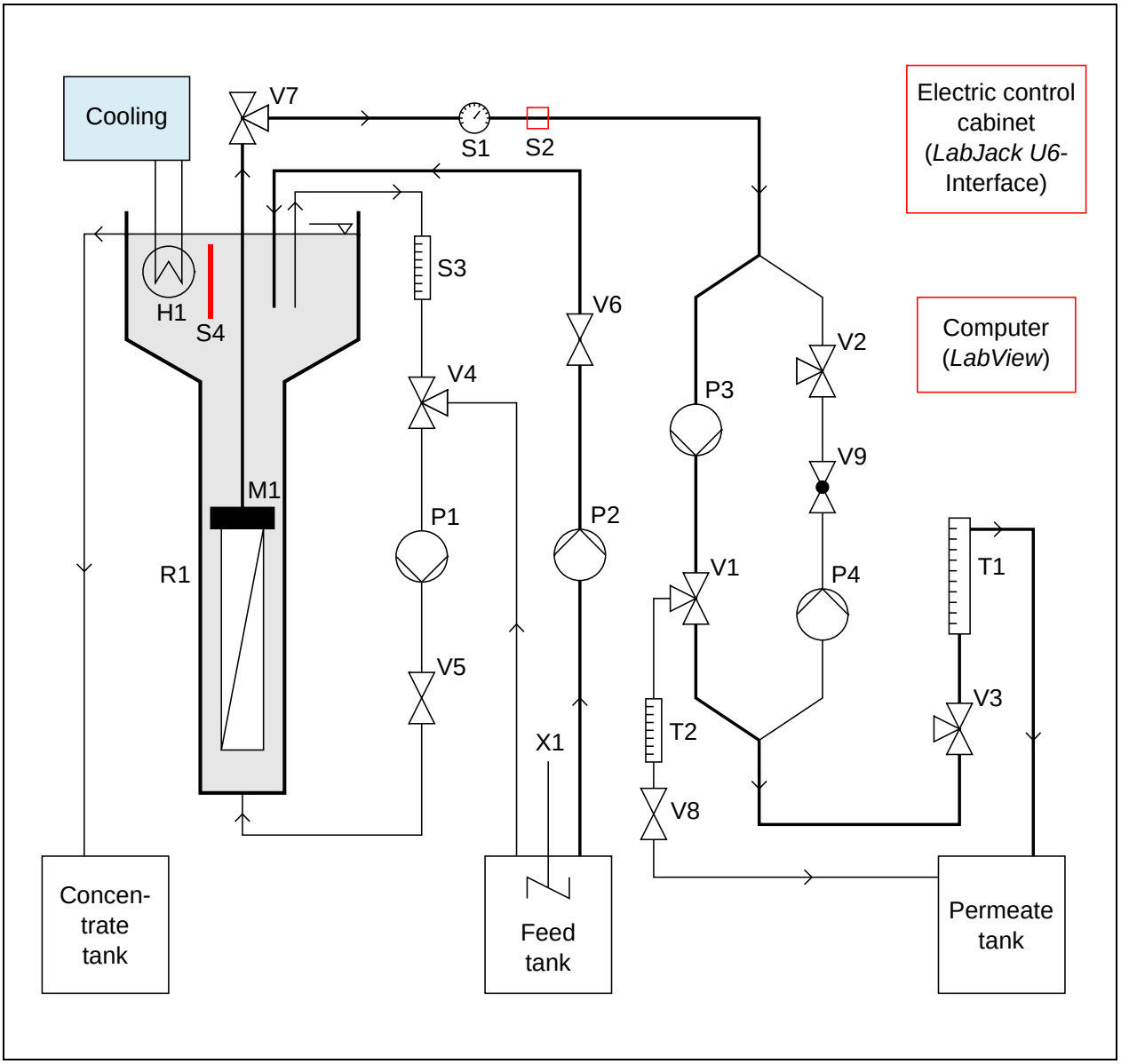

Figure 22. Flow chart of the ultrafiltration bench test stand and components specifications.

Table 12. PURON® hollow fibre membrane characteristics (Koch Membrane Systems 2014).

PURON® – Hollow Fibre Membrane (Koch Membrane Systems, Inc.)	
Nominal pore size	0.03 µm
Outside fibre diameter	2.6 mm

Membrane type	Proprietary PVDF
Maximum TMP (filtration / backwash)	60 kPa / 60 kPa
Maintenance cleaning	NaOCl: (125 – 1,500 ppm; backwashing at 6 LMH; 30 – 45 min) Citric acid: (1,000 – 1,500 ppm; backwashing at 6 LMH; 30 – 45 min)
Recovery cleaning	NaOCl: (1,000 – 2,000 ppm; soak for ≥ 5 h) Citric acid: (1,500 ppm; soak for ≥ 5 h)
Clean water permeability	≥ 500 LMH/bar (Judd and Judd 2011)
Maximum permeability	340 LMH/bar (Judd and Judd 2011)

Pumping was realized by modular peristaltic pumps (*Heidolph Instruments GmbH & Co.KG; Schwabach, Germany*). Whereas each test column had its own filtration (P3), backwashing (P4), and recirculation pump (P1), a single feed pump (P2) was used for both columns (see Figure 22). The feed stream was portioned through a Y-fitting, which was located behind P2 (not displayed in Figure 22). For adjusting the pump revolution rates, each pump had an individual control device with a control dial. These control devices were connected to an electric cabinet and could be switched on and off via a *LabJack U6* (*LabJack Corporation*; Lakewood, CO, USA) interface. The *LabJack* interface was controlled by *LabVIEW*™ (version 16.0; *National Instruments*; Austin, TX, USA). Also, the two temperature probes and the two pressure transducers were connected to the *LabJack* interface, which transmitted the signals to the computer where the *LabVIEW*™ application recorded the values. A visualization of the test-skid is presented in Figure SM2, supplementary material, Appendix D.

6.2 Laboratory analysis

6.2.1 Total organic carbon (TOC) and dissolved organic carbon (DOC)

TOC/DOC measurements were conducted with a HighTOC analyzer (Elementar Analysensyteme GmbH, Langensebold, Germany). Each sample was measured once. TOC/DOC was measured according to standard procedures. If necessary, samples were diluted to a concentration range of 5 – 100 mg/L. Samples were filled into 20 mL glass vials. Each sample was acidified with concentrated hydrogen chloride solution (HCl, 32 %) to a pH below 2 and stored in the fridge at

4 °C pending analysis. For DOC measurements the samples were filtrated with a 0.45 µm filter before measuring. Because samples downstream of UF treatment (0.03 µm) already constituted filtered samples the measured TOC corresponds to the DOC value.

6.2.2 Total suspended solids (TSS)

The total suspended solids content (TSS) was measured by filtrating 500 mL sample through a filter paper (*Quantitative Grade 388*; by *Sartorius*; Göttingen, Germany) and drying it at 105 °C. The TSS was determined as the weight difference of the dry loaded filter and the dry clean filter. As a pretreatment, the filters were flushed with ultrapure water (*Milli-Q*) to remove the loose fibre fraction before the unloaded dry weight was determined.

6.2.3 Chemical oxygen demand (COD)

Chemical oxygen demand (COD) was analyzed using *Hach*/*Lange* (Loveland, CO, USA) cuvette tests (LCK 515: 100 – 2000 mg(O_2)/L COD). Samples were not diluted or homogenized and just measured once. After pipetting the appropriate amount of 2 mL into the ready-to-use cuvette, the sample was digested at 170 °C for 15 min in a thermostat (*HT 2000S* by *Hach/Lange*). The cooled cuvette was finally measured in the *DR 600* (by *Hach/Lange*) photometer at 605 nm.

6.2.4 Ultraviolet absorbance at 254 nm (UVA_{254}) and specific ultraviolet absorbance (SUVA)

UV absorbance of the samples at 254 nm (UVA_{254}) expressed in the unit [1/m] was measured using an UV-visible light spectrophotometer from Shimadzu (UV-1601) and a QS high precision cell cuvette made of quartz SUPRASIL® from Hellma Analytics. The specific UV absorbance (SUVA) was calculated from the ratio of UVA_{254} to DOC. The SUVA is expressed in [L/(mg cm)]. Samples were measured undiluted.

6.2.5 Total protein and carbohydrate quantification

Protein concentrations in prepared samples were measured using the Pierce® BCA protein assay kid from Thermo Scientific©. Protein concentrations are given in bovine serum albumin (BSA) equivalents. This method is based on a colorimetric detection and the reduction of Cu^{2+} to Cu^{1+} by proteins in an alkaline medium. By adding bicinchoninic acid (BCA) a purple-colored complex is formed by the chelation of two molecules of BCA with one cuprous ion and its absorbance at 562 nm can be read. The absorbance of this colored complex is nearly linear with increasing protein concentrations over a working range of 20-2000 µg/mL. For measurement, the samples

were analyzed according to the microplate procedure as described in the manual provided with the assay kit.

Total carbohydrates were estimated by the phenol-sulfuric acid method according to DuBois et al. (1956) and are given in glucose-monohydrate equivalents. All classes of carbohydrates including poly-, oligo- and disaccharides are broken down to monosaccharides by high concentrated sulfuric acid. Pentoses and hexoses are then dehydrated to furfural and hydroxymethyl furfural, respectively. By adding phenol those furfural derivates react with the phenol to produce a yellow-gold color. For quantification, the absorption at 485 nm is read. The absorption of the sample is directly proportional to the total carbohydrate concentration. The calibration is commonly provided with a glucose standard. Here, a calibration was prepared with a D-(+)-glucose standard stock solution of 0.1 mg/mL and calibration standards in the concentrations 20, 40, 60, 80 and 100 µg/mL. For measurement, 1 mL of the sample or calibration standard is prepared in a sterile plastic centrifuge tube. 5 mL of sulfuric acid (> 96 %) and 1 mL of 5 % phenol solution (w/v) were added and tubes were mixed completely. The samples were placed in an oven at 105 °C for 10 min. to accelerate the reaction. Afterwards the samples were cooled to room temperature and the absorbance was read at 485 nm using a photometer.

6.2.6 Liquid chromatography-organic carbon detection (LC-OCD)

Liquid chromatography-organic carbon detection (LC-OCD) was applied for selected NF/RO samples. The LC unit separates organic compounds according to their molecular size through the size exclusion column. For that, selected samples (initial NF feed and permeate from exp. 1, initial RO feed and permeate from exp. 3) were sent to the LC-OCD laboratory at the Department of Water Quality Control at the TU Berlin (Prof. Dr.-Ing. Martin Jekel). At the LC-OCD laboratory, the water sample constituents were fractionated using LC (manufacturer DOC-LABOR Dr. Huber, Karlsruhe, Germany) with a size exclusion chromatography HW55S (Alltech-GROM GmbH, Germany) followed by a detector for UV_{254} (Ultramat 6, Siemens, Germany). The LC column is bypassed to obtain a DOC value at the dead volume time of each chromatographic run. The system is further equipped with a dissolved organic nitrogen detector using UV_{220} absorption (Well Chrom fixed wavelength detector K2001- UV220 Knauer, Germany). For LC-OCD analysis water samples were pre-filtered using cellulose nitrate filters (Sartorius Stedim Biotech GmbH) with a pore size of 0.45 µm and diluted to DOC concentrations in the range of 2 to 5 mg/L using ultrapure water. For data evaluation the software FIFIKUS® (DOC Labor Dr Huber, Karlsruhe) was used.

6.3 3D-fluorescence excitation-emission matrix (3D-EEM) measurement

3D-EEM measurements of all samples were measured at room temperature (20 ± 1 °C) using the Aqualog™ by HORIBA Scientific and Aqualog™ V3.6 software. A QS high precision cell cuvette made of quartz SUPRASIL® by HellmaAnalytics with a light path of 10x10 mm was used. Settings for 3D-EEM measurements are listed in Table 13. Each sample was measured once. Samples were measured diluted or undiluted, depending on the DOC values and determined signal intensities of the Aqualog™. Therefore, linearity measurements were applied for all sample types (i.e., raw wastewater, UF feed, UF permeate, NF/RO feed, NF/RO permeate). Thus, samples were diluted to have a DOC < 20 mg/L. The sample types raw wastewater and UF feed were filtered through a 0.45 µm filter before measurements. Samples were measured maximum two weeks after sampling.

Table 13. Experimental settings of the Aqualog™ for 3D-fluorescence excitation-emission matrix (3D-EEM) measurement.

Integration time	1 s
Excitation spectra	599-230 nm, 3 nm steps
Emission spectra	211.62-621.32 nm, 1.64 steps (4 pixel)
CCD gain	medium

First, a 3D-EEM blank of fresh ultrapure water was recorded. The Raman peak area of the blank was measured by the “Raman Scattering Area Unit Tool” provided with the Aqualog™ software. During measurement of the samples, the blank 3D-EEM was substracted from the sample 3D-EEM to remove most of the Raman scatter peaks. A compensation for the inner filter effect as well as the removal of Rayleigh scatter lines was applied by an algorithm provided by the Aqualog™ software. All 3D-EEM data was Raman calibrated by normalizing to the area under the Raman scatter peak of the blank. Thus, maximum fluorescence intensities were expressed in Raman Units (R.U.)

6.4 Parallel factor (PARAFAC) analysis

To create a parallel factor (PARAFAC) model, a total number (n) of 115 data points was used. 3D-EEM data from the raw wastewater (n=12), influent microsieving (n=5), effluent microsieving (n=17), UF feed (n=23), UF permeate (n=37), NF/RO feed (n=12), and NF/RO permeate (n=9)

was used. The model possessed a core consistency of 96 %. A split-half analysis was performed in which the dataset is split in two halves whereby each half is modeled independently. If both halves found to be identical the model can be considered as robust. Performed split-half analysis indicated 94 % agreement between excitation and emission loadings modeled for the two parts of the whole data set.

Three components (C1-C3) were identified by the chosen PARAFAC model. The representative contour plots are shown in Figure 23. C1 and C3 each consist of a double peak, whereby C2 is only one clear peak. An attempt has been made to create a 5-component model in order to split the double peaks of C1 and C3. However, core consistency, split-half analysis and explained variance parameters were not satisfactory for a 5-component model.

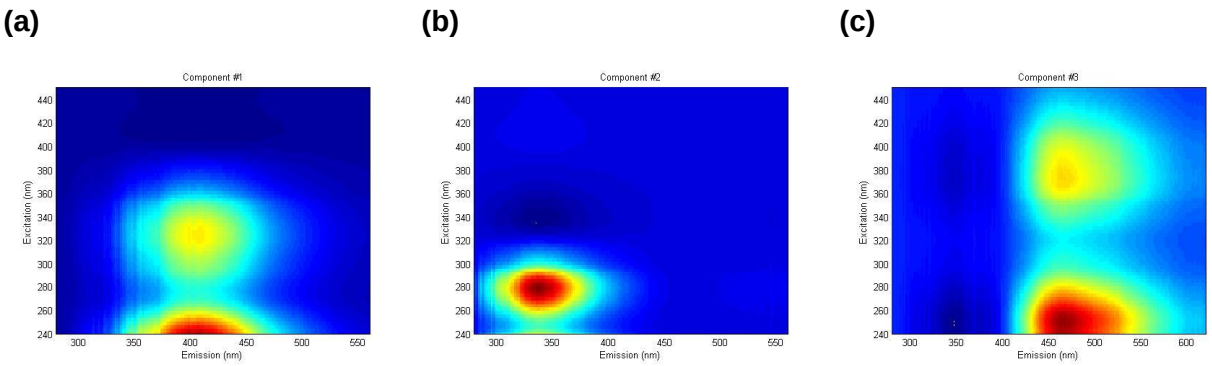

Figure 23. 3D-fluorescence excitation-emission matrix (3D-EEM) spectra of isolated components (a) C1, (b) C2 and (c) C3 during parallel factor (PARAFAC) analysis.

The fluorescence ranges of C1-C3 are reported in Table 13 along with related identified compounds from published studies. Based on the data of previous investigations, C2 can be related to protein-like fluorescence associated with microbial activity (Coble 1996, Baker et al. 2008, Murphy et al. 2011, Seredyńska-Sobecka et al. 2011). C3 can be related to humic-like fluorescence, which is supported by Coble (1996), Murphy et al. (2011) and Baghoth et al. (2011). Whereby the fluorescence maxima given by Murphy et al. (2011) characterized as terrestrial humic-like fluorescence in high nutrient and wastewater impacted environments fits only to the upper peak of C3. The lower peak of C1 overlaps on the one hand the region of hydrophobic acid fluorescence defined by (Chen et al. 2003), and on the other hand the region of humic-like fluorescence. The upper peak originates most likely also from (marine) humic-like fluorescence.

Table 14. Excitation (Ex) and emission (Em) ranges of the identified components 1-3 (C1-C3) from the parallel factor (PARAFAC) analysis model and relating compounds identified in previous studies.

	Fluorescence range		Previous studies	
Component	**Ex (nm)**	**Em (nm)**	**Related compounds**	**Reference**
C1	Upper peak: 240-275, Lower peak: 280-360	Upper peak: 340-475, Lower peak: 355-460	Humic-like, marine and terrestrial humic fluorescence, hydrophobic acids	Chen et al. (2003), Baghoth et al. (2011)
C2	245-305	290-400	Protein, tryptophan-like Protein-like fluorescence associated with microbial activity and biological productivity	Murphy et al. (2011), Seredyńska-Sobecka et al. (2011)
C3	Upper peak: 240-320, Lower peak: 330-430	Upper peak: 415-595, Lower peak: 445-570	Humic- and fulvic-like, terrestrial humic-like fluorescence in high nutrient and WW impacted environments	Murphy et al. (2011), Chen et al. (2003), Baghoth et al. (2011)

For data evaluation, F_{max} values were calculated according to equation 13:

$$\mathrm{F_{max_n}} = \mathrm{Score_n} \cdot \mathrm{Ex_n}(\lambda_{max}) \cdot \mathrm{Em_n}(\lambda_{max}) \quad (13)$$

Where:

$\mathrm{F_{max_n}}$ Maximum fluorescence intensity for the nth component [R.U.]

$\mathrm{Score_n}$ Relative intensity of the nth component

$\mathrm{Ex_n}(\lambda_{max})$ Maximum of the excitation loading of the nth component

$\mathrm{Em_n}(\lambda_{max})$ Maximum of the emission loading of the nth component

6.5 Inorganic measurements

The inorganic characterization included the following parameters: Calcium (Ca), chloride (Cl), iron (Fe), potassium (K), copper (Cu), magnesium (Mg), manganese (Mn), sodium (Na), and zinc (Zn).

Samples were determined by flame atomic absorption spectrometry (Varian Spectrometer AA-240FS) and graphite furnace atomic absorption spectrometry (Varian Spectrometer AA-240Z with GTA 120) according to Standard Methods 3111 and 3113 (APHA, 2005), respectively. Quality control was maintained by taking standard solution quantity checks every five samples and using blank samples.

6.6 Cake layer (CL) measurements (NF/RO)

Cake layer (CL) measurements were applied for NF/RO membrane tests. After the fouling experiments were finished, the NF/RO membranes were carefully replaced from the cross-flow test cell and air dried. Ziplock® bags were used to store the fouled membrane specimens in a fridge at 4 °C for further investigation. For CL analysis, 5 membrane pieces of a defined size (4 cm^2) were cut from the membrane. To minimize large deviations, each membrane was sampled diagonally as illustrated in Figure 24. Sample spots 1, 2 and 3 were used for protein and carbohydrate quantification, the spots 4 and 5 for an additional DOC and 3D-EEM sample. For DOC measuremtns the CL samples were 1:80 diluted to a total volume of 20 mL with DI water. For 3D-EEM measurements, the CL samples were 1:8 diluted to a total volume of 8 mL with DI water.

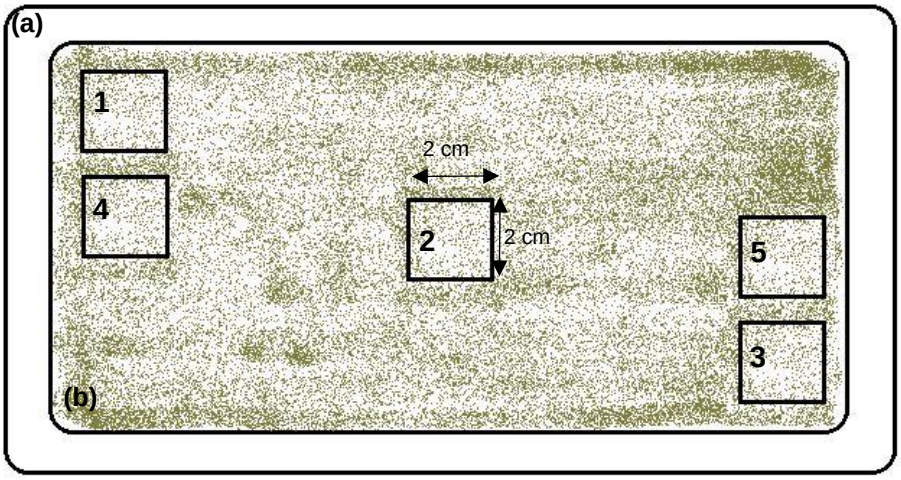

Figure 24. Graphical illustration of the sampling locations of a fouled membrane specimen. (a) Membrane, (b) fouled membrane surface, 1, 2 and 3 = sampling spots for protein and carbohydrate quantification, 4 and 5 = sampling spots for DOC and 3D-EEM sample.

In order to analyze the main foulants on the NF/RO membrane surface, the organic CL needs to be extracted without destroying parts of the sample. DI water and a 0.1 M sodium hydroxide

(NaOH) solution were tested in order to find the best solvent for CL extraction from the membrane surface. A protein measurement revealed similar concentrations when using DI water or NaOH solution so that DI water was selected for CL extraction of all samples during this study. For that, (I) the cut membrane pieces were placed in a tube containing glass beads and 1.5 mL DI water. (II) The tubes were shaken at 6 m^2/s using a FastPrep®-24 Instrument for 25 s. Following this protocol, the attached CL was grinded from the membrane surface and homogenized in the DI water. (III) Finally, the “resolved CL” was pipetted and transferred in a 1.5 mL Eppendorf tube and frozen for further protein, carbohydrate and DOC quantification, as well as 3D-EEM analysis. Parts of the resolved CL do not attach on the glass beads.

7 Ultrafiltration (UF) membrane treatment of municipal wastewater

The proposed conceptual design of a more energy-efficient potable water reuse schemes consists of the treatment of municipal wastewater with UF prior to subsequent RO treatment. This concept follows the idea to physically separate particulate and dissolved fractions of the wastewater constituents by UF treatment and subsequent concentration of dissolved fractions by RO treatment. Applying this approach, it is possible to enable separated energy recovery platforms for carbon and nitrogen. In addition, the load of the subsequent treatment stages is reduced. This chapter is targeting the design, construction and analysis of the first proposed membrane process (UF) within the postulated more energy-efficient potable water reuse scheme, stated as hypothesis #2:

> *"A fluidized bed UF reactor is able to treat reliably (regarding membrane fouling, cleaning intervals and generated water quality) pretreated raw municipal wastewater and generate a permeate quality which is suitable for subsequent NF or RO treatment."*

Hypothesis #2 was tested and discussed within this chapter. It was possible to separate particulate and dissolved fractions of the wastewater constituents, measured as fractions of carbon and nitrogen. By implementing successfully hydrodynamic optimizations and additional fouling control by mechanical cleaning with GAC in a fluidized bed, it was possible to operate reliable the UF system for over 576 days (chapter 7.1). The overall treatment performance (membrane fouling, cleaning intervals) of the UF treatment system was at an acceptable level. The water quality was regularly measured to assess the feasibility of downstream membrane treatment with NF or RO membranes. The results indicate that downstream treatment of the UF permeate with NF or RO is possible. However, the ultimate feasibility of downstream membrane treatment (NF/RO) will be investigated in chapter 8 and the corresponding hypothesis #3. Hence, hypothesis #2 could be confirmed. However, further studies indicated that further improvements regarding sustainable treatment operation are possible. In this context, the fouling behavior and mitigation potential with different recirculation rates and GAC concentration (fluidized bed / packed bed) are presented in chapter 7.2. Fouling mitigation based on vibrations induced by electroactive polymers (EAPs) is presented in chapter 7.3.

7.1 A hydraulically optimized fluidized bed UF membrane reactor (FB-UF-MR) for direct treatment of raw municipal wastewater to enable potable water reuse with integrated energy recovery (Publication #5)

Nils Horstmeyer[a], Cornelius Thies[a], Thomas Lippert[a] and Jörg E. Drewes[a]

[a]Chair of Urban Water Systems Engineering, Technical University of Munich, Am Coulombwall 3, 85748 Garching/München, Germany.

The following publication is submitted with editorial changes in:

Horstmeyer, N., Thies, C., Lippert, T., Drewes, J.E. (submitted) A hydraulically optimized fluidized bed UF membrane reactor (FB-UF-MR) for direct treatment of raw municipal wastewater to enable potable water reuse with integrated energy recovery. *Separation and Purification Technology*.

Abstract: A hydraulic optimized pilot-scale fluidized bed ultrafiltration membrane reactor (FB-UF-MR) for water reclamation with integrated energy recovery was designed and operated for 576 days with raw municipal wastewater from a local wastewater treatment plant (WWTP). The fluidized bed flow regime was optimized by a computational fluid dynamic (CFD) model and a tailored impact plate. Thus, the recirculation flow rate and energy demand could be reduced by approximately 38%. Granular activated carbon (GAC) was used as fluidized medium and proofed as successful fouling mitigation strategy, even at low concentration of 1.7–3.3 g/L (relating to the total reactor volume) or 21–41 g/L (relating to the fluidized bed volume). The optimal operational conditions of the FB-UF-MR were identified at (i) a flux of 7–11 LMH, (ii) an optimal backwash flux of 1.2 times of the permeate flux (8–13 LMH), (iii) a time cycle operation of 10 min consisting of 9 min filtration and 30–60 sec backwashing and optional 30 sec relaxation. Chemical cleaning was applied every 4–6 weeks during long-term operation. Main foulants of the wastewater matrix were identified with 3D-fluorescence excitation-emission matrix (3D-EEM) measurements coupled with parallel factor (PARAFAC) analysis suggesting that protein-like organic matter were the main constituent of the cake layer. The results of this study indicate that direct treatment of raw municipal wastewater with UF is a promizing option. Thus, it is possible to concentrate C and N (in a subsequent treatment step) for improved energy recovery while facilitating water reuse.

Keywords: Fouling mitigation; energy efficiency; fluidized bed; hydraulic optimization; wastewater treatment; potable water reuse

Highlights:

- Hydraulic optimized membrane reactor with fluidized bed (GAC) as fouling mitigation

- Design of a computational fluid dynamic (CFD) model with a tailored impact plate resulted in ~38% less recirculation flow rate and energy demand
- Transmembrane pressure increase was reduced by 51–97% by using a GAC fluidized bed
- Identification of main foulants with 3D-EEM measurements coupled with PARAFAC

7.1.1 Introduction

Water scarcity is becoming a major challenge in many regions worldwide. Potable water reuse offers the opportunity of a safe and sustainable water supply option and is commonly characterized by usage of conventional activated sludge (CAS) treatment plant effluent followed by different advanced water treatment (AWT) process combinations. Typically, these potable water reuse schemes are characterized by relative high energy demands (~1.2 kWh/m³) (Tchobanoglous et al. 2011, Cooley and Wilkinson 2012, Horstmeyer et al. 2018), mainly depending on the specific treatment configuration, wastewater characteristic, effluent criteria, facility´s capacity and other boundary conditions. The potential chemical-bound energy content of wastewater is approximately 2 times higher (~2.5 kWh/m³) (McCarty et al. 2011, Horstmeyer et al. 2018). Since energy-efficiency becomes a key issue in future wastewater treatment, alternative potable water reuse schemes are needed with improved and enhanced energy recovery strategies from carbon (C) and nitrogen (N). These alternative potable water reuse schemes can integrate improved and enhanced energy recovery strategies and can reduce the net energy balance by 38–80% (Horstmeyer et al. 2018). Thereby, membrane treatment can be considered not only as a barrier for the removal of contaminants to guarantee a sufficient water quality but also for the intended production of concentrated C and N water streams to enable improved and enhanced energy recovery. Direct treatment of raw municipal wastewater with ultrafiltration (UF) membrane treatment is one option to separate particulate (UF retentate) and dissolved (UF permeate) fractions of the wastewater constituents. The UF retentate contains mainly particulate carbon which can be utilized in an anaerobic digester for improved methane production. The UF permeate contains only dissolved fractions, including ammonia-nitrogen (NH_4-N) which can be further concentrated for nitrogen recovery by downstream reverse osmosis (RO) membrane treatment. The RO concentrate can be subsequently fed to an anaerobic digester to utilize the dissolved organic carbon for methane production. The digester effluent (still containing concentrated NH_4-N) can be transferred to the coupled aerobic–anoxic nitrous decomposition operation (CANDO) process as an enhanced energy recovery strategy from nitrogen. The CANDO process is a double-stage biological process which converts the NH_4-N into nitrous oxide (N_2O) (Scherson and Criddle 2014, Scherson et al. 2014, Weißbach et al. 2018). The N_2O can be utilized as an oxygen source together with the produced methane in combined heat and power (CHP) units.

Membranes are pressure driven systems, either operated at net positive pressure (RO spiral wound membranes) or at net negative (vacuum) pressure (e.g. outside-in hollow fibre UF

membranes). Thereby, the transmembrane pressure (TMP) is the pressure that is built up between the feed and permeate side of the membrane. At constant flux operation, the increase of TMP during filtration due to coverage of the membrane pores and surface by deposits with a subsequent loss in permeability (membrane fouling phenomena) can be used as a fouling indicator. Existing membrane fouling mitigation strategies are based on hydrodynamics (e.g. higher shear stress by higher cross flow velocities) or shear stress enhancement by scouring. These membrane fouling strategies require a high energy demand (mean 5 kWh/m³ for cross flow systems; mean 1.5 kWh/m³ for submerged gas sparging) (Aslam et al. 2017a). Sustainable and energy efficient membrane treatment (e.g. with UF and RO) is a key element of the alternative treatment trains and require the development of energy efficient membrane fouling mitigation strategies. Anaerobic treatment of municipal wastewater offers the possibility to establish more energy-efficient wastewater treatment (McCarty et al. 2011). However, anaerobic treatment (i) increases the fouling potential of membrane treatment applications and (ii) requires membrane fouling strategies without air scouring. A promising fouling mitigation strategy for improved operational performance of the membrane systems are fluidized bed reactors (FBRs) that allow membrane fouling control via mechanical cleaning with a fluidized inert material (e.g. GAC) and specific hydraulic conditions that increase the shear stress on the membrane surface. FBRs with GAC as fluidized material proofed to be a successful fouling mitigation strategy for wastewater treatment applications (Aslam et al. 2017a, Aslam et al. 2014, Aslam and Kim 2017, Aslam et al. 2017b). Kim et al. (2011) investigated a combined anaerobic fluidized bed reactor (AFBR) with an anaerobic fluidized bed membrane reactor (AFMBR) in bench-scale application and UF hollow fibre membranes. The AFBR reactor was operated with synthetic wastewater as feed, while the AFBR effluent was fed to the AFMBR. In the AFMBR GAC was used as fluidized medium (225 g/L). Bae et al. (2014) reduced the 2-stage system to a single stage operation (only AFMBR) and also used synthetic wastewater. The achieved flux varied between 6–9 LMH. The AFMBR was operated for 200 days with no backwash and two chemical cleanings.

In this study, we investigated the feasibility and optimal operational conditions of a pilot-scale fluidized bed UF membrane reactor (FB-UF-MR) with an optimized flow regime for a fluidized bed with GAC (no AnMBR). The hydraulic conditions were optimized by a CFD model to establish controlled shear forces along the membrane fibres. As feed matrix, raw municipal wastewater from a local WWTP was used. In a parameter study, the effect of GAC in a fluidized bed as fouling mitigation strategy and the optimal operation conditions were analyzed over a period of 576 days of continuous operation.

7.1.2 Materials and methods

7.1.2.1 Membrane reactor design / Establishment of a fluidized bed flow regime

The pilot-scale FB-UF-MR was designed with a single header UF demo membrane module with 245 hollow fibres in outside-in operation (PURON®, Koch Membrane Systems Inc., Wilmington, MA, USA). Nominal membrane pore size was 0.03 µm, fibre outside diameter 2.6 mm, fibre length 250 mm, total membrane surface area 0.5 m², and membrane material polyvinylidene fluoride (PVDF). The membrane module was installed in the reactor tank with the end of the fibres directed to the top of the reactor.

The membrane reactor design was pre-evaluated with hydraulic optimization (see chapter 7.1.3.1) and resulted in a reactor design with a conical bottom part (V=5 L), a cylindrical middle part (V=20 L), and a settler unit on top of the reactor (V=56 L) (Figure 25). Thus, the total volume of the membrane reactor was 81 L, the effective reactor volume was 75 L (membrane module dead volume 6 L). The total height of the reactor tank was 1.5 m, the height of the cylindrical middle part with the membrane module was 0.7 m with a diameter of 0.19 m. The settler unit was designed with a CFD model and tested in real operation with GAC to guarantee full retention of the GAC in the reactor (see chapter 7.1.3.1). The geometric design resulted in a height of 0.6 m and a top diameter of 0.42 m (2.2 times of membrane reactor middle part diameter resulting in 4.8 times less average up-flow velocity).

The hydraulic cycle of the membrane reactor consisted of the feed tank (V=1,000 L), the membrane reactor itself, and the permeate tank (Figure 25). The feed water was supplied by a peristaltic pump (Heidolph 52213 PK 3, Heidolph Instruments GmbH & Co. KG, Schwabach, Germany) to the membrane reactor tank. A second peristaltic pump (Watson-Marlow 314FDM/DX2, Watson-Marlow Fluid Technology Group, Falmouth, UK) was used for filtration and reversed flow direction for backwashing. The permeate was collected in an acrylic glass tank (V=60 L). Recirculation was realized by a centrifugal pump (Lowara CO4 500/03K/A, Xylem Inc., Rye Brook, NY, USA). The whole reactor was gas tight in order to inhibit biological and chemical reactions by the entry of oxygen.

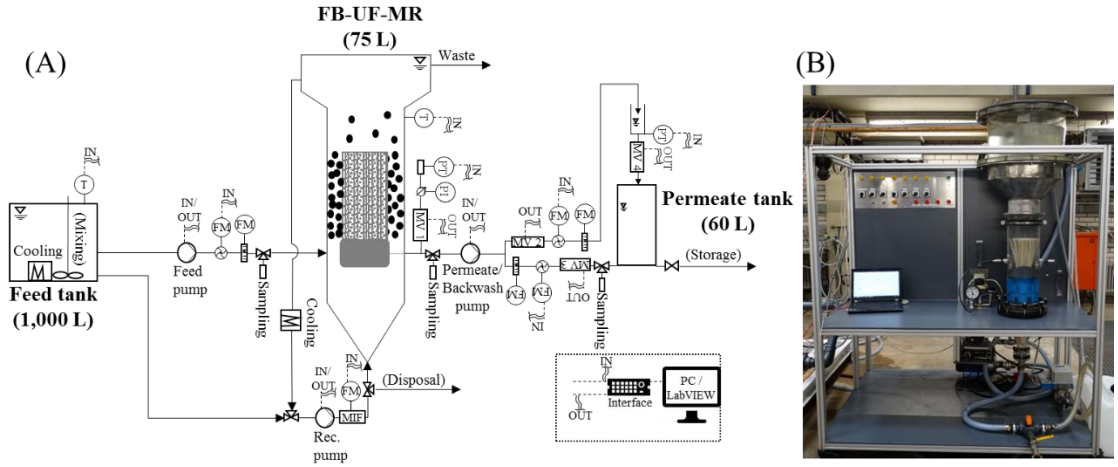

Figure 25 (A). Schematic of the fluidized bed ultrafiltration membrane reactor (FB-UF-MR), **(B).** Photo of the FB-UF-MR assembling. T=Temperature, FM=Flowmeter, PT=Pressure transducer, PI=Pressure indicator (manometer), MV=Magnetic valve, MIF=Magnetic-inductive flowmeter.

The establishment of the fluidized bed flow regime was ensured by considering the hydraulic conditions and characterization of the fluidized medium. A CFD model was programmed in Siemens NX™ (version 8.0, Siemens PLM Software Inc., Plano, TX, USA) to simulate the velocity distribution of the fluid in the reactor and configurations in reactor design and impact plate. Geometrical variations (reactor height and diameter, design of an impact plate) were tested with various recirculation flow rates until an optimum was found. The CFD model was set up under application of a shear stress transport turbulence model. The solving approach was the finite volume method, using tetraedic cubes with an edge length of 5 mm on average. The incompressible fluid was programmed as pure water (T=15 °C, ρ=999.1 kg/m³, μ=1.039x10^{-3} kg/(m*s)).

As fluidized medium GAC CYCLECARB 401® (Chemviron, Feluy, Belgium) was used. To characterize the flow behavior of the GAC, both the fluid and the particles were analyzed and described in rheology tests. The fluid was analysed regarding temperature, density, kinematic and dynamic viscosity. The analysed parameters of the GAC were mean particle diameter, density, sphericity and the stationary settling time of the particles. The determination of the settling velocity of the particles at zero recirculation flow was important for the mathematical description of a fluidized bed regime, as it reveals information about the geometrical deviation of the particles from an idealized sphere. In a settling test, 5 g of wetted GAC was put in a cylindrical column (height = 0.8 m) filled with tap water and the time was measured until it settled to the bottom. Measurements were applied with 50 repetitions. Since the smallest fraction of GAC particles was generally flushed away or was swimming on top of the reactor, the fraction of particles smaller than 1 mm and larger than 2 mm was excluded from the bulk by sieving to provide a more uniform particle size

distribution (see Cyclecarb 401®, modified, see Table SM4, supplementary material, Appendix E).

Modeling results were validated at a pilot-scale application with tapwater and raw wastewater to (i) verify the CFD model results, (ii) characterize the fluidized bed flow regime, (iii) to identify the minimum recirculation flow rate, and (iv) to define the reactor geometries inlet and outlet and final reactor with opening at the top. Pre-validation-tests were conducted with a membrane dummy module (see chapter 7.1.3.1, Figure 26). Different particle size and concentration were tested to determine an optimum for a stable and equal distributed fluidized bed. GAC concentration was varied from 1–5 g/L (based on total reactor volume) or 12.5–62.5 g/L (based on fluidized bed volume of 6 L and expansion of 20 cm). Long-term operation was performed with a mean concentration of 2.5 g/L (reactor volume) or 31.3 g/L (fluidized bed volume). These concentration are low in comparison to other studies (e.g., Kim et al. (2011) used 225 /L, Bae et al. (2014) used 189 g/L).

7.1.2.2 Raw wastewater generation / Feed matrix characteristics

Raw wastewater was provided weekly from the WWTP Garching, Germany (PE 31,000; flowrate 1.7 Mm³/year). Wastewater was transferred after a bar rack (8 mm) and 4 mm drum screen via pipeline to the laboratory. The pipeline was flushed for a minimum of 20 min before the wastewater was collected. The collected raw wastewater was further pretreated by 20 min sedimentation and microsieving (100 µm) before it was stored as feed matrix for the FB-UF-MR. Table 15 summarizes the key parameters of the raw, settled and microsieved wastewater from the WWTP Garching. From November until December 2016 wastewater was collected from the WWTP Munich – Gut Marienhof (PE 1.7 M, flowrate 80 Mm³/year). Wastewater was collected after a bar rack (40 mm and 20 mm) and grit chamber in 1 m³ tanks and was directly transported to the laboratory. Wastewater pre-treatment was the same like for the wastewater from the WWTP Garching. The parameters of the raw, settled and microsieved wastewater from the WWTP Munich are summarized in Table SM5, supplementary material, Appendix E.

Table 15. Key parameters of the raw, settled and microsieved wastewater matrix (WWTP Garching).

		Raw Wastewater	Settled Wastewater	Microsieved Wastewater
TOC	**[mg/L]**	96 ± 31 (41)	92 ± 29 (28)	84 ± 26 (56)
COD	**[mg/L]**	492 ± 122 (56)	449 ± 91 (50)	399 ± 99 (60)

EC	**[µS/cm]**	1,444 ± 240 (43)	1,439 ± 239 (43)	1,442 ± 228 (46)
SUVA	**[L/(mg cm)]**	0.78 ± 0.20 (10)	0.81 ± 0.19 (7)	0.87 ± 0.27 (16)
NH_4-N	**[mg/L]**	52 ± 7 (19)	51 ± 9 (8)	51 ± 7 (31)

7.1.2.3 Reactor operation, data acquisition and processing

The FB-UF-MR was operated fully automated with a LabVIEW™ control (LabVIEW™ 2016, National Instruments, Austin, TX, USA), remote control and electromechanical safety cabinet. Automatic data acquisition was realized with an interface (LabJack™ U6 Pro, LabJack Corporation, Lakewood, CO, USA) and LabVIEW™ logging in Microsoft Excel (.csv-files). TMP, flow rates (feed, recirculation, permeate, and backwash flow), temperature were logged automatically. Sensor calibration was applied on a weekly basis. Bubble test of the membrane was applied on a monthly basis. Membrane fouling development was determined by evaluating the TMP over time. The TMP was measured as fouling indicator with a pressure sensor (JUMO dTRANS p30, JUMO GmbH & Co. KG, Fulda, Germany) with a measurement range between -1.0 to 0.6 bar. Cleaning during operation was applied by backwash-cycles in cycle operation mode with permeate water. Chemical enhanced backwashing (CEB) was applied with a 1,000 ppm sodium hypochloride (NaOCl) solution if the pressure limit of 0.3 bar was reached or a test campaign required comparable starting conditions of TMP (e.g. parameter study). After cleaning the relative pressure p_{perm} was 50 mbar.

7.1.2.4 Analytical methods

For TOC measurements a Vario TOC cube analyzer from Elementar Analysensyteme GmbH was used. The UV absorbance of samples at 254 nm (UVA_{254}) was measured using an UV-visible spectrophotometer from Shimadzu (UV-1601) and a QS high precision cell cuvette made of quartz SUPRASIL® from Hellma Analytics. COD and NH_4-N were analysed using the Hach Lange tests (HACH Company) and the Hach Lange spectrometer DR 6000 (HACH Company). Conductivity was measured using the inolab cond 730 with the TeraCon® 325 sensor, manufactured by WTW GmbH & Co. KG. TSS..

3D-fluorescence excitation-emission spectroscopy and PARAFAC analysis were used as characterization methods for DOM as main foulant. Samples were filtered through a 0.45 µm filter

and measured diluted. The fluorescence 3D-EEMs of all samples were measured at room temperature (20 ± 1 °C) using the Aqualog™ by HORIBA Scientific and Aqualog™ V3.6 software. A QS high precision cell cuvette made of quartz SUPRASIL® by HellmaAnalytics with a light path of 10x10 mm was used. For the PARAFAC analysis, a 3-component model was established. To create the model, a total number (n) of 115 data points was used. The model possessed a core consistency of 81 %. Performed split-halve analysis indicated 96 % agreement between excitation and emission loadings modeled for the two parts of the whole data set.

7.1.3 Results and discussion

After commissioning of the test skid a stable fluidized bed with a certain GAC concentration was established. A parameter study was performed over 30 days with six measurement campaigns to identify the optimal operational conditions. Key optimization parameter were (i) GAC concentration, (ii) permeate flux, (ii) backwash flux, and (iii) cycle operation time. Long-term operation of the FB-UF-MR was performed over 576 days to analyse long-term effects and verify the results from the parameter study. A campaign using another feed wastewater (WWTP Munich) verified the feasibility of the direct treatment of municipal raw wastewater by FB-UF membrane treatment.

7.1.3.1 Establishment of a fluidized bed flow regime

The hydraulic conditions of the FB-UF-MR are illustrated by a flow diagram (Figure SM3, supplementary material, Appendix E). By illustration of the flow regime with the parameters, the dimensionless superficial fluid velocity U* and the particle diameter d_p*, measured values in a specific fluidized bed could be dedicated to one of three flow regimes: (i) the fixed bed regime, where the superficial velocity is insufficient to fluidize the particles, (ii) the fluidized bed regime, where particles are fluidized, and (iii) the transport regime, where the superficial velocity is too high for a stable fluidization and particles are carried out of the reactor. The stationary settling velocity was determined to be u_0=0.11 m/s.

To optimize the fluidized bed a CFD model was applied (Figure 26). The variation of the geometrical variations (reactor height and diameter, design of an impact plate) resulted in a final design including a tailored impact plate to guarantee a turbulence flow regime along the membrane fibres (and equal distributed fluidized bed) while reducing the recirculation flow rate to a minimum level (Figure 26). The flowrate required for a 100% fluidized bed expansion (fluidization to a height of 950 mm) without the impact plate was determined to be approximately 4 m³/h. After installation of the impediment, the recirculation flow could be reduced to 2.5 m³/h. Thus, the flowrate was reduced by 38% (Figure 26B). The results were verified with tapwater and raw wastewater and fluidized material (Figure 26D).

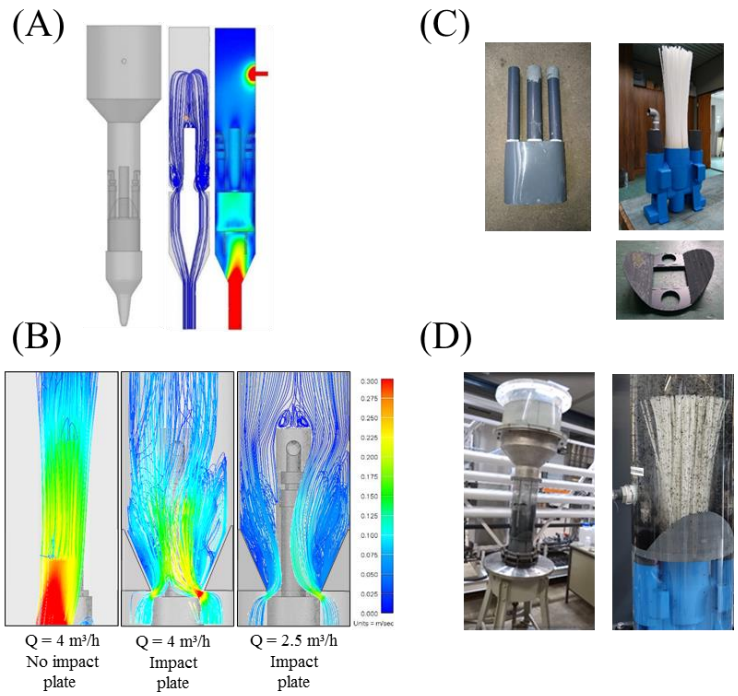

Figure 26 (A). Computational fluid dynamic (CFD) front view of the cylindrical reactor design, **(B).** Shear stress model with a recirculation flow of 4 m³/h with and without impact plate and 2.5 m³/h with impact plate, **(C).** Visualization of the membrane module dummy, real membrane module and impact plate, **(D).** Experimental setup for the hydraulic pretests to verify CFD results.

7.1.3.2 Optimal operational parameters

Effect of GAC concentration

The main goal of the following experiments was to determine the quantitative influence to fouling mitigation by using a fluidized bed of GAC. The applied concentration of GAC was 2.5 g/L (determined during pretests, see chapter 7.1.3.1). The effect of an established fluidized bed with GAC was analyzed with varying permeate flow and backwash time in a series of experiments (Figure 27). Without GAC in the reactor the membranes are blocked severe. With GAC in the reactor the TMP slope is significant lower compared to a non-fluidized bed with GAC. These results proof that GAC in a fluidized bed is an excellent anti-fouling mitigation strategy. The GAC particles scrub along the membrane and exert a considerable shear force. While this does not have significant effects on the different types of pore blocking, it successfully scrubs off the cake layer as soon as it forms. These findings regarding the influence of GAC are in agreement with the results from Kim et al. (2011).

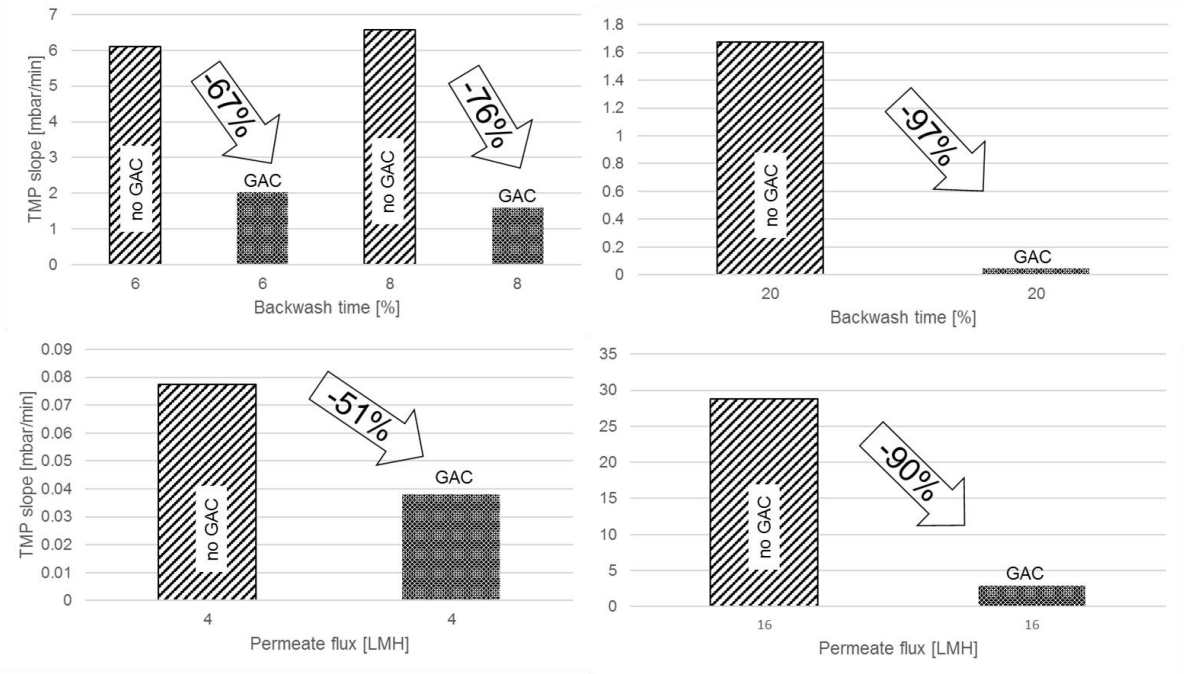

Figure 27. Effect of granular activated carbon (GAC) addition of 2.5 mg/L and varying permeate flow and backwash time on the TMP slope = fouling rate in mbar/min.

Permeate flux

The optimal permeate flux regarding fouling mitigation in this study was identified at 8-10 LMH during the parametric study (Figure 28). At this permeate flux the TMP slope is low enough to guarantee a sustainable membrane operation. Depending on the cleaning intervals the TMP slope needs to be elected. E.g. for a 4-week operation without membrane cleaning the TMP slope has to be lower than 0.028 mbar/min to guarantee sustainable operation.

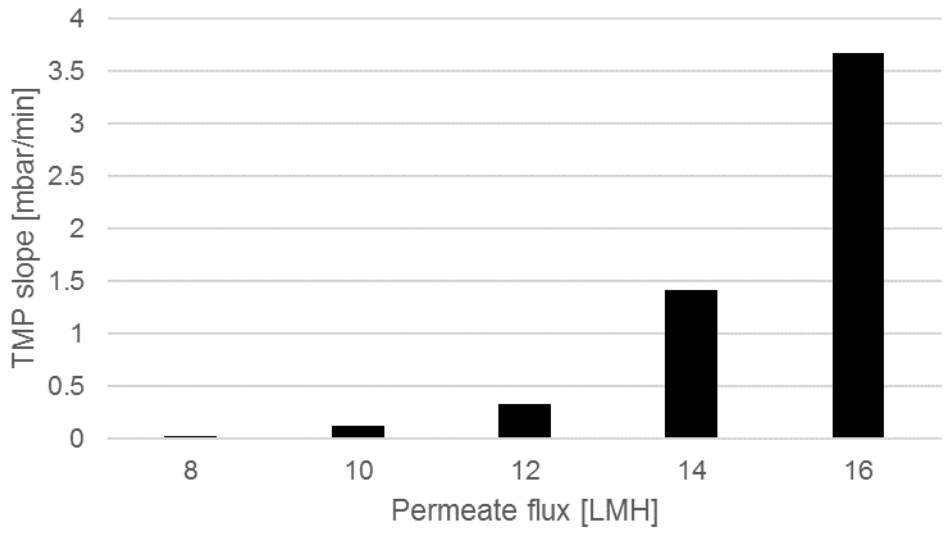

Figure 28. Investigation of permeate flux as a function of TMP pressure slope. Cycle length 5min, recovery 70%, backwash flow 6 L/h, backwashtime 20%.

A typical pressure development during two cycles is presented in Figure 29. After starting the filtration mode, the TMP first rises sharply then continually less strongly. During backwash, the pressure is not monitored indicated as a horizontal line. The new cycle starts at approximately the same pressure as the one before after 10 minutes, so a sudden drop appears at that point in time. The evaluation indicates an exponential increase of the pressure slope with the permeate flow rate. Melin (2007) also confirm the exponential development of the fouling rate (pressure slope) with permeate flow.

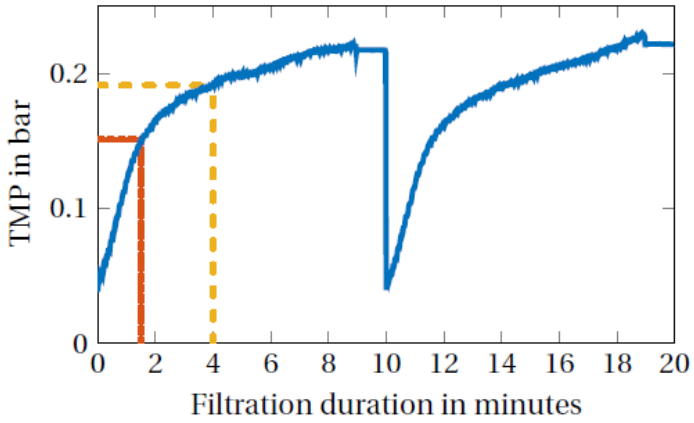

Figure 29. TMP development during two operating cycles.

Cycle length

The total cycle length was systematically varied between 300 and 900 sec (Figure 30). The optimal cycle operation regarding membrane fouling was identified with 540 sec filtration, 30 sec backwashing, and 30 sec settling.

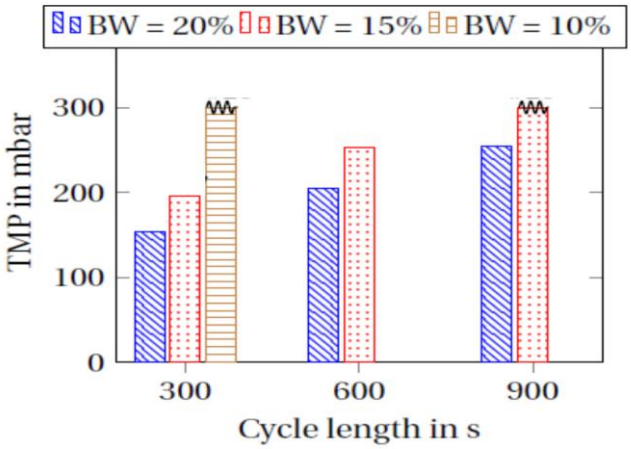

Figure 30. Comparison of the TMP during variation of the cycle length. BW = Backwashing. BW = 20% indicates that the time duration of BW was 20% of the total cycle time.

Backwashing

The effect of backwashing was evaluated on two parameters, the backwash flow and the backwash time/duration (Figure 31). The different backwash settings, varying between 4 and 16 LMH are displayed in Figure 31. At higher backwash flow rates the TMP pressure slope decreases. When the backwash flow was further increaed to 16 LMH, the pressure slope increase was higher as compared to 12 LMH. This could either be due to a temporal effect or could indicate that increasing the backwash flow rate above a certain limit (here 12 LMH) does not further improve the cleaning effect, but rather results in some adverse impacts. Thus, we determined the optimal backwash flow to be 1.2 times the permeate flow. Ye et al. (2010) and Chua et al. (2003) confirmed these findings. Ye et al. (2010) investigated the effects of different backwash settings on fouling in an UF bench-scale module and determined an optimum of a backwash flux 1.5 times higher than the permeate flux. Chua et al. (2003) confirms these finding with a 2 times higher backwash volume.

The second varied parameter was the backwash time/duration. The changing backwash time values between 2 and 16% can be obtained from Figure 31. The optimal backwash duration was determined with 5-10% of cycle length (30–60sec.) Ye et al. (2010) also reported a decreasing

pressure slope for longer backwash durations. However, their filtration time of 3,600 sec was much longer because of the completely different feed (seawater), so the required backwash time was much smaller between 2.77% (10 sec backwashing) and 1.64% (60 sec backwashing).

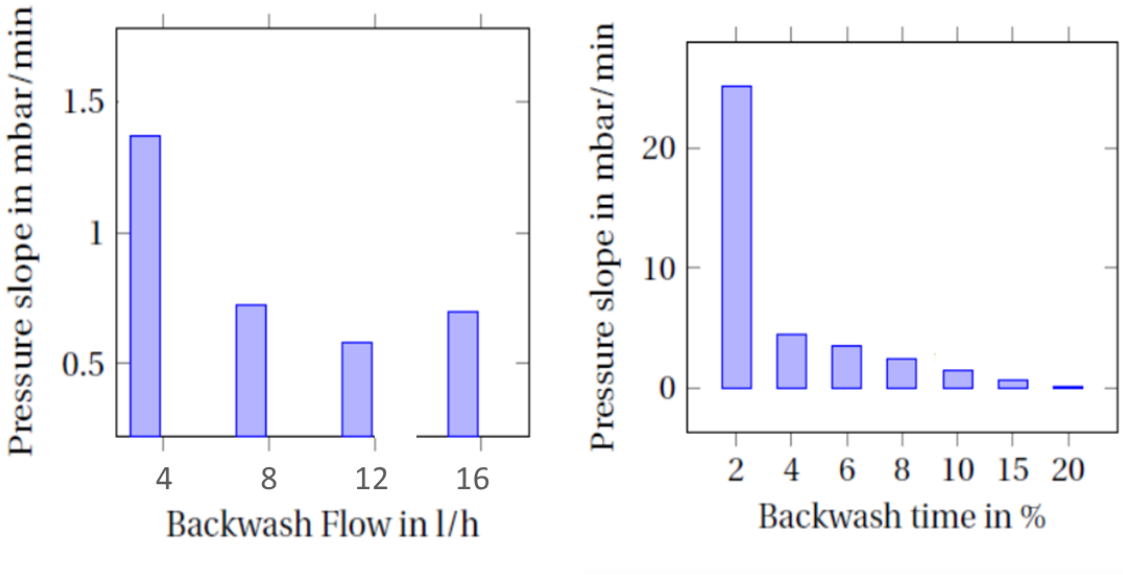

Figure 31. Investigation of backwash flow and backwash time as function of TMP pressure slope. Cycle length 5 min, recovery 70%. Backwash time is defined as the partial time of backwashing of the total cycle time.

7.1.3.3 Performance during long-term operation

The FB-UF-MR was operated for 576 days (Figure 32). After a start-up phase and commissioning of the reactor, the parametric study was applied (Day 1–36). During the parametric study the optimal operational conditions were identified. Long-term operation started from day 36–576 with the general settings of 8–10 LMH of permeate flux, a cycle operation of 540 sec filtration, 30 sec backwashing, and optional 30 sec settling. Recovery was set to 70–85 %. Backwashing was applied with a flux of 12–16 LMH and 30–60 sec. The operation of the FB-UF-MR was possible without major disturbances. However, the TMP development was partially highly variable. Chemical cleaning was applied after the TMP reached 0.3 bar, appromimately every 4–6 weeks. GAC in a fluidized bed resulted in a positive effect against fouling. The mean removal rates of the core parameters indicate that the FB-UF-MR was able to separte the particulate and dissolved fractions of the constituents (Table 16). Thus, the mean removal rate of TOC was 60%, meaning that only the dissolved fraction of organic carbon is present in the permeate as DOC. The dissolved

NH_4-N fraction was not removed during UF treatment as intended for the subsequent concentration in downstream RO treatment (Horstmeyer et al. 2018).

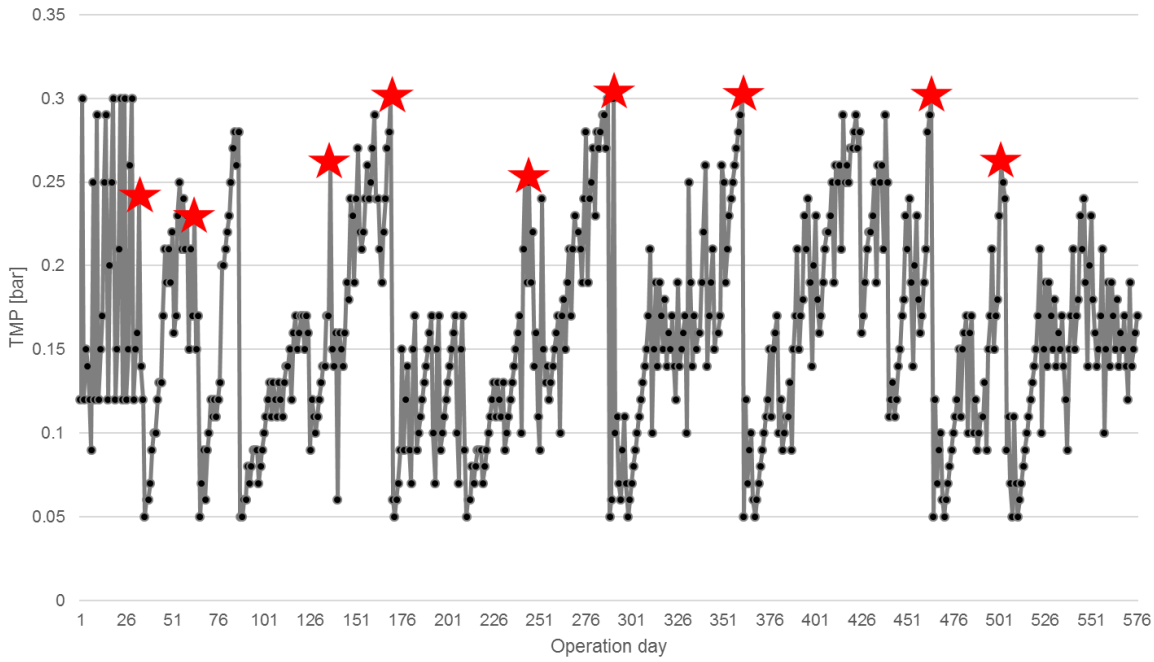

Figure 32. Long-term performance of the FB-UF-MR. Chemical cleanings are marked with a red star.

Table 16. Mean removal rates of the FB-UF-MR.

		Settled Wastewater	UF Permeate	Mean Removal [%]
TOC	**[mg/L]**	84 ± 26 (56)	34 ± 6 (66)	60
COD	**[mg/L]**	399 ± 99 (60)	70 ± 19 (57)	82
EC	**[µS/cm]**	1,442 ± 228 (46)	1,391 ± 328 (56)	3
SUVA	**[L/(mg cm)]**	0.87 ± 0.27 (16)	0.78 ± 0.12 (17)	10
NH_4-N	**[mg/L]**	51 ± 7 (31)	58 ± 9 (37)	-14

7.1.3.4 Identification of main membrane foulants

To identify the main membrane foulants of the feed matrix, 3D-fluorescence spectroscopy was applied. The feed matrix was analyzed over aperiod of 1 year to identify the main dominant peaks in the 3D-EEM spectras. With a PARAFAC analysis it was possible to isolate three characteristic components in the matrix (Figure 33). Thus, in the present matrices, basically all type of NOM (protein-, fulvic- and humic-like matter) can be found. Component 1 was identified as protein-like (tryptophan) peak, component 2 as humic-like (marine and terrestrial) peak, and component 3 as humic-like (terrestrial delivered) peak. After 6 month of operation the cake layer of one UF hollow-fibre was scraped off, dissolved and diluted in DI water. Subsequently the sample was analyzed with 3D-EEM measurements. The protein-like matter fluorescence peak was identified as dominant cake layer peak (Figure 34).

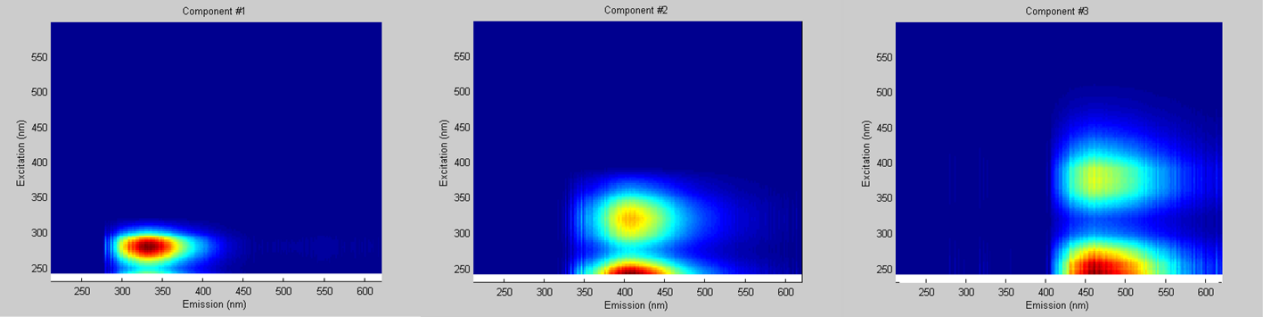

Figure 33. 3-component model of UF feed and permeate samples.

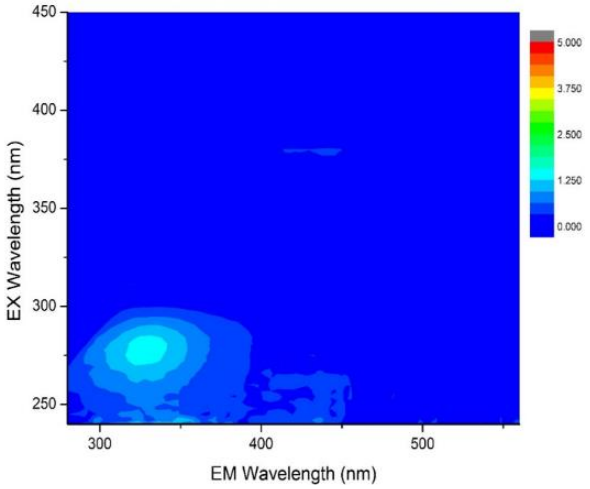

Figure 34. 3D-fluorescence excitation-emission matrix (3D-EEM) spectra of the isolated cake layer.

7.1.4 Conclusions

In this study, a FB-UF-MR was designed, constructed and operated to evaluate the possibility of direct treatment of raw municipal wastewater by UF membrane treatment. Based on the results within this study, it can be revealed that GAC proofed to be a successful anti-fouling strategy. Thus, it was possible to operate the FB-UF-MR over a long-term period of 576 days without major disturbances. Chemical cleaning was necessary every 4–6 weeks. As main foulant within the wastewater matrix, protein-like matter was identified. The particulate and dissolved carbon and nitrogen constituents can be seprated by UF treatment and enable the intended production of concentrated C and N water streams. In detail, the mean TOC removal rate of the FB-UF-MR is 60 %, while the NH4-N is not removed during UF treatment and can be subsequently utilized in downstream water treatment.

7.1.5 Acknowledgements

This research was funded by the Oswald-Schulze Foundation and seed funds provided by the Chair of Urban Water Systems Engineering at TUM. The membrane module was provided by KOCH. Philipp Sperle supported the 3D-EEM measurements and data evaluation.

7.2 Further optimization of the FB-UF-MR (fluidized bed vs. packed bed experiments)[1]

The operational feasibility of an FB-UF-MR pilot-scale system as an initial membrane stage for the treatment of raw raw municipal wastewater of a potable reuse train was demonstrated in chapter 7.1 (Publication #5). However, further investigation and improvement was intended and necessary, in particular in context of establishing a higher system efficiency (i.e., higher permeate flux, improved fouling mitigation, less required chemical cleanings, and less required energy demand required for fouling mitigation). The bulk recirculation for fouling control, used to create the fluidized bed, causes a high-energy consumption. Thus, this chapter focuses on the following objective:

> *Can lower or similar fouling rates be achieved with higher GAC concentrations, allowing a reduction in bulk recirculation, which in turn, would enable a more energy efficient operation?*

For this purpose, a laboratory-scale UF test-skid (downscaled to ~1:10, see chapter 7.1) has been assembled to investigate the fouling mitigation potential of different GAC concentrations, in combination with distinct recirculation flow rates. To find suitable fouling control conditions, a series of combinations were conducted with lower concentrations (fluidized bed) as well as with

[1] This chapter contains information based on a student project conducted by Jonas Aniol (2017)

high GAC levels (packed bed). For the consideration of possible energy conservation, the energy requirements for the individual test settings were computed by modeling the hydraulic head losses within the recirculation line. A final test compared the best combinations that were found in the previous test phases. In addition, the adsorption capacity of GAC and its effect on the fouling rate was investigated.

Granular activated carbon (GAC)

For all conducted experiments a reactivated GAC (*CYCLECARB 401*) from *Chemviron Carbon* (Feluy, Belgium) was used. The fluidized bed test phase as well as the packed bed test phase were carried out with pre-loaded GAC. To reduce possible adsorption effects on the fouling behavior (adsorption of foulants), the GAC was exposed to the actual feed matrix for around twelve hours (4 mL/g GAC). For the direct comparison test phase, long-term loaded carbon (also *CYCLECARB 401*) was used to further minimize fouling effects. This long-term loaded GAC was previously used in a granular filter test and was treated with the tertiary effluent of the wastewater treatment plant Garching for approximately one year. For this study, this GAC was additionally exposed to raw wastewater (500 µm sieved) for more than one week (daily replacement of the wastewater) before it was used for fouling behavior experiments. To avoid deposition of finer GAC fractions on the membrane surface, the GAC was always wet sieved (0.5 – 2.5 mm). Pore blocking due to fine activated carbon particles (PAC) was observed by Ying and Ping (2006) and Shin et al. (2016). However, a later release of leftover fine particles or the formation of new fine particles during the experiments, probably due to abrasion, could be observed in the experiments.

Fluidized bed formation

The formation of a fluidized bed, the magnitude of GAC particle motion and transport height, depends on the hydraulic conditions created in a reactor. One important parameter is the upflow velocity that exists in the respective vessel or basin. However, for this test-skid a comparison of two different bottom nozzle diameters showed that the height of the fluidized bed highly depends on the turbulence caused by a high injection velocity. Hence, a rather slim nozzle diameter of 6.2 mm was chosen for this study.

To select adequate fluidized bed settings (GAC concentrations and recirculation flow rates) for the actual test phases, regarding fouling mitigation and energy consumption, a preliminary examination was carried out. This examination indicated that the fluidized bed height increases with higher flow rates and decreases with higher GAC concentrations. Figure 35 shows fluidized beds from the pretest, with the two concentrations (50 g ≙ 7.1 g/L and 100 g ≙ 14.3 g/L) as applied in the actual test phases, at different recirculation rates. The subsequent experiments were conducted with shorter membrane modules (246 mm) to guarantee a complete fluidized bed along the membrane fibres (246 mm). The final magnitude of the fluidized bed is determined by the mentioned conditions as well as the geometry of the vessel, which influences the hydraulic behavior of the system. Here the maximal possible flow rate was determined as 3.66 L/min.

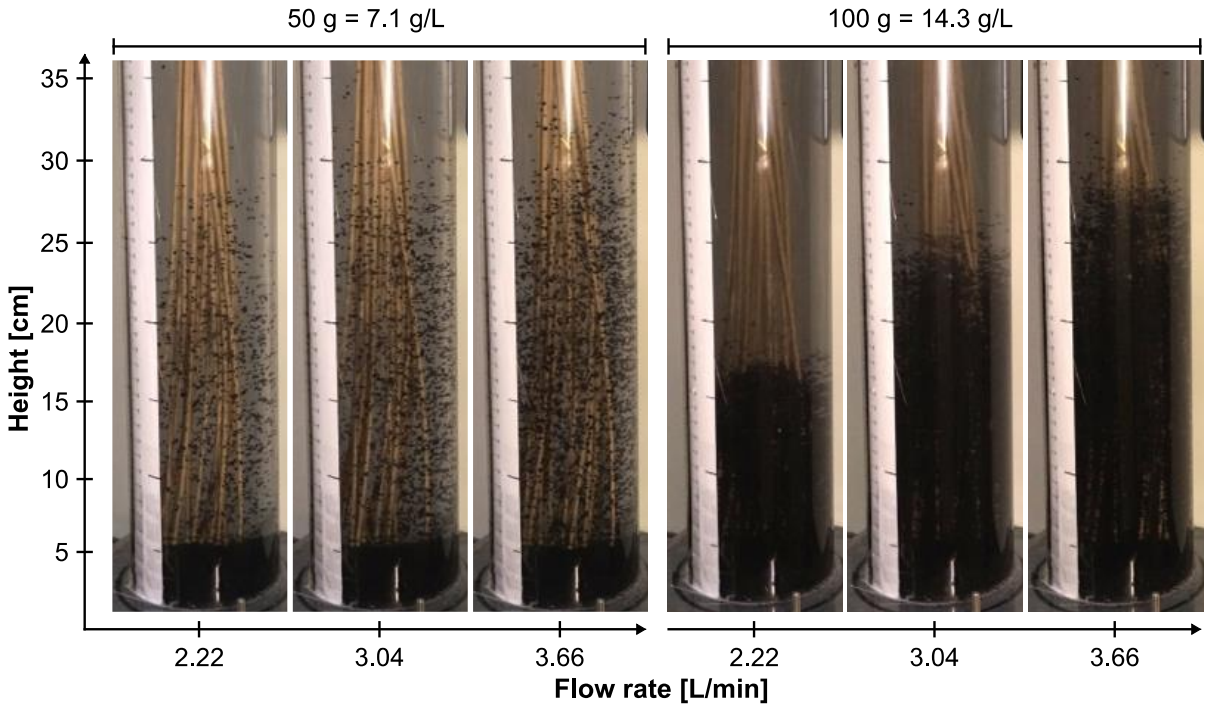

Figure 35. Appearance of the granular activated carbon (GAC) fluidized bed with different recirculation rates and GAC concentrations.

Packed bed

For the packed bed, the fibre area was half (50 % packed bed) or completely (100 % packed bed) filled with GAC. As mentioned, for the first two test phases twelve-hour pre-loaded GAC was used. For these tests, a mass (dry, fresh, and sieved GAC) of 896.1 g (100 %) or 522.7 g (50 %) was used, respectively. For later tests, where already loaded GAC (not dry) was used a volume of 2 L bulk cargo was applied (≙ 100 % packed bed). The packed bed differed from the fluidized bed in the magnitude of particle motion. Accordingly, the term packed bed does not describe a fixed bed like in GAC filters. Rather, it corresponds to a granulate bed that can be imagined with slowly and steady migrating GAC particles.

Energetic considerations

In hollow fibre membrane filtration processes the required amount of energy consists of the filtration work itself as well as of the energy demand for some kind of fouling control strategy. The latter normally comprises the creation of enhanced shear forces by mixing, aeration or recirculation (Judd and Judd 2011). The total dynamic head losses (h_{ls}) of the assumed

recirculation system were calculated (Figure SM4, supplementary material, Appendix E). The resulting characteristic curves, illustrated in Figure 36, show the high contribution of the reactor bottom nozzle (outlet). The nozzle accounts for an average of 63 % of the total dynamic head loss in the examined range of 0 – 4.0 L/min. The reason for this is the abrupt deceleration of the fluid as soon as it enters the reactor bulk media. The computed head loss values were employed to determine the respective energy demand of the bulk recirculation for the different settings of the fluidized and packed beds.

As shown before, the hydraulic loss caused in the recirculation pipes is a function of the flow velocity, which in turn depends on the used pipe diameters. Consequently, the final specific energy demand ($E_{spec,reci}$) of the recirculation, which's reduction is one of the questions assessed in this chapter, also depends on the assumptions made for the piping dimensions.

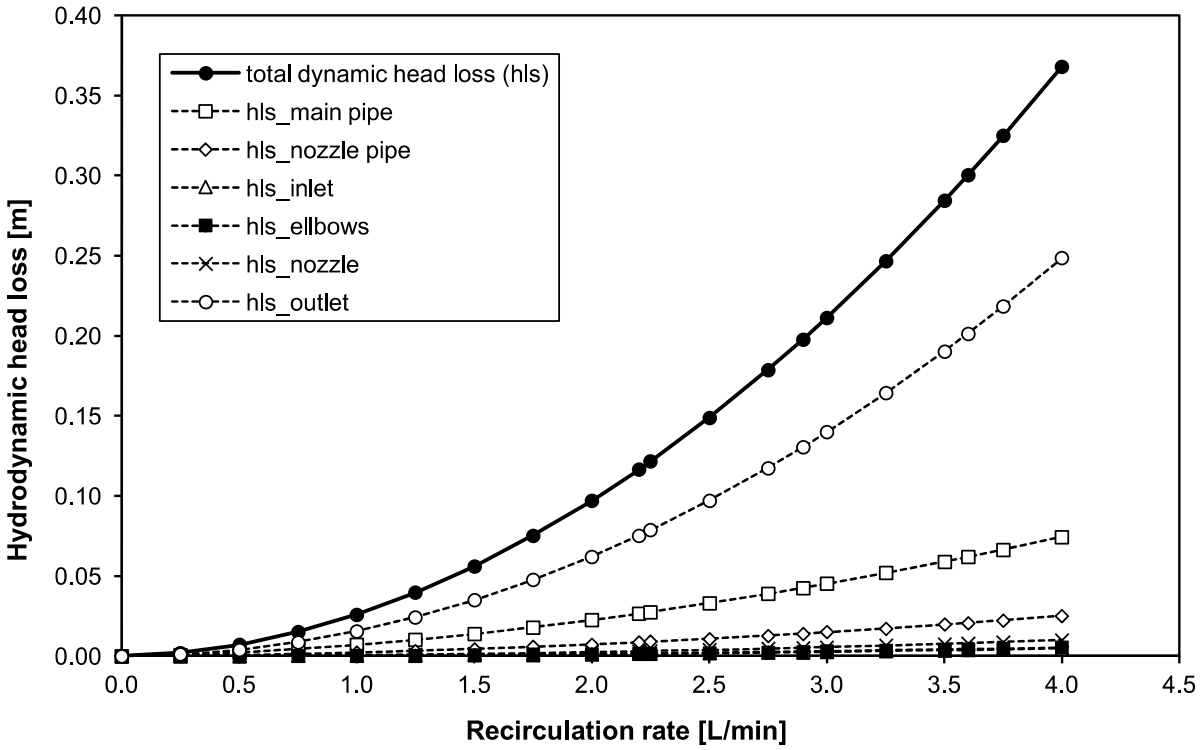

Figure 36. Characteristic curve of the recirculation pipe system, showing the total hydrodynamic head loss ($\boldsymbol{h_{ls}}$) as well as the individual parts contributing to the pressure loss as a function of the flow rate (with $\boldsymbol{\rho_{20°C}}$ = 998.2 kg/m^3, $\boldsymbol{\nu_{20°C}}$ = 1.004 * 10^{-6} m^2/s).

7.2.1 Fouling behavior with different recirculation rates and GAC concentration

The question, if a sufficient or improved fouling control in a FB-UF-MR can be achieved with higher GAC concentrations combined with lower bulk recirculation rates was examined through the fluidized bed and packed bed test series. The outcomes of these experiments are presented and discussed in the following sections.

Fludized bed

Three different flux-steps (i.e., 20, 26, 32 LMH) with each step comprising four filtration periods were tested. The pressures during these filtration periods were measured and the TMP increase over time was computed as a surrogate parameter for the fouling effect. The test results for the fluidized beds with the different combinations of recirculation flow rates and GAC concentrations are shown in Figure 37.

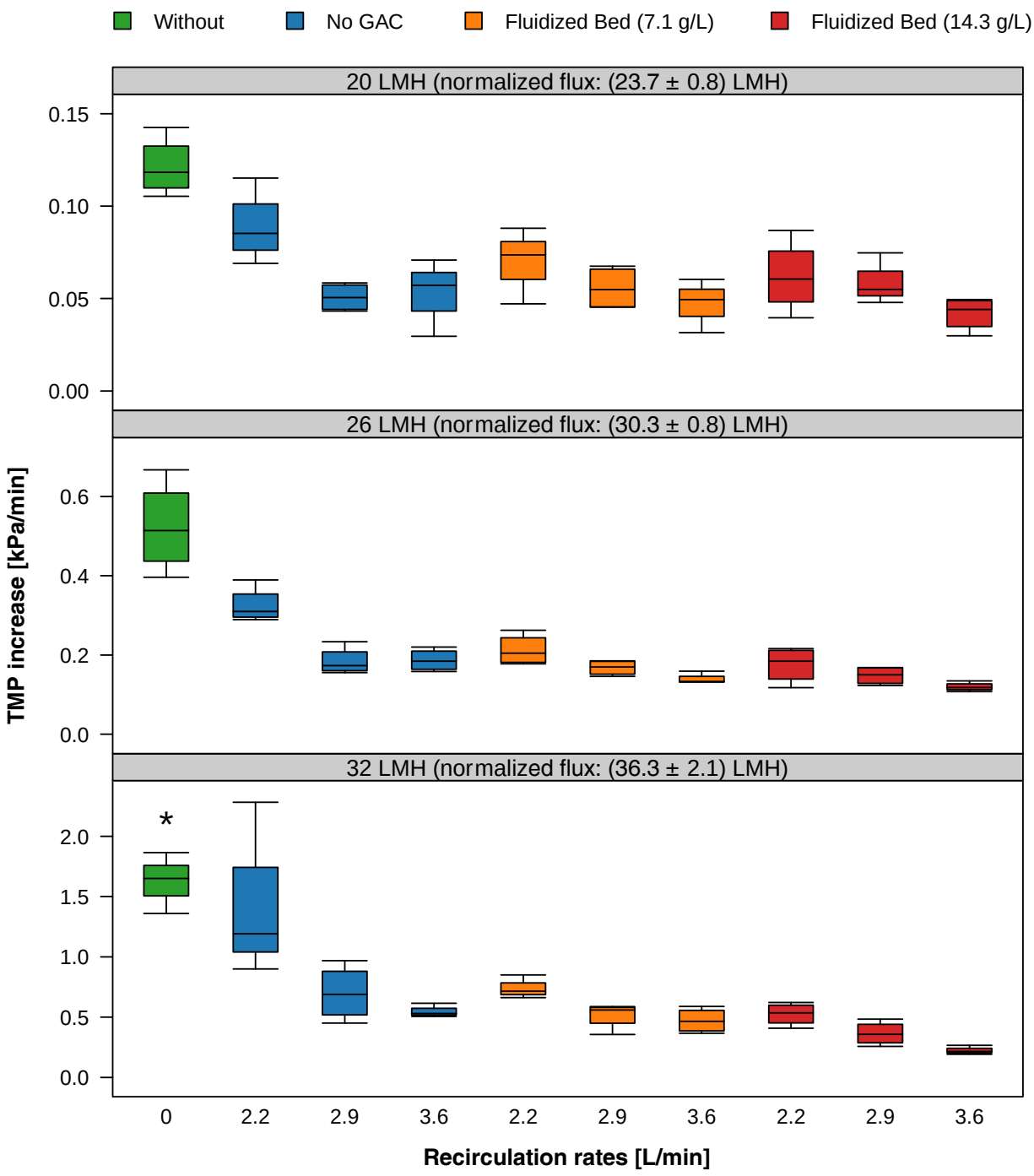

Figure 37. Fouling mitigation efficiency of fluidized beds with three different granular activated carbon (GAC) concentrations, four different recirculation flow rates, and their combinations, at three different filtration rates (four filtration periods (n = 4) per flux-step; * less or no filtration periods because pressure limit was reached).

The data of each combination are split according to the flux-steps 20, 26, 32 LMH, thus the fouling behaviors are plotted for each filtration intensity. For the flux-steps 20, 26, and 32 LMH the temperature corrected flux flows were 23.7 (± 0.8) LMH, 30.3 (± 0.8) LMH, and 36.3 s(± 2.1) LMH, respectively.

Firstly, it should be clarified that the dispersion (spread) of the above-shown data points around their respective medians have two reasons. One is the variation of practice gained measurement values, caused by small temperature differences, slight flux differences due to the limited pump control accuracy, or by unknown impacts. The second reason is the observed tendency of the total TMP as well as the TMP increase (fouling) to ascend with successive filtration periods (continuing operation). This phenomenon which was common among all the experiments was more severe the more ineffective a fouling mitigation measure became. Therefore, besides the position of the plotted medians, also the quartiles and whisker distances indicate if the fouling rate was actively expanding or not.

The blank test without fouling control (no GAC/no recirculation) had the highest fouling rates and underlines the necessity of any kind of alleviating measure. In that case, fouling acceleration was very high, and the filtration operation had to be stopped after the second last filtration period because the pressure limit of 60 kPa would have been exceeded in the next filtration cycle. Independent of the GAC mass (0, 7.1, 14.3 g/L), the impact of higher recirculation rates led to weaker fouling, which can be seen by the TMP/time decline within each GAC level. The comparisons of the fouling behavior on equal recirculation bases revealed a slight alleviating effect with higher GAC concentrations. Looking at the extremes in this test series, the vigorous and the gentler flow conditions, which are located on the right and the left side in Figure 37, differences are apparent. These relate to the total TMP, which reached 50 kPa and 26 kPa for the lowest and medium bulk recirculation without GAC, respectively, but just reached 13 kPa and 17 kPa for the highest and the medium bulk recirculation at the 14.3 g/L GAC level. The differences also relate to the TMP rise (fouling) that was very low for high GAC concentrations and very high without GAC. But considered as a whole, there seem to be no serious differences among the majority of the test combinations (middle section in Figure 37). This conclusion coincides with the results of the *Kruskal-Wallis H test* that showed a statistically significant difference of the TMP increase over time among the different batch tests (different GAC concentrations and recirculation rates) for all flux-steps (intensities). With χ^2 = 31.425, degrees of freedom (df) = 9, and p = 0.0003 at the 32 LMH flux-step level. The following post hoc test revealed differences on a 5 % significance level only between the following pairs:

- no GAC/ no recirculation – high GAC/medium recirculation (2.9 L/min)
- no GAC/ no recirculation – high GAC/high recirculation (3.6 L/min)
- no GAC/low recirculation (2.2 L/min) – high GAC/medium recirculation (2.9 L/min)

- no GAC/low recirculation (2.2 L/min) – high GAC/high recirculation (3.6 L/min)

7.2.2 Packed bed

The fouling mitigation potential of high GAC concentrations was investigated with the packed bed test series. The results are presented in Figure 38. Here, two different recirculation rates (1.5 and 3.0 L/min) and three different GAC amounts (0 %, 50 %, and 100 %) as well as one blank, without any mitigation measures, were tested. Compared to the fluidized bed examinations a lower recirculation rate (1.5 L/min) could be used for the packed bed. The reason for that were the high flow velocities necessary to drag GAC particles into the bulk solution and to develop a fluidized bed, which were not required for the packed bed. For the latter one, lower flow rates were capable of lifting the bed and causing gentle migration/movement of the GAC particles that was still visually discernible. Another difference compared to the first test phase was the much higher wastewater loading (423 – 420 mg/L COD instead of 281 – 284 mg/L COD; see Table SM7, supplementary material, Appendix E), which posed more severe fouling conditions.

On the other hand, these conditions emphasized the good fouling control potential of the packed bed. In this test phase, the membrane fouling was very high for the blank test, so that the pressure limit was already reached at the end of the second flux-step (Figure 38). Nonetheless even the pure bulk recirculation was not efficient enough to prevent serious fouling. The combination of the low recirculation rate (1.5 L/min) and no GAC had to be interrupted after the first filtration period at the highest flux-step level (Figure 39). Although the high bulk recirculation (3.0 L/min) without GAC was able to moderate the transport of wastewater constituents towards the membrane at lower filtration rates, it was not capable of controlling the fouling at the highest filtration rate. In contrast, the 100 % packed bed showed almost no fouling. Marginal TMP shifts (< 4 kPa) were recognized when the next higher flux-step was applied, and the TMP remained at a low level with maximal 13 kPa and 9 kPa for the low and the high recirculation, respectively. However, a detailed view on the two 100 % packed beds showed a slightly higher fouling propensity for the lower recirculation rate compared to the one with the high recirculation flow. The 50 % packed beds were also able to keep the fouling rate on a much lower level than the pure bulk recirculation. While the 50 % bed with the high recirculation showed a performance as good as the 100 % beds, the 50 % bed with the low recirculation was more prone to fouling. However, the 50 % packed beds are difficult to judge because even with their bed expansion, due to the up-flow recirculation, the membrane fibres were not completely covered with GAC particles. In these two cases, approximately one-third of the hollow fibres were not scoured by the GAC particles. It is expected that the excellent fouling mitigation property of the packed bed (as found for the 100 % bed) was also acting very well in the GAC covered fibre area, and that therefore, a rather high fouling in the top section was compensated.

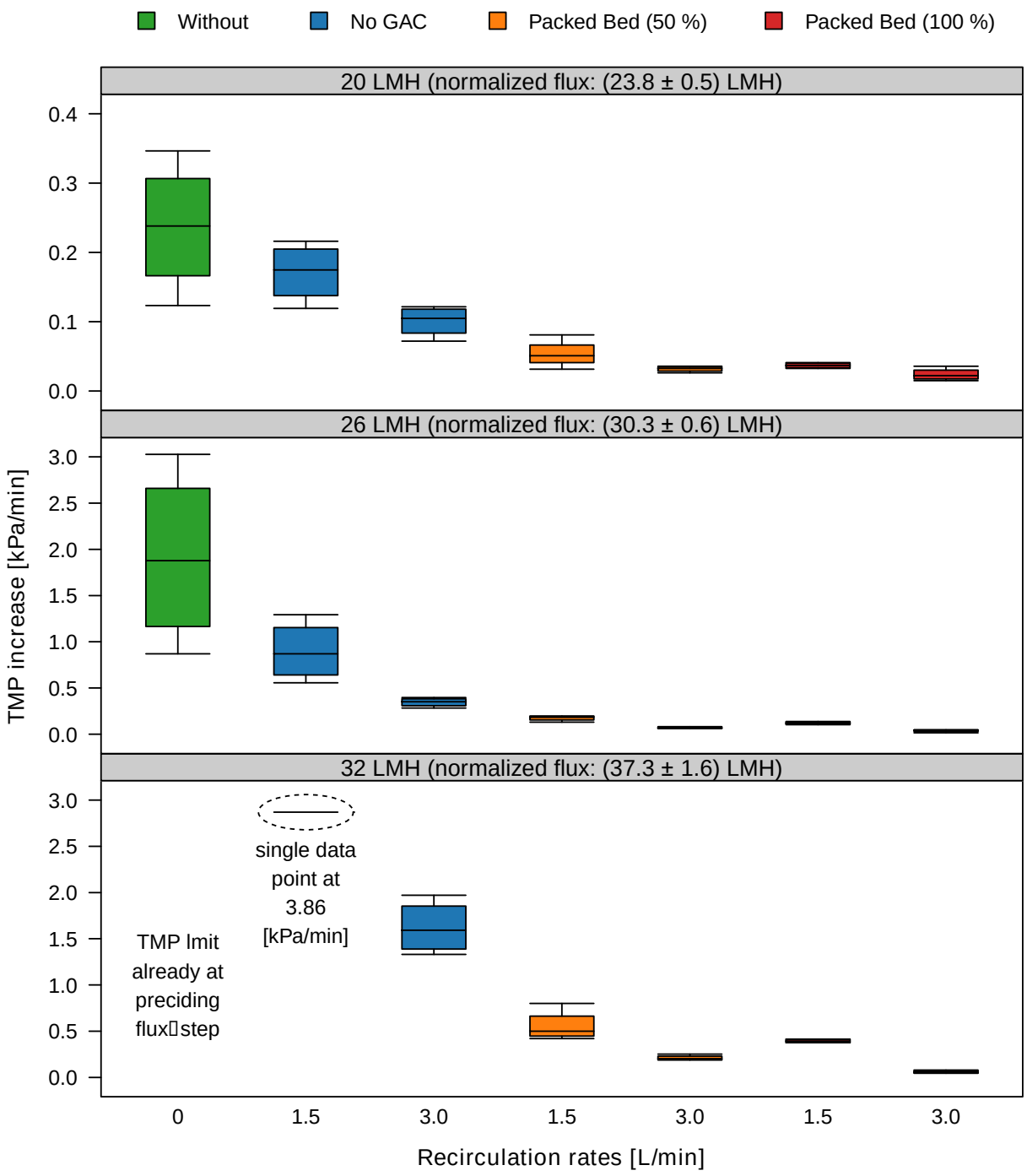

Figure 38. Fouling mitigation efficiency of packed beds with two different granular activated carbon (GAC) concentrations, two different recirculation flow rates, and their combinations, at three different filtration rates (with four filtration periods (n = 4) per flux-step).

Here the *Kruskal-Wallis H test* also delivered a significant difference on all flux-step levels, with χ^2 = 18.286, df = 4, and p = 0.0011 at the 32 LMH flux-step level (conducted without the two test that had to be interrupted). A pairwise comparison revealed differences on the 5 % significance level between:

- no GAC/ high recirculation (3.0 L/min) – 50 % GAC/high recirculation (3.0 L/min),
- no GAC/ high recirculation (3.0 L/min) – 100 % GAC/high recirculation (3.0 L/min),
- 50 % GAC/low recirculation (1.5 L/min) – 100 % GAC/high recirculation (3.0 L/min),

The severe fouling of the blank test as well as of the one without GAC and low recirculation (1.5 L/min) (not considered in the post hoc test), compared with all other tests in this test phase, is evident.

The findings from the fluidized and the packed bed revealed no significant differences in the fouling behavior for most of the tested combinations of bulk recirculation and GAC. This situation suggests that some of these operation settings are interchangeable regarding their fouling mitigation. This, in turn means that in the range of similar fouling behavior, operating conditions can be chosen on the basis of other parameters like the energy consumption of a respective process.

7.2.3 Effect of the adsorption capacity of GAC on the fouling rate

The permeate water quality assessment for the two previously depicted test series was carried out by TOC measurements. The filtrate samples were taken at the end of an experiment during the second last filtration period of the highest intensity (32 LMH flux-step). On the one hand, relative similar TOC contents were detected within the test groups with equal GAC concentrations, except from one batch test (Table SM7, supplementary material, Appendix E). The fluidized bed test with medium GAC concentration and low recirculation (7.1 g/L – 2.2 L/min) showed a TOC content very similar to the group without GAC. On the other hand, different TOC ranges among test groups with distinct GAC levels were detected. The TOC concentrations were lower the more GAC was added to the reactors. These results prove an enhanced effect of activated carbon on the permeate quality. From a practical point of view, such an additional reduction of pollutants is desirable. This improves the performance of the UF stage within an integrated membrane treatment train, and therefore, attenuates the burden for a subsequent NF/RO stage. For the first two test phases, adsorption of water constituents should be the reason for less organic content in the permeate. Park et al. (1999) also found a reduction of COD in their reactor supernatant as well as in the permeate with increasing PAC additions. Though, these outcomes raise two questions:

How long does this effect, probably adsorption, last?

How intense do the intrinsic GAC properties influence membrane fouling behavior?

The latter one was relevant for the investigations of this study because an additional purification mechanism would superimpose the mechanical particle scouring mechanism. Although the GAC that was used for the fluidized and the packed beds was pre-loaded overnight with the actual feed matrix, the adsorption capacity could apparently not be exhausted within this time span. To obtain further knowledge about the fouling mitigation contribution of the GAC material itself, two extra tests with various GAC states have been conducted. The intention for these experiments was to gain a qualitative impression of the adsorption impact regarding the membrane fouling. A first experiment was carried out as a comparison between a packed bed with virgin GAC and one with one-week-loaded GAC. Two portions of 896.1 g of GAC (100 % packed bed) were distributed to 2 x 4 two-liter polyethylene bottles and were rotated (~13 rpm) for one week with DI water and wastewater, respectively. The supernatant in the bottles was renewed twice a day (except for the weekend). In total, the packed beds were pretreated with ca. 40 L of wastewater (collected every day from the WWTP Garching and 500 µm sieved) or with ca. 40 L DI water. The used flux-step pattern was: 10 x 25 LMH followed by 14 x 30 LMH and 10 x 35 LMH. Because of the efficient fouling mitigation of the packed bed, the filtration rate was increased two times to trigger fouling. The results revealed a clearly better fouling control by the virgin GAC (data not shown). On that basis, the follow-up question raised was as follows: Is the adsorption capacity of the GAC already exhausted after one week? Therefore, a second GAC-state investigation was conducted.

For this second investigation (the adsorption test phase) virgin, one-day-loaded, one-week-loaded, as well as with long-term-loaded GAC were utilized in packed bed filtration batch tests. The long-term-loaded GAC activated carbon was taken from an adsorption filter, treated with WWTP effluent (Garching) for approximately one year (also *CYCLECARB 401* from *Chemviron Carbon*). This GAC was additionally treated with raw wastewater for a few days. Then, similar to the first GAC state test one portion long term-loaded GAC and two portions virgin GAC were pretreated with wastewater and DI water for one week. In this case, also two-liter polyethylene bottles but a horizontal shaker (~ 150 m^{-1}) was used. After six days another portion of virgin GAC was treated with wastewater for one day. The filtration tests were carried out with 35 LMH actual flux for around two hours and 1.5 L/min recirculation. Figure 39 illustrates the fouling propensity of the four packed beds. The additional fouling reduction by virgin GAC with its full adsorption capacity is apparent. Fouling behaviors of the one-day- as well as the one-week-loaded GAC were relatively similar. The strongest TMP increases were measured with the long-term-loaded GAC.

These results demonstrated the adsorption of foulants by activated carbon and also showed that the adsorption capacity was not exhausted within one week, under the given conditions. This means that the values obtained for the fluidized bed and packed bed test phases involve a separate fouling reduction mechanism. The adsorption acts simultaneously to the scouring effect, which was the actual factor of interest. However, there are three points that indicate a minor contribution of the adsorption potential compared to the scouring mechanism. First, the GAC applied in the first two test phases was pre-loaded overnight, so at least a proportion of the

adsorption capacity was already exhausted. Second, a much smaller amount of GAC was used for the fluidized bed than in the packed bed (50, 100 g compared to 896 g), meaning less adsorption for the fluidized beds. Third, the comparison of the long-term-loaded packed bed with the non-GAC test from the packed bed test phase, still shows much less fouling by the long-term-loaded GAC, even under more severe conditions (flux, operation time, high feed loading). This indicates scouring as the dominant fouling mitigation. The last point compares tests that were conducted with different wastewater charges, but with relative similar feed characteristics (Table 17). It has to be noted that no quantitative conclusions can be drawn from these results, which would require separate investigations.

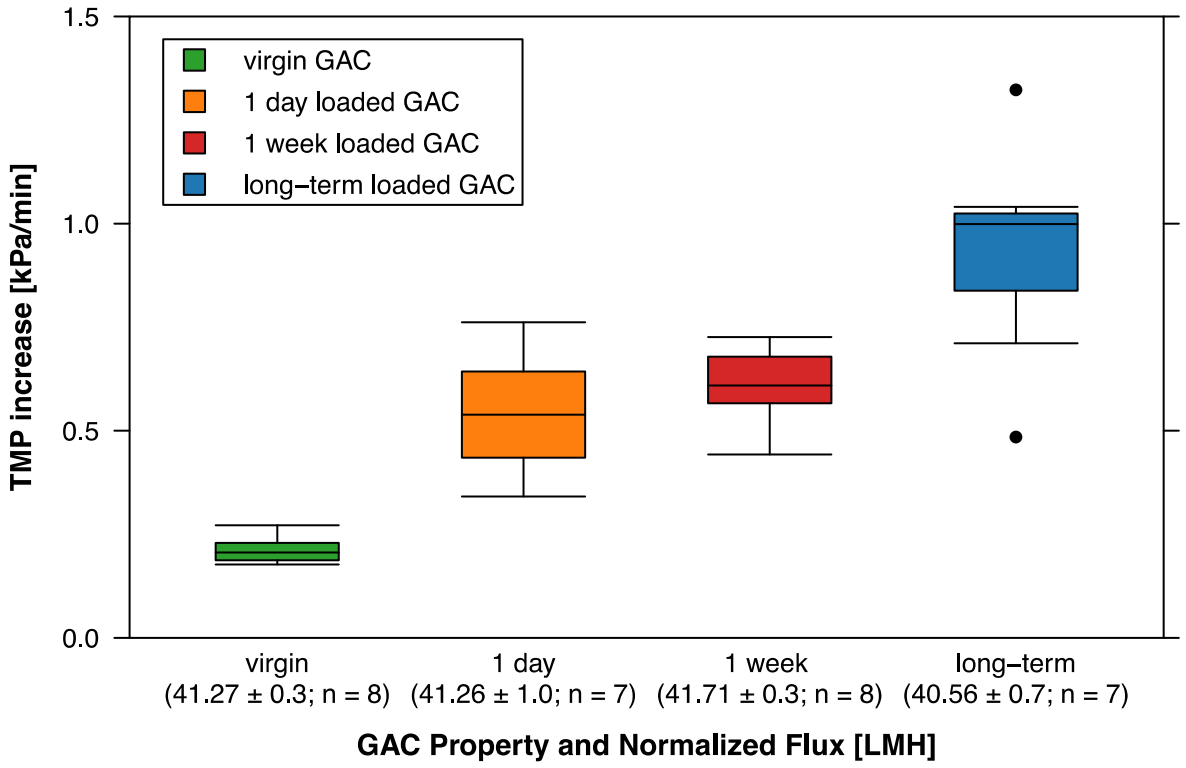

Figure 39. Influence of granular activated carbon (GAC) state on fouling behavior in a packed bed at 35 LMH, with the normalized flux ± standard deviation and n filtration periods given in brackets (12.5 min filtration duration, each followed by 2 min of backwashing).

For this test phase, three permeate samples were taken per batch test, the first one after around 30 minutes and two more during the second half of the test durations (1.7 – 1.9 h). TOC and UV_{254} absorbance were analyzed to determine the organic load in the filtrate. No significant trends were discernible within the three samples of an individual batch test with a particular GAC state.

Table 17. Permeate water quality and removal rates for packed beds with different granular activated carbon (GAC) states.

	virgin (n = 3)	**one-day (n = 3)**	**one-week (n = 3)**	**long-term (n = 3)**
TOC (mg/L)	14.4 ± 2.5	45.5 ± 0.7*	46.8 ± 2.1	28.3 ± 1.4
mean Rejection (%)	88.8	63.9*	63.7	77.5
UV_{254} (1/m)	1.1 ± 0.1	1.2 ± 0.1	2.0 ± 0.1	6.0 ± 0.1
mean Rejection (%)	97.2	97.1	95.0	84.8

* one outlier value removed.

Whereas the UV_{254} values presented plausibly higher absorption the more pre-loaded the GAC was, this trend was not entirely consistent with the TOC contents. As expected, the lowest TOC concentrations were measured for the virgin GAC. The permeate samples of the one-day- and one-week-loaded GAC contained approximately 32 mg/L more TOC than the fresh one but were both in the same range. Surprisingly, the TOC level for the long-term-loaded GAC test was located between the virgin and the one-day-/one week-loaded activated carbon. This is an unexpected outcome, as it was assumed that the adsorption capacity of the long-term-loaded GAC was mostly exhausted. Therefore, the highest TOC was expected to be found in that samples. A possible explanation for this could be the history of the long-term-loaded activated carbon. This GAC was treated with real tertiary effluent as a biofilter for around one year. Potentially, to the GAC surface attached and well-established microorganisms were responsible for the lower TOC concentrations in the permeate. It is conceivable that the adsorption area of this GAC was already loaded and therefore no further sorption of foulants (colloidal and macromolecular agents) was possible. Whereas, low molecular and readily biodegradable organics, which easily penetrates the UF membrane and therefore would end up in the permeate, were degraded by the microorganisms.

The additional adsorption effect of fluidized activated carbon to mitigate membrane fouling was also found in other studies (Aslam et al. 2017a). Aslam et al. (2014) tested fluidized beds with fresh activated carbon and with different particle sizes and observed much fewer fouling the smaller the particle diameters were (greater surface area). As they repeated the filtration tests with pre-adsorbed activated carbon the previously observed phenomenon vanished, and contrarily, the larger particles showed slightly better fouling alleviation. Nonetheless the intrinsic properties of activated carbon influencing fouling are presumably more complex under fluidized conditions than in fixed filter beds. During all batch tests in this study, a GAC abrasion could be observed by a color change of the reactor fluid during operation. Depending on the recirculation intensity, the bulk medium color above the fluidized or the packed bed turned into a dark gray or even into a

complete black. Attrition and pulverization of PAC particles from 40 – 50 µm to 1 – 10 µm, in dependence of the flow regime, was observed by Pirbazari et al. (1996). Such an abrasion possibly produces new GAC surfaces, and so continuously new adsorption capacity would be generated. In MBR systems, further effects like reduction of soluble microbial products (SMP) or extracellular polymeric substances (EPS) in the mixed liquor were revealed by Johir et al. (2011). However, for biological environments, it seems to be unclear to what extent this is caused by physical-chemical adsorption, rather than caused by biological reasons.

To reduce the adsorption influence as much as possible for the last test phase, where pure bulk recirculation, a fluidized bed, as well as a packed bed were directly compared to each other, only the long-term-loaded GAC was used.

7.2.4 Energy consumption of different recirculation rates and granular activated carbon (GAC) concentrations for the fluidized and the packed bed

The determined fouling behaviors were combined with the energy requirements of the individual operation conditions. A graphical comparison was used to select the best fluidized bed and packed bed settings for a benchmark test (best of test phase). The energy demand is calculated as the product of liquid throughput and the counteracting pressure. In low-pressure membrane processes (e.g. UF), the filtration power is often many times smaller than the power for cross-flow generation. Indeed, feed pumping as well as backwashing also require some energy and have to be considered for full-scale facilities. In this chapter, only the filtration and bulk recirculation are taken into account. It should be moreover mentioned that the additional mass of fluidized granulates also influences the head loss in such a system (Epstein 2003).

The modeled hydraulic pressure losses in the recirculation line as well as the mean TMP (average during each filtration period) were used to calculate the energy consumption per volume of produced permeate (specific energy demand). Figure 40 displays the results of the fluidized bed test phase, where the determined fouling rates are plotted against the specific energy demand. The individual tests with their respective conditions are grouped into boxes. Recirculation and GAC concentration values are displayed by the blue and the gray bars, respectively. Data points are pictured with different symbols, which represent the three applied flux-steps. Differences among the flux-steps (within one test) could be explained by the smaller permeate production, leading to higher specific power consumptions. Altogether, the diagram demonstrates the trade-off between small energy requirement and greater fouling rates on the one hand, as well as the possible fouling reduction potential with higher energy inputs on the other hand.

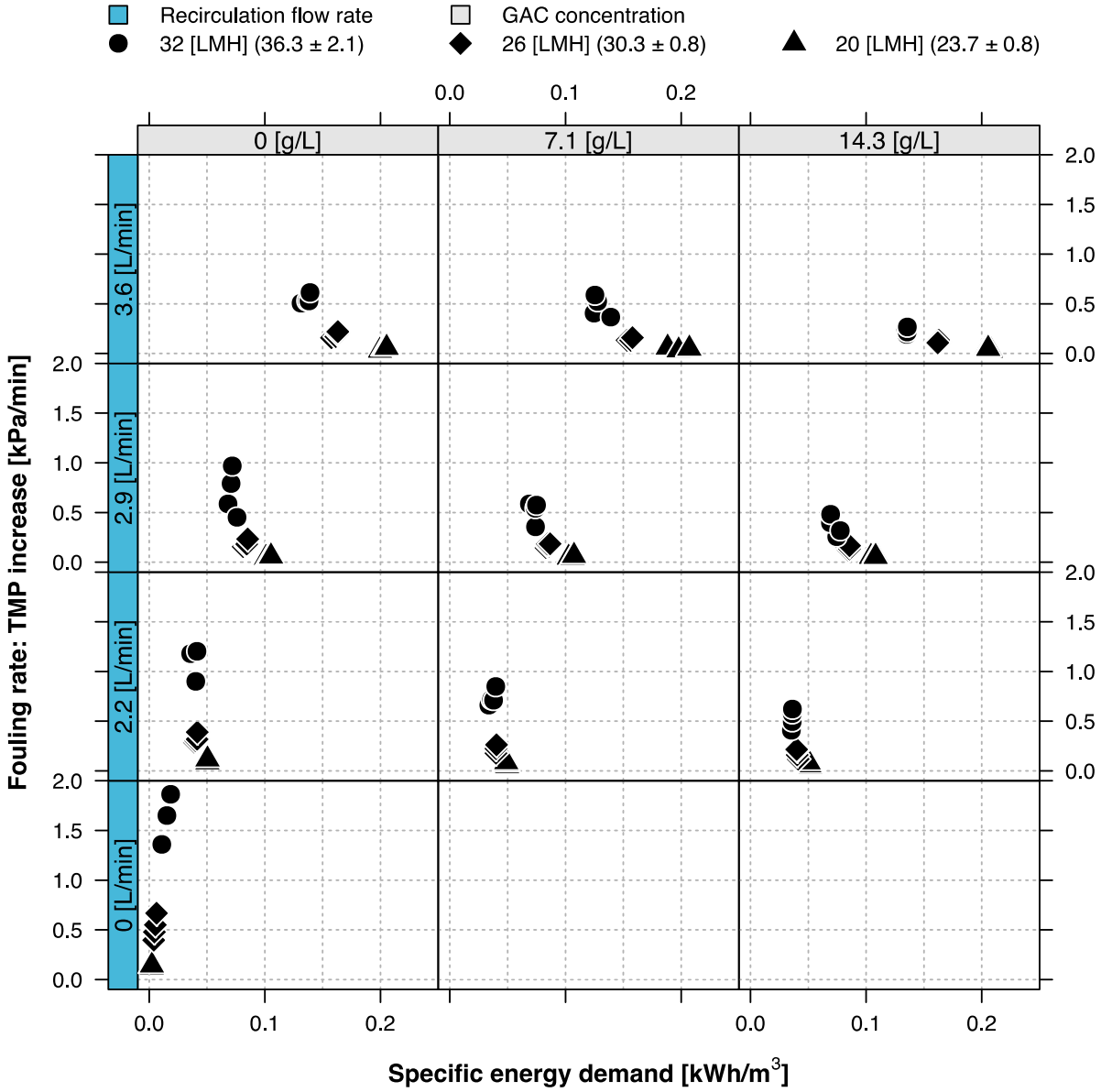

Figure 40. Comparison of the fouling rate in dependence of the specific energy demand per volume permeate, with different recirculation flow rate and granular activated carbon (GAC) concentration combinations in a fluidized bed.

The blank test without recirculation and GAC showed the relatively low specific energy demand that is required to overcome the TMP. At 10 kPa and 50 kPa TMP, only 0.004 kWh/m^3 and 0.019 kWh/m^3 (η = 75 %) are required for the filtration operation, respectively. Whereas 0.028 - 0.050 kWh/m^3 and 0.120 – 0.206 kWh/m^3 were determined for the recirculation at 2.2

L/min and 3.6 L/min, respectively (referred to the measured and standardized flux rates at all flux-steps).

Analogous to Figure 41, Figure 42 illustrates the fouling behavior over the specific energy demand for the packed bed test phase. Due to the more challenging fouling conditions and the lower recirculation rates, in that test series, a different scaling was chosen. The two diagrams (Figure 41 and Figure 42) offered useful graphical means to select the best recirculation-GAC combinations from the fluidized bed as well as from the packed bed investigations. These best settings were examined in a direct comparison, together with pure bulk recirculation, under the same conditions (same feed). For this selection, only the data at the highest filtration rate (32 LMH flux-step) were considered because this data fraction represents the fouling mitigation/propensity with the highest sensitivity. The recirculation-GAC combinations of interest are the ones which allow operation with adequate fouling mitigation under low energy consumption.

For the fluidized bed, these conditions were given for low and medium recirculation rates (2.2 / 2.9 L/min), together with the two GAC concentrations 7.1 g/L and 14.3 g/L. Out of these four, the 2.2 L/min – 14.3 g/L option had the best fouling alleviation capability and was therefore selected for the benchmark test. With respect to the packed bed, the 100 % packed bed at 1.5 L/min of recirculation flow was chosen. The 50 % packed beds were not taken into account because here the upper third of the membrane fibres did not receive any scouring treatment. The decision for the 100 % packed bed with the lower recirculation (1.5 L/min) was made due to the small energy requirement and an excellent fouling control. In the first two test phases, pure bulk recirculation revealed an insufficient fouling control under the harsh fouling conditions in this study. Therefore, the maximal pump capacity (3.6 L/min) was applied for the pure recirculation mode in the final comparison test. The test setup with its two columns allowed the conduction of two batch tests at the same time, and therefore, an additional fourth test could be run. Hence, the packed bed proved high fouling control potential in the previous examinations, even under low recirculation rates, an extra packed bed was investigated in the last test phase. This should show if the recirculation rate can be reduced further, while still sufficient fouling can be ensured. Therefore, the additional packed bed had a recirculation rate of 1.0 L/min.

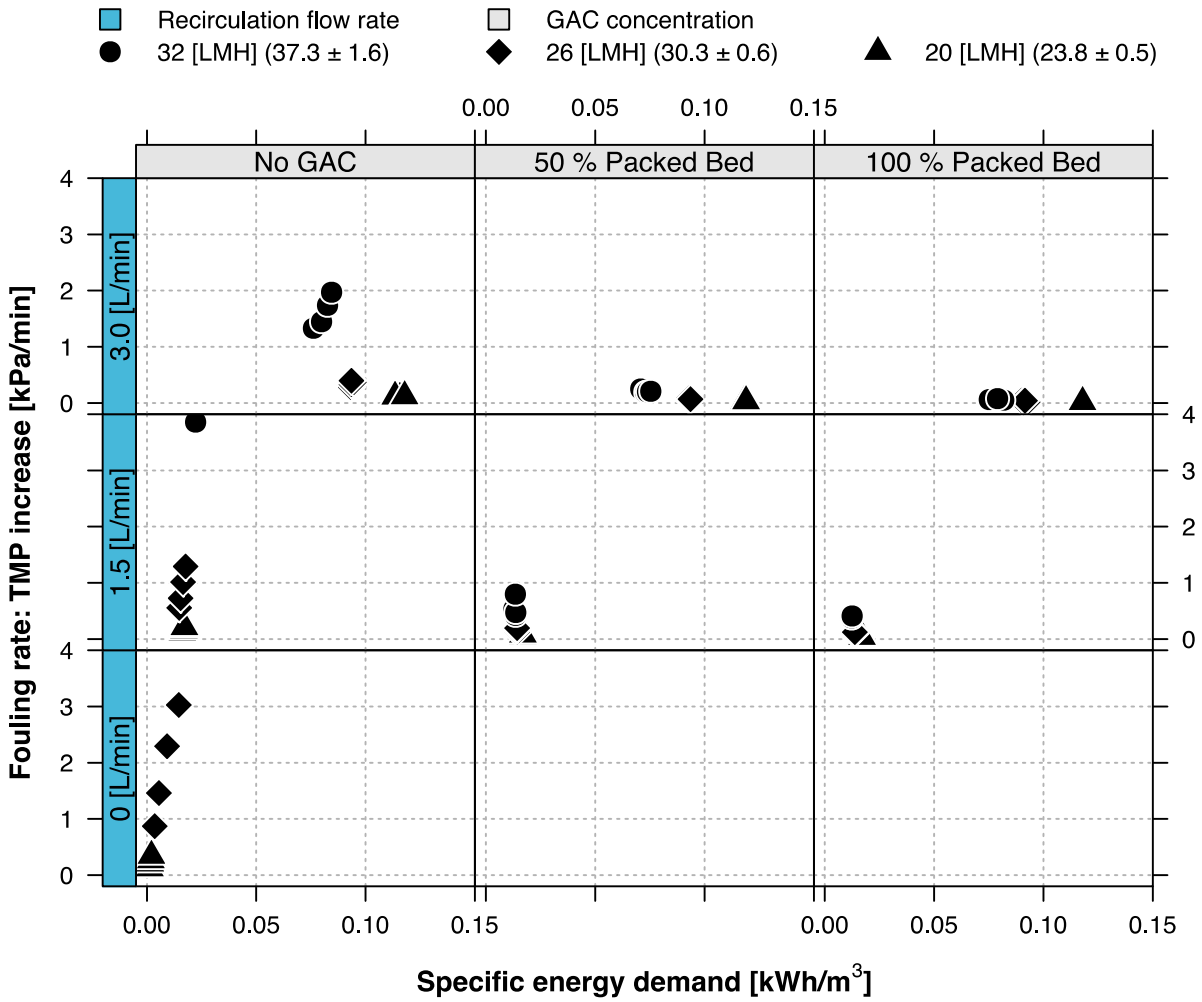

Figure 41. Comparison of the fouling rate in dependence of the specific energy demand per volume permeate, with different recirculation flow rate and granular activated carbon (GAC) concentration combinations in a packed bed.

7.2.5 Comparison of bulk recirculation, fluidized bed, and packed bed

The benchmark test with equal conditions (same feed) for all operation modes enabled the direct comparison of different fouling control strategies. It was conducted with:

- pure bulk recirculation with 3.6 L/min
- fluidized bed with 14.3 g(GAC)/L + 2.9 L/min
- packed bed with 100 % GAC + 1.5 L/min

- packed bed with 100 % GAC + 1.0 L/min.

For this investigation, the flux was adjusted to 35 LMH (actual flux), and the alternating filtration-backwashing pattern (12.5 min / 2 min) ran for several hours. The first filtration period was used to adjust the filtration pumps and was not considered for the evaluation. Table 18 summarizes the determined and normalized flux rates during the best of test phase.

Table 18. Measured and normalized flux during the best of test phase.

pure recirculation (LMH)	**fluidized bed (LMH)**	**packed bed (1.5 L/min) (LMH)**	**packed bed (1.0 L/min) (LMH)**
40.45 ± 0.84 (n = 13)	40.60 ± 2.22 (n = 16)	41.75 ± 0.91 (n = 16)	41.59 ± 1.81 (n = 26)

Figure 42 illustrates the determined fouling rates in dependence of the specific energy demand.

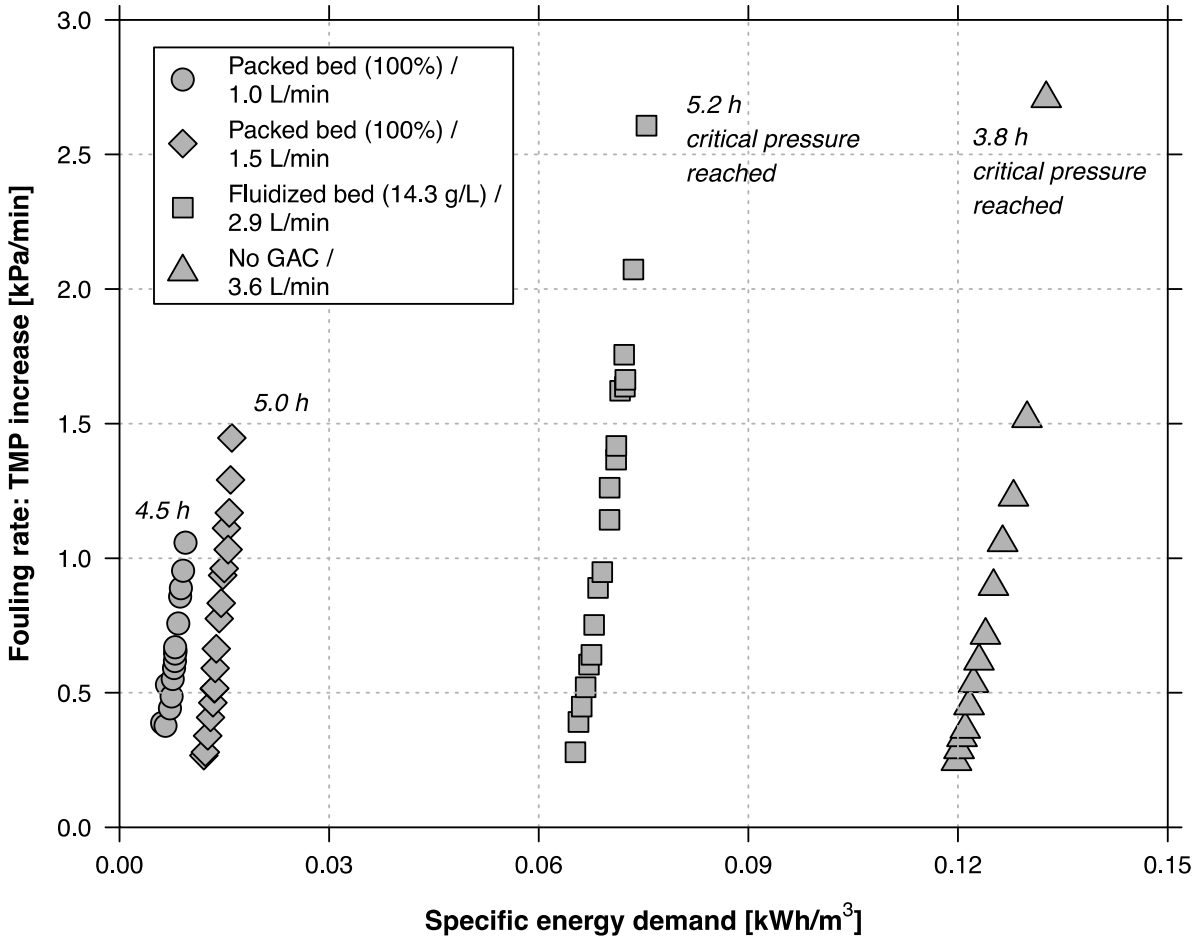

Figure 42. Comparison of fouling rates with different fouling mitigation strategies and their specific energy demand per volume permeate.

In all four batch tests, increasing fouling rates were observed with continuing operation. Hence, it is pointed out that the data points in Figure 42 also indicate a temporal development. As expected the highest fouling was measured for pure bulk recirculation, which also had the highest energy demand with more than 0.12 kWh/m^3. Here the pressure limit was already reached after 3.8 h. The fluidized bed revealed better fouling control at 0.065 – 0.075 kWh/m^3, and an operation span of 5.2 h before the pressure limit was reached. The lowest fouling was recorded with the two packed beds. The packed bed with the stronger recirculation (1.5 L/min) reached a maximum pressure of 30.6 kPa at the end of the second last filtration period, whereas, the packed bed with the weaker recirculation (1.0 L/min) just reached 26.0 kPa. The first mentioned ran about 30 min longer and therefore developed a higher TMP. Due to little difficulties with the right pump adjustments during the first filtration periods, slightly steeper TMP increase slopes have been produced at the beginning of the 1.0 L/min packed bed test. Both packed bed tests ran with the

lowest power consumptions of 0.012 – 0.016 kWh/m^3 and 0.006 – 0.009 kWh/m^3 at the 1.5 L/min and 1.0 L/min recirculation rate, respectively.

According to these small values, the energy demands for bulk recirculation could be reduced to the level of filtrate pumping. The ratios of recirculation to filtration regarding the specific energy requirements are given in Table 19. Hence, the filtration energy increases (growing total TMP) with continuing operation while the energy for recirculation remains on the same level, thus the $E_{spec,reci}$ / $E_{spec,fil}$ ratio changes over time. These ratio values should underline in which low energy range the packed beds operate.

Table 19. Ratio of the specific energy demand for bulk recirculation to the specific energy demand for filtration ($E_{spec,reci}/E_{spec,fil}$) at different filtration steps.

	pure recirculation	**fluidized bed**	**packed bed (1.5 L/min)**	**packed bed (1.0 L/min)**
Filtration period 1 – 4	28.65 ± 3.78	14.12 ± 1.99	2.36 ± 0.26	0.70 ± 0.08
Filtration period 5 – 8	18.49 ± 2.91	9.89 ± 0.86	1.82 ± 0.06	0.55 ± 0.02
Filtration period 9 – 12	10.81 ± 2.01	7.22 ± 0.69	1.57 ± 0.11	0.51 ± 0.02

The organic loading of the permeate samples was assessed through TOC concentration and UV_{254} absorption (Table 20). Although only pre-adsorbed GAC (long-term-loaded) was used, a considerable improvement of the filtrate quality due to the amount of added GAC was shown. The highest TOC and UV_{254} levels were measured for the pure bulk recirculation mode. For the two packed beds the TOC and UV_{254} values were approximately two and a half as well as five times lower than to the test without GAC. For the fluidized bed, this reduction was not as high, but the GAC influence was still ascertainable. Possible reasons for the GAC influence include the generation of new adsorption surfaces through attrition or biological impacts.

Table 20. Permeate quality and rejection rates for the bulk recirculation, the fluidized bed, and the packed beds.

	pure recirculation	**fluidized bed**	**packed bed (1.5 L/min)**	**packed bed (1.0 L/min)**
TOC [mg/L]	28.9 ± 1.0	23.1 ± 1.2	12.0 ± 1.6	12.2 ± 0.2

mean Rejection [%]	43.1	61.5	80.0	76.1
UV_{254} [1/m]	29.4 ± 0.7	19.0 ± 1.1	5.8 ± 0.1	6.0 ± 0.3
mean Rejection [%]	9.2	41.3	82.1	81.5

7.3 Fouling mitigation based on vibration induces by electroactive polymers (EAPs)[2]

The enhancement of shear forces on the membrane surface for fouling mitigation can also be realized by dynamic membrane systems. The collective term dynamic membrane system encompasses several techniques which all aim for enhanced shear forces between the membrane surface and the surrounding fluid without feed pumping or recirculation (Beier and Jonsson 2008). Generally, this is achieved by some kind of movement, like e.g., rotation, toroidal oscillation, or vibration of the membrane or of a separate body in the vicinity of the membrane. Vibration as a shear-enhancing countermeasure has already been proved to be a possible strategy against fouling (Bilad et al. 2012, Kola et al. 2014, Li et al. 2016a). These applications are alo in similar form commercially available as vibratory shear enhanced processing (VSEP) modules. In general, there are four mechanisms for inducing sinus-like vibrations:

- Mechanically by a shaker or motor of either the whole membrane module or the whole liquid (Beier et al. 2006, Kola et al. 2012, Li et al. 2016a),
- An engine magnetically inducing the vibrations (Bilad et al. 2012),
- Or like in the commercial available solution (VSEP) by circular membranes attached to a vertical mounted shaft, which is rotating/oscillating azimuthal inducing torsional vibration parallel to the surface (New Logic Research n.d., Jaffrin 2008).

However, due to the high energy demand in scale-up, VSEP is especially applied for difficult feed waters (Jaffrin 2008, Kola et al. 2014). As the limit of VSEP is due to the needed energy, it is searched for a more energy efficient possibility to induce the vibration to the membranes. The new approach investigated in this chapter is trying to directly induce the vibrations to hollow fibre UF membranes instead of vibrating the whole module as it was done so far. To do so, electro active polymers (EAPs) will induce the vibrations on holdings, connected to the membranes. In addition to the advantage that the vibrations are induced directly to the membranes, EAPs are fast responding (Pei et al. 2016), flexible in frequency and amplitude, as well as they might offer an energy-efficient vibration. Furthermore, complex oscillations like square waves or superposed

[2] This chapter contains data based on a student project conducted by Jonas Aniol (2018) and Philipp Sperle (2018)

sinus waves can be performed. With the integration of the EAP modules into casings, located at different fibre positions, it is possible to realize a more direct and efficient transfer of the vibration. Together with the versatile EAP formability and possible future EAP-integrated designs, kept in mind, a very direct induced vibration can be realized.

7.3.1 Electroactive polymer (EAP) modules

As the name “electroactive polymer” (EAP) implies, EAPs are polymers which respond to applied electricity. Depending on the physical mechanism, electroactive polymers can be grouped into distinct subgroups. The here used EAPs belong to the category of dielectric elastomers (DEs). However, in this thesis, the general term EAP is synonymously used for the specific DEs. In the following, the fundamentals of DE actuators are briefly explained. The driving force of DEs is the attraction or repulsion of like or unlike electrical charges, respectively (Pelrine and Kornbluh 2008). Their basic structure consists of a thin, elastic polymer film which is coated with electrode material on both sides (Hau et al. 2018). Apart from the flexible material traits, this design (two flat electrodes separated by a dielectric material) is equal to the construction of an electrical capacitor. The flexible or compliant electrodes are often realized through a graphite powder coating. Such electrodes allow the necessary and simultaneous deformation together with the separating polymer when the EAP configuration stretches or contracts (Kofod and Sommer-Larsen 2008) (Figure 43). Due to the manifold formability of the base components, EAPs can be shaped in various geometries with distinct deformation directions.

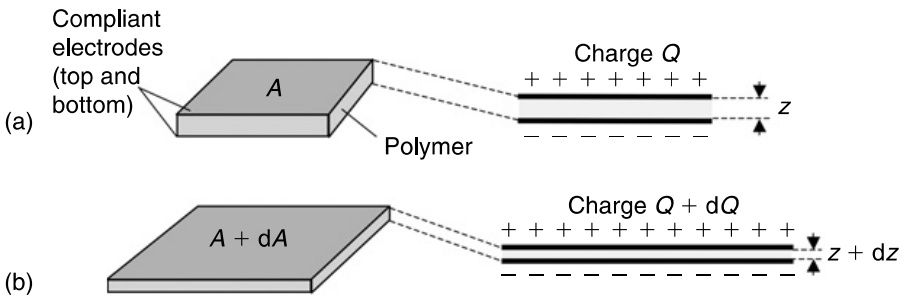

Figure 43. The basic operating principle of a dielectric elastomer (DE) actuator with an initial state (a) and a final state (b) after a change of electrical charge (Pelrine and Kornbluh 2008).

For this study, actuator modules with EAP sheets fabricated by *Parker-Hannifin Corporation* (Cleaveland, OH, USA) were used (Figure 44). These were initially made for tactile/haptic response applications, like for example in video game controllers or deep bass (sound) imitating headphones (House 2013). The sheets have measurements of about 43.1 x 36.5 x 0.5 mm and

consist of a rigid plastic frame, a transparent silicone layer/film with the six active EAP fields, three movable plastic bars, and a ribbon cable for electrical supply (Figure 44). All active EAP fields are located between the rigid frame and a movable plastic bar, respectively. When the EAP sections stretch, in the planar direction of the sheet due to the force of an electrical field, the movable bars are pushed in the same direction relative to the rigid frame. In case of the particularly shown EAP sheet (Figure 44) three of the six EAP sections contracts simultaneously while the other three sections also contracts simultaneously but with a phase shift of 90° (= one quarter of the period of the excitation frequency). However, there are also EAP sheets with only three active fields.

To convert the generated movement to a tactile/noticeable vibration the motion is transferred to a moving mass that repels from the rigid holding frame. This means that the mass (metal plate) is mounted onto the EAP sheet but is only fixed to the three moving bars. The used EAP actuator modules were available with two types of masses – metal plates with and without a hole. Further, the rigid plastic frame is attached to a solid plastic casing. In addition, two leaf springs at each end of the moving mass create the necessary restoring force between the mass and the casing. To prevent any contact with moving or electrical parts of the modules, these are covered by thin, transparent plastic sheets at the bottom and top of the modules.

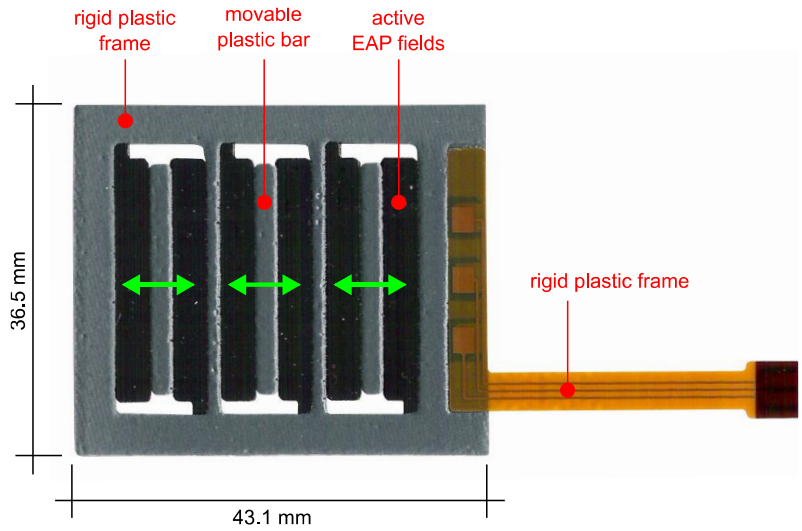

Figure 44. Utilized electroactive polymer (EAP) sheet with measurements, description, and indicated direction of movement (green arrows).

DEs usually require high voltages to generate necessary forces to deform the elastic polymer films. For the investigations here, the EAP modules were individually controlled by USB-transducers which converted a low-volt audio signal to a high-volt signal of around 1 kV. For all experiments, we used a sinusoidal signal and the maximal intensity (volume control at the used

computers) to cause the most powerful vibrations. Since there was no measuring instrument to assess the vibration intensity, the vibration was assessed by holding the EAP modules between fingers or placing them on a metal table (causing noise and movement) while different signals were applied. This very subjective approach led to an appropriate frequency of 80 Hz. The 80 Hz sinusoidal signal was generated with the software *Audacity*® (by Audacity Team; version 2.1.2).

7.3.2 Vibrating hollow fibre UF membrane module (Prototype 1)

The considerations that led to the design of the vibrating hollow fibre UF membrane module (Prototype 1) were determined by the geometry of the EAP actuator modules, the desired transverse vibration direction of the fibres, and the requirement that the EAPs could not come in direct contact with water. Additionally, the UF unit should have a surface area of around 0.05 m^2 and should be excited at the top and bottom end as well as at the middle position of the fibres. To meet the mentioned conditions, elements were designed which acted as casings for the EAP actuators and which enabled a coupling to the fibres as well. The elements were drawn with the computer-aided design (CAD) software *Autodesk Inventor* (Version 2017; Autodesk GmbH, Munich, Germany) and later 3D printed from acrylonitrile butadiene styrene (ABS) filaments with the *Xeed* printer (by Leapfrog, Netherlands). *Simplify3D* (Version 3.1.1; by Simplify3D LLC) was used as slicing software. Here “slicing” refers to the process of translating a 3D geometry from a CAD file and specific settings (e.g. temperatures and speed) into commands (work steps) for a particular printer. One of the EAP casings and the assembly scheme are shown in Figure 45. For the assembling process of the UF module, first, copper cables were soldered to the ribbon cables of the EAP on one end and to the USB voltage transducer on the other end. To place the EAP actuators tightly and watertight in their casings the casings’ insides were coated with synthetic resin (two-component adhesive) before the EAPs were pressed in. Subsequently, the topsides of the EAPs were sealed with synthetic resin. All other pieces like the individual print parts, fittings, and the UF-hollow fibre membranes were also stuck together with synthetic resign. The 16 membrane fibres were cut into approximately 45 cm long pieces to achieve free membrane sections of around 20 cm between the vibration modules. Minus the membrane area loss due to synthetic resin covered sections the total membrane area was determined with 0.0494 m^2. For this study *PURON*® UF hollow fibres fabricated by *Koch Membrane Systems, Inc.* (Wilmington, MA, USA) were used.

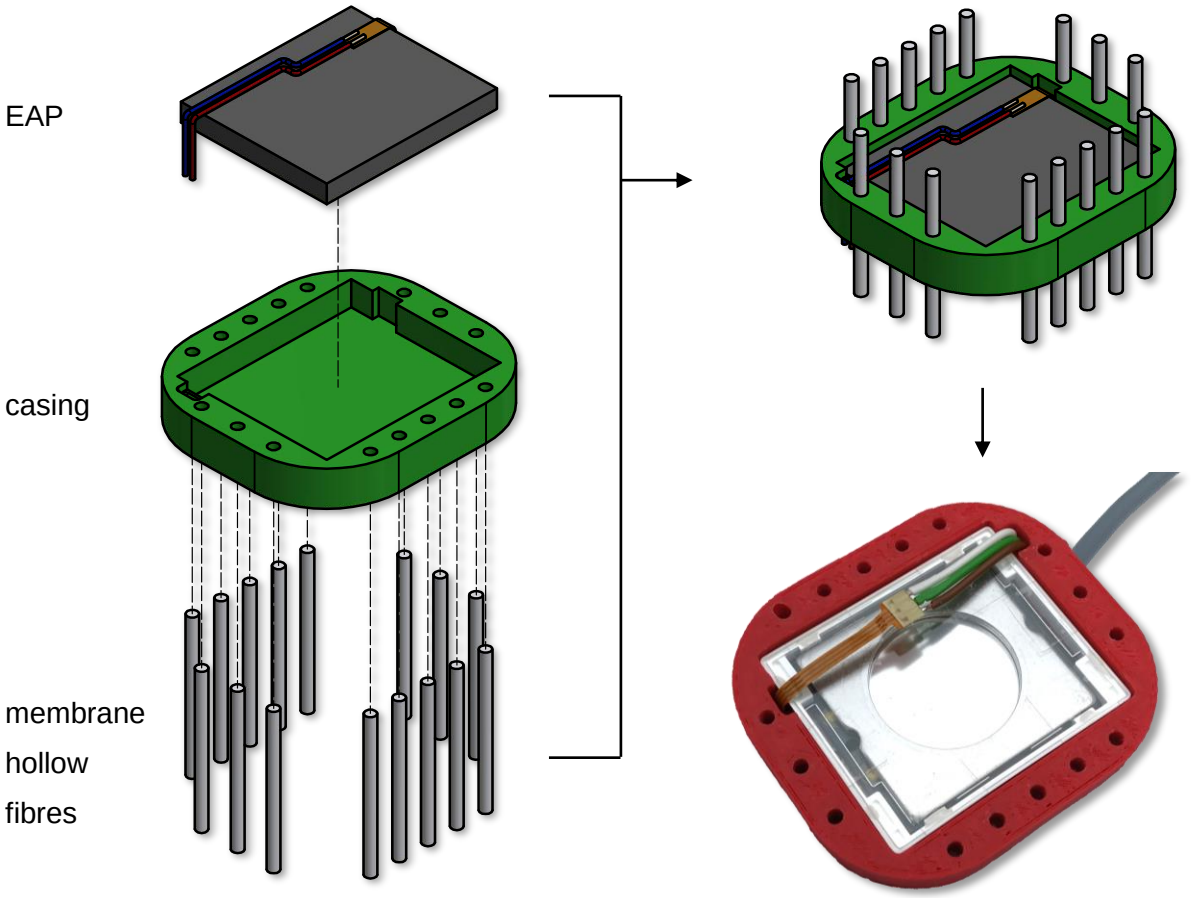

Figure 45. Middle unit assembly and a unit photograph (perspective upside down) of the vibrating hollow fibre prototype.

7.3.3 Experimental set-up and procedure

The experiments were conducted with the UF laboratory-scale test-skid (see chapter 6.1.2). The feed media, municipal wastewater from the WWTP Garching was pretreated by sedimentation (20 – 30 min) and microsieving (100 µm). The feed solution was then stored at 4 °C in a 300 L tank. In total, it was possible to conduct two vibration test runs with prototype 1. Vibration test 1 was conducted with consecutive filtration (15 min, different flux-steps) and backwashing (2 min, 39 ± 3 LMH (normalized)) periods as well as with 2.0 L/min of recirculation. A blank test was subsequent repeated without running EAPs, to evaluate the potential vibration impact. Vibration test 2 was carried out in a reverse order (first without vibration followed by applied vibration) to demonstrate the effect once more and to ensure that the effect was not affected or even determined by the virgin membrane conditions in the first test run.

7.3.4 Results

The applied vibration enabled a more extended filtration operation with less fouling than without fibre excitation (Figure 46). For all applied flux-steps durin vibration test 1, the TMP was lower with the vibration-enhanced filtration. The average reduction of the TMP (total TMP at half-time of each filtration period) was:

- (24.9 ± 3.9) % at 6 LMH,
- (17.2 ± 4.2) % at 12 LMH,
- (23.2 ± 2.5) % at 18 LMH, and
- (42.6 ± 7.6) % at 21 LMH.

The blank test run had to be interrupted after approximately 7 min during the last filtration period (regularly 15 min) at 21 LMH because a critical pressure value was already reached. This was not the case with the vibration-enhanced filtration.

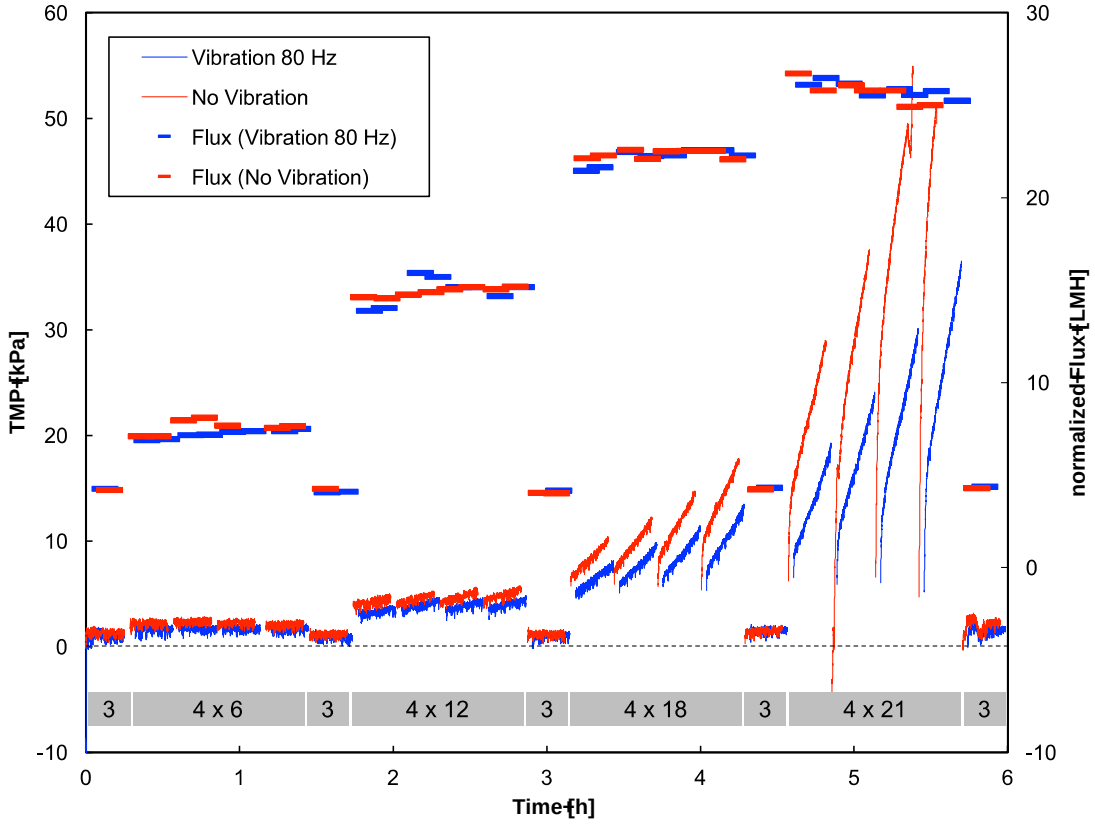

Figure 46. Flux-step UF hollow fibre experiment with vibration (80 Hz, full power, just top & and middle EAP working) and without vibration; applied flux-steps (actual flux) indicated by grey bars.

The findings of the second experiment with a reversed test run order (no-vibration then vibration), confirmed the positive effect of vibrating hollow fibre membranes regarding fouling behavior. Here the average TMP reduction was (9.1 ± 0.4) % at 18 LMH and (14.5 ± 5.1) % at 21 LMH (actual flux). The outcomes of experiment 2 are presented in Figure 47.

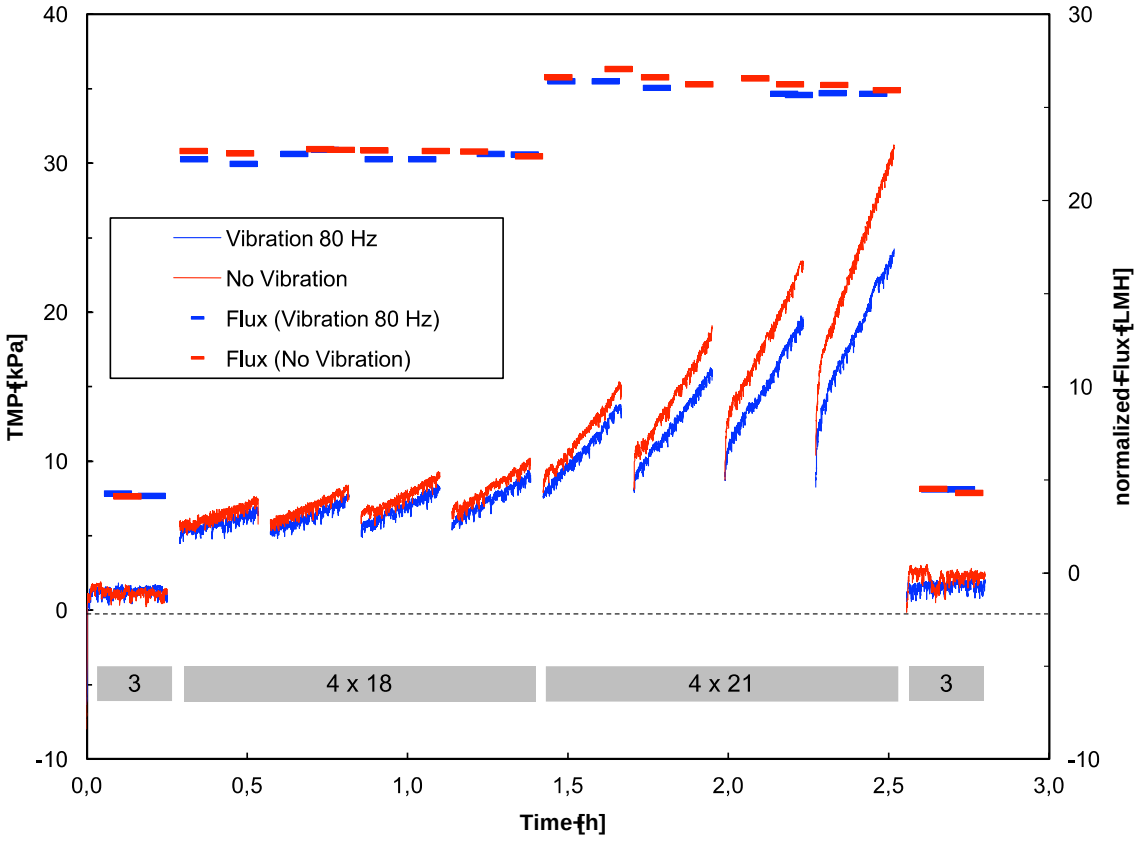

Figure 47. Flux-step UF hollow fibre experiment with vibration (80 Hz, full power, just middle EAP working) and without vibration; applied flux-steps (actual flux) indicated by grey bars.

Regrettably, for the second vibration test the top EAP was not working. This can be due due to water ingress, a broken electrical contact or because some pressure point onto EAP, which hindered the moving mass in the actuator module from moving freely. Thus, it can be explained why the fouling mitigation effect is not that positive compared to test run 1. After the second experiment, all EAPs were out of function due to water ingress. The reason for this was a degradation of the utilized synthetic resin, which began to soften and crumbled. Thus, it can not be stated how long which EAP was working. However, a positive effect of the vibration was 2 times approved.

7.3.5 Outlook

To ensure a better control of the EAP (controlled triggering, aibility to check the function of EAP during experiments) and to ensure a better watertightness, another prototype was designed and constructed (Prototype 2). The improvements comprised a new material selection, better placement of the EAP modules in the casings, a reliable sealing, as well as constructional changes facilitating an easier assembly, and the possibility to exchange broken actuators. The material selection was changed to polyvinyl chloride (PVC) due to its mechanical stability and chemical resistance regarding wastewater and detergents. With the new material, also another fabrication process was chosen. Instead of 3D printing, the parts of the second prototype were CNC milled out of solid PVC parts. One critical point was to ensure proper fixation of the EAP actuator within the casings without pressing them at the wrong sides (disabling the oscillating mass from moving). To account for this, extra contact points were created to touch the EAP modules only in the corners of their bottom and top side. To realize a tight connection between the EAP modules and the casings in the excitation plane, without using glue or synthetic resin, spacer strips were inserted. The spacers were cut from thin but firm plastic sheets and pressed in the gaps between casings and EAP modules at two sides (spacers are not shown in the figures). The essential aspect of waterproofness was enhanced due to the addition of a solid lid. The lid had a tongue which fit into a groove in the of the corresponding casing. In this area, a thin gap of 0.5 mm was realized between the surfaces of the tongue and groove to create a free space for a sealing agent. To enable a later opening/removal of the lid, sanitary silicon was used as a sealing which was filled into the groove and the cable outlet drill holes. The lid was held in place by five 2 mm screws and nuts. Compared to prototype 1, the membrane fibres were only placed at two sides to enable the access to the lid. Regarding the prototype assembly, the fibre fixation points were designed as open bores. This allowed an easier placement of the single fibres and their attachment. The open drill holes also prevented the probability of membrane damages during the mounting process. To avoid the degradation or fatigue of the utilized glue, as happened with the first prototype and the used synthetic resin, an adhesive (*Tangit PVC-U Spezial-Klebstoff* by *Henkel,* Düsseldorf, Germany) more resistant to detergents (chloride compounds) and regarding the range of application was applied. A schematic view of the assembled prototype 2 is given in Figure 48.

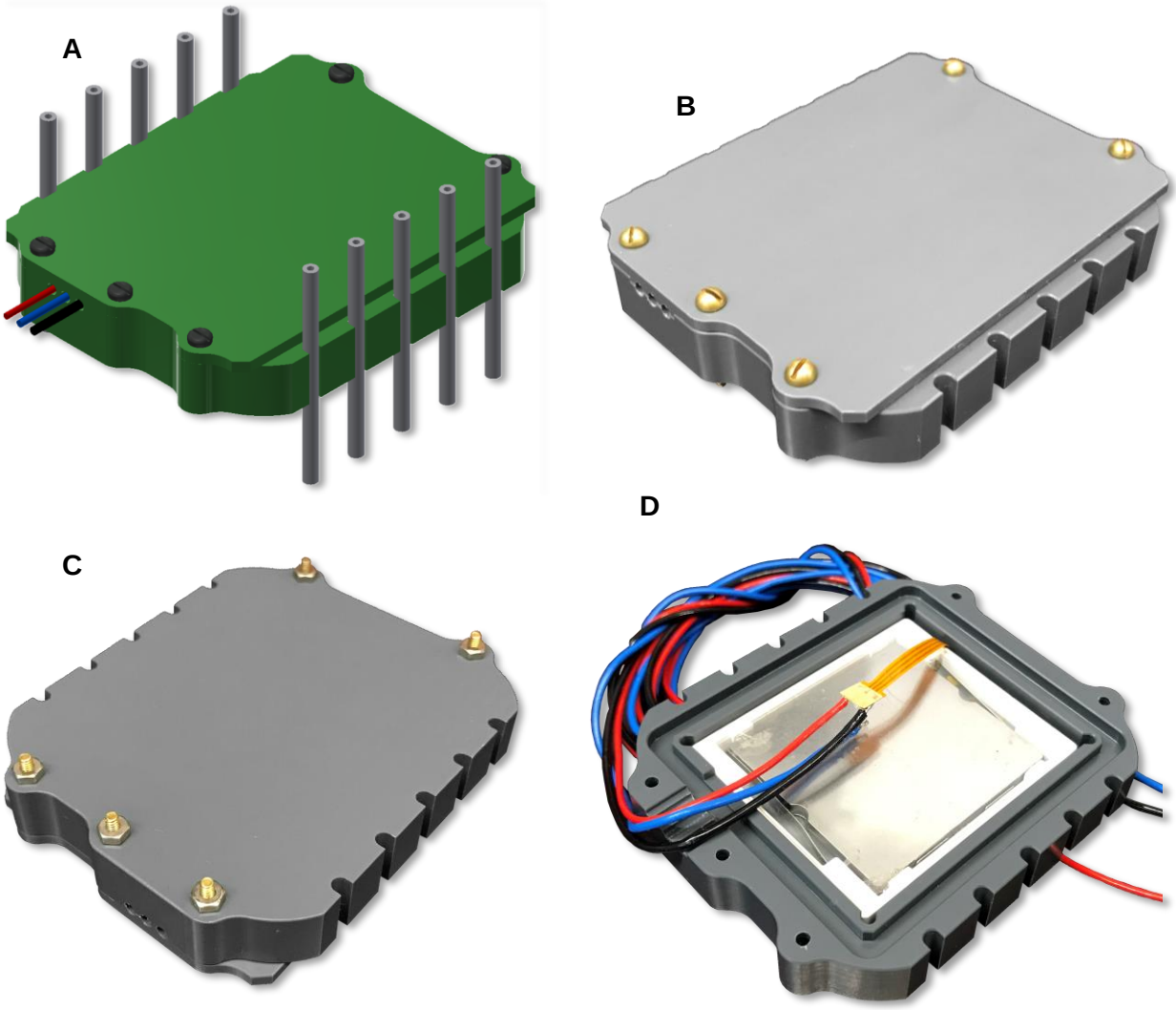

Figure 48. CAD drawing of the assembled prototype 2 middle casing and photographs of the real assembling.

In addition to an improved experimental setup also the proof of the induced vibrations to the UF hollow fibres and its dispersion along the fibres was investigated. In cooperation with the Saarland Univerity (intelligent Material Systems Lab, Prof. Seelecke) it was possible to establish a method to measure the vibration of the UF prototype 2. Therefore a PSV-500-3D scanning vibrometer (Polytec GmbH, Waldbronn, Germany) was used (Figure 49). It is measuring the vibration velocity in three directions, over a whole frequency spectrum or at a single frequency. To do so, points on the prototype have to be defined. The amount of velocity calculated is then the mean value over all selected points.

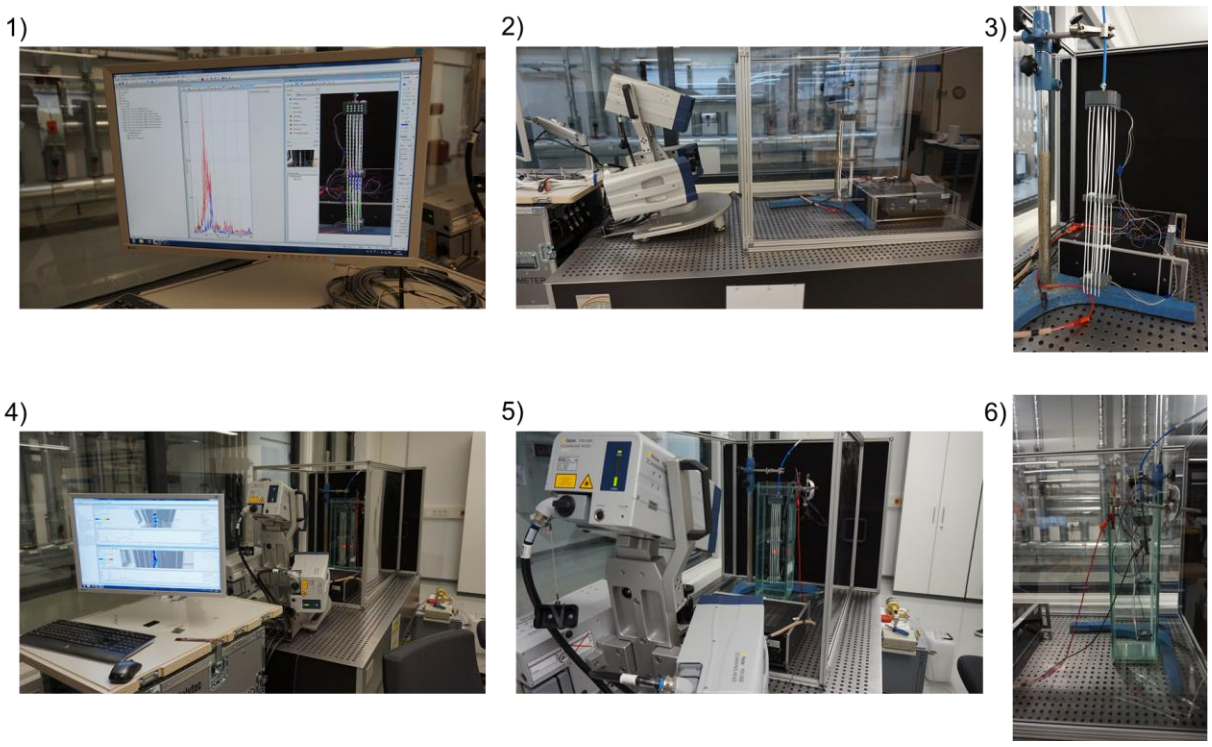

Figure 49. Vibration measurement; 1) view from software; 2) & 3) meausuring prototype in air; 4), 5) and 6) measuring prototype in water.

The vibrometer measurements enabled to analyze and visualize the vibrations induced to the fibres and its dispersion along the fibres. Since the method was not applied before to measurements in water, the establishment of the method was of key interest. A serious of measurements in air and water was conducted. In Figure 50 a fixed image of the measured vibrations of the prototype can be seen. Figure 51 and Figure 52 indicate the difference of vibration dispersion in air and water due to the absorption effect of water.

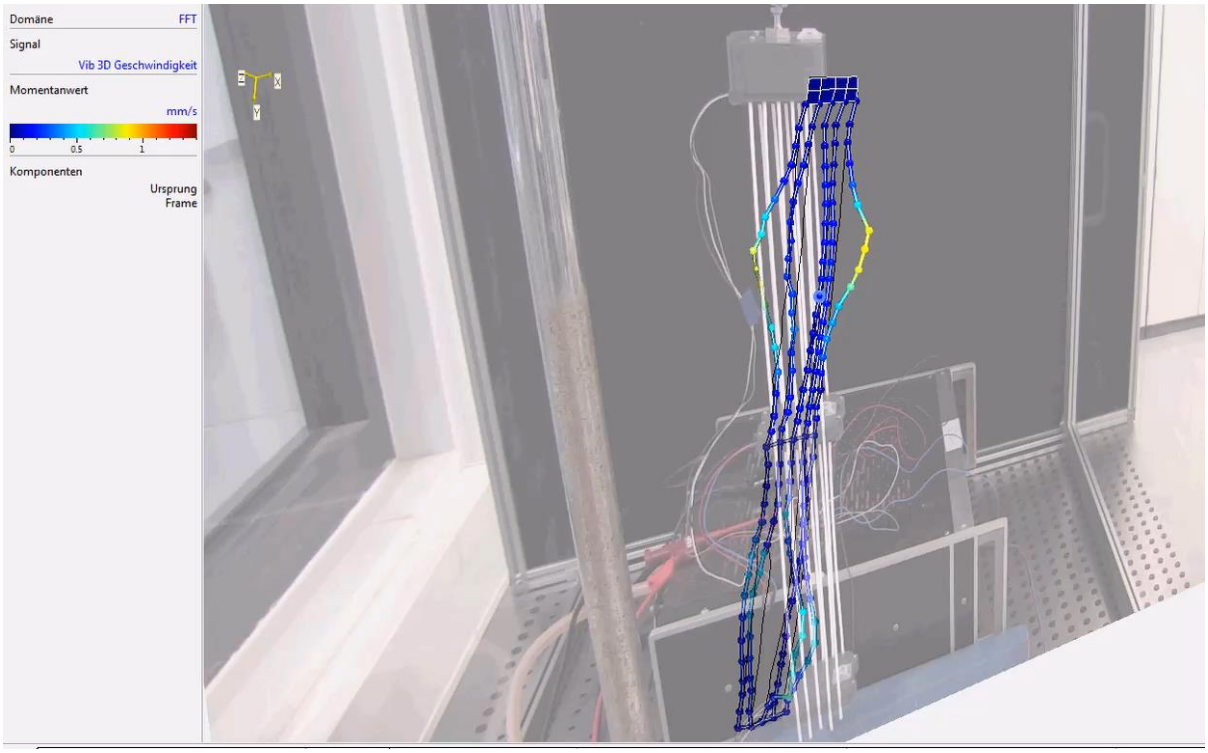

Figure 50. Result of fixed image of vibration measurement.

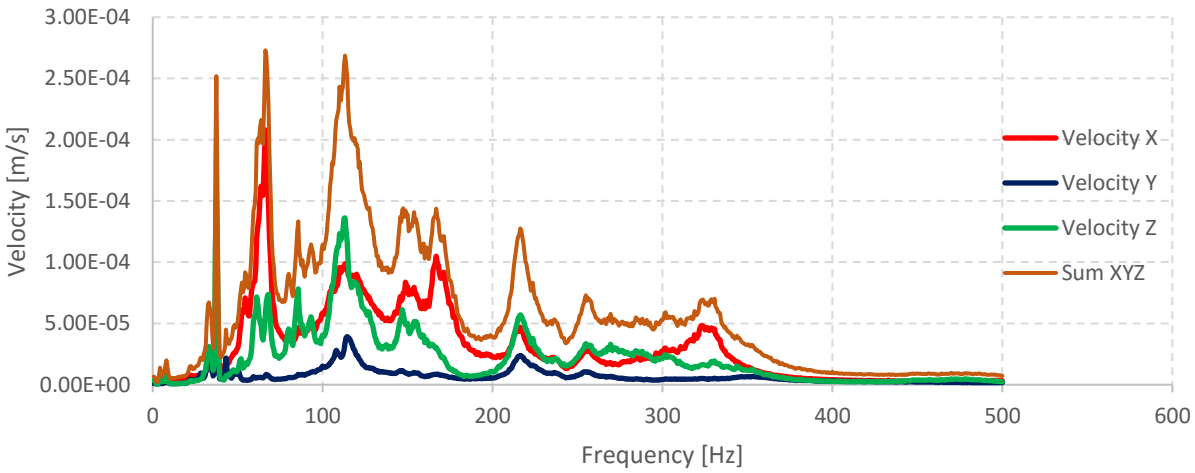

Figure 51. Vibration spectrum, air and mass.

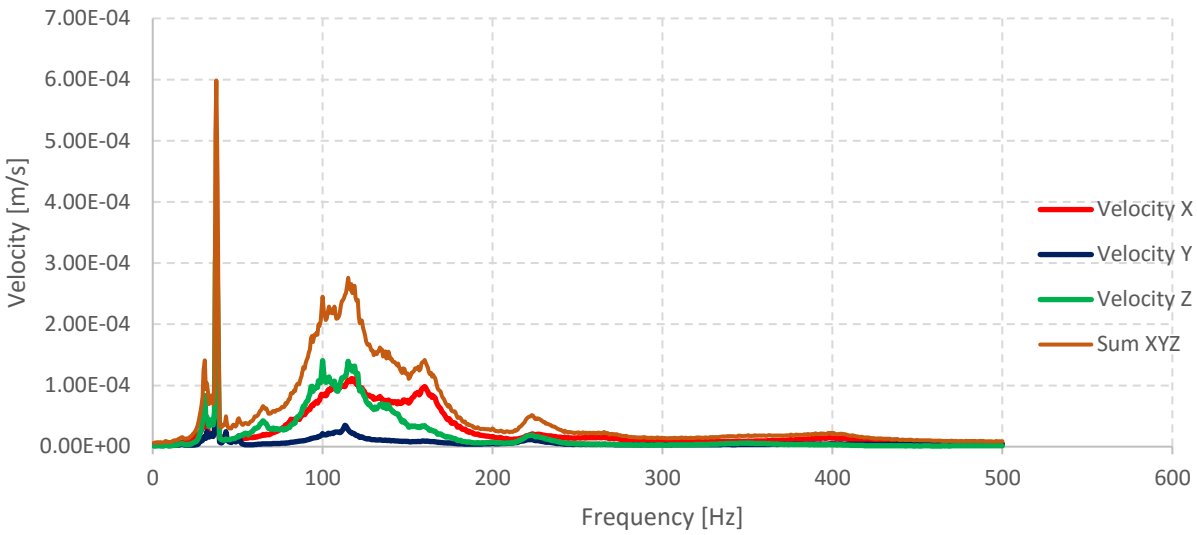

Figure 52. Vibration spectrum, water.

With the successful implementation of EAPs into case holding and inducement of vibration to the UF fibres, it was possible to determine a positive effect of the induced vibrations on the fouling mitigation. However, the conducted tests serve as preliminary results and need to be investigated in more detail. The necessary intensity of vibration and the optimal triggering of the EAPs need to be analyzed more detailed. In addition the effect on different fouling mechansims (e.g. organic fouling vs. scaling) or the implementation as preliminary fouling mitigation or its utilization as additional cleaning effect are future research objectives. It has to be noted that the applied EAPs are not optimized for the utilization in water or for membrane vibration purposes. Thus, completely different EAP geometries can be possible to optimize the effect of fouling mitigation and the positive integration in existing and new designed membranes. For this purpose a research proposal is in preparation.

8 Downstream membrane treatment with nanofiltration (NF) or reverse osmosis (RO)[3]

A hybrid membrane system, consisting of UF treatment followed by NF or RO treatment, is considered as concept to enable more energy-efficient potable water reuse schemes. While the UF treatment stage is investigated in chapter 7, within this chapter the subsequent membrane treatment (NF/RO) is investigated. Core focus is the operational feasibility of NF/RO membrane treatment with a UF pretreated municipal wastewater. Beside the operational feasibility the produced water quality is analyzed to assess the possibility of downstream treatment with further required treatment stages to ensure potable water quality. Stated as hypothesis #3:

> *"NF/RO membrane treatment downstream of a fluidized bed UF reactor can be sustained while generating a suitable water quality for downstream BAF, UV-AOP with the purpose to generate potable water quality."*

Hypothesis #3 is tested and assessed within this chapter. Therefore, NF and RO membrane treatment was evaluated as downstream membrane treatment stage of UF pretreated municipal wastewater. The comparison of NF and RO membrane fouling test showed average permeate flux declines below 30% (NF ~18%, RO ~26%). Thus, it is indicated that NF/RO membrane treatment can be sustained. However, considering the conceptual approach of concentrating ammonia for subsequent energetic utilization in the CANDO process, NF is not a suitable membrane (ammonia rejection capability NF: ~30%, RO: ~97%). Thus, RO is considered more suitable to concentrate NH_4-N in the reject stream, which is subsequently used for energetic utilization via the CANDO process. The produced water quality of NF and RO membrane treatment was determined with DOC removals of approximately 90%, resulting in permeate DOC concentration of 2.0 ± 0.7 mg/L. This indicates to be a suitable water quality for downstream treatment with BAF and UV-AOP. However, long-term performance and potential upscaling effects needs to be considered. Hence, hypothesis #3 is only partly confirmed.

8.1 Fouling beheviour of NF/RO with UF pretreated wastewater / Comparison of NF and RO fouling performance

To assess the feasibility of NF and RO treatment subsequent to UF treatment, the UF permeate from the FB-UF-MR was collected and further treated over a time period of approximately 5 month. The UF sampling, sample storage and an overview of all performed fouling experiments can be found in the appendix (Appendix F). The average membrane performance parameters for the NF and RO membrane are summarized in Table 21. On

[3] This chapter contains information based on a student project conducted by Jan Schmitz (2017)

average, the NF membrane showed low flux decline (< 20 %), but with a high variation. This can be mainly explained by batch 4 (exp. 6 & 7) which showed a flux decline > 30 %. Compared to NF, flux decline of the RO membrane was generally higher (> 25 %). The RO is a non-porous membrane and exhibits the greater size exclusion capability compared to the NF membrane, which leads to a stronger CP, adsorption and accumulation of solutes and particles on the membrane surface resulting in an increased inclination for flux decline. The DOC rejection for the NF membrane was determined to be 89.1 % on average (Table 21). This is slightly lower but similar to the TOC rejection capability of 93.5 ± 1.6 % for the NF-270 reported by Bellona et al. (2008). Consistent with the DOC, also the UVA_{254} value in the permeate of both membranes is small, which indicates also a good removal of aromatic DOC. For the RO membrane the rejection was determined to be 92.3 % on average. Also the Toray TMG10 was investigated by Bellona et al. (2008) and they found a TOC rejection capability of 96.7 %.

Table 21. Average membrane performance parameters for the DOW NF-270 and Toray TMG10 RO membrane.

Parameter	DOW NF-270 membrane	Toray TMG10 RO membrane
Average flux decline (%)[a]	18.1 ± 15.1	25.6 ± 6.5
Average DOC feed (mg/L)	22.2 ± 10.3	27.3 ± 13.1
Average DOC permeate (mg/L)	2.2 ± 1.4	2.0 ± 0.7
Average DOC rejection (%)	89.1 ± 6.0	92.3 ± 2.7
Average UVA_{254} feed (1/m)	0.15 ± 0.06	0.18 ± 0.04
Average UVA_{254} permeate (1/m)	0.02 ± 0.01	0.02 ± 0.02
Average SUVA feed (L/(mg cm))	0.72 ± 0.28	0.77 ± 0.30
Average SUVA permeate (L/(mg cm))	1.06 ± 0.55	1.63 ± 1.28

[a]The average flux decline after 80 h of operation is shown in order to compare all experiments.

In addition, flux decline curves of the performed experiments are shown in Figure 53. Since not all experiments had the same operation time, the rTCSF is only shown for an operating time of 80 h to compare all experiments and their flux decline curves. The RO membrane indicates two fouling phases. Phase one with an initial flux drop within the first hours of operation (0-20 h), followed by phase two with a decreased linear flux decline (20 h-end). Here, a steady-state flux would be expected during long-term operation (> 120 h). The NF membrane shows a rather linear flux decline and steady-state flux did not set in during 80 h of operation, but is also expected during long-term operation. Clearly visible is the stronger flux decline recorded for exp. 6 and 7 with the NF membrane. Specific fouling phases according to the flux decline curves cannot be considered for the NF membrane (Figure 53).

For both membranes, a second drop in flux during long-term operation can be also expected due to biofouling and the further increased hydraulic resistance. In conclusion, the general extent of flux decline of both membranes is classified as low (< 30 %) during short-term operation when considering the high DOC values and high fouling potential of the feed matrices. Especially the NF membrane was able to maintain a high flux during 80 h of operation (flux decline < 20 %). In addition to that, the high DOC rejection capacities of both membranes (~90 %) demonstrate high membrane efficiencies.

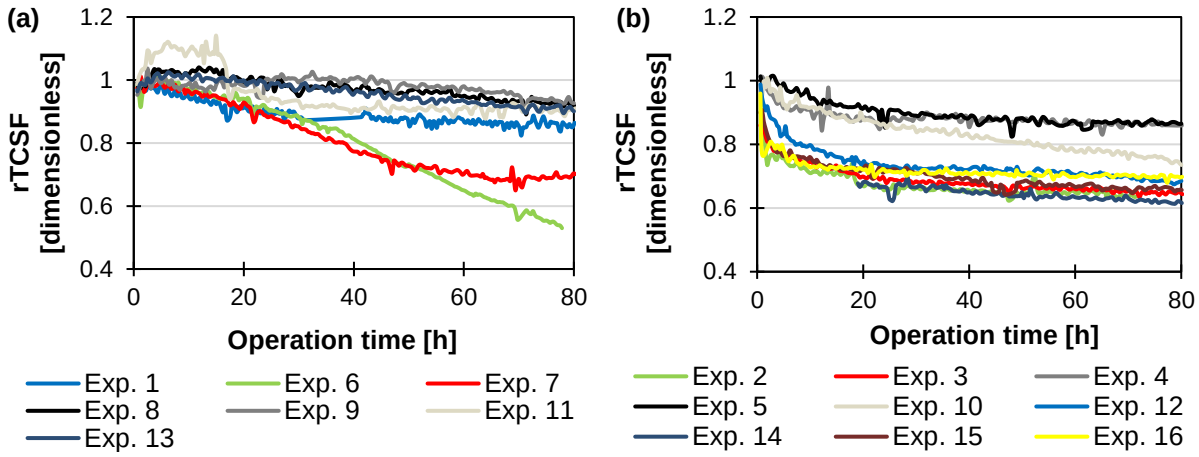

Figure 53. Flux decline curves of all fouling experiments performed with (a) the DOW NF-270 and (b) the Toray TMG10 RO membrane. Relative temperature corrected specific flux (rTCSF) plotted against operation time (80 h). Experiments 1-12 conducted with raw wastewater matrix from WWTP Garching, experiments 13-16 performed with raw wastewater matrix from WWTP Gut Marienhof (Munich).

Thus, when considering only the maintenance of a high flux and removal efficiencies of DOM, an implementation of the present NF and RO membranes in the proposed potable water reuse scheme (see chapter 4) is possible when excluding long-term operation behavior and further biofouling formation which were not investigated during this study. Due to its lower energy requirements, the NF-270 would be preferred over the non-porous RO membrane for the IMS. However, for the presentd potable water reuse scheme, also the concentration of C and NH_4^+ to produce CH_4 and N_2O for co-combustion in the CANDO process is considered. Both membranes showed good DOC retention capabilities, which would definitely allow a sufficient concentration of carbon at this membrane stage in the IMS. However, for a sufficient NH_4^+ concentration, the RO would be the membrane of choice. The NH_4^+ rejection capability of the NF-270 and Toray TMG10 RO membranes were tested along with the fouling experiments for this study. The NF-270 was found to have a poor NH_4^+ rejection of only 29.7 ± 1.8 %. The RO in turn was found to reject NH_4^+ up to 91.7 ± 1.3 %. Those values are slightly lower compared to the rejection capabilities reported by Bellona et al. (2008), which observed a rejection of 35.9 % for the NF membrane and 97.2 % for the RO membrane.

Also trace organic chemicals in water are parameters of interest. Their rejection is based on complex interactions such as steric hindrance of those, electrostatic repulsion, solution effects on the membrane, and solute/membrane properties (Bellona et al. 2004). However, with regard to trace organics, it can be stated, that RO membranes providing better permeate qualities compared to NF membranes. Bellona et al. (2008) showed in a study that several tested RO membranes possessed a greater removal efficiency of trace organics compared to NF membranes including the NF-270.

8.2 Investigation of NF/RO membrane fouling

The overall membrane performance was found to be good, a high flux could be maintained for both membranes (flux NF > RO). However, two experiments performed within batch 4 showed a strong flux decline (51 % and 32 %). In order to investigate the reason for that and to potentially get an insight why the membranes could maintain a high flux within ~90 h of operation, two fundamental questions will be considered:

- Do the NF and RO membranes react more sensitive to the total load of DOM in the feed matrix and FLs (total mass of biopolymers described by the DOC concentration)?, or
- do they react more sensitive to specific organic compounds or compositions of the feed matrices?

The UF pretreatment is able to reduce to total load of organic colloids and particles, but the majority of the DOC still passes this barrier and might increase fouling probability in the downstream NF/RO stage. In order to better understand membrane fouling behavior in the NF/RO stage and thereby increasing the system efficiency of the whole treatment chain, it is important to investigate the influence and makeup of the DOM fraction which penetrates the UF stage and serves as feed matrix for the NF/RO membranes.

8.2.1 NF/RO feed matrices

First, the NF/RO feed matrices are characterized regarding their makeup in order to better understand what fraction interacts with the membranes and potentially might determine membrane fouling. In addition to DOC, UVA_{254} and SUVA, also conductivity, pH, carbohydrate and protein concentrations were determined. Average values of those parameters in the NF/RO feed matrices originating from WWTP Garching and Gut Marienhof (Munich) are shown in Table 22.

Table 22. Measured bulk water quality parameters of the NF/RO feed matrices with standard deviations. UF pre-treated raw wastewater from wastewater treatment plant (WWTP) Garching and Gut Marienhof (Munich).

Parameter	WWTP Garching	WWTP Gut Marienhof (Munich)
DOC (mg/L)	26.2 ± 12.3	21.9 ± 11.2
Conductivity (µs/cm)	1735 ± 166	1544 ± 103
pH	7.8 ± 0.1	7.9 ± 0.1
UVA_{254} (1/m)	0.183 ± 0.044	0.126 ± 0.058
SUVA (L/(mg cm))	0.8 ± 0.3	0.6 ± 0.3
Proteins (µg/mL)	88.8 ± 22.5	66.1 ± 20.9
Carbohydrates (µg/mL)	5.9 ± 3.8	4.3 ± 1.1

Number of data (n), WWTP Garching n=11, WWTP Gut Marienhof n=4.

As Table 22 shows, initial DOC values of both used feed matrices tend to vary strongly. This can be partially explained by the used feed matrices itself. Weekly, the UF feed matrix is renewed, and thus, also the UF permeate matrix changes in their organic composition, so that initial DOC values of the NF/RO feed matrices may vary for each batch. The lower average DOC value for the matrix originating from WWTP Gut Marienhof (Munich) can be explained by the matrix used for exp. 13 (DOC = 12.3 mg/L). During sampling at the WWTP, the internal recirculation of the full-scale activated sludge system was on so that the raw WW sample was diluted resulting in a low DOC concentration, which lowers in turn the average value.

However, regarding to current literature, a DOC concentration > 20 mg/L can be classified as comparable high. The majority of studies deals with (1) UF pretreated secondary effluents from (waste)water reclamation plants with DOC concentrations ranging from 6.5-10.5 mg/L, (2) UF pretreated or sand-filtered water from drinking water plants using river water as source with DOC values ranging from 1.9-3.2 mg/L, or (3) synthetic model solutions with a DOC concentration of e.g. 5.3-10.5 mg/L (Li and Elimelech 2006, Her et al. 2007, Zhao et al. 2010a, Zhao et al. 2010b, Lamsal et al. 2012, Tang et al. 2014). The initial pH values of the feed matrix (7.8 ± 0.1 and 7.9 ± 0.1) were quite stable among all conducted fouling experiments, similar to the initial conductivity values. Due to the varying organic composition of the feed matrices the measured UVA_{254} values also tend to fluctuate strong (0.183 ± 0.044 and 0.126 ± 0.058). Same as concluded before, the very low SUVA values indicate hydrophilic matter. Protein concentrations as well as the concentrations of the carbohydrates are relatively constant – proteins ~88.8 µg/mL and ~66.1 µg/mL and carbohydrates ~5.9 µg/mL and ~4.3 µg/mL.

For a further characterization of the NF/RO feed matrices, 3D-EEM spectroscopy was used. First, Figure 54 shows the percentage portion of the average F_{max} values calculated for C1-C3 in the NF/RO feed matrices originating from both raw wastewaters from WWTP Garching and

WWTP Gut Marienhof (Munich). Besides, two 3D-EEM spectra of one RO feed matrix originating from WWTP Garching and one from WWTP Gut Marienhof (Munich) at the start of the experiments are shown. It basically shows that the general makeup of both matrices is nearly identical when considering only the 3 components identified by the PARAFAC analysis (Figure 54 (a)). The 3D-EEM spectra also show a similar fluorescence pattern of the two matrices (Figure 54 (b) and (c)). Due to that, for further discussion the water matrices are not examined separately.

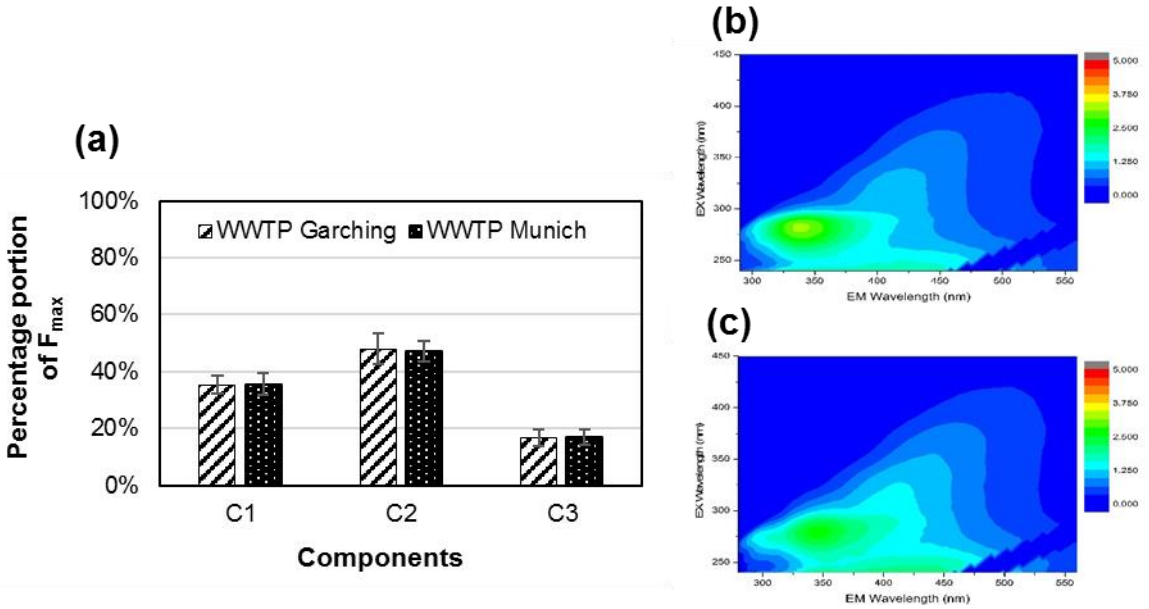

Figure 54. (a) Compositions of NF/RO feed matrices from wastewater treatment plant (WWTP) Garching and Gut Marienhof (Munich). Percentage portions of the average Fmax values from C1-C3 are shown. 3D-fluorescence excitation-emission (3D-EEM) spectra of (b) exp. 12 (WWTP Garching) and (c) exp. 16 (WWTP Gut Marienhof Munich).

For a detailed 3D-EEM characterization, 3 characteristic feed spectra of used NF feed matrices at the start of the experiments are illustrated in Figure 55. Besides, the 3D-EEM spectrum illustrated in Figure Figure 55(a) is divided according to the typical 3D-EEM characterization of raw (waste)waters. In the present matrices, basically all type of NOM (protein-, fulvic- and humic-like matter) can be found to different degrees indicated by stronger or lower fluorescence intensities in the spectra. However, for all feed matrices the protein-like matter fluorescence peak was always the most intense in relation to the other fluorescence regions. A detailed characterization of the present matrix with regard to the PARAFAC model is discussed later.

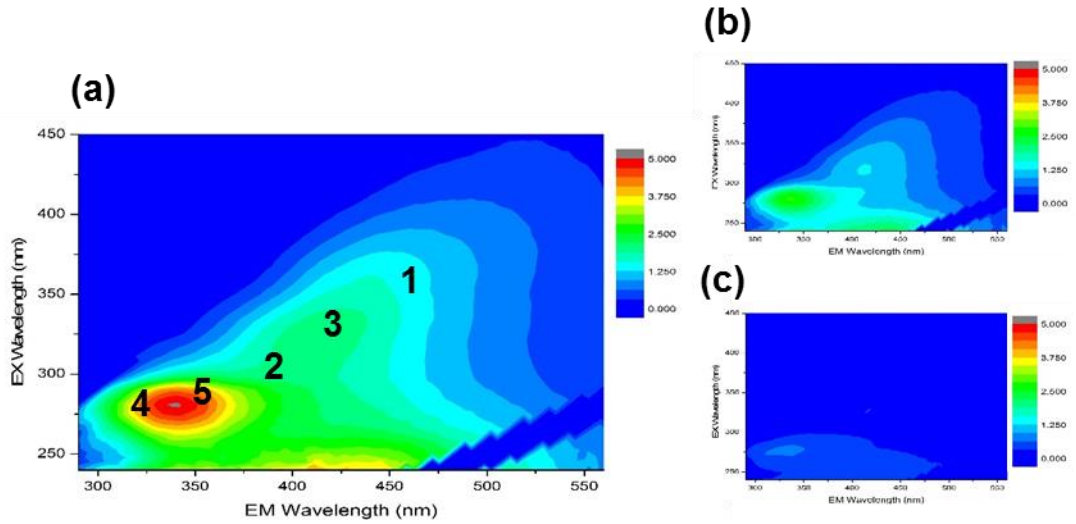

Figure 55. 3D-fluorescence excitation-emission (3D-EEM) spectra of typical NF/RO feed matrices. (a) dissolved organic matter (DOM) rich matrix, (b) and (c) less DOM rich matrices. (a) Matrix from exp. 9, DOC = 30.7 mg/L; (b) matrix from exp. 6, DOC = 17.2 mg/L; (c) matrix from exp. 13, DOC = 12.3 mg/L. Also, main fluorescence regions of NOM in raw waters are shown in spectra (a). Region 1 and 2 can be related to humic-like matter, region 3 to fulvic-like, region 4 to tyrosine protein-like and region 5 to tryptophan protein-like matter.

Selected representative feed matrix samples were further analyzed using LC-OCD. The LC-OCD chromatograms of a NF and RO feed matrix as well the corresponding permeate matrices are shown in Figure 56. Certain characteristic peaks in the NF/RO feed matrices are labeled with letters a-d in Figure 56, which marks specific DOM fractions. Peak a can be attributed to biopolymers including carbohydrates and proteins. The difference signal intensity demonstrates the varying amount of this fraction in the present NF/RO feed matrices. Peak b eluting at around 60 minutes indicates the presence of humic substances. Peak c and d can be attributed to building blocks, low molecular-weight acids and low molecular-weight neutrals (Haberkamp et al. 2008, Huber et al. 2011). The chromatogram demonstrate also that all fractions can be nearly completely removed by the NF-270 and Toray TMG10 RO membrane, when considering the peak intensities of the NF and RO permeate.

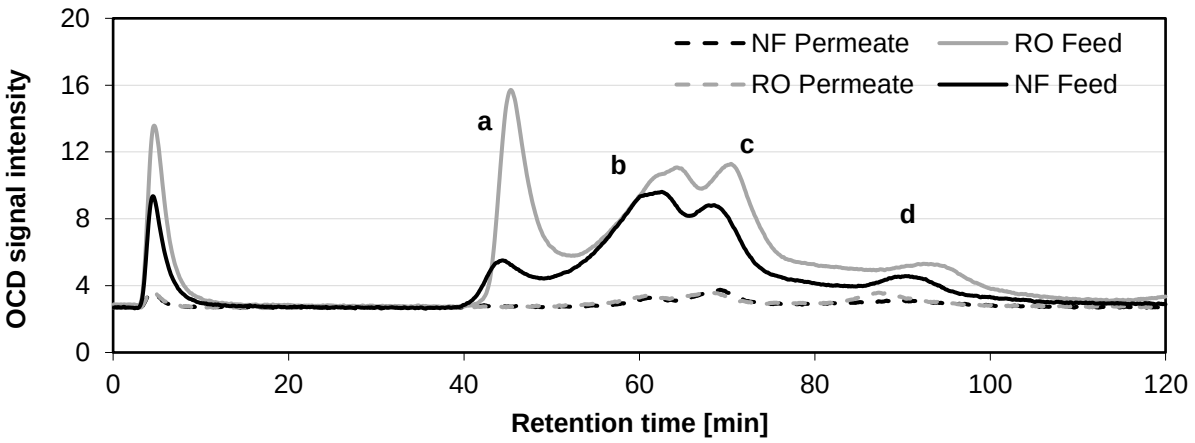

Figure 56. Liquid-chromatography-organic carbon detection (LC-OCD) chromatogram of NF feed and permeate of exp. 1 and RO feed and permeate of exp. 3. Certain characteristic peaks are labeled (a-d). Initial DOC concentration of NF/RO feed from exp. 1 = 15.2 mg/L, exp. 3 = 24.0 mg/L.

The presented data indicates the complex makeup of the used NF/RO feed matrices during this study. The membranes were exposed to an UF pre-treated raw wastewater matrix with high DOC concentrations (> 20 mg/L) and further, with a frequently changing makeup covering the whole NOM spectrum and strong presence of protein-like matter (Figure 55). This makes it more complicated to break down the matrix and perhaps also the forming CLs into their main foulants. It is likely that rather an interplay of certain foulants lead to a membrane flux decline than only one specific compound. Furthermore, it can be suggested that the fouling formation here is of complex origin and an interplay of different fouling mechanisms. The role of particular interactions between different types of foulants in the feed matrix and between the foulants and the feed matrix itself, which may strengthen or contribute towards fouling, need to be considered as well. Nevertheless, protein-like matter is expected to mainly contribute towards membrane fouling due to their high presence in the NF/RO feed matrices.

As a result, the varying complex organic compositions of the present feed matrices and further, the variety and different loads of membrane foulants displayed a challenge for the NF and RO membrane in this study. Thus, the membranes were expected to be highly covered with DOM which would result in a strong flux decline (> 50 %). As a conclusion, it is all the more surprising that the general flux decline for both membranes was “low” over an operation time of more than 80 h. In particular for the RO membrane, which is a non-porous membrane. Further long-term fouling experiments (> 120 h) are necessary to define steady-state flux conditions for both membranes and to characterize their long-term flux behavior in general.

8.2.2 Optical membrane inspection

Membrane images from NF and RO membrane specimen were investigated after operation to analyze the NF/RO membrane CLs in more detail. Figure 57 shows fouled NF membrane specimen after operation of ~90 h. For comparison, Figure 57(a) shows the NF membrane of

exp. 9 with a total flux decline of 11 % and (b) the NF membrane of exp. 6 with a flux decline of 51 %. Unlike the suggestion that the membrane of exp. 6 must possess a higher degree of surface coverage due to the stronger flux decline, both membranes show more or less the same extent of surface coverage by DOM. Moreover, the initial DOC concentration of the feed of exp. 9 was nearly twice as high compared to exp. 6, but as the images demonstrate, this difference had no effect on the extent of membrane surface coverage and flux decline.

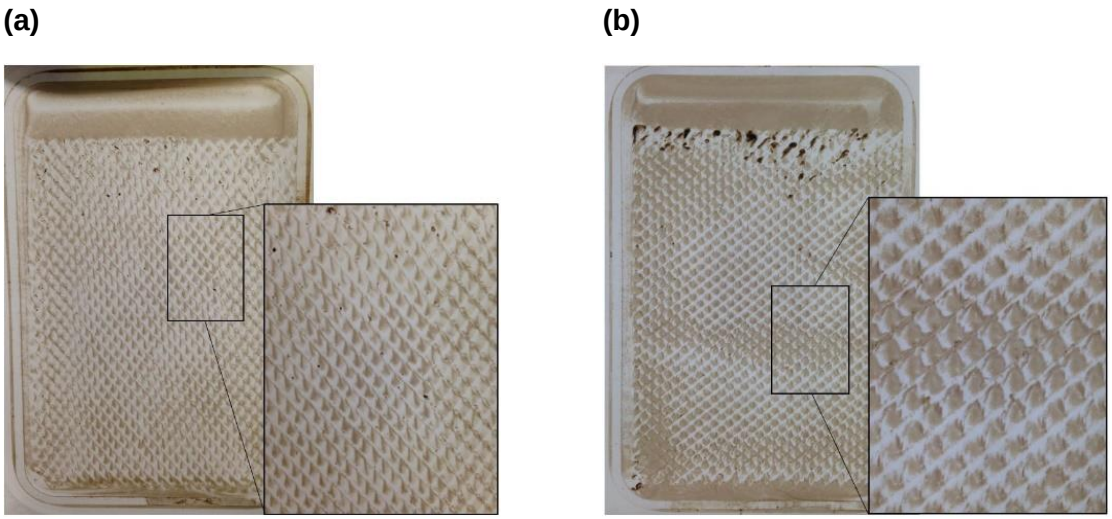

Figure 57. Images of fouled DOW NF-270 membrane specimen after operation of ~90 h. (a) exp. 9 and (b) exp. 6. Initial DOC concentrations of the feed matrix: Exp. 9, DOC = 30.7 mg/L; exp. 6, DOC = 17.2 mg/L.

Images of fouled RO membranes are shown in Figure 58. Compared to the NF membrane, the surface coverage of the RO membrane was less. However, the extent of flux decline on average was higher. This can be mostly explained by the fact that the RO membrane is non-porous. A slight layer of foulants on the membrane surface might be enough to reduce the flux across the membrane stronger than on the NF membrane. Besides, especially the images of the RO membranes show a “CL” which is not uniformly distributed across the membrane surface. This might be due to uneven flow conditions within the cross-flow test cell. Accumulated DOM on the surface might partially be removed by higher CFVs in some parts of the test cell. This uneven CFVs are likely feed spacer induced. The feed spacer was cut by hand and renewed for each experiment, which led to differences in its size. Also placement “errors” can occur so that the spacer is not completely planar on the membrane surface which can affect the flow conditions. The NF in contrary did show this uneven pattern of surface coverage, but to a lesser extent.

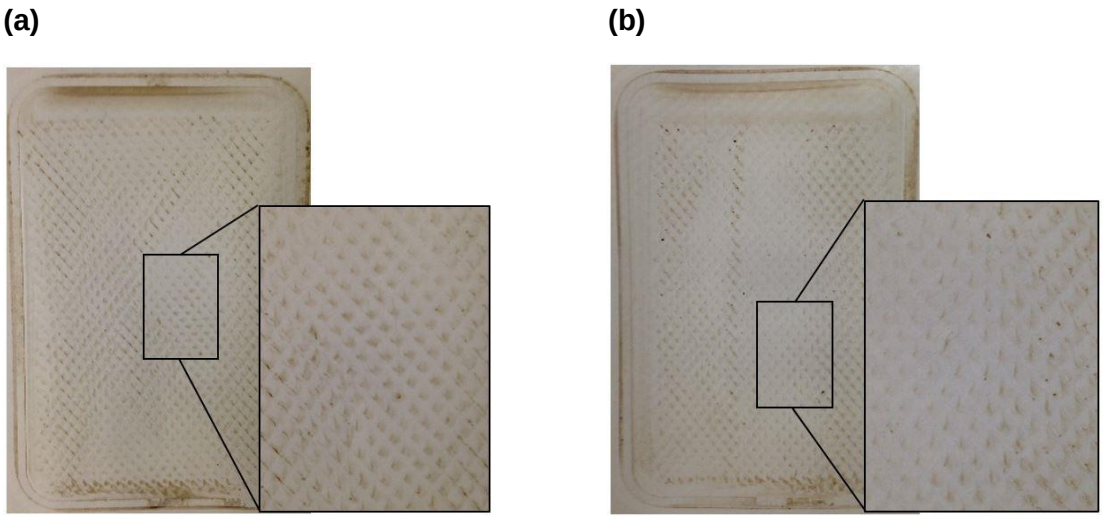

Figure 58. Photos of fouled Toray TMG10 RO membrane specimen after operation of ~90 h. (a) exp. 5 and (b) exp. 12. Initial DOC concentrations of the feed matrix: Exp. 5, DOC = 22.6 mg/L; exp. 12: DOC = 19.2 mg/L.

8.2.3 Influence of varying initial DOC concentrations in NF/RO feed matrices

The optical membrane inspection already indicates that initial DOC concentrations had no influence on the extent of surface coverage of the membranes. Now, the relationship between the initial DOC concentrations of the feed matrices and the resulting flux decline after 80 h of operation of the NF and RO membrane is shown in Figure 59.

Figure 59(a) indicates that high initial DOC concentrations in the feed matrix do not have a significant influence on NF membrane flux decline. High flux declines have been rather recorded with initial feed DOC concentrations of 12 and 17 mg/L, respectively, whereas high initial DOC concentrations led to low flux declines. Same conclusion can be made for the RO membrane (Figure 59(b)). Despite the fact that one experiment with the highest DOC of about 55 mg/L resulted in the highest flux decline and one experiment with a DOC of only 16 mg/L led to a comparable low flux decline of 16 %, the majority shows a flux decline between 25-32 % with initial DOC concentrations ranging from 19 to 38 mg/L. This all indicates no strong relationship between initial DOC concentration in the feed and extent of NF/RO flux decline. The flux decline curves illustrated in Figure 53 support this result.

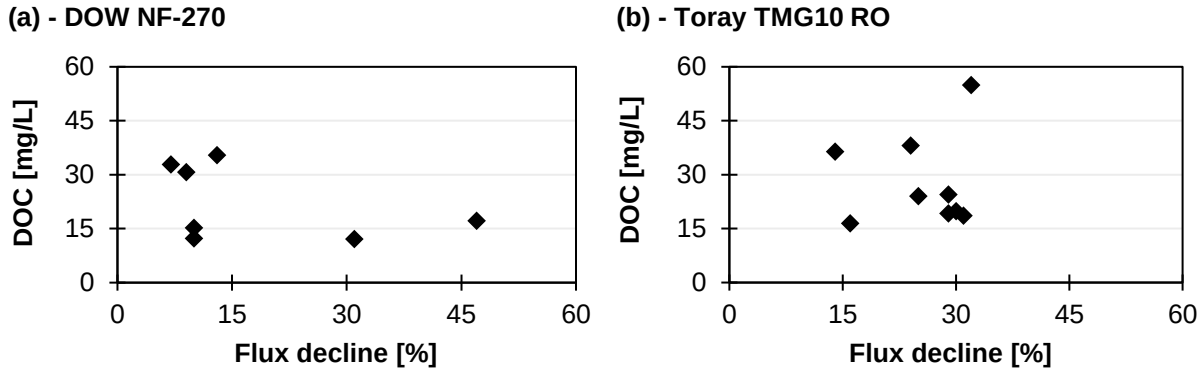

Figure 59. Initial dissolved organic carbon (DOC) concentrations of the feed matrices plotted against resulting percentage flux decline of the (a) DOW NF-270 and (b) Toray TMG10 RO membrane.

Considering the NF-270 membrane, this result can be partly explained by its unique properties which make the membrane resistant to organic fouling. The membrane is highly hydrophilic and has a low surface roughness. The surface polyamide layer of the membrane contains both carboxylic (-COOH) and amine (-NH) functional groups that can deprotonate in aqueous solution giving the membrane surface a negative charge at high pH values (pH > 6). Since biopolymers are present in a net negative charge in aqueous solution at neutral pH values, an electrostatic repulsion between foulants and membrane surface is formed (Mänttäri et al. 2004, Vogel et al. 2010). Indeed, during fouling experiments, the pH values of the present feed matrices were always ~8 so that functional groups of both membrane and biopolymers were likely deprotonated.

However, batch 4 (exp. 6 and 7) conducted with the NF membrane is different to the other NF experiments. Even though the optical inspection of the NF membranes after operation showed similar surface coverage at high and low flux decline conditions, and no strong relationship between initial DOC concentration and flux decline of the NF membrane (Figure 57 and Figure 59(a)). Both experiments of batch 4 were conducted with the same feed matrix. Despite the initial DOC was only ~15 mg/L, the flux decline was significantly higher compared to all other NF experiments. Thus, other parameters such as specific membrane-foulant interactions seem to greatly determine the extent of flux decline – at least for the NF membrane.

Mustafa et al. (2016) also reported that specific membrane-foulant interactions governed by feed chemistry have a bigger influence on NF membrane fouling for a variety of membranes with different surface chemistries than the total load of OM. Also, Zularisam et al. (2007) proved, although for a polysulfone and cellulose acetate UF membrane, rejection and fouling are not significantly dependent on DOC concentrations but mostly on the rejection mechanisms resulting from membrane-feed interactions.

As a result, it can be concluded, that specific membrane-foulant/membrane-feed interactions likely limit the accumulation of DOM determined by the drag force towards the membranes and that those interactions are potentially more contributing towards fouling than the total amount

of DOM present in the feed matrix. This can be proven from optical inspections of the fouled membranes and low influence of initial DOC concentrations on the extent of flux decline.

8.2.4 Influence of accumulated dissolved organic matter (DOM) on the membrane surface

In addition to the influence of the initial DOC concentrations of the NF/RO feed matrices on membrane fouling, also the total mass of DOM which actually accumulates on the membrane surface during operation is important to fully assess NF/RO membrane fouling. For that, membrane specimen of a defined size were cut from the fouled membrane specimen and its DOC concentration was measured. The measured DOC concentration was considered as indication for the total mass of DOM on the membrane surface. For evaluation of the results, account should be taken that each DOC was only measured once and that not all fouling experiments exhibited the same operation time. Therefore, the DOC expositions of the membranes were calculated according to equations 11 and 12 to better compare the results in a simplified way. The data is summarized in Table 23.

Table 23. Measured dissolved organic carbon (DOC) concentrations in the NF/RO cake layers (CL) as well the total DOC exposition of the membranes (E_T) and the DOC exposition per hour (E_h).

Experiment/ Membrane	Flux decline (%)	Operation time (h)	DOC_{CL} (µg/cm²)	E_h (mg_{DOC}/h)	E_T (mg_{DOC})
Exp. 1, NF	13	92	19.9	3.8	350.7
Exp. 2, RO	34	71	31.8	8.7	618.1
Exp. 3, RO	25	93	6.9	3.7	348.9
Exp. 4, RO	16	84	10.4	3.6	300.6
Exp. 5, RO	17	88	8.6	7.8	675.8
Exp. 6, NF	51	90	34.4	4.0	358.3
Exp. 7, NF	32	133	16.9	3.2	419.4
Exp. 8, NF	8	92	161.3	9.3	857.3
Exp. 9, NF	11	92	133.5	8.7	803.2
Exp. 10, RO	33	93	112.0	4.6	430.3
Exp. 11, NF	15	92	47.1	10.4	958.8
Exp. 12, RO	32	92	19.0	4.2	388.4
Exp. 13, NF	11	115	80.9	3.4	386.3
Exp. 14, RO	32	120	206.4	3.7	446.1
Exp. 15, RO	31	115	28.8	5.3	640.0

Exp. 16, RO	24	115	/	8.1	967.2

Considering the results reported in Table 23, DOC expositions of the membranes vary for each experiment depending on the individual initial DOC concentrations of the feed. Higher DOC concentrations in the feed logically lead to a higher DOC load encountered to the membranes. The data in Table 23 suggests that higher expositions (E_h and E_T) do not automatically lead to a higher flux decline.

Further, consistent to the results from chapters 8.2.2 and 8.2.3, also no correlation with the total amount of DOM ($DOCC_L$) and the NF-270 membrane can be determined ($r = -0.811$, $p < 0.05$). Once more, the results show, that not the total load of DOM nor its concentration in the feed, determines the strength of fouling of the NF membrane. Still, an indication for the high flux decline during batch 4 (exp. 6 and 7) with the NF membrane cannot be revealed. DOC_{CL} concentrations of the exp. 6 and 7 were measured to be 34.4 µg/cm^2 and 16.9 µg/cm^2, respectively. For comparison, the DOC_{CL} concentration of exp. 11 was 47.1 µg/cm^2 with a corresponding flux decline of only 15 % in total.

Slightly different the results for the RO membrane. Here, a “correlation” can be determined ($r = 0.743$, $p = < 0.05$). The more DOM accumulates on the membrane the stronger was the extent of flux decline. Contrary to the NF, the RO is a non-porous membrane. As soon as a monolayer of foulants forms on the membrane surface, the membrane flux decreases rapidly. This first adsorption occurs usually in a short period of time. Thereafter, the foulants are gradually adsorbed onto the membrane surface which enhances membrane flux decline (Li et al. 2016b). Furthermore, the principle of size exclusion is intensified in RO membrane filtration resulting in an enhanced rejection of DOM and CP compared to the NF.

Again, the results should be interpreted carefully. Operating times of the experiments are not fully comparable and thus, neither the total mass of DOM in the CL is comparable. The gradual adsorption of DOM is not an infinite process – usually an adsorption limit is reached. This means that the adsorption limit of DOM on the membrane can be reached after e.g. 90 h, but flux decline continues until 120 h of operation due to the hydraulic compression of the CL. Moreover, the total mass of DOM on the membrane surface correlates not linearly with its flux decline. A highly porous and thick CL (high mass of DOM) can result in a lower flux decline than a dense and thin CL (less mass of DOM). For this very reason, also the Spearman Rho correlation is indeed one way to evaluate the data, but it excludes absolute concentrations of DOM in the CL. Nevertheless, the present results go hand in hand with the general fouling behavior of RO membranes, but should be only considered as indication. A high flux decline of the RO membrane in the present IMS and with the present matrix might of course be due to a higher accumulation of DOM, but this needs to be investigated in further detail.

8.2.5 Influence of proteins and carbohydrates on NF/RO membrane fouling

Protein and carbohydrate concentrations were measured in order to further break down the present DOM on the basis of their nature as main NF/RO membrane foulants (Speth et al. 1998, Lee et al. 2006, Her et al. 2007, Ding et al. 2016). Therefore, Table 24 shows the protein and carbohydrate concentrations measured in the initial NF/RO feed matrices and CLs of all experiments performed with the matrices originating from WWTP Garching and WWTP Gut Marienhof (Munich). In addition, corresponding individual total flux declines for all experiments are listed and will serve as basis for the following discussion in order to classify the strength of membrane fouling.

Table 24. Measured protein and carbohydrate concentrations in NF/RO feed matrices and NF/RO cake layers as well as relating determined flux declines.

Experiment/ Membrane	Total flux decline (%)	Feed (µg/mL)		Cake layer (µg/cm²)	
		Proteins	Carbohydrates	Proteins	Carbohydrates
Exp. 1, NF	13	154.3 ± 25.2	5.9 ± 0.1	60.0 ± 2.5[b]	13.8 ± 0.9[b]
Exp. 2, RO	34	84.7 ± 0.6	4.6 ± 0.0	75.0 ± 10.0	8.0
Exp. 3, RO	25	87.3 ± 9.7	5.6 ± 0.0	31.2 ± 5.1[b]	4.4[b]
Exp. 4, RO	16	76.3 ± 2.5	5.4 ± 0.1	48.8 ± 6.7	7.3
Exp. 5, RO	17	75.1 ± 3.6	17.4 ± 0.1	35.8 ± 1.8[b]	3.7[b]
Exp. 6, NF	51	72.9 ± 3.6	4.8 ± 0.1	99.2 ± 18.8[b]	20.3 ± 3.8[b]
Exp. 7, NF	32	72.2 ± 1.5	4.2 ± 0.2	73.7 ± 3.2	15.1 ± 3.8
Exp. 8, NF	8	100.7 ± 3.7	5.2 ± 0.1	90.6 ± 1.7[b]	18.0 ± 2.2[b]
Exp. 9, NF	11	94.0 ± 0.6	4.8 ± 0.1	61.2 ± 5.0[b]	11.8 ± 1.6[b]
Exp. 10, RO	33	90.6 ± 0.8	6.6 ± 0.1	51.8 ± 6.2[b]	11.2 ± 3.2[b]
Exp. 11, NF	15	81.6 ± 1.3	4.2 ± 0.0	73.2 ± 6.3[b]	18.7 ± 4.8[b]
Exp. 12, RO	32	75.7 ± 3.7	4.0 ± 0.0	32.4 ± 5.5[b]	4.7 ± 1.5[b]
Exp. 13, NF[a]	11	41.9 ± 0.9	5.4 ± 0.1	35.0 ± 0.8	7.1 ± 0.2
Exp. 14, RO[a]	32	57.5 ± 2.9	3.1 ± 0.1	66.4 ± 7.4	13.0 ± 1.4
Exp. 15, RO[a]	31	75.2 ± 1.5	5.0 ± 0.0	58.0 ± 2.4	9.4 ± 0.8
Exp. 16, RO[a]	24	89.9 ± 2.0	3.7 ± 0.3	33.5 ± 4.1	2.3 ± 0.7

[a]NF/RO feed matrix originating from raw wastewater from WWTP Gut Marienhof (Munich).

[b]Marked values of experiments with similar operation time (~90 h). Only those values are comparable with regard to the flux decline.

In contrast to the varying DOC concentrations in the NF/RO feed matrices, the concentrations of proteins and carbohydrates in the feed were relatively constant. The measured high protein concentration for exp. 1 and high carbohydrate concentration for exp. 5 are remarkable, but the respective individual flux declines of about 13 and 17 % are under the average flux decline obtained for the NF and RO membrane (Table 21). Thus, it can be assumed that higher protein and carbohydrate concentrations in the initial NF/RO feed matrices did not consequently lead to a higher flux decline. Supporting that, exp. 6 and 7 performed with the NF membrane exhibited significant high flux declines of 51 % and 32 %, but considering the results reported in Table 24, the concentration of neither the proteins nor the carbohydrates was significantly high or low. As a result, it can be stated that the extent of flux decline here did also not depend on the concentrations of proteins or carbohydrates. A performed correlation analysis after Spearman Rho to determine possible correlations between the initial protein and carbohydrate concentrations in the feed and the extent of flux decline for all experiments with the NF and RO membrane claims this assumption. Calculated correlation coefficients do not indicate a relationship between those parameters (see Table SM9, supplementary material, Appendix F).

Regarding the concentrations of proteins and carbohydrates in the CLs the evaluation of potential relationships between their concentration and flux decline is more difficult. When the absolute concentrations of proteins and carbohydrates are considered as illustrated in Figure 60 and Figure 61, no trend can be determined.

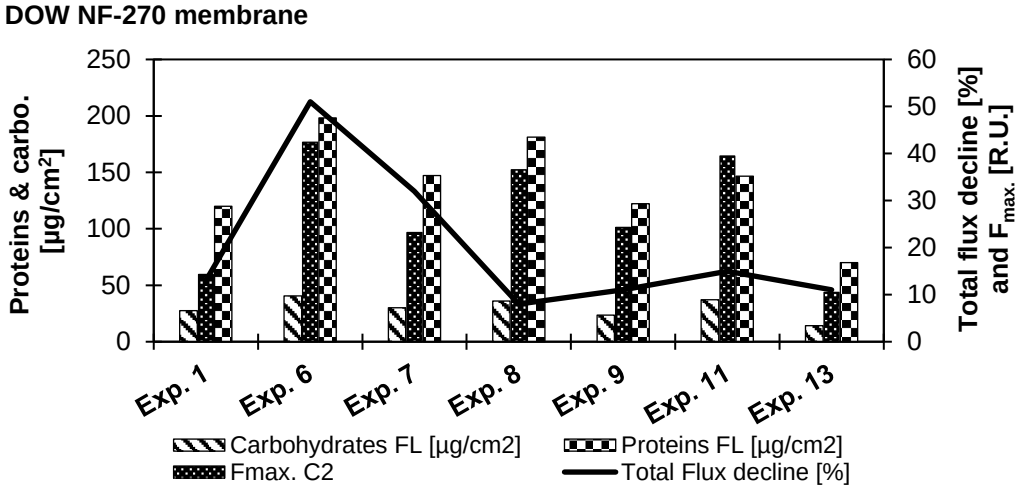

Figure 60. Relationship between the absolute concentrations of proteins and carbohydrates (carbo.) and Fmax. values of component 2 (C2) in the DOW NF-270 cake layers (CL) and the total flux decline.

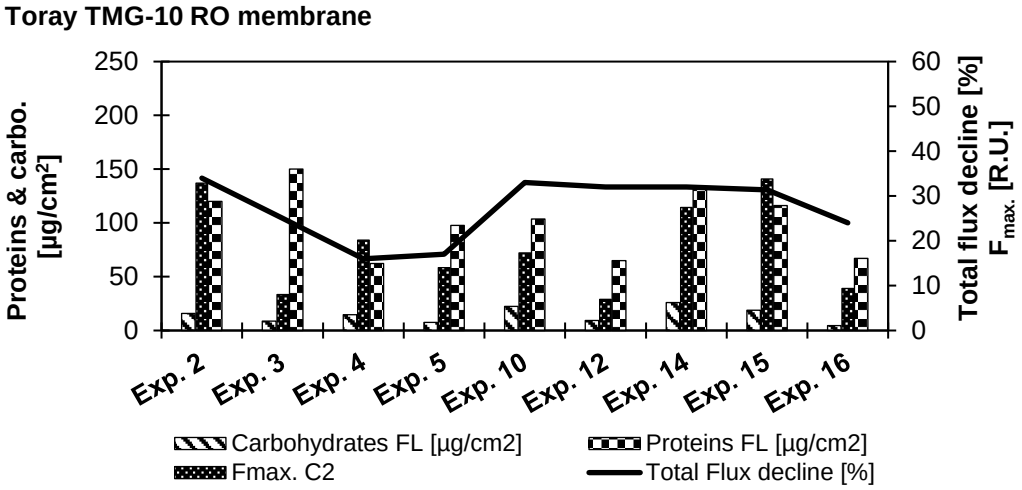

Figure 61. Relationship between the absolute concentrations of proteins and carbohydrates (carbo.) and Fmax. values of component 2 (C2) in the Toray TMG10 RO cake layers (CL) and the total flux decline.

Protein and carbohydrate concentrations tend to vary strongly. Analogous to the varying protein concentrations the $F_{max.}$ values of C2 vary similarly.

However, in contrast to that, the performed Spearman Rho correlation analysis indicates slight correlations, but rather for the carbohydrates (NF: $r = 0.559$, $p = > 0.05$, RO: $r = 0.611$, $p = < 0.05$). This is a bit surprising since the 3D-EEM spectra of the CLs, which are discussed in detail in chapter 8.2.6, indicate “solely” protein-like matter.

Analogous to the DOC_{CL} data, operation times of the experiments are not fully comparable and thus, neither the total concentrations of proteins and carbohydrates in the CLs. The data must be examined more critically since the Spearman Rho correlation excludes the absolute concentrations and indicates only that higher flux decline correlates slightly with higher carbohydrate concentrations. Moreover, the data suggests that NF/RO CLs consists mainly out of protein-like matter indicating that proteins seem to be the main membrane foulants.

For exp. 6 and 7 for the NF membrane, a high flux decline was observed, but Figure 60 shows that the concentrations in the CLs of proteins and carbohydrates separately were not significantly higher compared to the other experiments. Also the sum of the protein and carbohydrate concentrations do not provide indications. Exp. 6 with the highest flux decline in total (51 %), indeed shows the highest amount of proteins and carbohydrates in its CL when combining their concentration, but this does not apply for exp. 7 with the second highest flux decline. Its combined carbohydrate and protein concentration is lower than for e.g. exp. 4 with the lowest determined flux decline. In fact, also the ratio of carbohydrates to proteins (C/P) was calculated in order to check for anomalies in exp. 6 and 7, but again, no evidence for the higher flux decline was determined. In addition, the exposition of proteins and carbohydrates of the membranes was calculated according to equations 10 and 11. Regarding the protein and carbohydrate exposition per hour (E_h) also no trend can be determined regarding the flux

decline for the NF/RO membranes. Considering exp. 6 with the highest recorded flux decline, E_h of carbohydrates was calculated to be the highest.

Regarding Figure 61, the same can be stated for the RO membrane. A clear trend which would identify either carbohydrates or the proteins as main fouling contributors cannot be recognized. Interestingly, protein and carbohydrate concentrations measured in RO CLs are lower compared to the NF membrane. This goes along with the lower surface coverage observed for the RO membrane. Calculated C/P ratios do also not indicate a trend which correlates with the flux decline. Also here, CLs consist mainly out of protein-like matter suggesting that they seem to play a major role in fouling formation of the RO membrane.

Nevertheless, average values of the C/P ratios were calculated for the NF and RO membrane and it can be stated that the NF is more affected by carbohydrates than the RO membrane, which is indicated by the higher ratio: NF = 0.21 ± 0.02, RO = 0.14 ± 0.05. However, for the tested membranes it becomes more and more clear that the mass of biopolymers and DOM does not determine the extent of flux decline solely. But, it has to be considered that this merely applies only for the tested operation conditions (Flux = 20 LMH, CFV = 0.18 m/s).

8.2.6 Isolated components C1-C3 and NF/RO membrane fouling

Figure 62 shows 3D-EEM spectra of NF/RO CLs. It has to be taken into account, that the spectra were measured after operation. This means, that the different operation times of the experiments needs to be considered. Nevertheless, the spectra show that the CLs were mainly protein-like matter which supports the results from chapter 8.2.5. For the NF membrane the spectra of exp. 6 (flux decline 51 %) and exp. 11 (flux decline 15 %) are similar if not almost identical. This can be claimed by the calculated F_{max} values which were determined to be 42.4 and 40.0, respectively. This further supports the previous findings that a high presence of proteins alone does not determines the flux decline of the NF membrane. For the RO membrane, exemplarily the spectra of exp. 2 (flux decline 34 %) and exp. 12 (flux decline 32 %) is shown. Here, a difference can be seen, whereby only for the peak intensities. The fluorescence intensity of the protein-like region is higher for exp. 2 compared to exp. 12 (exp. 2: F_{max} = 32.9 R.U.; exp. 12: F_{max} = 6.9 R.U.). Analogous to the NF membrane, the higher presence of protein-like matter in the RO CL of exp. 2 did not consequently result in significant higher flux decline indicating that the extent of flux decline is not mass-dependent.

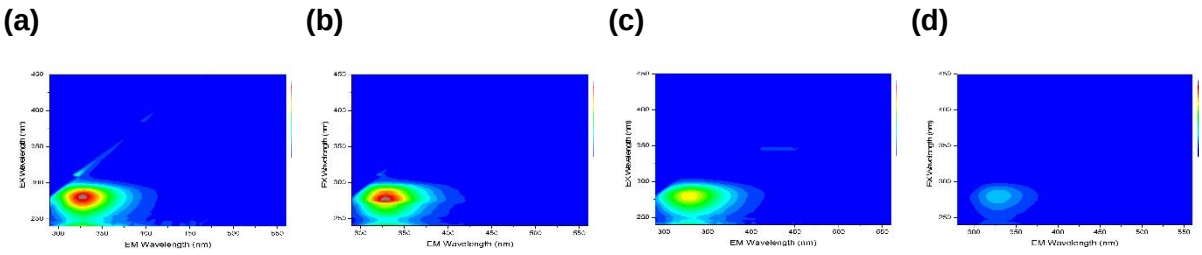

Figure 62. 3D-fluorescence excitation-emission matrix (3D-EEM) spectra of DOW NF-270 cake layers from (a) exp. 6 and (b) exp. 11, and Toray TMG10 RO cake layers from (c) exp. 2 and (d) exp. 12. Intensity scale 0-50. Corresponding DOC concentrations, DOC_{FL}: (a) exp. 6 = 34.4 µg/cm²; (b) exp. 11 = 47.1 µg/cm²; (c) exp. 2 = 31.8 µg/cm²; (d) exp. 12 = 19.0 µg/cm².

However, considering the results presented in chapter 8.2.5, also carbohydrates were found in the NF/RO CLs next to proteins and the correlation analysis indicates rather a slight correlation between the carbohydrate concentration and the resulting flux decline. Whereby this needs to be handled rather as an indication than an explicit proof due to the difficult evaluation of this data as described in chapter 8.2.5. Nevertheless, as already mentioned, a relationship between carbohydrates and the extent of flux decline cannot be confirmed by the determined 3D-EEM spectra of the CLs, which show only an intense peak of protein-like matter as it is shown in Figure 62. This can be explained by the fact that pure polysaccharides (carbohydrates) cannot be detected by fluorescence (Her et al. 2007). Therefore, also the 3D-EEM spectra need to be interpreted carefully. Not only due to the different operation times of the experiments and that carbohydrates potentially cannot be detected by EEM spectroscopy, but also due to the fact that 3D-EEM spectra are just a qualitative analysis.

In order to evaluate 3D-EEM data also quantitatively, the PARAFAC analysis is used. Also here, a correlation analysis after Spearman Rho was conducted to analyze the F_{max} values. Corresponding correlation coefficients of C1-C3 in the initial feed matrices and CLs are listed in Table 25.

Table 25. Correlation coefficients between C1, C2 and C3 concentrations in the initial feed matrices and the extent of flux decline for the DOW NF-270 and Toray TMG10 RO membrane.

		DOW NF-270			**Toray TMG10 RO**		
Feed[a]		C1	C2	C3	C1	C2	C3
Flux decline (%)	Correlation coefficient	-0.559	-0.721	-0.559	0.067	0.100	-0.017
	Significance (1-sided)	0.096	0.034	0.096	0.432	0.339	0.483
	Number of data, n	7	7	7	9	9	9
Cake layer[b]							

Total flux decline (%)	Correlation coefficient	0.000	0.378	0.541	-0.138	0.251	0.525
	Significance (1-sided)	0.500	0.201	0.105	0.362	0.257	0.073
	Number of data, n	7	7	7	9	9	9

[a]F_{max} values for C1-C3 were correlated with the extent of flux decline after 80 h of operation for better comparison.

[b]F_{max} values for C1-C3 were correlated with the total extent of flux decline after the total operation time of each experiment.

The correlation coefficients obtained for C1-C3 in the initial feed matrices support the previous results. In fact, no correlation between the quantity of the components in the initial feed matrices and the extent of flux decline could be determined. Regarding the results obtained for C1-C3 in the NF/RO CLs, it can be shown that in fact likely no correlation exists between protein-like matter (C2) and extent of flux decline. Correlation coefficients of 0.378 (NF) and 0.251 (RO) do not indicate a strong correlation, also because they are not significant ($p > 0.05$). C1 (humic-like fluorescence, hydrophobic acids) could not be detected in the CLs. Interestingly, “strongest” correlations could be determined for C3 which can be related to humic- and fulvic-like fluorescence. Coefficients of 0.541 and 0.525 for the NF and RO membrane were estimated indicating a weak correlation. Considering that the correlations are still not significant, but more significant as for C1 and C2 (see significance in Table 25). With regard to the fact that CL data is not totally comparable due to the different operation times of the experiments, which was discussed more detailed in chapter 8.2.4, it slightly indicates that humic- and fulvic-like substances are present and might play a role in fouling formation. Correlation analysis reveals that they are contributing “more” towards fouling than protein-like matter (C2). However, Figure 63 shows that the NF/RO CLs consisted of more than 90 % out of C2 (protein-like matter) as it was already stated in chapter 8.2.4 and by the 3D-EEM spectra shown in Figure 62. A strong influence of C3 can rather not be assumed. The results shown for exp. 6 and 7 in Figure 63 support this. During both experiments, a strong flux decline was detected. Exp. 6 with the strongest flux decline shows rather the same CL composition than all other NF experiments, which suggest than C3 was not a determining factor for flux decline. Only, for exp. 7, a higher portion of C3 can be detected. However, a supporting role of humic- and fulvic-like substances in fouling formation is obvious since fouling formation is rather a complex process where all DOM fractions contribute towards fouling to different degrees.

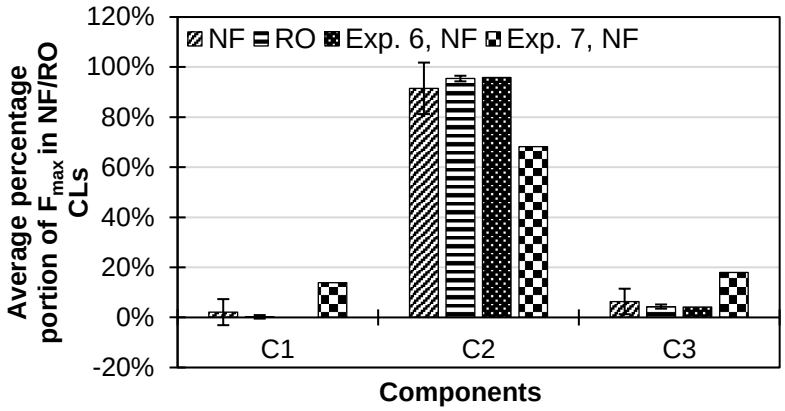

Figure 63. Average percentage portions of Fmax of C1-C3 in NF/RO cake layers (CLs). Besides the compositions of the cake layers of experiments (exp.) 6 and 7 are shown.

Those results show that all CLs, on NF and RO, consist mainly out of protein-like matter. However, a relationship between the protein-like matter and the extent of flux decline cannot be determined.

8.3 Discussion

Three fundamental reasons can be basically considered for the results, which will be discussed in the following.

1. The selected operation conditions in this study (flux = 20 LMH, CFV = 0.18 m/s) were optimal to efficiently reduce the extent of membrane fouling during the experiments and over the tested period of ~90 h.

When excluding exp. 6 and 7 of batch 4, most experiments with the NF membrane showed a flux decline between 8 and 15 % over an operating time of ~90 h or even higher as for exp. 13 (115 h). This can be partially related to the hydrophilic surface of the NF-270 membrane and its low surface roughness, which makes the membrane highly resistant to organic fouling (Mänttäri et al. 2004, Vogel et al. 2010). Another study conducted by Wang and Tang (2011) demonstrated that the NF-270 effectively mitigated organic fouling, but only under low hydrodynamic forces. During their study the NF-270 was exposed to a model solution spiked with 20 mg/L BSA and 10 mM NaCl to simulate organic fouling. Over a filtration time of 96 h the membrane shows no flux decline at a flux of 30 LMH at both pH 5.8 and 7. Slight flux decline effects could be observed at 60 LMH (Wang and Tang 2011). It has to be noted that the present matrix during this study is more complex and possess a substantial challenge for the membranes due to the broad spectrum of present NOM and the high DOC values of the feed matrices, so that the fouling phenomenon in general is supposed to be more pronounced and different to the ones presented in the mentioned studies. All parameters, the solution chemistry, diversity and characteristics of foulants as well as the operation conditions are not completely transferable.

However, the NF-270 membrane was challenged with a higher flux (60 LMH) during a last batch using an UF permeate matrix from 13.01.2017 as NF feed to check whether fouling is more pronounced when the drag force towards the membrane is enhanced. For comparison, another experiment with the same matrix was conducted at the usual conditions with 20 LMH. Both experiments were performed over ~90 h (Figure 64).

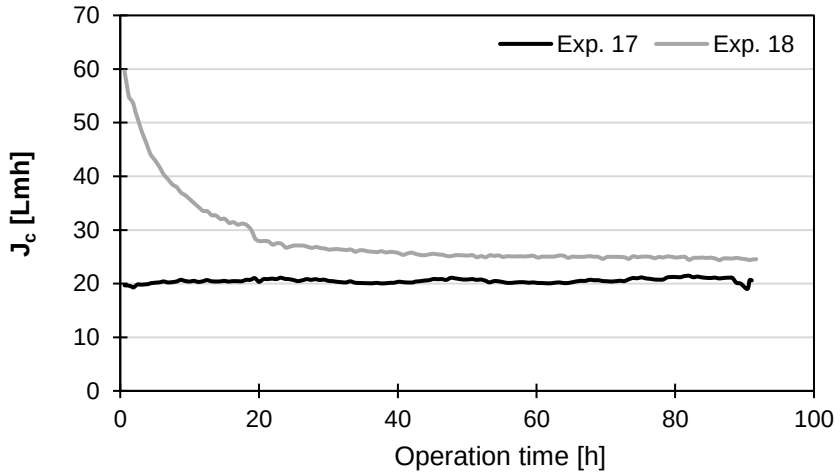

Figure 64. Temperature corrected flux (Jc) over time for experiment 17 and 18. Initial DOC concentrations of the feed: Exp. 17 = 40.9 mg/L, exp. 18 = 25.0 mg/L.

Here, clearly visible no flux decline occurred at 20 LMH, which is not really consistent to the previous described flux decline behaviour of the NF-270. Considering Figure 53, a flux decline was always observed, although only between 8–15 %. Nevertheless, substantial flux decline occurred at 60 LMH, which actually was expected. The enhanced drag force towards the membrane increases the mass flow which facilitates CP, adsorption of DOM and finally CL formation resulting in a stronger initial flux decline (Seidel and Elimelech 2002). However, after 20 h the flux decline proceeds linear and is slowed significantly. It can be assumed, that in case of exp. 18, the fouling mitigating clean membrane properties of the NF-270 were rapidly masked by deposited DOM at a flux of 60 LMH, because the hydrodynamic force overcomes the electrostatic repulsion between the DOM and the membrane. As a result, at lower operation fluxes the hydrodynamic force is reduced and specific clean membrane properties (electrostatic repulsion of DOM) are effective for a longer time during filtration mode so that fouling formation is slowed and a “stable flux” can be maintained for a longer time. The formation of a rapid CL at higher initial fluxes is likely more severe for the RO membrane due to its non-porous character. Size exclusion mechanisms are more pronounced compared to the NF membrane. With the restriction that valid data for the RO membrane to proof this is missing.

With regard to the long-term flux for the NF and RO membranes in the present treatment scheme and with the present matrix, it might be interesting to check whether the flux converges

towards a final flux irrespective from the initial flux as it was observed in previous fouling studies with synthetic model solutions (Seidel and Elimelech 2002, Wang and Tang 2011). Also the risk of biofouling becomes more relevant, which is another parameter which needs to be addressed in long-term fouling experiments. Moreover, regarding the flux curves illustrated in Figure 53, for both NF and RO membrane no real steady-state flux was achieved. Especially for the NF membrane the typical fouling pattern showing two “phases” of flux decline with a rapid initial flux decline within the first ~20 h of operation, and a slower flux decline or even steady-state conditions within a second phase, as it can be seen for the RO membrane, cannot be determined.

2. Physicochemical properties of the foulants and the feed matrix are more decisive for fouling formation than the total amount of DOM in the feed matrix.

During this study it could be revealed that initial concentrations of DOM had minor influence on the extent of flux decline, which could be also stated in previous studies (Mustafa et al. 2016). Similar to that, Zularisam et al. (2007) concluded that the DOC fractions which are most abundant in the feed matrix, are not necessarily the ones responsible for membrane flux decline. Consequently, this suggests that membrane flux is primarily determined by the fraction which interacts “best” with the membrane, so that, the properties of DOM, the membrane material, surface roughness and porosity, surface chemistry as well as feed water characteristics have an influence on membrane fouling (Al-Amoudi 2010). Whereas this effects become less important at higher flux conditions with increased hydrodynamic forces as discussed before.

Nevertheless, in general, low fouling of the NF/RO membranes was observed throughout the study so that exp. 6 and 7 conducted with the NF membrane are especially noteworthy due to their strong flux decline. Exemplarily, in Figure 65 the flux decline curves of exp. 6 and 7 as well as exp. 13 are shown.

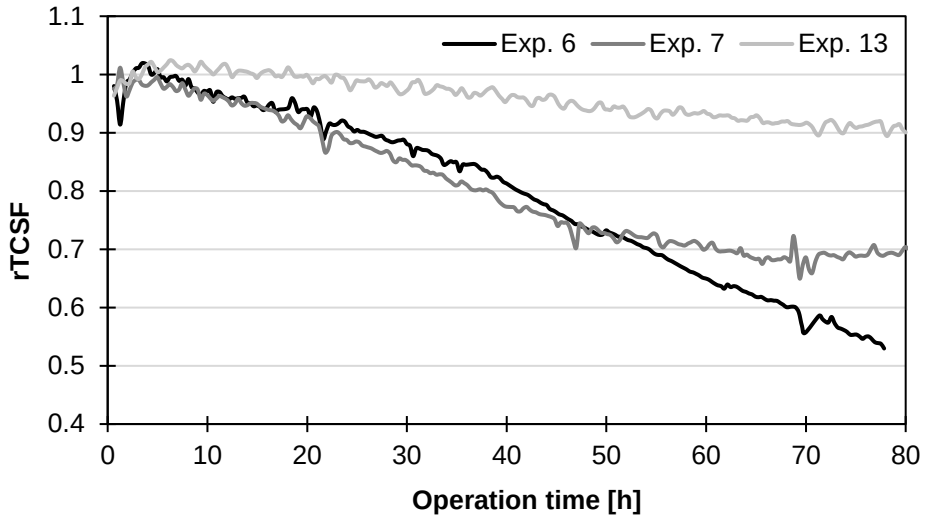

Figure 65. Relative temperature corrected flux (rTCSF) over operation time for exp. 6, 7 and 13 with the DOW NF-270 membrane. Initial DOC concentrations of the feed matrices:
Exp. 6 = 17.2 mg/L, exp. 7 = 12.1 mg/L and exp. 13 = 12.3 mg/L.

The flux decline curve of exp. 13 represents the typical flux decline curve determined during a low fouling experiment with the NF membrane. Approximately stable flux conditions can be observed within the first 20 h of operation. Thereafter the flux decreases. To remember, during all measurements of this study no differences of the CL compositions of the NF experiments were found which would explain the higher flux declines within exp. 6 and 7 of batch 4. However, within batch 4 a strong flux decline was observed. The course of the corresponding flux curves (exp. 6 and 7) indicate a direct formation of a CL so that the flux decreases significantly from the start of the experiments. Potentially, it can be assumed that certain DOC fractions which were solely present in the initial matrix of batch 4, immediately adhered onto the membrane surface, which suggests that for this DOC fraction, the negative surface charge and the hydrophilic properties of the NF-270 were ineffective. Both, zeta potential and surface angle measurements of the membrane as well as an advanced DOC fractionation of the matrix would be required to fully clarify this and in order to achieve better insights in the physicochemical interactions between membrane and feed matrix constituents.

The continuous flux decline of batch 4 suggests that a CL was continuously build-up. Once fouled, the membrane surface is masked by deposited NOM and its surface properties change. In fact, Bellona et al. (2010b) demonstrated that the surface of the NF-270 becomes more hydrophobic and less negatively charged when fouled by OM. The more hydrophobic character of the membrane surface in turn increases the risk of further attachment and flux decline by hydrophobic NOM such as humic- and fulvic acids, which would have been repelled by the clean membrane surface (Nghiem and Coleman 2008). Hydrophobic matter is present in the NF/RO feed matrices as indicated by the 3D-EEM spectra in Figure 55, but the CL spectra shown in Figure 62(a) and (b) and also Figure 63 do not indicate a strong presence of humic- and fulvic like compounds. Also the PARAFAC analysis did not indicate higher quantities of

C1 or C3 in the CLs from batch 4. This suggests that the stronger flux decline within batch 4 is likely not caused by an additional deposition of humic- and fulvic acids or deposition of other fractions which interact with the NF membrane. However, it is advisable to fractionate the present DOC fractions of both the feed and the CLs based on their physicochemical properties. It can be assumed that those properties determine more the deposition of DOM on the membranes than their absolute amount which is supported by the results that no strong correlations could be determined for absolute concentrations of proteins, carbohydrates and DOM in the CLs (see chapters 8.2.4 and 8.2.5).

Another option for the stronger flux decline within batch 4 might be the stronger NOM deposition due to a charge neutralization of the membrane surface and shielding of the interchain charges of NOM by Ca^{2+} and/or other ions in the feed matrix. For that, those experiments were analyzed in terms of their inorganic compositions in order to check this. The corresponding data is summarized in Table 26.

Table 26. Results of the inorganic characterization of the NF/RO feed matrices of selected experiments.

Experiment		Parameter								
		Ca (mg/L)	**Cl (mg/L)**	**Fe (mg/L)**	**K (mg/L)**	**Cu (µg/L)**	**Mg (mg/L)**	**Mn (µg/L)**	**Na (mg/L)**	**Zn (mg/L)**
NF	Exp. 6	65	149	< 0.1	20	< 50	20	< 25	133	0.6
	Exp. 8	63	164	< 0.1	23	< 50	22	< 25	145	0.4
RO	Exp. 2	87	272	< 0.1	18	< 50	24	< 25	176	0.3
	Exp. 5	74	117	< 0.1	17	< 50	20	< 25	98	0.2
Average		72 ± 11	176 ± 67	/	20 ± 2	/	21 ± 2	/	138 ± 32	0.4 ± 0.2

The data of exp. 2, 5, 6 and 8 represent four independent UF permeate matrices used as NF and RO feed matrices and it can be determined that Fe, Ka, Cu, Mg and Mn do not vary strongly. Ca, Cl, Na and Zn in turn fluctuate stronger. Especially Ca needs to be considered for fouling formation since it may function as bridging ion in the feed matrices and CLs.

Therefore, regarding the data shown in Table 26, it can be stated that the concentration of Ca^{2+} during exp. 6 (65 mg/L) with high flux decline (51 %) was not significantly higher compared to exp. 8 (63 mg/L) with a flux decline of only 8 %. Also other inorganic parameters show no anomalies for exp. 6.

3. Cake layer formation is not completed – rather in the initial stage, so that a clear correlation between specific foulants and flux decline is ambiguous.

During this study, an attempt has been made to investigate the role of specific DOM fractions on NF/RO membrane fouling. For none of the studied fractions such as proteins and carbohydrates, as well as three identified components during PARAFAC analysis, a significant correlation between their presence in the feed matrix or CL and the extent of flux decline could be determined. Moreover, surface coverage of the membranes (see Figure 57 and Figure 58) show that CL formation during ~90 h of operation was not as strong as expected due to the high presence of DOM in the feed matrices. The membranes are not completely covered by a CL. The flux decline curves in Figure 53 show that for both the NF and RO membrane a steady-state flux could not be maintained during 90 h of operation. This points to the assumption that CL formation was not completed. Thus, it is difficult to correlate the extent of flux decline with certain DOM fractions when the fouling process is not finished. An operation time of 90 h can be considered as short-term operation time also for bench-scale applications. When upscaling the NF/RO application to pilot-scale or even full-scale applications, usual operation times are in the range of several thousand hours (Bellona et al. 2010a).

8.4 Conclusion

During this study, fouling behavior of a NF and RO membrane implemented in an IMS for the treatment of raw municipal wastewater was investigated. UF pre-treated wastewater acquired from the WWTPs Garching and Gut Marienhof (Munich) served as feeding matrix for the downstream NF/RO membranes. The findings of this study revealed that the UF pre-treatment is capable to efficiently reject colloidal and particulate matter. However, dissolved fractions are only poorly removed, so that the downstream NF/RO membranes were exposed to a highly challenging feed matrix with a high fouling potential. The membranes were encountered to a feed matrix with DOC concentrations ranging from 12-55 mg/L, which represents a high organic load compared to secondary effluents or surface waters. Further, 3D-EEM analysis of the feed matrix revealed that the matrix covers the whole NOM spectrum. Proteins, carbohydrates as well as humic- and fulvic like matter was found to different degrees. This implies a high fouling potential since all, proteins, carbohydrates and humic substances have been identified as main NF/RO fouling contributors during previous studies. Further, it was also shown that the two acquired raw matrices from the WWTPs Garching and Gut Marienhof (Munich) are nearly identical with regard to the three identified components during PARAFAC analysis.

The NF and also the RO membrane featured average flux declines below 30 % during short-term (90-120 h) fouling experiments at 20 LMH and high DOC rejection capacities. The average flux declines of the NF and RO membrane were found to be 18.1 and 25.6 %, respectively. The flux decline was expected to be higher due to the highly challenging feed matrix. The RO membrane indicated the typical fouling pattern with a stronger initial flux decline due to the rapid adsorption of DOM and a further slow linear decline of the flux which can be

attributed to the further continuous formation of a CL. In contrary, the NF membrane showed rather a constant linear flux decline without the achievement of a steady-state flux. With the exception of batch 4, the flux decline of the NF was only between 8-15 % for the majority of experiments.

Due to that, a detailed characterization of the NF/RO membrane fouling was difficult. Membranes were not comprehensively and severe fouled by DOM. The RO was in general less covered by DOM than the NF membrane. However, the results indicate that initial DOC concentrations of the feed matrices most likely have no strong impact on the extent of flux decline of the tested membranes. Higher DOC concentrations of the feed matrices did not consequently result in a higher surface coverage. This is consistent to the absolute concentrations of carbohydrates and proteins in the feed which both do not correlate with the extent of flux decline either. Those findings indicate that the total amount of DOM and specific fractions in the feed matrix do not affect the extent of fouling of the tested NF and RO membrane.

The data collected for CL analysis must be considered carefully since the different operation times and hence the different organic loads encountered to the membranes over time must be taken into account when evaluating the experiments and in particular the composition of the CLs. The sampling method of the UF permeate was improved throughout the study in order to provide the matrix as fresh as possible for NF/RO fouling experiments without storage, cooling, etc. Because of that, a uniform operation time of the experiments was not always possible. However, CLs were analyzed in terms of protein, carbohydrate and DOC concentrations as well as analyzed by 3D-EEM and PARAFAC.

The total amount of DOM accumulated on the membranes, which was indicated by the DOC concentrations, supports the results that no strong correlation exists between the mass of DOM and the extent of flux decline. The total amount of DOM on the membranes during this study had no influence on the extent of membrane fouling. Not surprisingly, that absolute protein and carbohydrate concentrations in the CL samples do not contribute to CL formation in any relationship. It can be assumed, that the deposits on the membranes during the experiments are partially rather adsorbed particles in the initial stage than a pronounced gel or cake layer.

More pronounced CLs would be actually required to eventually determine the specific role of certain DOM fractions in CL formation on the NF and RO membranes.

A Spearman Rho correlation analysis was conducted, to check whether relationships exist when excluding absolute concentrations. Slight correlations were only detected for the carbohydrate concentrations in the CLs and the extent of flux decline (NF: $r = 0.559$, $p = > 0.05$, RO: $r = 0.611$, $p = < 0.04$).

3D-EEM spectroscopy was utilized in order to display the DOM which accumulated on the membranes. The spectra indicated nearly solely protein-like fluorescence. Moreover, the PARAFAC analysis indicates also humic- and fulvic-like fluorescence. All in all, the data reveals that the CLs are mainly protein-like matter, which suggests that they play a major role for the fouling formation of the NF/RO membranes operating with this raw wastewater matrix.

This was expected since 3D-EEM spectra of the feed matrices show strong proteinaceous fluorescence.

Regarding the PARAFAC model, a 3-component model was established with the available data. C1 and C3 were allocated with humic- and fulvic like matter, C2 with protein-like matter. Another Spearman Rho correlation analysis with C1-C3 and the extent of flux decline indicates rather correlations with humic-like matter.

In fact, all DOC fractions could be found in NF/RO Fls to different degrees, but none of them could be really related to flux decline due to the poor CL formation. Results showed that mainly proteins build up the CLs, but correlations with the extent of flux decline were rather found for carbohydrates and humic-like substances. However, the data should be considered carefully. Total amount of DOM in the feed and on the membrane did not determine flux decline during this study. It is assumed that the major contributing factor are specific membrane-foulant interactions.

For the NF membrane this low fouling behavior can be mainly explained by its surface characteristics. The negatively charged and hydrophilic surface effectively repel (hydrophobic) DOM, which limits the formation of organic membrane fouling. It can be further concluded that the operation conditions were favorable to limit the adsorption and rapid build-up of a CL since a strong flux decline was determined at 60 LMH due to the enhanced hydrodynamic forces, but not at 20 LMH.

However, one batch with the NF membranes showed a high linear flux decline much different to the ones usually detected. On the basis of the collected data in this study regarding protein and carbohydrate concentrations as well as 3D-EEM spectroscopy and PARAFAC, this outcome cannot be explained. Water quality parameters such as pH, conductivity or UVA_{254} and an inorganic characterization of the feed matrix did not indicate any differences to all other experiments.

9 CT scanning of membrane feed spacers – Impact of spacer model accuracy on hydrodynamic and solute transport modeling in membrane feed channels (Publication #6)

Membrane treatment applications are considered within this thesis in more energy-efficient potable water reuse schemes. Beside UF treatment, NF and RO treatment are key treatment barriers for contaminants present in municipal wastewater. NF and RO membrane applications are mainly applied in spiral-wound applications. Likewise all membrane processes, spiral-wound membrane applications are mainly hindered by membrane fouling. Spacers are utilized to (i) provide a feed channel between sheets of neighboring membranes and (ii) enhance mass transfer by inducing an intricate flow pattern. However, there is a clear need for the optimization of the spacer geometry, as it is accountable for an increased fouling propensity due to the creation of stagnant water zones with elevated fouling concentration. Thus, hypothesis #4 is stated as:

> *"A new spacer design can be developed for NF/RO membranes which can significantly reduce pressure drop and concentration polarization. An altered shape and orientation of the filaments can generate an unsteady flow regime, conventional spacers are not able to produce. The unsteadiness will further enhance depolarization and hence reduce the fouling potential."*

Hypothesis #4 is tested and answered within this chapter. This chapter is mainly based on publication #6, which serve as basis for reliable investigation and development of novel spacer geometries. It was found that the spacer model accuracy has a significant impact on the hydrodynamic and solute transport modeling results. Therefore, a new CT scan approach was proposed. However, novel spacer geometries are not presented in publication #6. Based on the findings of publication #6, in chapter 9.5 the potential of novel spacer geometries with improved fouling propensities are discussed. Hence, hypothesis #4 is assessed as positive.

Nils Horstmeyer[a], Thomas Lippert[a], David Schön[a], Felizitas Schlederer[a], Cristian Picioreanu[b], Klaus Achterhold[c], Franz Pfeiffer[c,d] and Jörg E. Drewes[a]

[a]Chair of Urban Water Systems Engineering, Technical University of Munich, Am Coulombwall 3, 85748 Garching/München, Germany.

[b]Department of Biotechnology, Delft University of Technology, Van der Maasweg 9, 2629 HZ Delft, The Netherlands.

[c]Chair of Biomedical Physics, Department of Physics and Munich School of BioEngineering, Technical University of Munich, James-Franck-Str. 1, 85748 Garching, Germany.

[d]Department of Diagnostic and Interventional Radiology, Klinikum rechts der Isar, Technical University of Munich, Munich, Germany.

The following publication was published with editorial changes in:

Horstmeyer, N., Lippert, T., Schön, D., Schlederer, F., Picioreanu, C., Achterhold, K., Pfeiffer, F., Drewes, J.E. (2018) CT scanning of membrane feed spacers – Impact of spacer model accuracy on hydrodynamic and solute transport modeling in membrane feed channels. *Journal of Membrane Science*, 564, 133–145.

Abstract: This study evaluated the impact of precise representation of spacer geometry on numerical simulations of hydrodynamics and solute transport in feed channels of membrane processes. Three levels of increasing geometry accuracy were assessed: i) cylindrical filaments, ii) filaments with circular sections of variable diameter based on microscopic measurements, and iii) geometries obtained from X-ray computed tomography (CT scans) in three resolutions (22 µm, 11 µm, and 5.5 µm). The three-dimensional CT scans revealed quasi-elliptic, not circular, cross-sections of the filaments. Microscopic measurements fail to account for this ellipticity, resulting in overestimation of pressure drop calculated at industry-typical average velocities (0.07–0.15 m s^{-1}) by a factor of 1.8 compared to CT-based geometries. On the other hand, the cylindrical spacer filaments representation overestimates concentration polarization at the membrane surface compared to CT-based geometries. Experimental results of pressure drop and particle deposition were in close agreement with simulations using CT scanned geometries. This work demonstrates that modeling results depend significantly on the spacer geometry accuracy. Within the investigated CT scan accuracies 20 µm was found sufficient for modeling hydrodynamics and solute transport in spacer-filled feed channels. The results may be useful for reliable investigation and development of novel spacer geometries.

Keywords: Computational fluid dynamics (CFD); feed channel; feed spacer 3-D geometry; scan accuracy; X-ray computed tomography (CT); particle deposition; mass transfer

9.1 Introduction

Feed spacers are used in spiral-wound (SW) membrane modules to create a flow channel between two sheets of adjacent membrane leaves and to potentially enhance feed water mixing so that the build-up of concentration polarization at the membrane surface is attenuated (Melin and Rautenbach 2007). The most widely applied spacer geometry in practice is the bi-planar net made of extruded polypropylene. It comprises two layers of parallel filaments (non-woven), which commonly form a diamond-shaped layout at a thickness of typically 0.6 - 0.9 mm (24 - 36 mil) (Vrouwenvelder et al. 2010, Johnson and Busch 2010). Spacer filaments deviate from a straight cylindrical shape and exhibit varying thickness (“necking”) with the largest diameters at the intersection points (Johnson and Busch 2010, Bucs et al. 2015). Therefore, spacers exhibit a rather complex and irregular geometry.

Spacer geometry is critical to module performance as it directly relates to hydrodynamic and solute transport (Haidari et al. 2018). The flow field also determines the local distribution of foulants (Radu et al. 2014). Thus, for quantitatively reliable fluid flow and solute transport simulations employing computational fluid dynamics (CFD), spacer model geometries close to the original conditions are crucial. However, current spacer geometry modeling is still carried out using far-ranging simplification of the geometry. Two-dimensional (2-D) representations of the cross-flow channel that are used to quickly obtain qualitative results (e.g. by modeling the spacer as an array of circular flow obstacles) were reported to oversimplify the intricate three-dimensional (3-D) hydrodynamics within cross-flow channels (Picioreanu et al. 2009, Shakaib et al. 2007). Various 3-D CFD studies were conducted to overcome the insufficiency of 2-D models, but were largely limited to simple cylindrical spacer representations (Shakaib et al. 2007, Saeed et al. 2012), thus neglecting the variability of the filament diameters. A more accurate representation of spacer geometry was proposed by Picioreanu et al. (2009). In that work, the non-uniform spacer filaments were measured by optical microscopy and the conventionally applied cylindrical strands were replaced by an array of truncated cones with varying diameters. The study revealed that for instance pressure drop computed with the more complex spacer geometry could be twice as high as the one resulting from a simple cylindrical approximation, at flow rates typically applied in engineering practice (Picioreanu et al. 2009). This modeling method was further refined, so that the spacers were not only assembled out of truncated cones with edges at the contact boundaries, but also modeled by use of characteristic dimensions and cubic extrusion guides creating smooth filament surfaces (Radu et al. 2014). At the same time, measurement techniques also evolved and recently scanning electron microscopy (SEM) was employed to more accurately assess the characteristic dimensions of spacer geometry (Bucs et al. 2015, Radu et al. 2014).

The latest development in the evolution of spacer geometry accuracy was proposed by Haaksman et al. (2017). In that work, an X-ray computed tomography (CT) scan was carried out to obtain accurate 3-D geometries for any given spacer design. CFD results revealed that the CT scan approach allows for a better quantification of local distribution of velocity and shear (Haaksman et al. 2017). However, a study that simulates solute transport on CT scanned spacer geometries is still lacking, while recent studies aiming on CFD modeling and mass transfer still use the cylindrical geometry (Gu et al. 2017, Kavianipour et al. 2017). Also, a conclusive assessment on how the CT scan accuracy effects hydrodynamics and solute transport simulations in the feed channel is missing. Siddiqui et al. (2017a) investigated the accuracy of different porosity quantification methods of spacer-filled feed channels and the impact on hydrodynamic predictions. Results showed that the microscopic techniques deviate significantly from the more accurate methods for feed-channel porosity measurements (i.e., volume displacement technique, weight and density technique, CT scanning technique) (Siddiqui et al. 2017a). Deviations in porosity measurement accuracy can result in a significantly different prediction of the pressure drop of -31% to 43%, with CT scanning being the recommended porosity measurement technique aimed for numerical studies (Siddiqui et al. 2017a). However, the accuracy of geometry (and thus, porosity) determination depends

heavily on the CT scan resolution. Thus, this study aims (i) to validate the proposed CT scanning approach by modeling hydrodynamics, particle deposition and solute transport within the feed channel, (ii) to verify modeling results of pressure drop and particle deposition through experimental tests, and (iii) to apply the most accurate CT scan up to date to investigate the influence of the CT scan accuracy on CFD and solute transport simulations. In addition, we present here a simplified workflow of converting raw CT scan data to solid shape data to generate the model geometry usable in CFD and solute transport simulations. The development of a periodic computational domain, which is also delineated within this work, allows to reconstruct a spacer net and is applied for numerically efficient particle deposition and solute transport modeling.

9.2 Materials and methods

9.2.1 CT scanning procedure

The geometry of a commercially available diamond-shaped spacer (Toray Industries, Inc., Tokyo, Japan) with a thickness of 34 mil (0.86 mm) was assessed by use of computed tomography (CT) scans. The scan of a piece of this spacer comprising 2×3 full rhomboidal mesh elements was executed with a ZEISS Xradia 500 Versa X-ray CT microscope (Carl Zeiss AG, Oberkochen, Germany), using the cone beam of a transmission tube (nt100, Nordson Dage) at a voltage of 60 kVp, power of 4.5 W with a tungsten target and no additional filter. 3601 projections were collected for full (360°) rotation of the sample. The sample was mounted with polystyrene on the sample holder. Figure 66 displays images of the investigated spacer mesh and the fixed layout of the measurement in the X-ray microscope. The region of interest (ROI) for all measurements was the mesh element nearest the support but still uncovered by the polystyrene (avoidance of potential movement of the spacer during measurement). The data reconstruction was done with the Scout-and-Scan™ Control System Reconstructor (version 11.1.5707) and saved in digital imaging and communications in medicine (DICOM) format as attenuation values. The DICOM data where read into VGStudio MAX (version 2.0, Volume Graphics GmbH, Heidelberg, Germany), converted into isosurfaces by thresholding, and stored as 3-D stereo lithography (STL) file.

The ZEISS Xradia 500 Versa CT microscope uses a two-step magnification of the sample. A geometric magnification of the sample projection onto a scintillator screen is done via the source to object distance (SOD), and the object to scintillator distance (OSD). With the SOD fixed at 70 mm and the OSD at 18 mm, the geometric magnification was M_{geo} = (SOD+OSD)/SOD = 1.26 in all experiments. The scintillator converts X-rays into visible light. Switchable magnifying optics between scintillator and detector (iKon-L DW936N BV, Andor) magnifies the scintillator image further. The 4x optical magnification (M_{opt}) of the ZEISS CT microscope was used in the experiment due to the optimal combination of resolution and scintillator efficiency. The detector has 2048 x 2048 pixels of 13.5 x 13.5 µm. Binning into 1024 x 1024 pixel of 27 x 27 µm (bin2), 512 x 512 pixel of 54 x 54 µm (bin4) and 256 x 256

pixel of 108 x 108 µm (bin8) was performed for the three measurements at the three effective, i.e. binned, pixel sizes r_D = 27, 54 and 108 µm. The spot size of the X-ray source was determined by the knife-edge method to be S = 2.2 µm at 60 kVp and 4.5 W. Due to the small geometric magnification , this spot size S has only a minor effect on the effective voxel size r_{eff} of the reconstruction (equation 14).

$$r_{eff} = \frac{\sqrt{\left(\frac{r_D}{M_{opt}}\right)^2 + S^2 \cdot (M_{geo} - 1)}}{M_{geo}} \tag{14}$$

with r_D the binned detector pixel size, S the spot size of the X-ray source, M_{opt} the optical magnification (M_{opt} = 4) and M_{geo} the geometric magnification (M_{geo} = 1.26). Repeating the tomography with changed detector pixel sizes r_D by binning, the resolution was changed without changing the other parameters of the measurement. The effective voxel size of the reconstructed object was r_{eff} = 5.44 µm (bin2), 10.77 µm (bin4) and 21.50 µm (bin8), referred to in the following as 5.5, 11 and 22 µm CT scan accuracies.

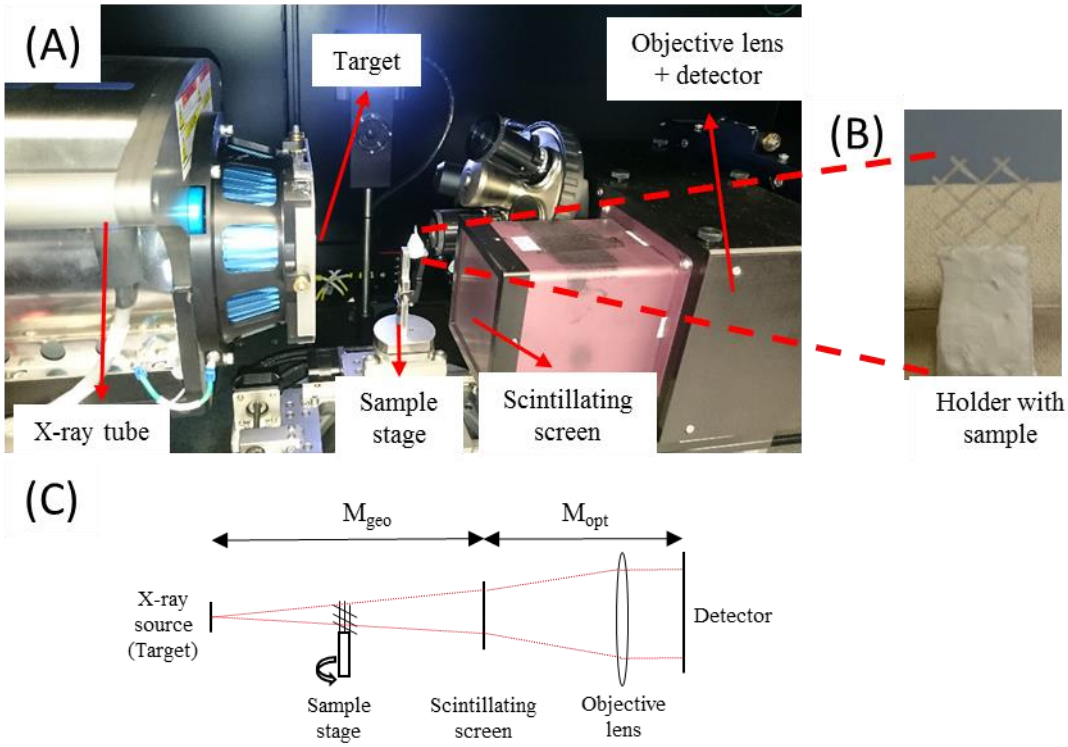

Figure 66. Microscopic CT scan setup. **(A)** X-ray microscope with system components: X-ray tube (including electron gun, cathode and electron focus), target, sample stage and detector assembling (including scintillating screen, objective lens and detector). **(B)** Analyzed feed spacer mesh with 2 x 3 spacer mesh rhomboids mounted into a polystyrene holder fixed in the X-ray microscope. **(C)** Schematic of the system components with the two-step magnification of the sample. A geometric magnification (Mgeo) of the sample projection onto a scintillator screen is done via the X-ray source, the optical magnification (Mopt) is achieved by a 4x objective.

9.2.2 Surface fitting of the CT scanned feed spacer, solid shape and periodic geometry conversion

The transformed output data format of the CT scanner, a 3-D STL file of the spacer specimen, was not directly usable within the employed CFD software, COMSOL Multiphysics (version 5.3, Comsol Inc., Burlington, MA, USA). Moreover, the STL mesh deviated slightly from the geometric periodicity of the repetitive spacer mesh pattern, possibly due to a slight heterogeneity of the extruded polypropylene fibres resulted during the manufacturing process. However, a periodic geometry is highly desirable for CFD simulations because it allows a significant reduction in the size of a representative computational domain. A solution strategy to overcome these impediments is to precisely remodel the complex geometry, so that a perfectly periodic geometry is created while the utmost of the CT scan accuracy is preserved. This was achieved by use of the Geomagic Design X (3D Systems Inc., Rock Hill, SC, USA) mesh healing and surfacing functionalities, which allow creating solids from a non-uniform polygon mesh. First, the mesh was aligned in an XY-plane and all irrelevant point clouds (due to background noise during CT scanning) lying outside of the spacer geometry were removed via cutting operations. Afterwards the spacer surface was cleared of any holes and defects were repaired (as in Haaksman et al. (2017)), which was done with the further meshing functionalities of Geomagic. To create a precise freeform geometry true to the original scan output, the “Auto Surface Function” of Geomagic was used. This function was able to achieve a high accuracy in the conversion from STL surface triangles into a freeform solid by preserving the full detail of the scan (up to 1,222 single surface elements in one rhomboid for the 5.44 µm scan accuracy). Subsequently, the geometry was cut on all four intersecting edges. Figure 67A illustrates the workflow starting with the “real” spacer up to the solid shape conversion for usage in COMSOL Multiphysics.

To impose exact periodicity on the unit geometry the filament openings were matched, i.e. both edges were projected onto one sketch, where a closed spline was created that averages the two original circumferences (Figure 67B). The closed spline was then used to construct a 0.05 mm thick loft at the edges. This artificial alteration of the CT geometry for the gain of a periodic domain was deemed acceptable, as the difference between the two opening edges was minimal. A spacer mesh was finally created by merging the four lofts with the spacer unit (Figure 67B). The procedure was subsequently performed for all three CT scan accuracies (22 µm, 11 µm, and 5.5 µm), with results presented in Figure 68C-E. This new method ensures domain periodicity which allows for an efficient data processing and easy construction of larger spacer nets.

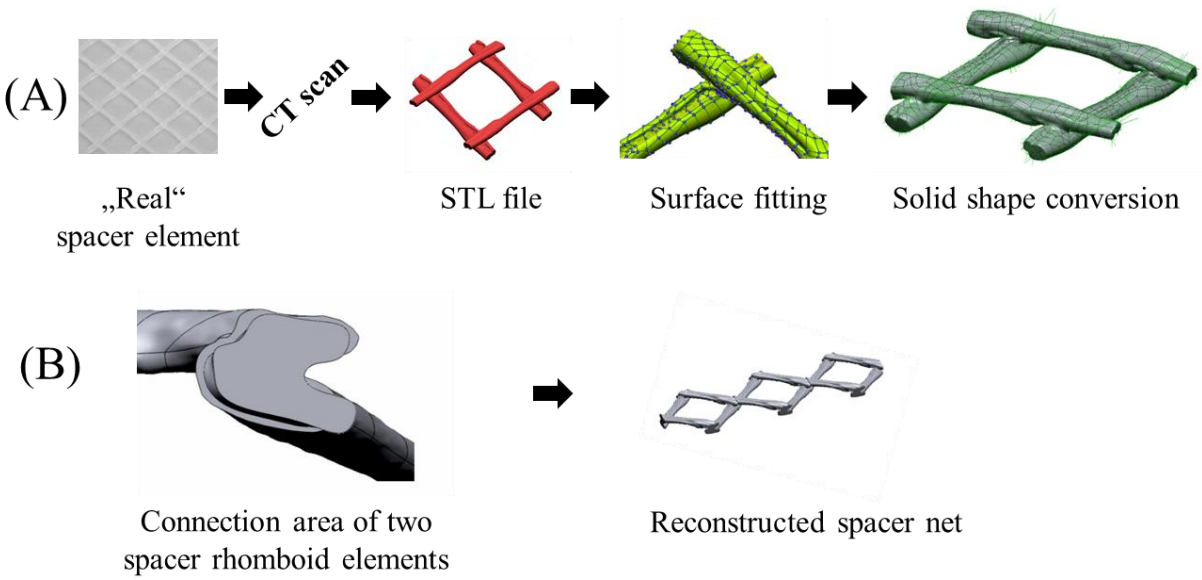

Figure 67. (A) Workflow of the CT scan approach. The “real” feed spacer was CT scanned, then the STL mesh file was processed for mesh alignment in plane, noise was removed and mesh defects repaired. Subsequently, the repaired geometry was used for surface fitting and conversion into a solid shape. **(B)** Realization of a periodic feed spacer net. The connection area between two rhomboid spacer elements was matched with a closed spline to create a spacer net.

9.2.3 Derivation of simplified feed spacer geometries

The 3-D CT scan was further displayed in top view in Geomagic Design, corresponding to the conventional microscopic perspective used to measure the spacer dimensions (e.g., in Picioreanu et al. (2009), Bucs et al. (2014)). The varying horizontal diameters of each filament were then measured at seven locations on each strand. Based on the measured diameters, circles were drawn and the spacer was rebuilt by extrusion operations, similar to the procedures reported in previous studies (Picioreanu et al. 2009, Haaksman et al. 2017, Bucs et al. 2014). The resulting two filament segments were vertically placed in a way that the prescribed channel thickness of 0.86 mm (34 mil) was met (Figure 68B). Finally, the same procedure as in Section 9.2.2 was applied to create lofts on opposing edges to generate a periodic domain. This simplified spacer geometry is termed here “microscopy-based”.

The simplified cylindrical spacer representation in Figure 68A was obtained by replacing the irregular filament geometries by cylinders, with diameters set to half of the channel height (0.43 mm). This is the same procedure used in several earlier 3-D CFD studies (Shakaib et al. 2007, Saeed et al. 2012, Li and Tung 2008a, Mojab et al. 2014, Al-Sharif et al. 2013, Lau et al. 2009, Karode and Kumar 2001).

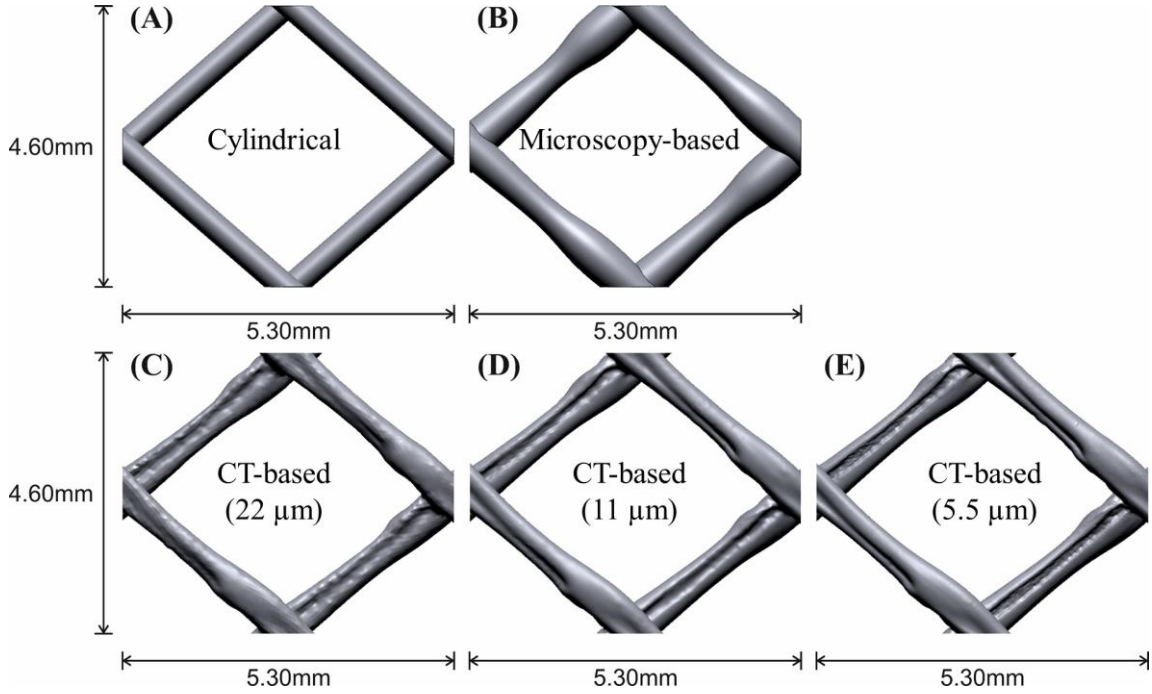

Figure 68. Comparison of the different feed spacer model geometries and CT scan accuracies. **(A)** Cylindrical filaments; **(B)** Top-view microscopy-based filaments with circular section; **(C–E)** Remodeled geometries in increasing CT scan accuracy (22 µm, 11 µm, and 5.5 µm). The spacer height is 0.86 mm in all cases.

9.2.4 Fluid domain modeling

The geometries of the fluid domains surrounding the spacers were obtained by subtracting the different spacer geometries (Figure 68) from blocks with size $4.60 \times 5.30 \times 0.86$ mm. This differential volume corresponds to the water body encasing one spacer mesh element between the lateral faces (periodic in the two lateral directions) and the two membrane surfaces (top and bottom faces). The computational domain for the CT-based spacers is shown in Figure 69.

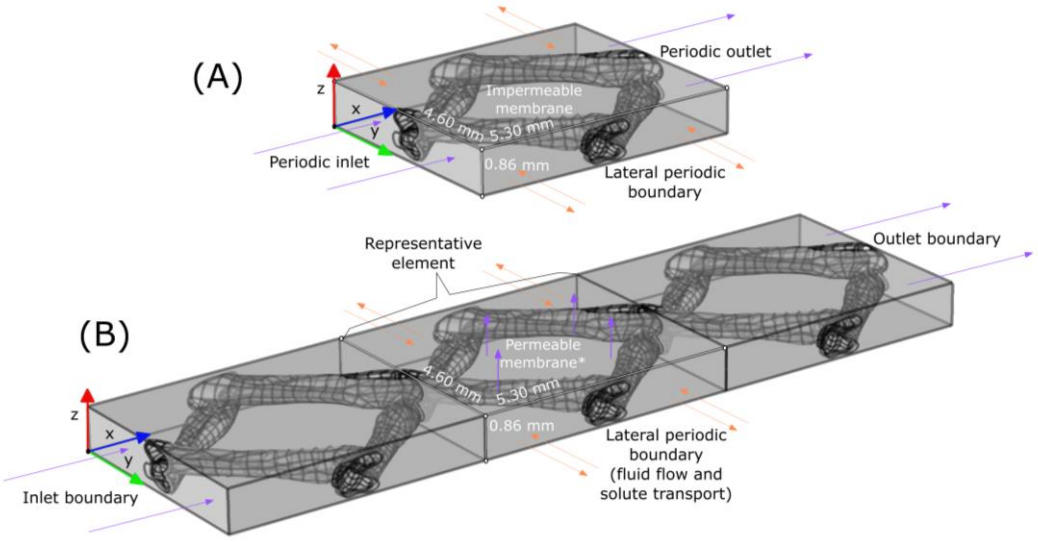

Figure 69. (A) Periodic domain used for CFD only, with CT-based feed spacer geometries. The flow domain is the difference between a rectangular block and the spacer geometry. The flow with a desired average velocity was driven by a pressure difference set between the periodic inlet and the opposite outlet boundary. No pressure difference was imposed between the lateral periodic boundaries. Top and bottom membrane walls were considered impermeable to flow. **(B)** Three-element domain used for solute mass transfer calculations. Laminar inflow and ambient pressure outflow were imposed, while the lateral boundaries were periodic. *1 membrane wall was considered permeable for water but impermeable for solutes. Please note that we visualize due to illustration reasons the top membrane permeable in Figure 69B, while all results show the bottom membrane as permeable membrane.

9.2.5 Flow model

Water flow through the spacer-filled feed channel was computed according to the incompressible, laminar, steady-state Navier-Stokes equations 15 and 16:

$$\rho(\mathbf{u} \cdot \nabla)\mathbf{u} + \nabla p = \nabla \cdot (\mu \nabla \mathbf{u}) \quad (15)$$

$$\nabla \cdot \mathbf{u} = 0 \quad (16)$$

with $\mathbf{u}$ = (u_x, u_y, u_z) representing the velocity vector, p the pressure, μ and ρ the dynamic viscosity and density of water at 20°C, respectively. The assumption of laminar flow is justified as solely industry-typical flow velocities (u_{in} = 0.07–0.15 m s^{-1}) for the given geometries were tested, corresponding to Reynolds numbers between 84 and 203 (according to Schock and

Miquel (1987)), in which unsteady or turbulent flow features were shown to be minimal (Bucs et al. 2015, Fimbres-Weihs and Wiley 2010).

To model fluid flow in a single spacer mesh element and still undisturbed by entrance, exit or lateral wall effects, periodic boundary conditions were set on each pair of parallel lateral faces. The flow was driven by a pressure difference between the periodic inlet and the opposite outlet boundary. An additional constraint (equation 17) iterates this pressure difference until the actual flow rate q_{in} matches the prescribed flow rate $q_{set} = u_{in} \cdot A_{in}$. Hereby, A_{in} is the area of the inlet face (width x height), not accounting for the spacer imprint. Consequently, A_{in} is equal for all tested geometries regardless of spacer accuracy, so that the same q_{set} (and thus q_{in}) is imposed on all different geometries. The total inlet area A_{in} for all domains was equal to 0.86×4.60 mm (similar to the approach in Haaksman et al. (2017) and Radu et al. (2014)). Therefore, velocity u_{in} is defined as the average x-component of the flow velocity (normal to the inlet surface) over the total inlet section, with zero velocity taken in the spacer-occupied inlet area.

$$\int_{A_{in}} u_x dA = q_{set} = q_{in} \tag{17}$$

No pressure difference was imposed between the lateral periodic boundaries. For the hydrodynamic simulations, the membrane walls were considered to be impermeable, as the permeation rates typical for NF and RO membranes are less than 0.1% of the channel flow rates. This would not affect the flow fields and pressure drop in any significant way (also according to the studies of Radu et al. 2014, Shakaib et al. 2007, Lau et al. 2009, Karabelas et al. 2015). Except the periodic boundaries, all surfaces were therefore modeled as no-slip walls. Domain dimensions and boundary conditions are summarized in Figure 69B and in Table 27.

Table 27. Boundary conditions for the solute transport model.

Boundary surface	**Flow model**		**Solute transport model**
	1 – hydrodynamics only	2 – hydrodynamics with solute transport	
Inlet	Periodic with outlet	Laminar inflow	Reference Concentration
$x = 0\ mm$		$u_{in} = 0.07\ m \cdot s^{-1}$ $u_{in} = 0.11\ m \cdot s^{-1}$ $u_{in} = 0.15\ m \cdot s^{-1}$	$c_{ref} = 1\ mol \cdot m^{-3}$
Outlet	Periodic with inlet	Pressure	No diffusion
$x = 15.9\ mm$		$p = 70\ psi\ (4.8\ bar)$	$D_i(\partial c_i/\partial x) = 0$

Lateral boundaries	Periodic condition	Periodic condition	Periodic condition
$y = 0\ mm$	$u(x,0,z) = u(x,4.6,z)$	$u(x,0,z) = u(x,4.6,z)$	$c(x,0,z) = c(x,4.6,z)$
$y = 4.6\ mm$	$p(x,0,z) = p(x,4.6,z)$	$p(x,0,z) = p(x,4.6,z)$	
Membrane	No-slip condition	Outlet	No flux
$z = 0.86\ mm$	$u = 0$	$v_{perm} = \Delta p/(R_m \cdot \mu) - v_{corr}$	$D_i(\partial c_i/\partial x) = 0$
Cellholder	No-slip condition	No-slip condition	No flux
$z = 0\ mm$	$u = 0$	$u = 0$	$D_i(\partial c_i/\partial x) = 0$
Spacer filaments	No-slip condition	No-slip condition	No flux
	$u = 0$	$u = 0$	$D_i(\partial c_i/\partial x) = 0$

9.2.6 Solute transport model

A simplified transport of a model solute through an RO membrane module was also evaluated in this study. When used in conjunction with solute transport, the hydrodynamic model was subjected to several alterations.

First, to calculate 3-D concentration polarization (CP) effects, the membrane boundaries were changed to be permeable for water according to the Darcy model:

$$v_{perm} = \frac{TMP}{R_m \cdot \mu} \tag{18}$$

with v_{perm} representing permeation velocity, TMP transmembrane pressure, R_m hydraulic resistance of the membrane, and μ dynamic viscosity of water (20°C). As the pressure drop along the computational domain was found to be less than 1/1000 of the operating pressure, a constant permeation velocity of 8 μm/s was chosen based on equation 18 for the entire membrane boundary with a TMP of 4.8 bar (70 psi). For R_m, a value of 5.97×10^{13} m^{-1} was determined in separate lab measurements for the Toray SUL-G20FTS RO membrane (Toray Industries, Inc., Tokyo, Japan) according to the procedure proposed by Rajabzadeh (2010).

Second, membrane permeation caused an unclosed mass balance of water if periodic flow conditions between inlet and outlet were applied. Hence, a laminar flow profile was imposed at the inlet with the prescribed flow rate q_{set}. To avoid strong entrance or exit effects on the solute concentration fields, the domain was extended to a row of three rhomboidal mesh elements and only the middle element was evaluated with respect to hydrodynamics and CP modulus (Picioreanu et al. 2009). At the outlet, ambient pressure was set, whereas the lateral boundaries remained unaffected as periodic boundaries.

The transport of solute within the cross-flow channel was modeled by the steady-state convection-diffusion equation, solved using the already calculated flow field **u**:

$$\nabla \cdot (-\mathrm{D}\nabla \mathrm{c}) + \mathbf{u} \cdot \nabla \mathrm{c} = 0 \tag{19}$$

with D representing the diffusion coefficient (set to 1×10^{-9} m² s^{-1}) and c the solute concentration. The diffusion coefficient was kept constant, as modeling of a concentration-dependent diffusivity was shown to add considerable computational cost for an only marginal improvement of model accuracy (Lyster et al. 2009). The membrane was assumed to reject the model solute completely and osmotic effects on permeation velocity were disregarded for this qualitative consideration. With this, the normal component of solute convective flux ($v_{perm}\cdot c_m$) equals the back-diffusion flux ($D\cdot(\partial c/\partial z)_m$) at the membrane surface. These simplifications allow uncoupling the calculation of hydrodynamics from the concentration field. At the inlet, an arbitrary reference concentration of 1 mol m^{-3} was set (since osmotic pressure was not considered), while the outlet boundary was defined as no-diffusion condition. At the lateral boundaries, periodic conditions were applied, and the spacer walls were set as impermeable (no-flux condition).

9.2.7 Mesh generation

To ensure comparability between the simulation results, all geometries were discretized with the same mesh generation parameters for finite element computations in COMSOL Multiphysics. The domains were meshed by use of a hybrid approach employing both tetrahedron cells for the bulk volume and hexahedron cells for surface mesh refinements (SMRs). The heavily boundary-influenced fluid flow and solute transport required such SMR to sufficiently resolve the steep velocity and concentration gradients in the wall vicinity at a reasonable number of mesh elements. Bulk volume of the fluid domain was discretized by use of tetrahedron cells, with a maximum and minimum cell size of 138 and 41 um, respectively, for both fluid flow and mass transport simulations. The tetrahedron mesh was subsequently complemented by adding several layers of an additional hexahedron mesh on the surface boundaries. Decreasing tetrahedron cell size with no usage of such surface mesh refinements proved to be highly inefficient with respect to grid convergence (see Figure SM5, supplementary material, Appendix G). Final meshes featured 8 layers of hexahedron elements for fluid flow and 12 layers of hexahedron elements at the membrane boundary for the mass transport simulation. For fluid flow and solute transport simulations, average total cell counts amounted to 0.65 and 1.15 million elements, respectively. A further increase in cell numbers (by size reduction of the tetrahedron elements or by increasing the number of SMRs) did not lead a notable change in the results. For instance, decreasing tetrahedron cell size by 10% or adding another layer of SMRs (total 9 SMRs) changed the results for pressure drop and average membrane CP modulus by less than 1%.

9.2.8 Model solution

The stationary laminar flow simulations were carried out in COMSOL Multiphysics 5.3, by using the fully coupled nonlinear solver with PARDISO as the linear solver. Solute transport was subsequently solved based on the previously determined flow field. The simulations were carried out on a workstation with eight Intel(R) Xeon(R) central processing units (CPUs) with 3.16 gigahertz (GHz) each and 32 GB total random access memory (RAM). The computing time varied between 5 and 48 hours per simulation of flow field and between 72 and 96 hours per simulation of mass transfer. Simulations were terminated after the residual error between iterations was less than 10^{-3}.

9.2.9 Particle transport and deposition modeling

Particle transport in the feed channel and deposition on the membrane surface was simulated with a 3-D numerical model, according to Radu et al. (2014). The flow field resulted from COMSOL Multiphysics simulations was exported on a 3-D Cartesian grid for particle distribution calculations in MATLAB (MATLAB R2017a, MathWorks, Natick, MA, USA). The model was applied in three steps: (i) geometric construction, (ii) calculation of fluid flow field around a spacer element, and (iii) particle transport along the fluid streamlines. The movement of particles was computed by a Lagrangian approach, with massless particles following the fluid streamlines. The particles were defined to deposit on the membrane when (i) a particle crossed a threshold distance (5 µm) to the membrane or (ii) when its velocity was approaching zero. The already deposited particles were considered not to influence the next depositing particles. Particle deposition was simulated with the membrane surface on top of the spacer. More information about this approach can be found in (Radu et al. 2014).

9.2.10 Experimental tests of pressure drop and particle distribution and deposition

9.2.10.1 Pressure drop

The spacer was placed in a flowcell (200 x 40 x 0.86 mm) with a flat-sheet membrane (Toray SUL-G20FTS RO membrane), but without permeation (Haaksman et al. 2017, Vrouwenvelder et al. 2006, Vrouwenvelder et al. 2009, Bucs et al. 2016). The spacer had the same orientation in respect to the flow direction as the model spacer mesh. The flow was controlled precisely with a mass flow controller (Flow X3, Italy). During pressure drop measurements the inflow velocity was increased stepwise (0.07–0.15 m s^{-1}) until steady values were reached. Pressure drop was converted into mbar per 20 cm spacer-filled feed channel. Conversion in Pa/spacer element was determined with 38.5 meshes/20 cm (5.2 mm per mesh). The average inflow velocity (m s^{-1}) was calculated by conversion of the mass controlled flow rate (kg h^{-1}) to volumetric flow rate (m^3 s^{-1}), then divided by the cross-section area

(40 x 0.86 mm=34.4 mm²), corrected with the porosity (see Table 28). Measurements were replicated three times.

9.2.10.2 Particle deposition

Particle deposition was followed experimentally in flat-sheet membrane experiments with cross-flow operation and no permeation, as Radu et al. (2014) reported the same particle deposition patterns regardless of permeation or no permeation operation. The particle deposition tests were performed with a flowcell of a 146 x 96 x 1 mm, using 34 mil Toray spacer (0.86 mm) and Toray SUL-G20FTS RO membrane. Feed channel height of 0.86 mm was ensured by an acrylic glass of 0.14 mm thickness between flowcell bottom and spacer. A particle feed suspension with red colored latex particle beads (Polybead, Polysciences Inc., Warrington, PA, USA), diameter 2.74 µm, containing approximately 5.6 x 10^8 particles L^{-1} was used for the test in full recycle mode. The duration of the experiment was 6 h. Cross-flow velocity (CFV) was set to (i) 0.35 L min^{-1}, and (ii) 0.74 L min^{-1} (0.07 m s^{-1} and 0.15 m s^{-1} with a cross-section area of 82.6 mm² (89 x 0.86 mm)) and controlled by a flowmeter (Blue White Industries, Huntington Beach, CA, USA). Membrane and spacer were analyzed visually directly after the test within the flowcell and with an optical microscope.

9.3 Results and discussion

9.3.1 Geometric feed spacer characteristic accuracy

The CT scans of the spacer allowed for an accurate 3-D measurement of its geometry. CT scans revealed that filament cross-sections strongly deviate from the previously assumed rotationally symmetric shape (Figure 70). The horizontal diameters (i.e. along the main flow direction) of the irregular sections were found to be considerably larger than the vertical diameters (i.e. along the channel height) for the examined spacer (34 mil, Toray). The cross-sections of the CT-based geometries, depicted in Figure 70 for the 22 µm and 5.5 µm CT scan accuracy, visualize the quasi-ellipticity of the spacer strands. These findings are in agreement with Haaksman et al. (2017) and confirm the need of the CT scanning approach for numerical simulations. The applied surface fitting method seems to be an appropriate method to i) preserve the accuracy of the CT scan, while ii) enabling efficient CFD simulations by use of periodic domains.

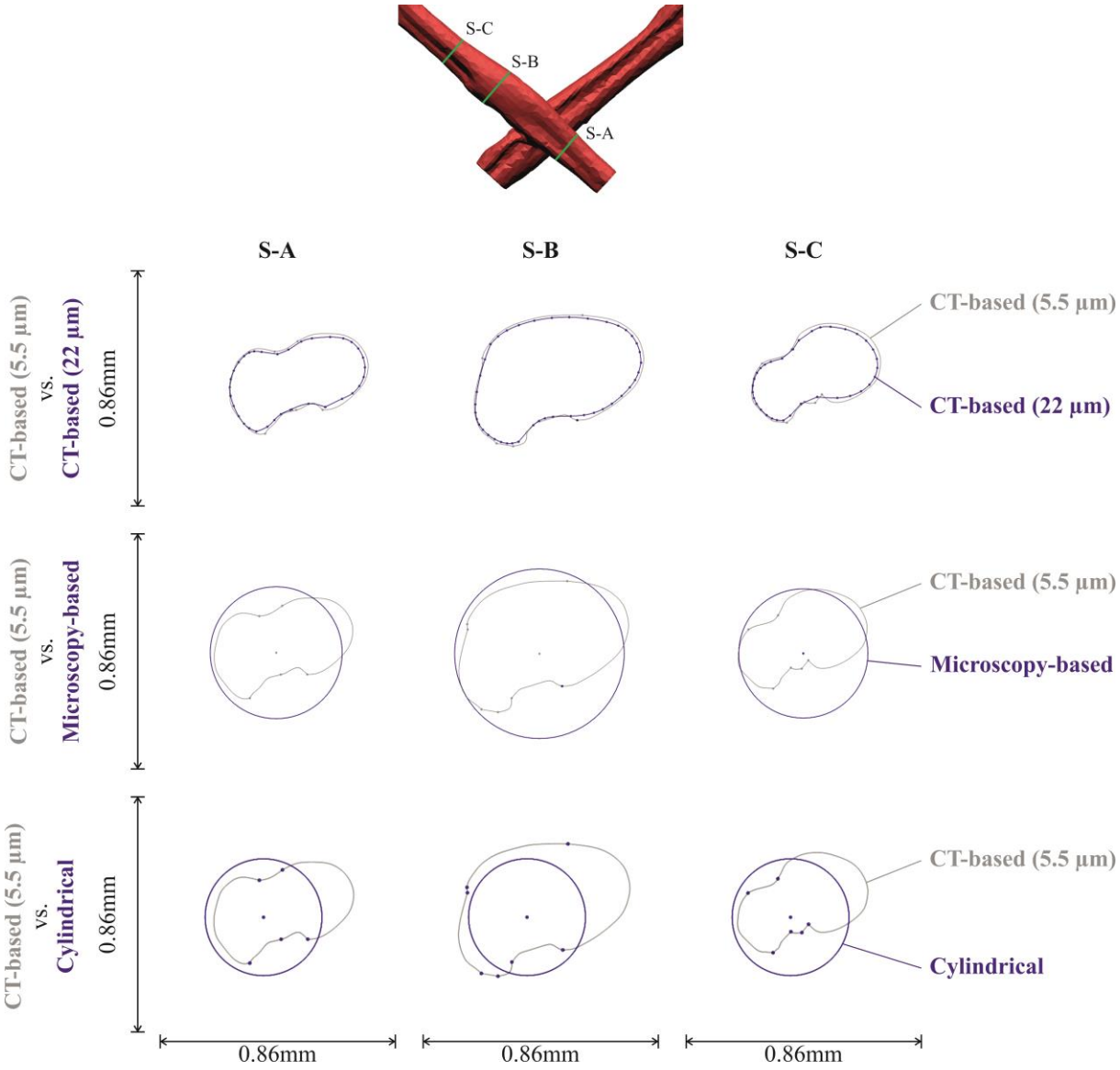

Figure 70. Comparison of cross-sections of the lowest and highest CT-based feed spacer model (22 µm, 5.5 µm) among each other and with the microscopy-based and cylindrical feed spacer model. Each row compares two cross-sections with a black and blue curve, labeled in the left column.

Based on the CT scans, conventional spacer microscopy view from the top was mimicked. No compelling compliance between the two geometry types could be achieved (Figure 70). While section width and position of the upper domain limit both agree well for raw CT geometries and microscopy-based spacer, filament height (i.e. vertical diameter) is strongly overestimated. As microscopes are only capable of assessing the horizontal diameter accurately, the vertical diameter is inevitably overestimated in a rotationally symmetric spacer model. The prescribed channel height of 0.86 mm dictates a shift of the overly thick filaments towards the middle of the channel in order to fit the microscopy-based spacer model within. As expected, the simple cylindrical model did not achieve a high compliance with the CT-based geometries either (Figure 70). The deviation between the cross-sections of cylindrical model and CT scan

geometry is not as pronounced as for the microscopy-based model with respect to height overrating and vertical offset. The microscopy-based model deviates clearly from the CT-based geometries as porosity and hydraulic diameter were considerably smaller, whereas filament surface was larger (Table 28). The cylindrical model shows reversed deviations as the surface area is much smaller and the hydraulic diameter is larger.

In contrast to the simplified geometries, the three CT-based geometries (22 µm, 11 µm, 5.5 µm) do not exhibit significant deviations, as presented in the supplementary material (Figure SM6 and SM7, Apendix G). Flow channel porosity and hydraulic diameter were identical for the 11 µm and 5.5 µm CT scan geometry, whereas the spacer surface area, spacer thickness and “canyon” width and depth were in close agreement. The “canyon”-like slots in the filaments were more precisely reproduced at the high CT scan accuracies (as visualized in Figure 70 and listed in Table 28). The more precise reproduction of the “canyon”-like slots in the spacer strands could be important if (bio)fouling aspects are considered, since these recesses provide a suitable place for the attachment of particles and bacteria. Additionally, the spacer surface appeared rougher with increasing CT scan accuracy. Overall, a lower scan accuracy can lead to a reduced spacer surface area and more imprecise reproduction of the “canyon”-like slots.

Coincidentally, the CT-based and cylindrical models yielded similar values for porosity but geometric compliance is not evident. In comparison with reference caliper measurements, the 11 µm and 5.5 µm CT scans presented the smallest deviations (Table 28). However, the impact of the identified differences and more imprecise reproduction of the 22 µm CT scan accuracy on hydraulic parameters (i.e., pressure drop, velocity profile and shear rate distribution) and solute transport needed to be investigated in detail.

Table 28. Key geometric parameters of the different feed spacer models and spacer thickness measurements. The hydraulic diameter calculation was done according to (Schock and Miquel 1987).

	Units	**CT-based (22 µm)**	**CT-based (11 µm)**	**CT-based (5.5 µm)**	**Microscopy-based geometry**	**Cylindrical geometry**
Porosity	[-]	0.89	0.88	0.88	0.82	0.91
Hydraulic diameter	[mm]	1.05	1.00	1.00	0.91	1.11
Spacer surface area [a]	[mm²]	23.34	25.20	25.56	27.62	20.22
Spacer thickness (CT scan) [b]	[µm]	810 ± 19	822 ± 7	821 ± 5	-	-
“Canyon” width [c]	[µm]	302	236	195	-	-
“Canyon” depth [c]	[µm]	67	125	100	-	-
Experimental thickness measurements						

Spacer thickness (caliper measurement) [d]	[µm]	848 ± 21	-	-

[a] Per spacer rhomboid element

[b] Measurements based on 4 measurements at each of the 4 crossings (total 16 measurements)

[c] Measurements based on the broadest and deepest point of the “canyon”-like slot

[d] Measurements based on 25 caliper measurements distributed over the spacer net

9.3.2 Impact of feed spacer geometry and CT scan accuracy on hydrodynamics

9.3.2.1 Pressure drop

The pressure drop over the one-element computational domain was evaluated for nine inflow velocities ranging from 0.07 to 0.15 m s^{-1} corresponding to a laminar Reynolds number range of 84–203 (Figure 71A). Pressure drop computed with the microscopy-based geometry was approximately 1.8 times higher than the pressure drop from the CT-based spacer models (22 µm: 1.86 times; 11 µm: 1.65 times; 5.5 µm: 1.77 times). The significant increase in pressure loss for the microscopy-based spacer geometry is due to two factors: i) the reduced channel porosity, which leads to higher average flow velocities and ii) the increased surface area, which results in more friction. Cylindrical and CT-based spacer geometries caused very similar pressure drop ($\Delta p_{Cylindrical}/\Delta p_{CT\text{-}based}$ = 1.20 (22 µm); 1.07 (11 µm); 1.15 (5.5 µm)). However, this effect needs to be interpreted with caution because the similarity stems (most probably) from a coincidentally almost equal porosity and not from a well-matching geometry (Table 28). Finally, the difference between the mean pressure drop (over the whole velocity range from 0.07 to 0.15 m s^{-1}) computed with the most and least accurate CT scan accuracy was less than 5%.

A comparison between experimental measurements of pressure drop function of flow velocity and simulated pressure drop results for the different CT scan accuracies is presented in Figure 71A. As expected, the measured pressure drop increased quadratically with an increase in velocity, following Bernoulli’s law. The experimental measured data were reproducible and in closest agreement with simulations with CT scan geometries with accuracies of 5.5 µm and 22 µm. However, the pressure drop simulations for the CT-based geometries provided higher values than the experimental measurements (in average, 6% at 0.07 m s^{-1} and 14% at 0.15 m s^{-1}). Haaksman et al. (2017) also reported a difference of -7% to 17% between simulated and measured pressure drop for several different spacer types. The discrepancy could be explained by at least three reasons. First, there could have been a mismatch between the CT scanned geometries and the existent geometry in the flowcell, resulting from different channel height. Parts of the CT scanned spacer geometry had to be cut off in constructing the modeling domain in order to fit a too thick spacer into the measured channel height, while in

experiments the spacer would simply be squeezed (Haaksman et al. 2017). Second, fluid inertia and potential jet effects at the inlet of the flowcell (Pánek et al. 2015) could result in higher pressure drops at higher flow velocities compared to numerical simulations. Thirdly, deviations in slope between experimental and model results at higher flow velocities suggest the transition from steady to unsteady flow, which would invalidate the assumption of steady laminar flow for these velocities. Santos et al. (2007) investigated the transition of steady to unsteady flow for 100 < Re < 300, Shakaib et al. (2007) reported an onset of unsteady flow for Reynolds numbers between 150 < Re < 175, Haaksman et al. (2017) stated an onset of unsteady flow condition for Reynold numbers above 175. Bucs et al. (2015) measured a deviation of 10% for Re=160 between the mean pressure drop from numerical simulations and applied particle image velocimetry measurements. However, direct comparison with other studies is impeded due to the utilization of different spacer model accuracies.

9.3.2.2 Velocity and shear rate

The observed differences for pressure drop are mirrored in the results for average velocity magnitude (over the whole channel volume) and average shear rates at the membrane (over both top and bottom walls). For the CT-based and cylindrical geometries, both hydrodynamic quantities are similar. However, in the microscopy-based channel geometry the average velocity is ~12% higher (22 µm: 9%; 11 µm: 11%; 5.5 µm: 15%) due to the lower porosity (Figure 71B) and average shear rates are also higher (11µm: 18%; 22 µm: 28%) compared to the CT-based spacer geometry (Figure 71C), except for the highest scan accuracy (5.5 µm: ±5%).

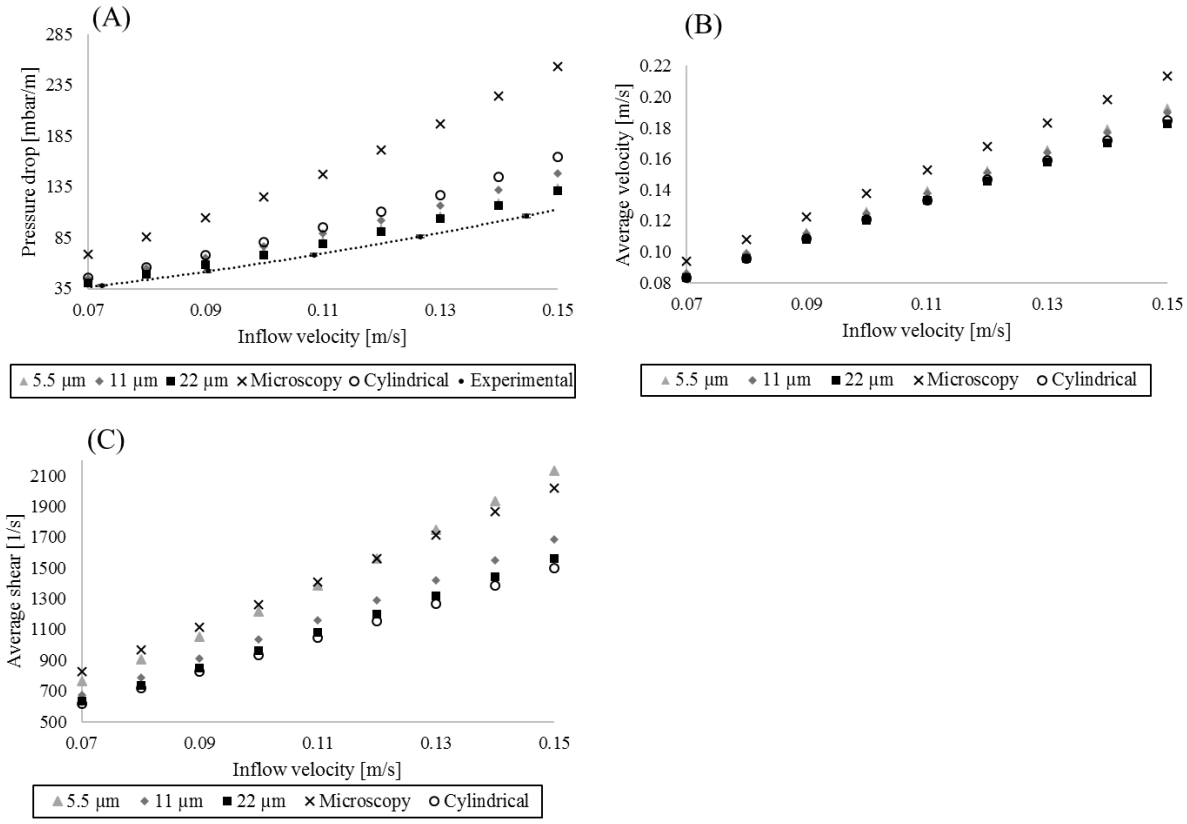

Figure 71. Computed dependencies of three hydrodynamic quantities on the average inflow velocities, uin. **(A)** Pressure drop per meter. Including the comparison of experimental measured mean pressure drop (error bars are shown and represent the standard deviation between determinations with n=3) and simulated pressure drop. A more detailed representation of the experimental measured data is shown in the supplementary material (Figure SM8, Appendix G). **(B)** Volume-averaged velocity. **(C)** Average shear rate on the membrane.

For all geometries, the shear rate on the membrane presented a largely heterogeneous pattern, with the highest values corresponding the narrow flow sections formed between filaments and membrane. Figure 72 depicts section plots of velocity profiles and the resulting shear rate distributions on the membrane for a selected velocity of 0.15 m s^{-1}. For CT- and microscopy-based geometries, smaller regions of high shear can also be identified along the filament thinnings (neckings), which allow some flow through the narrow gap between membrane and spacer filament. Cylindrical geometries on the other hand - entirely disregarding filament thinning - cannot represent the beneficial effect of filament necking on the shear rate, thus falsely predicting stagnant water zones (i.e. low shear rate) where spacer filaments touch the membranes.

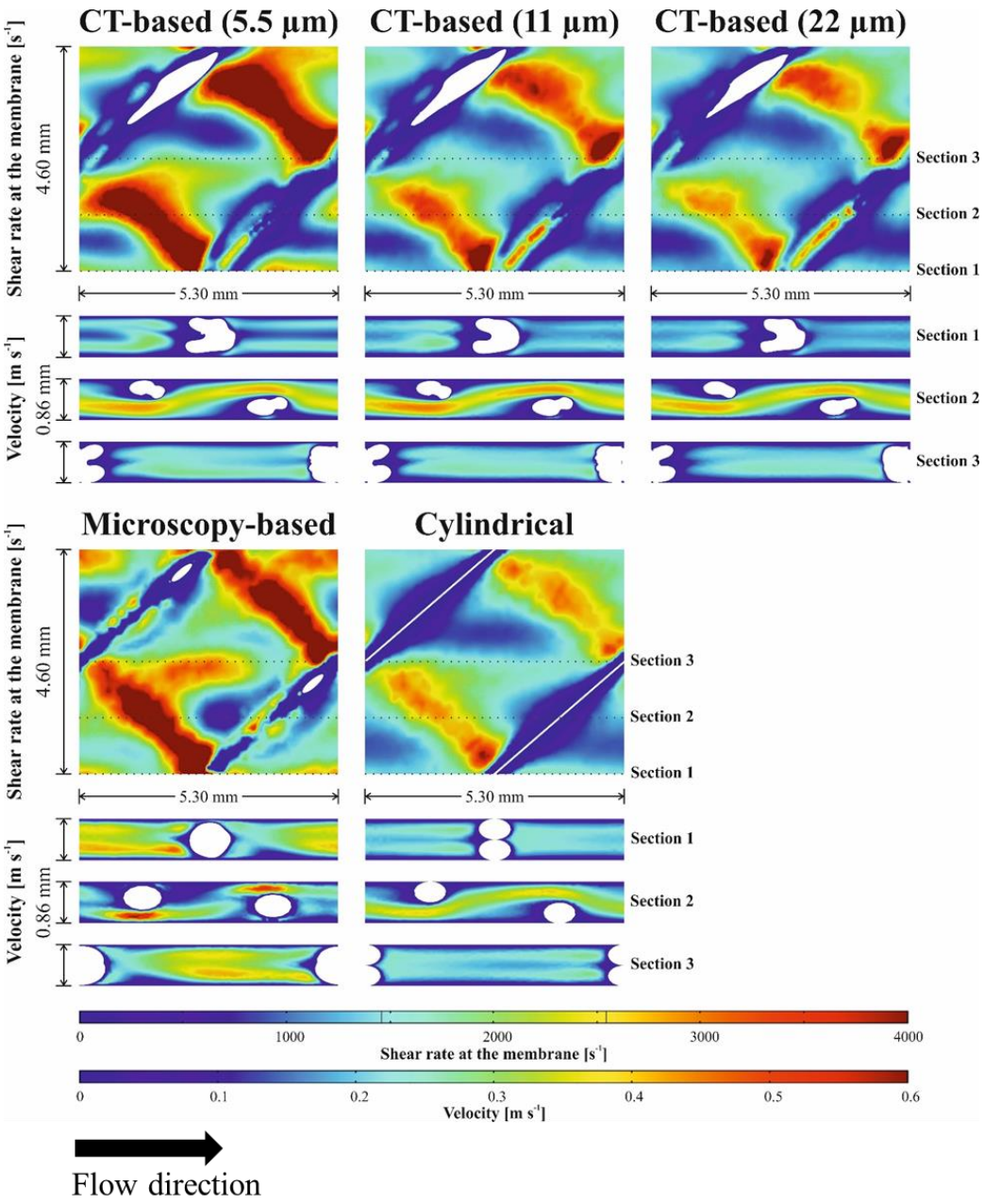

Figure 72. Comparison of the velocity profiles (bottom panels) and corresponding shear rate distributions at the membrane surface (top panels) for the different levels of feed spacer geometry accuracy, at uin=0.15 m s^{-1}. The bottom membrane wall is displayed. The high end of the color scale for shear rate was limited to 4,000 s^{-1} in order to make the comparison more visible, whereas the highest shear rate value for the microscopy-based calculations reached about 15,000 s^{-1}.

9.3.3 Impact of spacer model accuracy on solute transport

The concentration polarization (CP) modulus at the membrane was defined as the ratio between actual concentration and reference concentration of 1 mol m^{-3} in the bulk liquid. High

CP values indicate permeate flux reduction due to osmotic effects caused by accumulation of salt next to the membrane in regions with slow mass transfer. The calculated average CP modulus on whole membrane surface, for the different levels of spacer geometry accuracy and for three inflow velocities u_{in} (0.07, 0.11, 0.15 m s^{-1}) is displayed in Figure 73A. Clearly, the average CP modulus in case of cylindrical spacer exceeds those for the microscopy- and CT-based spacers at all inflow velocities.

On the other hand, the microscopy-based spacer geometry consistently delivered the lowest values for the average CP. The reason for the elevated average CP modulus obtained in case of a cylindrical spacer geometry representation is readily apparent from the solute concentration distribution over the membrane displayed in Figure 73B. The cylindrical strands are completely attached to the membrane, resulting in regions of quasi-stagnant flow along the strands, which cause reduced salt transfer and larger solute concentrations. In the other geometry models, the strand thinning allows for improved depolarization by convective transport. On the extreme, the microscopy-based geometry leaves the largest gaps between spacer strands and membrane, resulting in the least concentration polarization from all analyzed spacer geometries. The highest CT scan accuracy (5.5 µm) did not result in significantly different CP modulus results compared to the more imprecise CT scan accuracy (22 µm), as presented in the supplementary material (Figure SM9, Appendix G).

With increasing pressure drop the CP modulus decreases for all spacer geometries (Figure 73C). Overall, this study demonstrated the weakness of solute transport simulations if considering cylindrical spacer models. Neglecting the filament thinning leads to an overprediction of average membrane solute concentrations compared to both the microscopy- and CT-based spacer geometries. In particular the more precise computation of the CP modulus at the filaments becomes important if the (bio)fouling formation and potential mitigation strategies are investigated. However, the reliability of solute transport simulations should be critically evaluated. The employed solute transport model was largely simplified and could only demonstrate the dependency of solute distribution at the membrane on the geometric quality of the spacer. Osmotic effects, concentration-dependence of viscosity and/or electrostatic interactions were not considered. The impact of solute concentration on solution viscosity and solute diffusion coefficient may not be considerable on the CP levels, as demonstrated by Lyster et al. (2009). However, the omission of osmotic effects on permeation rate (e.g. the assumption of a constant permeation velocity) could be a more influential simplification. Nevertheless, the observed considerable differences in CP distribution between the largely different geometry models indicate that a sophisticated solute transport model is of little value without considering highly accurate spacer geometry, especially when quantitatively reliable concentration distributions are needed.

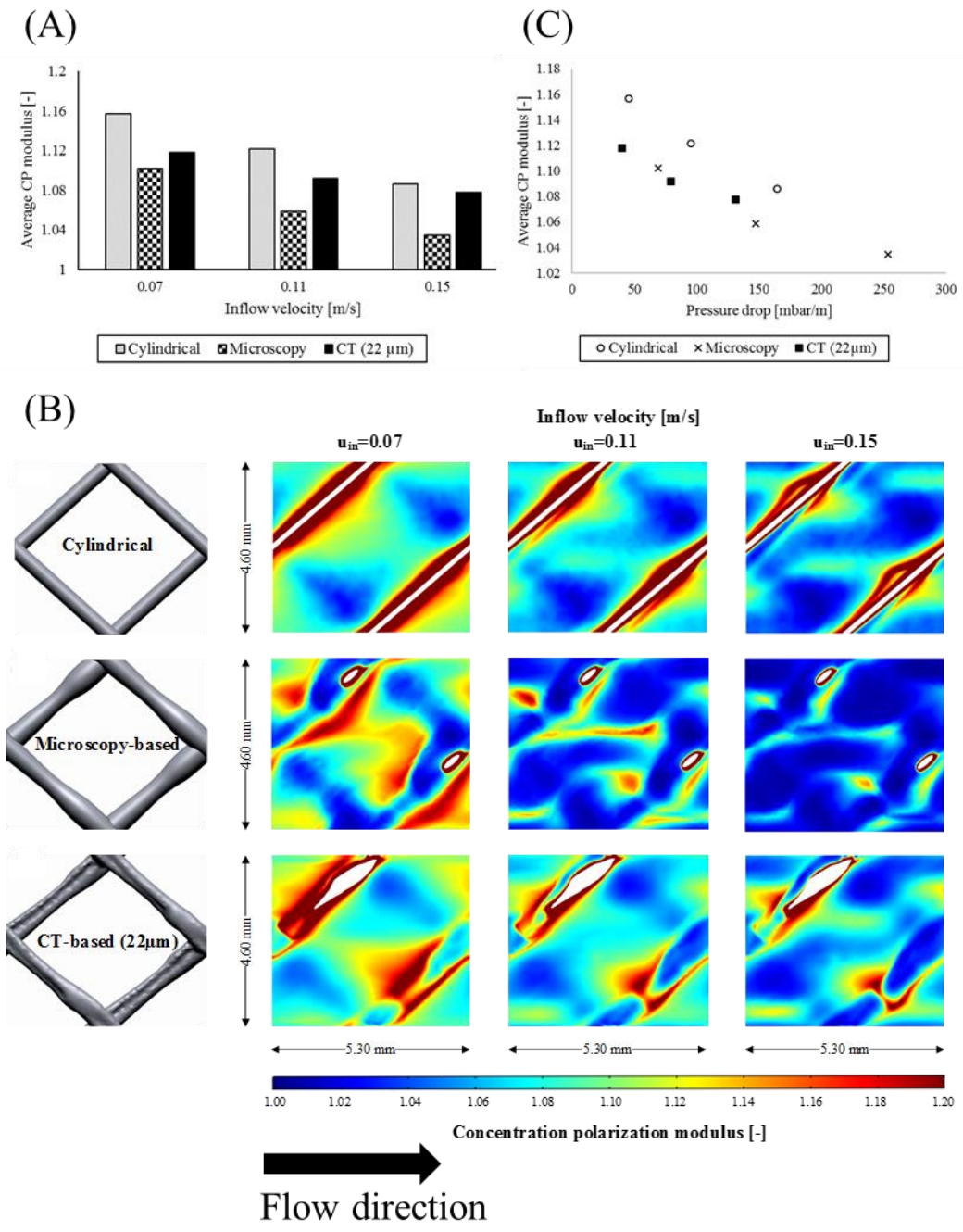

Figure 73. (A) Average CP modulus at the bottom membrane for the different accuracy levels of spacer geometry representation. **(B)** Spatial distribution of concentration polarization modulus on the bottom membrane wall surface, for the three levels of spacer representation and for three inflow velocities (0.07, 0.11 and 0.15 $m \cdot s^{-1}$). For the ease of visual comparison, the color range was limited to a top value of CP 1.2. **(C)** Average CP modulus at the bottom membrane for the different accuracy levels of spacer geometry representation in dependency of the pressure drop.

9.3.4 Particle deposition modeling and experimental tests

In order to evaluate potential effects of spacer geometry on the fouling patterns, particle transport and deposition simulations were performed for cylindrical, microscopy-based, and CT-based spacer geometries (Figure 74A). The deposition pattern computed for the cylindrical geometry showed mainly large triangular areas formed by particles attached on the membrane surface. These appear upstream the entrance to the flow constriction created between a spacer strand and membrane, where the flow is directed towards to membrane. Furthermore, streaks appear along the main flow direction in the middle of a spacer element. The Microscopy- and CT-based models produce different deposition patterns from the cylindrical model. For lower cross-flow velocities (0.07 m s^{-1}) the deposition areas from the CT-based models are also triangular. Additional attachments upstream filament crossings appear in a “boomerang”-shape. For higher cross-flow velocities (>0.11 m s^{-1}) the deposition patterns are only “boomerang”-shaped. On the other hand, the microscopy-based model produces only “boomerang”-shaped deposition zones at all velocities. With increasing cross-flow velocity the deposition pattern becomes more compact for all modeled geometries, while streaks start forming along the spacer element diagonal. Similar patterns were also identified by other modeling study (Radu et al. 2014) and observed experimentally in Fortunato and Leiknes (2017), West et al. (2016). However, additional studies focusing on the qualitative and in particular on the quantitative comparison of numerical and experimental results will strengthen the assessment for practical membrane applications. Within this study abiotic particles were used for deposition pattern studies. Since these particles offer the advantage of controlled conditions (defined size, shape, and density, no growth) and are highly comparable with the numerical results, the effects of bacterial strains could behave differently. Our experimental tests of particle deposition performed for 0.07, 0.11 and 0.15 m s^{-1} (Figure 74B) confirmed the model results. For 0.07 m s^{-1} the pronounced particle deposition membrane surface was recorded, with an area resambling the triangular deposition on the membrane. Very little particle deposition on the spacer filaments was noticed at the low velocity. In contrast, the experiments with 0.11 and 0.15 m s^{-1} show the presence of a “boomerang”-shape deposition area, together with more particles attached at the spacer filaments crossing. The experimental deposition patterns agree better with the microscopy-based model spacers and looser CT scan accuracies (all three CT scan accuracies particle modeling results are presented in the supplementary material, Figure SM10, Appendix G).

The developed approach could be useful in combination with the solute transport simulations as a (bio)fouling prediction tool (i.e. detecting areas on spacer and membrane more prone to fouling). In this context, Haidari et al. (2016) measured low-velocity zones with particle image velocimetry (PIV), indicating high (bio)fouling potential in these areas. In a step forward, Siddiqui et al. (2017b) investigated the impact of geometric modifications of spacers as potential (bio)fouling mitigation.

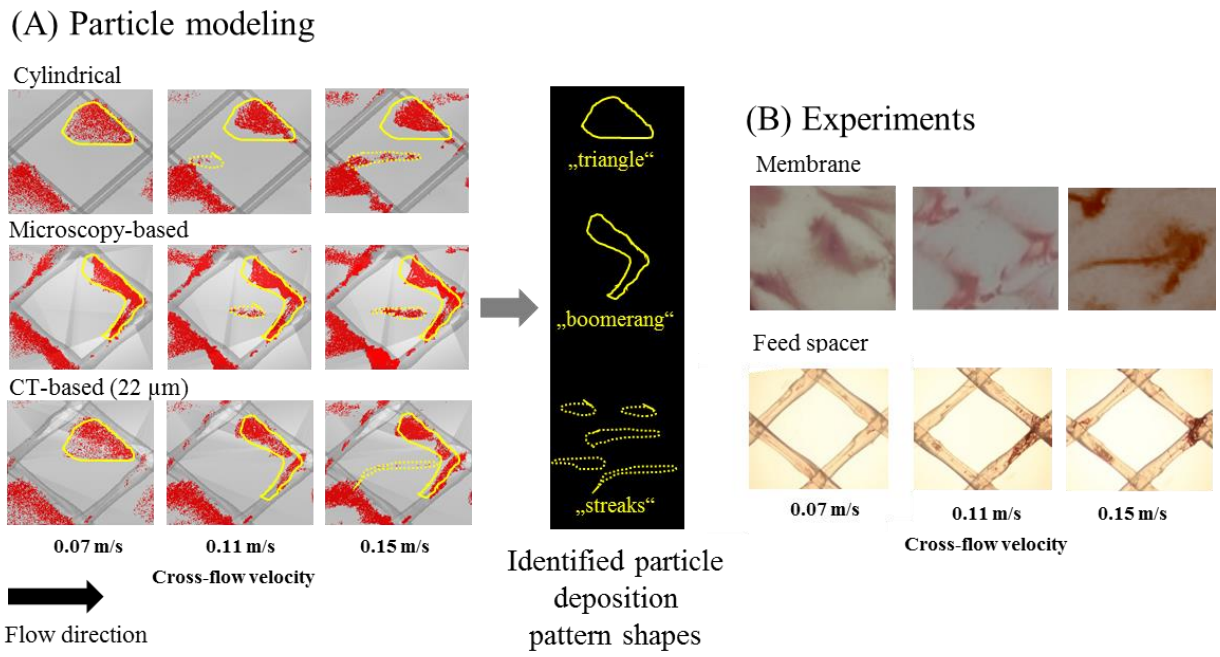

Figure 74. (A) Computed particle deposition patterns of the bottom membrane wall with spacer geometries based on cylindrical filaments, top-view microscopy and CT scan (22 µm scan accuracy). **(B)** Experimental particle deposition tests at different flow velocities. Images show separately the deposition patterns on the flat-sheet membrane and feed spacer.

9.4 Conclusions

The present work evaluated the impact of spacer model accuracy on numerical simulations of hydrodynamics and solute transport in feed channels of membrane processes. Based on three levels of geometric spacer model accuracy (cylindrical, microscopy-based, and X-ray computed tomography (CT)-based) and three CT scan accuracies, the conducted geometric evaluations, model solutions and experimental tests allowed the following conclusions:

- The CT scans yielded the most accurate spacer geometry model to date and revealed a more irregular, quasi-elliptic and not rotationally symmetric, shape of the filament cross-sections. Cylindrical and microscopy-based spacer models could not obtain this precise spacer geometry required for reliable simulations of hydrodynamics and solute transport.
- Thus, the spacer model accuracy affected significantly the hydrodynamics and solute transport simulations. Microscopic-based geometries failed to account the spacer ellipticity, resulting in overestimation of pressure drop by 80%, average velocity by more than 10% and average shear rate by ~20% compared to CT-based geometries. Cylindrical spacer geometries neglected the spacer filament thinning, resulting in an overestimation of the concentration polarization at the membrane surface compared to

CT-based geometries. However, the hydrodynamic simulations for cylindrical and CT-based spacers yielded relatively similar results for pressure drop, average velocity and average membrane shear rate. Please note that the agreement between cylindrical and CT-based spacer geometries regarding computed pressure drop, shear and velocity was only incidental, as the generated flow domain porosities were quite similar.

- The experimental measurements of pressure drop were in close agreement with simulations of pressure drop of the CT-based spacer geometries (highest deviation 14%)
- The particle deposition experimental test were in close agreement with the simulations of particle deposition of the CT-based spacer geometries. Experimentally-observed triangular areas at the membrane surface for the lower cross-flow velocity (0.07 m s-1) and “boomerang”-shapes for higher cross-flow velocities (>0.11 m s-1) were only reproduced by the CT-based simulations.
- Based on these results, we strongly recommend the use of the proposed CT scanning approach when quantitatively accurate CFD and solute transport simulations on cross-flow channels are targeted. However, an increased CT scan accuracy above a certain precision (i.e. less than 20 µm) in order to create more accurate spacer geometries did not result in significant changes in modeling results. The CT scan accuracy (within 5 and 20 µm) was found to have only marginal effects on the hydrodynamics and solute transport modeling results.

9.5 Outlook / Recommendations for future studies

The assumption of laminar flow is justified for the range of investigated Reynolds numbers and it is not expected to introduce a major error. In a recent study, Bucs et al. (2015) compared simulated laminar flow fields within spacer-obstructed cross-flow channels with PIV and found that for industry-typical flow velocities of 0.163 m s^{-1} (Re = 160) the laminar flow model can deliver closely matching results (Bucs et al. 2015). Still, a PIV measurement should also be conducted for the investigated Toray spacer in order to confirm the source of observed differences in hydrodynamic patterns between the different spacer model accuracies. Interestingly, almost all simulations conducted in Bucs et al. (2015) slightly overestimated the PIV observed velocities, which might stem from the potentially decreased flow domain porosity of the employed microscopy-based, rotationally symmetric spacer.

In this work only one commercial spacer was investigated. For this particular case of quasi-elliptic spacer strands, CT-based spacers constructed at all resolutions yielded similar results whereas both the cylindrical and the microscopy-based spacer models yielded strongly deviating results. For a spacer with more circular filaments, the observed differences between CT scanned and microscopically assessed spacer may not be so large. Therefore, the conclusions of this study may not be valid for all spacer types. Although Haaksman et al. (2017) reported the same strong deviations between CT scanned and microscopy-based spacers for

pressure drop for several, commercially available 34 mil spacers (Haaksman et al. 2017), more spacers should be evaluated in this regard in the future. In addition, different spacer types (e.g. woven spacers) should be analyzed.

The influence of the CT scan accuracy on the simulation results was investigated within an accuracy range of 5.5–20 µm. Within this range no significant influences of the CT scan on the simulations (hydrodynamics and solute transport) could be observed. With this knowledge it becomes evident that future studies could investigate the influence of courser CT scan accuracies (above 20 µm) and if there is a dependency of the detailed spacer geometry (e.g. comparison of very rough and very smooth spacer geometries).

Aside the investigated impact of spacer geometry accuracy on laminar flow and solute transport, the revealed quasi-elliptic shape of the filaments is expected to have also a considerable impact on the onset of unsteady and turbulent flow. Reported direct numerical simulations (DNS) on cross-flow channel hydrodynamics employed solely cylindrical filaments (Mojab et al. 2014, Koutsou et al. 2007, 2009, Li et al. 2002) or were conducted in 2-D domains (Amokrane et al. 2015, Ahmad and Lau 2006, Koutsou et al. 2004). In a next step, a DNS on the CT-based geometry will be conducted in order to evaluate the transient flow behavior and to determine the Reynolds numbers at which unsteady vortex shedding or full turbulence is reached. It is hypothesized that the quasi-elliptic, more streamlined shape of the filaments might delay the onset of unsteadiness and turbulence to higher Reynolds number than assumed to date (Mojab et al. 2014). On the other hand, the irregular, more complex shape could enhance the formation of unsteady vortices. DNS on a realistic geometry could confirm or challenge the hypothesis that spacers act as turbulence (mixing) promoters, with a far-ranging impact on future spacer design and optimization.

Finally, the presented procedure (i.e. CT scanning followed by surface fitting and generation of a periodic domain for fluid flow and solute transport simulations) could provide a useful workflow for membrane module developers to estimate reliably the performance of novel spacer geometries with optimized geometries. An optimal spacer geometry would be defined as a design that achieves a balance between competing factors, e.g. enhanced mass transfer vs. pressure drop and membrane fouling (Haidari et al. 2018). Combined with advances in 3-D-printing (Lee et al. 2016, Bucs et al. 2018), the numerically optimized geometries can be readily tested and validated in experiments, as was presented in Siddiqui et al. (2016). This validation by comparison of numerical and experimental tests would strengthen the practical impact of spacer geometry development. On the other hand, provided sufficient accuracy, *in situ* CT scanning could reveal non-intentional behavior of spacer placed in real modules, e.g., deformations, curvature effects, or even scaling patterns. Since simulations did not considering the curvature of spiral-wound membrane modules, future studies could investigate the deviation of flat and curvature geometries. However, in 2-D simulations of the pressure drop the influence of curvature was found to be less than 1% compared to flat geometries (Li and Tung 2008b).

Overall, the development of optimized spacer geometries resulting in optimized hydraulic conditions of the feed channel has potential to lower the energy requirements of membrane treatment and reducing (bio)fouling phenomena (Haidari et al. 2018, Siddiqui et al. 2017b, Bucs et al. 2018).

9.6 Acknowledgements

This research was funded by seed funds of the Chair of Urban Water Systems Engineering at TUM.

10 Conclusions, discussion and perspective

The core objectives of this thesis were twofold: (i) the evaluation of existing potable water reuse schemes regarding their energy demand and product water quality including the design of more energy-efficient potable water reuse schemes and (ii) the assessment of the operational performance of membrane treatment stages and membrane fouling mitigation strategies including their further development and improvement. To investigate the objectives four research hypotheses were defined and assessed in the corresponding chapters.

Three key research pillars were defined for sustainable water treatment: (i) energy-efficiency, (ii) operational performance / feasibility, and (iii) water quality. The overall possibility of more energy-efficient potable water reuse schemes was assessed by hypothesis #1. To evaluate the operational performance and feasibility of the core treatment stages of the proposed more energy-efficient treatment schemes (i.e. membrane treatment), the following hypotheses focused on (i) the treatment of raw municipal wastewater by ultrafiltration (UF) treatment (hypothesis #2) and (ii) the operational performance of downstream nanofiltration (NF) / reverse osmosis (RO) treatment (hypothesis #3). Since membrane treatment is mainly hindered by membrane fouling, hypothesis #2 included a membrane fouling mitigation strategy (i.e. granular activated carbon (GAC) in a fluidized bed). Additionally, fouling mitigation strategies were further investigated and improved (e.g., fluidized bed with different GAC concentration, GAC packed bed) or new fouling mitigation strategies were developed (i.e. vibration of membranes by electroactive polymers (EAPs)). For downstream membrane treatment in spiral-wound membrane applications (NF/RO) the potential of novel spacer geometries as fouling mitigation strategy was evaluated. The assessment of the four hypotheses is summarized and discussed in the following.

Hypothesis #1

Design of a more energy-efficient potable water reuse scheme (Chapter 4)

The results of the assessment of hypothesis #1 (chapter 4) revealed that the concept of energy recovery can be integrated into potable water reuse schemes. Overall, the energy consumption of conventional potable reuse schemes could be reduced up to 29% (overall energy balance up to 80%) compared to current reuse schemes, resulting in an overall net energy demand balance of 0.22 kWh/m³. This can mainly be achieved by (i) a lower energy input, (ii) physical separation of carbon and nitrogen removal, (iii) an increased biogas yield from carbon, and (iv) implementation of alternative nitrogen removal strategies (e.g. partial nitritation/anammox (PN/A), the coupled aerobic-anoxic nitrous decomposition operation (CANDO) process). The CANDO process for nitrogen removal allows a later energy recovery from nitrous oxide. Thus, hypothesis #1 was assessed positive. By comparing the oxygen and external carbon demand of different nitrogen removal strategies (e.g., nitrification/denitrification (N/DN), PN/A, CANDO process) it becomes evident that the removal of nitrogen is of key interest of both (i) energetic consideration and (ii) climate system considerations (Figure 75). The comparison revealed that the decoupling of the organic and nutrient removal by implementing the CANDO process

results in less oxygen demand and additional energy in form of N_2O. In addition to the assessed energy-efficiency and product water quality, also the sustainability of potable water reuse schemes related to greenhouse-gases (GHGs) should be considered. The (unintentional) production of N_2O and release to the atmosphere has a relevant contribution to the climate. The intentional utilization of N_2O in the CANDO process is probably more relevant than the additional energy yield. It was balanced that only approximately 0.04 kWh/m³ wastewater treated can be recovered by intended N_2O production and subsequent energetic utilization, mainly depending on the wastewater characteristic and ammonia content. The CANDO process was investigated regarding the technical and economic feasibility by Weißbach (2018). The results indicate that the CANDO process is a viable for real feed-stream conditions. However, potential scale-up, start-up phase behavior and operational stability needs to investigated in more detai. Finally, also the energetic benefit in CHP units needs to be investigated in future research.

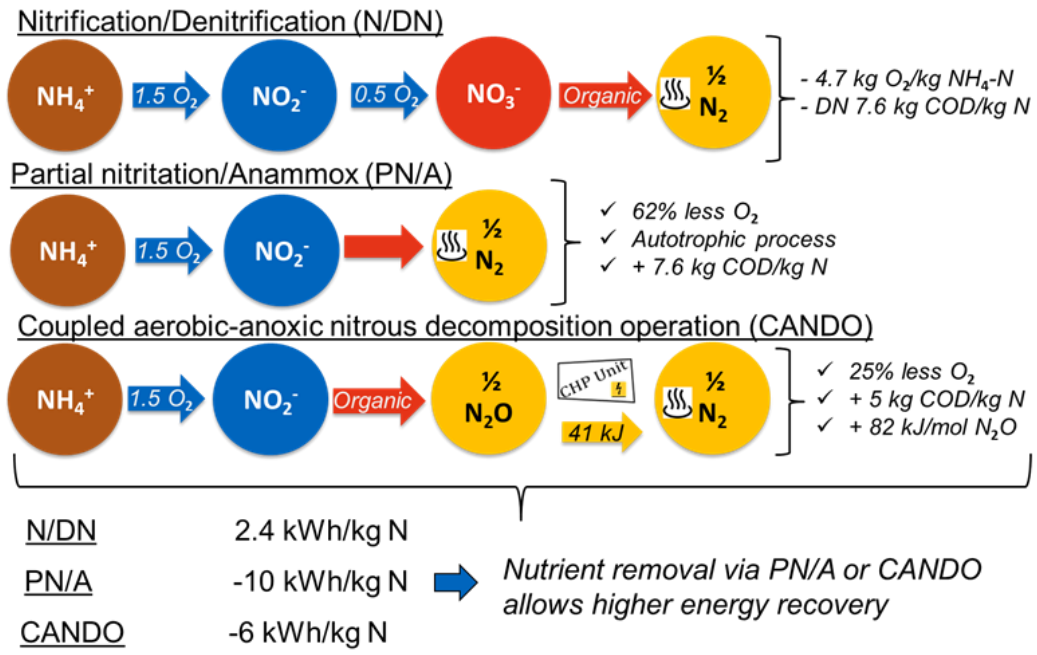

Figure 75. Oxygen and external carbon balance of different nitrogen removal strategies.

The proposed alternative of a more energy-efficient potable water reuse scheme was investigated in the subsequent hypotheses. However, more detailed research is needed including a detailed technical feasibility study. Within this thesis the feasibility was assessed in laboratory- and pilot-scale applications. The feasibility of the proposed physical treatment processes (microsieving, UF and RO) is also assessed in the subsequent hypotheses. From these results a general feasibility can be stated. However, long-term performance, biofouling issues, process stability, and upscaling potentials are some important aspects that have to be considered in future research. In addition, the downstream coupling with biological (BAF) and

disinfection processes require detailed research to proof and guarantee final water quality for drinking water purposes. Within this thesis the water quality was mainly considered on a conceptual level or regarding operational performance parameters. Thus, an overall assessment and proof of the final water quality still needs to be applied. Based on log-removal efficiencies of the proposed treatment steps according to the Treatment Train Toolbox from Trussell et al. (2017), the product water quality is meeting drinking water quality. Log-removal values (LRVs) were determined with 18 for enteric viruses, 12.5 for cryptosporidium and 21 for total coliform bacteria. The advantage of the integrated membrane system (IMS) with multiple-barriers is a good removal efficiency for the previous mentioned contaminants. However, municipal wastewater is a complex matrix with a wide range of contaminants. The proposed treatment train consist on pure physical treatment until the NF/RO treatment stage (no biological treatment). A critical assessment of constituents that are challenging for the proposed treatment train revealed that generally low molecular weight acids and low molecular weight neutrals (<100 Da) are most critical for the proposed treatment train. In addition, N-Nitrosodimethylamine (NDMA), 1,4-dioxane and N-Nitrosomorpholine (NMOR) are considered to be critical since their monitored concentration in conventionally treated secondary effluents were higher than the reported monitoring trigger levels (MTLs) (SWRCB 2018). Fujioka et al. (2018) revealed a good removal efficiency of 1,4-dioxane by RO treatment (~99%). In contrast, the removal efficiency of NDMA by RO treatment was lower (57-81%). However, NDMA removal efficiencies vary widely in a comprehensive analysis of laboratory-, pilot-, and full-scale data (Fujioka et al. 2012). Thus, a more detailed research focus on the removal mechanisms and efficiencies of NDMA should be applied in the future. NDMA formation control and removal is of key interest for potable water reuse schemes. To be able to guarantee a suitable water quality for drinking water, within this thesis subsequent BAF followed by UV-H_2O_2 are considered as final barriers for these compounds, in particular for low-molecular acids and neutrals and NDMA removal. In addition, no fouling control by chloramination is considered, since chloramination is the most common process that results in the formation of NDMA (Sgroi et al. 2018). Müller et al. (2017) introduced a novel approach using sequential biofiltration for enhanced biological removal of trace organic chemicals. This approach could be applied as potential design for the treatment of the NF/RO permeate. The NF/RO permeate water quality is below the investigated wastewater treatment plant effluent analyzed by Müller et al. (2017) (DOC: 6.9 vs. 2.0 mg/L; UVA_{254}: 13.4 vs. 0.02 1/m). Thus, a BAF with low empty bed contact time (EBCT) (~30 min) is considered to reduce the presence of low molecular weight acids and neutrals. The subsequent UV-H_2O_2 treatment stage is considered as final barrier for residual trace organic chemicals oxidation. UV treatment is preferred compared to ozonation due to its efficient removal effieciency of NDMA and lower formation of NDMA during operation (Sgroi et al. 2018).

Hypothesis #2

UF treatment of municipal wastewater (Chapter 7)

The conceptual design of a more energy-efficient potable water reuse scheme follows the idea to physically separate particulate and dissolved fractions of the wastewater constituents by UF

treatment and subsequent concentration of dissolved fractions by RO treatment. Thus, it is possible to enable separated energy recovery platforms for carbon and nitrogen. In addition, the load of the subsequent treatment stages is reduced. Therefore, a UF pilot-scale membrane treatment stage was designed and constructed. In a first study this reactor was operated for 576 days. GAC in a fluidized bed served as fouling mitigation strategy (see chapter 7.1). It was possible to separate particulate and dissolved fractions of the wastewater constituents, measured as fractions of carbon and nitrogen. The overall treatment performance (membrane fouling, cleaning intervals) of the UF treatment system was at an acceptable level. Overall, the hypothesis #2 could be confirmed. Additional experiments with different GAC concentration in a fluidized bed and GAC in a packed bed revealed further optimization and energetic improvements (see chapter 7.2). The fouling mitigation effect was more evident for the packed bed than for the fluidized bed tests. Within the latter one, only small differences could be seen between various GAC fluidization intensities. This leads to the conclusion that additional energy input does not inevitably cause more reduction of membrane fouling. Similar observations were made by Wang et al. (2016). A different view on the benchmark test outcomes should highlight the relevance of fouling minimization with respect to long-term operation. For the fouling rate (TMP increase) and the total TMP growth, with each filtration period and despite intermitting backwashing phases, an exponential development can be shown. For all fouling control options, as illustrated in Figure 76, exponential regression curves were determined. Coefficients of determination revealed $r^2 > 0.95$ and $r^2 > 0.92$ for the curves in Figure 76A and Figure 76B, respectively. To enable further comparison of the total TMP development, the intercepts of the individual TMP curves (Figure 76B) were added and divided by their number. With the help of this mean intercept, the regression curves were recalculated and forced to involve the mean intercept (equal start point).

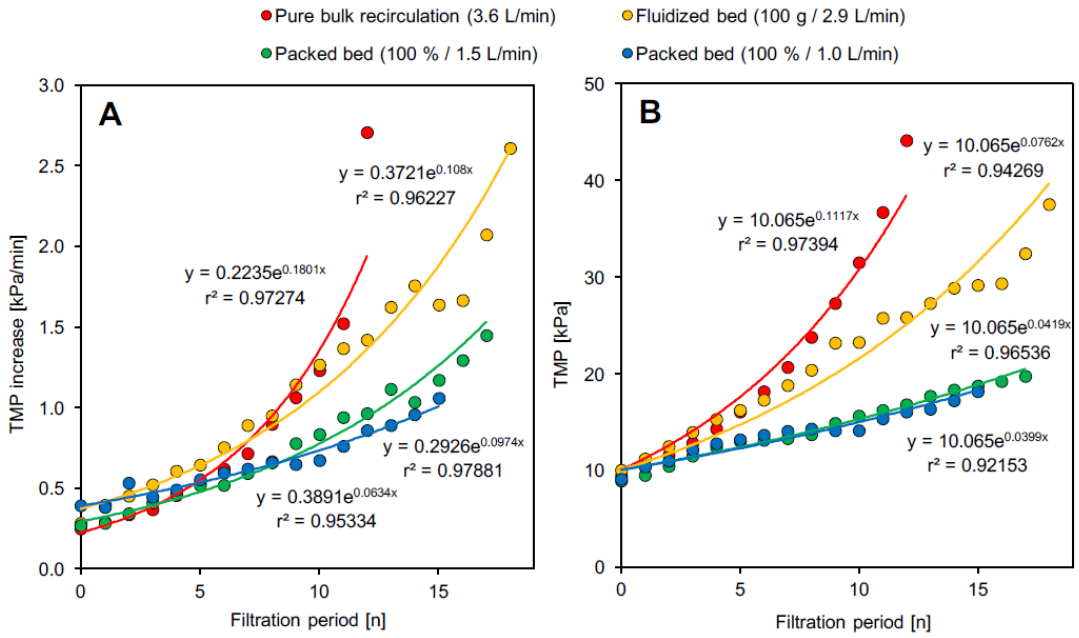

Figure 76. Exponential fouling rate and total TMP increase with successive filtration periods for distinct fouling control strategies.

The exponential characteristics of the fouling rate as well as the total TMP, emphasize the effective fouling reduction potential through particle scouring, particularly with the packed bed. This regression data can be used as an indicator for a development consideration (extrapolation). Based on the exponential equations, given in Figure 76B, and a 50 kPa set-point for the TMP the maximal operation periods can be calculated. Accordingly, the filtration can operate for 3.5, 5.1, 9.2, and 9.7 h with the pure bulk recirculation, the fluidized bed, the packed bed (1.5 L/min), and the packed bed (1.0 L/min), respectively. Thus, the packed bed enables the extension of the operation span by approximately three times compared to the bulk recirculation and by approximately two times compared to the fluidized bed. Indeed, these data were gained in short-term tests under severe fouling conditions (actual flux 35 LMH), and therefore any predictions for long-term filtration with lower flux rates have to be made with reservation. However, similar behavior was observed by Aslam and Kim (2017). Even greater extension rates of approximately four to seven were determined by these authors, comparing bulk recirculation and a fluidized bed (50 % v/v). In this publication, it was also shown that particle scouring is effective to reduce reversible membrane fouling (cake layer formation) but had no alleviating effect on irreversible fouling (internal fouling). This was also stated by Charfi et al. (2017). Due to the findings revealed in the present and also in other studies, it is concluded that intervals between chemical cleanings can be extended by at least a factor of two to three. This, in turn, would considerably reduce the demand for chemical detergents. Nonetheless, particle scouring is probably ineffective regarding pore blocking and constriction, and therefore chemical cleaning might be reduced significantly but cannot be omitted entirely.

The inducement of vibration via EAPs to the membrane surface indicated to be a very promising approach for the development of anti-fouling membranes. The induced vibrations demonstrated a positive fouling reduction compared to no-vibration. Because of some issues with the used sealing compound (synthetic resin) and intrusion of water into the electrical actuators, only a few test runs could be carried out. For further experiments, a second vibrating UF hollow fibre prototype was designed (Prototype 2). Considering the issues and difficulties from the first filtration unit, several improvements have been elaborated and realized in the design of a second prototype. However, further research is needed to evaluate the feasibility of long-term EAP operation in water conditions. Also, new possibilities of different EAP geometries and sufficient control signals (amplitude and frequency) need to be tested in future investigations. Since no-vibration measuring tool was available for the measurements with Prototype 1, vibration intensity was evaluated via a subjective haptic assessment. Consequently, investigations were conducted with a sinusoidal signal at 80 Hz. The successful application of vibrometer measurements proofed the inducement and dispersion of vibration along the hollow fibres.

Hypothesis #3

Downstream NF/RO treatment (Chapter 8)

Downstream water treatment with NF and RO treatment showed comparable performance for both membrane types. In total 16 fouling tests were performed with a DOW NF-270 nanofiltration and Toray TMG10 reverse osmosis membrane. The average permeate flux decline for both membrane types was below 30% during short-term experiments (90–120 h), with an average flux decline of 18% for NF treatment and 26% for RO, respectively. The results indicate that downstream treatment of the UF permeate with NF or RO is possible. RO is preferred due to better NH_4-N rejection. Thus, hypothesis #3 could be confirmed. However, the overall aim is the implementation of the RO application in the system for the treatment of UF pretreated raw municipal wastewater. Thus, upscaling of the RO system to pilot-scale application is the next step. When upscaling the RO application, long-term flux behavior and rejection capacities become more relevant. Furthermore, when concerning the long-term operation, biofouling of the RO membranes can be likely assumed due to the high nutritious feed matrices and the fact that mainly protein-like matter deposited onto the RO membrane surfaces during the course of this study which serves as a perfect nutrient basis for microorganisms. Therefore, the RO membrane applications must be investigated in terms of biofouling formation. Based on that, biofouling mitigation strategies must be investigated to enhance system efficiency for long-term operation. Thus, other pretreatment strategies such as coagulation, adsorption or even an anaerobic membrane bioreactor before the UF pretreatment need to be considered to potentially minimize the biological load for the downstream RO application. It is advisable to remove especially the proteinaceous matter before the RO stage to prevent biofouling. Besides that, the complex effects and influences of NOM and DOM on RO membrane fouling are still not well understood. Recent studies by Mustafa et al. (2016) and Chon and Cho (2016) demonstrate that further research about fouling formation by NOM and DOM is required and still matter of interest, especially in terms of IMSs

including different pretreatment steps which directly affects feed matrix composition and chemistry. The studies also show that the fouling by DOM is based on a complex interplay between the membranes and DOM fractions. The reason for the high flux decline for the NF membrane during experiments 6 and 7 from batch 4 could not be clearly attributed to any of the fractions investigated during this thesis. Thus, a further characterization of the physicochemical characteristics and properties of DOM and the membranes might be useful to get more insights into the underlying fouling phenomenon and moreover, to optimize the pretreatment strategies also in terms of physicochemical characteristics of the raw wastewater matrix. For this, DOM fractionation is a useful tool which is applied by many researchers to characterize membrane fouling (Her et al. 2007, Zhao et al. 2010b, Chon and Cho 2016). Besides to that, surface angle and zeta potential measurements of the clean and fouled membrane surfaces as well as attenuated total reflection fourier transform infrared spectroscopy could be applied to analyze the cake layer characteristics more in detail. The results of this thesis suggest that further analysis is required to reveal the complex interplay of DOM fractions with the membranes.

Hypothesis #4

Novel spacer geometries for fouling mitigation (Chapter 9)

The reliable investigation and development of novel spacer geometries require a detailed understanding of the hydrodynamic and solute transport mechanisms within spiral-wound membranes (SWMs). Therefore, a new CT scan approach was developed and proposed (see chapter 9). It was found that the spacer model accuracy has a significant impact on the hydrodynamic and solute transport modeling results. However, novel spacer geometries are not presented in publication #6. Based on the findings of publication #6 the development and evaluation of novel spacer geometries with improved fouling propensities is possible. The development of optimized spacer geometries resulting in optimized hydraulic conditions of the feed channel has potential to lower the energy requirements of membrane treatment and reducing (bio)fouling phenomena (Haidari et al. 2018, Siddiqui et al. 2017b, Bucs et al. 2018). An optimal spacer geometry would be defined as a design that achieves a balance between competing factors, e.g. enhanced mass transfer vs. pressure drop and membrane fouling (Haidari et al. 2018). Thereby, a wide range of ideas exists to improve current spacer designs. However, most follow the idea to change the geometry of feed spacers to improve their fouling propensities. Theoretically, an ideal spacer is defined as a spacer with the perfect hydrodynamic design. Thus, a spacer that neither causes stagnant regions nor blocks the membrane surface area (empty channel). Practically, an optimal spacer is defined as a design that achieves a balance between competing concerns. Mass transfer on one hand – pressure drop and fouling on the other hand. Combined with advances in 3-D-printing (Lee et al. 2016, Bucs et al. 2018), the numerically optimized geometries can be readily tested and validated in experiments, as was presented in Siddiqui et al. (2016). This validation by comparison of numerical and experimental tests would strengthen the practical impact of spacer geometry development.

11 References

Agus, E., Lim, M.H., Zhang, L., Sedlak, D.L. (2011) Odorous compounds in municipal wastewater effluent and potable water reuse systems. *Environmental Science and Technology*, *45*(21), 9347–9355.

Ahmad, A.L., Lau, K.K. (2006) Impact of different spacer filaments geometries on 2D unsteady hydrodynamics and concentration polarization in spiral wound membrane channel. *Journal of Membrane Science*, 286, 77–92.

Al-Amoudi, A.S. (2010) Factors affecting natural organic matter (NOM) and scaling fouling in NF membranes: A review. *Desalination,* 259**,** 1-10.

Al-Sharif, S., Albeirutty, M., Cipollina, A., Micale, G. (2013) Modelling flow and heat transfer in spacer-filled membrane distillation channels using open source CFD code. *Desalination*, 311, 103–112.

Alidina, M., Li, D., Drewes, J.E. (2014) Investigating the Role for Adaptation of the Microbial Community to Transform Trace Organic Chemicals during Managed Aquifer Recharge. *Water Research,* 56(6), 172-180.

Amokrane, M., Sadaoui, D., Koutsou, C.P., Karabelas, A.J., Dudeck, M. (2015) A study of flow field and concentration polarization evolution in membrane channels with two-dimensional spacers during water desalination. *Journal of Membrane Science*, 477, 139–150.

Angelakis, A.N., Gikas, P. (2014) Water reuse: Overview of current practices and trends in the world with emphasis on EU states. *Water Utility Journal*, 8, 67–78.

Aniol, J. (2017) Investigation of Membrane Fouling Mitigation with Fluidized Granular Activated Carbon in Ultrafiltration Membrane Treatment of Municipal Wastewater. Master Thesis. Technical University of Munich.

Aniol, J. (2018) Membrane Fouling Mitigation in Municipal Wastewater Treatment Applications. Study Project. Technical University of Munich.

Weißbach, M. (2018) Technical implementation and development of control strategies for the integration of the Coupled Aerobic-anoxic Nitrous Decomposition Operation (CANDO) into wastewater treatment schemes for simultaneous nitrogen removal and energy recovery from nitrogen. Doctoral Thesis. Technical University of Munich.

Appelbaum, B. (2002) *Water & Sustainability: U.S. Electricity Consumption for Water Supply & Treatment – The Next Half Century*. Electric Power Research Institute, EPRI, Palo Alto, CA, USA.

Arzbaecher, C., Parmenter, K., Ehrhard, R., Murphy, J. (2013) *Electricity Use and Manage ment in the Municipal Water Supply and Wastewater Industries*. Electric Power Research Institute, EPRI, Palo Alto, CA, USA.

Asano, T., Leverenz, H.L., Tsuchihashi, R., Tchobanoglous, G. (2007) *Water Reuse*. New York: McGraw-Hill.

Aslam, M., McCarty, P.L., Bae J., Kim, J. (2014) The effect of fluidized media characteristics on membrane fouling and energy consumption in anaerobic fluidized membrane bioreac tors. *Separation and Purification Technology*, 132, 10–15.

Aslam, M., Kim, J. (2017) Investigating membrane fouling associated with GAC fluidization on membrane with effluent from anaerobic fluidized bed bioreactor in domestic wastewater treatment. *Environmental Science and Pollution Research*, 1–11.

Aslam, M., Charfi, A., Lesage, G., Heran, M., Kim, J. (2017a) Membrane bioreactors for wastewater treatment: A review of mechanical cleaning by scouring agents to control mem brane fouling. *Chemical Engineering Journal*, 307, 897–913.

Aslam, M., McCarty, P.L., Shin, C., Bae, J., Kim, J. (2017b) Low energy single-staged anaer obic fluidized bed ceramic membrane bioreactor (AFCMBR) for wastewater treatment. *Bi oresource Technology*, 240, 33–41.

Bae, J., Shin, C., Lee, E., Kim, J., McCarty, P.L. (2014) Anaerobic treatment of low-strength wastewater: A comparison between and staged anaerobic fluidized bed membrane biore actors. *Bioresource Technology*, 165, 75–80.

Baghoth, S.A., Sharma, S.K., Amy, G.L. (2011) Tracking natural organic matter (NOM) in a drinking water treatment plant using fluorescence excitation–emission matrices and PAR AFAC. *Water Research,* 45**,** 797-809.

Baker, R.W. (2012) *Membrane Technology and Applications,* New York: John Willey & Sons.

Baker, A., Tipping, E., Thacker, S.A., Gondar, D. (2008) Relating dissolved organic matter fluorescence and functional properties. *Chemosphere,* 73**,** 1765-1772.

Batstone, D.J., Hülsen, T., Mehta, C.M., Keller, J. (2015) Platforms for Energy and Nutrient Recovery from Domestic Wastewater: A Review. *Chemosphere,* 140**,** 2–11.

Beier, S., Jonsson, G.E. (2008) *Dynamic Microfiltration: Critical flux and macromolecular trans mission.* Ph.D. thesis, Department of Chemical and Biochemical Engineering, Technical University of Denmark, Søltofts Plads.

Bellona, C., Drewes, J. E., Xu, P., Amy, G. (2004) Factors affecting the rejection of organic solutes during NF/RO treatment—a literature review. *Water Research,* 38**,** 2795-2809.

Bellona, C., Drewes, J.E., Oelker, G., Luna, J., Filteau, G., Amy, G. (2008) Comparing nano filtration and reverse osmosis for drinking water augmentation. *Journal (American Water Works Association),* 100**,** 102-116.

Bellona, C., Wuertle, A., Xu, P., Drewes, J.E. (2010) Evaluation of a bench-scale membrane fouling protocol to determine fouling propensities of membranes during full-scale water re use applications. *Water Science and Technology,* 62, 1198-1204.

Bellona, C., Marts, M., Drewes, J.E. (2010b) The effect of organic membrane fouling on the properties and rejection characteristics of nanofiltration membranes. *Separation and Puri fication Technology,* 74, 44-54.

Bilad, M.R., Mezohegyi, G., Declerck, P., Vankelecom, I.F.J. (2012) Novel magnetically in duced membrane vibration (MMV) for fouling control in membrane bioreactors. *Water Re search,* 46, 63-72.

Bolle, F., Pinnekamp, J. (2015) Energiebedarf von Verfahren zur Elimination von organischen Spurenstoffen – Phase II. Abschlußbericht Ministerium für Klimaschutz, Umwelt, Land wirtschaft, Natur- und Verbraucherschutz des Landes Nordrhein-Westfalen Aktenzeichen IV-7-042 600 003 J (in German).

Bucs, Sz.S., Radu, A.I., Lavric, V., Vrouwenvelder, J.S., Picioreanu, C. (2014) Effect of differ ent commercial feed spacers on biofouling of reverse osmosis membrane systems: A nu merical study. *Desalination*, 343, 26–37.

Bucs, Sz.S., Valladares Linares, R., Marston, J.O., Radu, A.I., Vrouwenvelder, J.S., Pi cioreanu, C. (2015) Experimental and numerical characterization of the water flow in spacer-filled channels of spiral-wound membranes. *Water Research*, 87, 299–310.

Bucs, Sz.S., Farhat, N., Siddiqui, A., Linares, R.V., Radu, A., Kruithof, J.C., Vrouwenvelder, J.S. (2016) Development of a setup to enable stable and accurate flow conditions for mem brane biofouling studies. *Desalination and Water Treatment*, 57, 12893–12901.

Bucs, Sz.S., Farhat, N., Kruithof, J.C., Picioreanu, C., van Loosdrecht, M.C.M., Vrouwen velder, J.S. (2018) Review on strategies for biofouling mitigation in spiral wound membrane systems. *Desalination*, 434, 189–197.

Bull, R., Crook, J. Whittaker, M., Cotruvo, J. (2011) Therapeutic dose as the point of departure in assessing potential health hazards from drugs in recycled municipal wastewater. *Regu latory Toxicology and Pharmacology*, 60(1), 1-19.

Burek, P., Satoh, Y., Fischer, G., Kahil, M.T., Scherzer, A., Tramberend, S., Nava, L.F., Wada, Y., Eisner, S., Flörke, M., Hanasaki, N., Magnuszewski, P., Cosgrove, B., Wiberg, D. (2016) Water Futures and Solution: Fast Track Initiative (Final Report). IIASA Working Pa per. Laxenburg, Austria, International Institute for Applied Systems Analysis (IIASA).

Charette, M.A., Smith, W.H.F. (2010) The Volume of Earth´s Ocean. *Oceanography,* Vol. 23, No.2.

Charfi, A., Aslam, M., Lesage, G., Heran, M., Kim, J. (2017) Macroscopic approach to develop fouling model under GAC fluidization in anaerobic fluidized bed membrane bioreactor. *Journal of Industrial and Engineering Chemistry,* 49, 219-29.

Chen, W., Westerhoff, P., Leenheer, J.A., Booksh, K. (2003) Fluorescence Excitation−Emis sion Matrix Regional Integration to Quantify Spectra for Dissolved Organic Matter. *Envi ronmental Science & Technology,* 37, 5701-5710.

Chon, K., Cho, J. (2016) Fouling behavior of dissolved organic matter in nanofiltration mem branes from a pilot-scale drinking water treatment plant: An autopsy study. *Chemical En gineering Journal,* 295, 268-277.

Chua, K.T., Hawlader, M.N.A., Malek., A. (2003) Pretreatment of seawater: Results of pilot trials in singapore. *Desalination*, 159(3), 225–243.

Coble, P.G. (1996) Characterization of marine and terrestrial DOM in seawater using excita tion-emission matrix spectroscopy. *Marine Chemistry,* 51, 325-346.

Cooley, H., Wilkinson, R. (2012) *Implications of Future Water Supply, Sources for Energy De mands*. WateReuse Research Foundation, WRRF, Alexandria, VA, USA.

Cornejo, P.K., Santana, M.V.E., Hokanson, D.R., Mihelcic, J.R., Zhang, Q. (2014) Carbon Footprint of Water Reuse and Desalination: A Review of Greenhouse Gas Emissions and Estimation Tools. *Journal of Water Reuse and Desalination*, 4(4), 238–252.

Crittenden, J.C. (2012) *MWH's water treatment*: *Principles and design, third edition,* 3rd ed. John Wiley & Sons, Hoboken, N.J.

Crone, B.C., Garland, J.L., Sorial, G.A., Vane, L.M. (2016) Significance of Dissolved Methane in Effluents of Anaerobically Treated Low Strength Wastewater and Potential for Recovery as an Energy Product: A Review. *Water Research,* 104, 520–31.

Daelman, M.R., van Voorthuizen, E.M., van Dongen, L.G., Volcke, E.I., and van Loosdrecht, M.C.M. (2013) Methane and Nitrous Oxide Emissions from Municipal Wastewater Treat ment – Results from a Long-Term Study. *Water Science and Technology,* 67(10), 2350.

Desloover, J., De Clippeleir, H., Boeckx, P., Du Laing, G., Colsen, J., Verstraete, W., Vlae minck, S.E. (2011) Floc-Based Sequential Partial Nitritation and Anammox at Full Scale with Contrasting N_2O Emissions. *Water Research,* 45(9), 2811–21.

Desloover, J., Vlaeminck, S.E., Clauwaert, P., Verstraete, W., Boon, N. (2012) Strategies to Mitigate N2O Emissions from Biological Nitrogen Removal Systems. *Current Opinion in Biotechnolog*y, 23(3), 474–82.

Dickenson, E.R.V., Drewes, J.E., Sedlak, D.L., Wert, E., Snyder, S.A. (2009) Applying Surro gates and Indicators to Assess Removal Efficiency of Trace Organic Chemicals during Chemical Oxidation of Wastewater. *Environmental Science & Technology,* 43, 6242-6247.

Dickenson, E., Drewes, J.E., Snyder, S.A., Sedlak, D.L. (2011) Indicator Compounds: An Ap proach for Using Monitoring Data to Quantify the Occurrence and Fate of Wastewater-Derived Contaminants in Surface Waters. *Water Research,* 45, 1199-1212.

Ding, S., Yang, Y., Li, C., Huang, H., Hou, L.-a. (2016) The effects of organic fouling on the removal of radionuclides by reverse osmosis membranes. *Water Research,* 95, 174-184.

DOW (n.d.). FILMTEC Membranes, FILMTEC NF 270 Nanofiltration Elements for Commercial Systems. Available: http://msdssearch.dow.com/PublishedLiteratureDOW

COM/dh_0074/0901b803800749e1.pdf?filepath=liquidseps/pdfs/noreg/609-00519.pdf&fromPage=GetDoc, Accessed 25.11.2018.

Drews, A. (2010) Membrane fouling in membrane bioreactors—Characterisation, contradict tions, cause and cures. *Journal of Membrane Science*, 363(1-2), 1–28.

Drewes, J.E., Sedlak, D., Snyder, S., Dickenson, E. (2008) *Development of Indicators and Surrogates for Chemical Contaminant Removal during Wastewater Treatment and Recla mation*. Final Report. Alexandria, VA: WateReuse Foundation.

Drewes, J.E., Khan, S.J., McDonald, J.A., Trang, T.T.T., Storey, M.V. (2010) Chemical moni toring strategy for the assessment of advanced water treatment plant performance. *Water Science and Technology*: *Water Supply,* 10(6), 961-968.

Drewes, J.E., Khan, S. (2011) Water Reuse for Drinking Water Augmentation. J. Edzwald (ed.) Water Quality and Treatment, 6th Edition. 16.1-16.48. American Water Works Association. Denver, Colorado.

Drewes, J.E., Anderson, P., Denslow, N., Olivieri, A., Schlenk, D., Snyder, S.A., Maruya, K.A. (2013) Designing Monitoring Programs for Chemicals of Emerging Concern in Potable Re use - What to include and what not to include? *Water Science and Technology,* 67(2), 433-439.

Drewes, J.E., Khan, S.J. (2015) Contemporary Design, Operation and Monitoring of Potable Reuse Systems. *Journal of Water Reuse and Desalination,* 5(1), 2-7.

Drewes, J.E., Horstmeyer, N. (2016) Recent developments in potable water reuse. Fatta-Kas sinos, D. et al. (eds.) Advanced Treatment Technologies for Urban Wastewater Reuse. The Handbook of Environmental Chemistry. Springer 45, 269–290.

Drewes, J.E., Anderson, P., Denslow, N., Jakubowski, W., Olivieri, A., Schlenk, D., Snyder, S. (2018) Recommendations of a Science Advisory Panel: Monitoring Strategies for Constit uents of Emerging Concern (CECs) in Recycled Water. State Water Resources Control Board.

DuBois, M., Gilles, K. A., Hamilton, J. K., Rebers, P. A., Smith, F. (1956) Colorimetric Method for Determination of Sugars and Related Substances. *Analytical Chemistry,* 28, 350-356.

Dürrenmatt, D.J., Wanner, O. (2014) A Mathematical Model to Predict the Effect of Heat Re covery on the Wastewater Temperature in Sewers. *Water Research,* 48, 548–58.

Environmental Protection and Heritage Council (EPHC) (2008). Australian Guidelines for Wa ter Recycling: Managing Health and Environmental Risks (Phase 2). Augmentation of Drinking Water Supplies. Canberra, Australia.

Epstein, N. (2003) Liquid–Solids Fluidization. *In:* YANG, W.-C. (ed.) *Handbook of Fluidization and Fluid-Particle Systems.* New York: Marcel Dekker.

European Union (EU) (1998) Council Directive 98/83/EC of the European Parliament and of the Council of 3 November 1998 on the quality of water intended for human consumption. European Commission. Brussels, Belgium.

European Union (EU) (2000) Directive 2000/60/EC of the European Parliament and of the Council of 12 December 2006 on the protection of groundwater against pollution and de terioration. European Commission. Brussels, Belgium.

European Union (EU) (2006) Directive 2006/118/EC of the European Parliament and of the Council of 12 December 2006 on the protection of groundwater against pollution and de terioration. European Commission. Brussels, Belgium.

European Union (EU) (2008) Directive 2008/105/EC of the European Parliament and of the Council of 16 December 2008 on environmental quality standards in the field of water policy, amending and subsequently repealing Council Directives 82/176/EEC, 83/513/EEC, 84/156/EEC, 84/491/EEC. European Commission. Brussels, Belgium.

European Union (EU) (2013) Directive 2013/39/EC of the European Parliament and of the Council of 12 August 2013 amending Directives 2000/60/EC and 2008/105/EC as regards priority substances in the field of water policy. European Commission. Brussels, Belgium.

European Union (EU) (2018) Proposal for a regulation of the European parliament and of the council on minimum requirements for water reuse. European Commission. Brussels, Bel gium.

Fan, L., Harris, J.L., Roddick, F.A., Booker, N.A. (2001) Influence of the characteristics of nat ural organic matter on the fouling of microfiltration membranes. *Water Research,* 35, 4455-4463.

Fimbres-Weihs, G.A., Wiley, D.E. (2010) Review of 3D CFD modeling of flow and mass trans fer in narrow spacer-filled channels in membrane modules. *Chemical Engineering and Pro cessing: Process Intensification*, 49, 759–781.

Fortunato, L., Leiknes, T. (2017) *In-situ* biofouling assessment in spacer filled channels using optical coherence tomography (OCT): 3D biofilm thickness mapping. *Bioresource Tech nology*, 229, 231–235.

Fricke, K., Haberkern, B., Jagemann, P., Kaste, A., Kobel, B., Koenen, S., Mitsdoerffer, R., Rißе, H., Schmellenkamp, P., Theilen, U., Thöle, D. (2015) Energiecheck und Energiean alyse - Instrumente Zur Energieoptimierung von Abwasseranlagen (in German), DWA-A 216. Deutsche Vereinigung für Wasserwirtschaft, Abwasser und Abfall e. V., DWA, Hennef, Deutschland.

Fujioka, T., Khan, S.J., Poussade, Y., Drewes, J.E., Nghiem, L.D. (2012) N-nitrosamine remo val by reverse osmosis for indirect potable water reuse – A critical review based on obser vations from laboratory, pilot and full-scale studies. *Separation and Purification Techno logy*, 98, 503–515.

Fujioka, T., Kodamatani, H., Takeuchi, H., Tanaka, H., Nghiem, L.D. (2018) Online monitoring of N-nitrosodimethylamine for the removal assurance of 1,4-dioxane and other trace orga nic compounds by reverse osmosis. *Environmental Science: Water Research & Techno logy*, 4, 2021–2028.

Gao, H., Scherson, Y.D., Wells, G.F. (2014) Towards energy neutral wastewater treatment: methodology and state of the art. *Environmental Science: Processes & Impacts*, 16, 1223–1246.

Gu, B., Adjiman, C.S., Xu, X.Y. (2017) The effect of feed spacer geometry on membrane per formance and concentration polarisation based on 3D CFD simulations. *Journal of Mem brane Science*, 527, 78–91.

Guo, W., Ngo, H.-H., Li, J. (2012) A mini-review on membrane fouling. *Bioresource Technol ogy*, 122, 27–34.

Gerrity, D., Pecson, B., Trussell, S., Trussell, R.R. (2013) Potable Reuse Treatment Trains throughout the World. *Journal of Water Supply: Research and Technology - Aqua,* 62(6), 321.

Gruber, N., Galloway, J.N. (2008) An Earth-system perspective of the global nitrogen cycle. *Nature*, 451(7176), 293.

Haaksman, V.A., Siddiqui, A., Schellenberg, C., Kidwell, J., Vrouwenvelder, J.S., Picioreanu, C. (2017) Characterization of feed channel spacer performance using geometries obtained by X-ray computed tomography. *Journal of Membrane Science*, 522, 124–139.

Haberkamp, J., Ernst, M., Böckelmann, U., Szewzyk, U., Jekel, M. (2008) Complexity of ultra filtration membrane fouling caused by macromolecular dissolved organic compounds in secondary effluents. *Water Research,* 42, 3153-3161.

Haidari, A.H., Heijman, S.G.J., van der Meer, W.G.J. (2016) Visualization of hydraulic condi tions inside the feed channel of Reverse Osmosis: A practical comparison of velocity be tween empty and spacer-filled channel. *Water Research*, 106, 232–241.

Haidari, A.H., Heijman, S.G.J., van der Meer, W.G.J. (2018) Optimal design of spacers in re verse osmosis. *Separation and Purification Technology*, 192, 441–456.

Hau, S., Bruch, D., Rizzello, G., Motzki, P., Seelecke, S. (2018) Silicone based dielectric elas tomer strip actuators coupled with non-linear biasing elements for large actuation strains. *Smart Materials and Structures,* 27(7), 074003.

Her, N., Amy, G., Plottu-Pecheux, A., Yoon, Y. (2007) Identification of nanofiltration membrane foulants. *Water Research,* 41, 3936-3947.

Hering, J.G., Waite, T.D., Luthy, R.G., Drewes, J.E., Sedlak, D.L. (2013) A changing frame work for urban water systems. *Environmental Science & Technology*, 47, 10721–10726.

Holloway, R.W., Miller-Robbie, L., Patel, M., Stokes, J.R., Munakata-Marr, J., Dadakis, J., Cath, T.Y. (2016) Life-Cycle Assessment of Two Potable Water Reuse Technologies:

MF/RO/UV–AOP Treatment and Hybrid Osmotic Membrane Bioreactors. *Journal of Mem brane Science,* 507, 165–78.

Hong, S., Elimelech, M. (1997) Chemical and physical aspects of natural organic matter (NOM) fouling of nanofiltration membranes. *Journal of Membrane Science,* 132, 159-181.

Horstmeyer, N., Weißbach, M., Koch, K., Drewes, J.E. (2018) A novel concept to integrate energy recovery into potable water reuse treatment schemes. *Journal of Water Reuse and Desalination*, 8(4), 455–467.

House, M. (2013) ViviTouch: A Conversation With CEO Dirk Schapeler On The Power of HD Feel Technology [Online]. Available: https://www.dualshockers.com/vivitouch-a-conversa tion-with-ceo-dirk-schapeler-on-the-power-of-hd-feel-technology/ [Accessed 25.11.2018].

Huber, S.A., Balz, A., Abert, M., Pronk, W. (2011) Characterisation of aquatic humic and non-humic matter with size-exclusion chromatography – organic carbon detection – organic nitrogen detection (LC-OCD-OND). *Water Research,* 45, 879-885.

Hyde, C.G. (1937) The Beautification and Irrigation of Golden Gate Park with Activated Sludge Effluent. *Sewage Works Journal*, 9(6), 929-941.

Ibrahim, N., Aziz, H.A. (2014) Trends on Natural Organic Matter in Drinking Water Sources and its Treatment. *International Journal of Scientific Research in Environmental Sciences,* 2, 94.

Iorhemen, O.T., Hamza, R.A., Tay, J.H. (2016) Membrane Bioreactor (MBR) Technology for Wastewater Treatment and Reclamation: Membrane Fouling. *Membranes,* 6, 33.

Jaffrin, M.Y. (2008) Dynamic shear-enhanced membrane filtration: A review of rotating disks, rotating membranes and vibrating systems. *Journal of Membrane Science*, 324(1-2), 7–25.

Johir, M.A.H., Aryal, R., Vigneswaran, S., Kandasamy, J., Grasmick, A. (2011) Influence of supporting media in suspension on membrane fouling reduction in submerged membrane bioreactor (SMBR). *Journal of Membrane Science,* 374, 121-8.

Johnson, J., Busch, M. (2010) Engineering Aspects of Reverse Osmosis Module Design. *De salination and Water Treatment*, 15, 236–248.

Judd, S., Judd, C. (2011) *The MBR book*: *Principles and applications of membrane bioreactors in water and wastewater treatment,* 2nd ed. Elsevier, Amsterdam, London.

Kalbar, P.P., Karmakar, S., Asolekar, S.R. (2013) Assessment of Wastewater Treatment Tech nologies: Life Cycle Approach. *Water and Environment Journal,* 27(2), 261–68.

Kampschreur, M.J., Wouter, R.L., van der Star, W.R.L., Wielders, H.A., Mulder, J. W., Jetten, M.S.M., van Loosdrecht, M.C.M. (2008) Dynamics of Nitric Oxide and Nitrous Oxide Emis sion during Full-Scale Reject Water Treatment. *Water Research,* 42(3), 812–26.

Kampschreur, M.J., Temmink, H., Kleerebezem, R., Jetten, M.S.M., van Loosdrecht, M.C.M. (2009) Nitrous Oxide Emission during Wastewater Treatment. *Water Research,* 43(17), 4093–4103.

Karabelas, A.J., Kostoglou, M., Koutsou, C.P. (2015) Modeling of spiral wound membrane desalination modules and plants – review and research priorities. *Desalination*, 356, 165–186.

Karode, S., Kumar, A. (2001) Flow visualization through spacer filled channels by computa tional fluid dynamics I. Pressure drop and shear rate calculations for flat sheet geometry. *Journal of Membrane Science*, 193, 69–84.

Kavianipour, O., Ingram, G.D., Vuthaluru, H.B. (2017) Investigation into the effectiveness of feed spacer configuraions for reverse osmosis membrane modules using Computational Fluid Dynamics. *Journal of Membrane Science*, 526, 156–171.

Khan, S.J. (2013) Drinking Water Through Recycling. A Report of a Study by the Australian Academy of Technological Sciences and Engineering (ATSE). Melbourne, Victoria, Australia.

Khan, S.J. (2015) Potable reuse of water. *Environmental Science: Water Research & Tech nology*, 1, 550–553.

Kim, J., Kim, K., Ye, H., Lee, E., Shin, C., McCarty, P.L., Bae, J. (2011) Anaerobic Fluidized Bed Membrane Bioreactor for Wastewater Treatment. *Environmental Science & Technol ogy,* 45(2), 576–81.

KOCH MEMBRANE SYSTEMS. (2014) Installation and Operation Manual - Puron® Singele Header Wastewater Treatment Module - PURON® Single Bundle Demo Module (0.5m2) for Bench Test Units [Online]. Aachen. Available: www.kochmembrane.com.

Kofod, G., Sommer-Larsen, P. (2008) Chapter 7 - COMPLIANT ELECTRODES: SOLUTIONS, MATERIALS AND TECHNOLOGIES. *In:* CARPI, F., ROSSI, D. D., KORNBLUH, R., PEL RINE, R. & SOMMER-LARSEN, P. (eds.) *Dielectric Elastomers as Electromechanical Transducers.* Amsterdam: Elsevier.

Kola, A., Ye, Y., Ho, A., Le-Clech, P., Chen, V. (2012) Application of low frequency transverse vibration on fouling limitation in submerged hollow fibre membranes. *Journal of Membrane Science,* 409-410, 54-65.

Kola, A., Ye, Y., Le-Clech, P., Chen, V. (2014) Transverse vibration as novel membrane fouling mitigation strategy in anaerobic membrane bioreactor applications. *Journal of Membrane Science*, 455, 320–329.

Koutsou, C.P., Yiantsios, S.G., Karabelas, A.J. (2004) Numerical simulation of the flow in a plane-channel containing a periodic array of cylindrical turbulence promoters. *Journal of Membrane Science*, 231, 81–90.

Koutsou, C.P., Yiantsios, S.G., Karabelas, A.J. (2007) Direct numerical simulation of flow in spacer-filled channels : Effect of spacer geometrical characteristics. *Journal of Membrane Science*, 291, 53–69.

Koutsou, C.P., Yiantsios, S.G., Karabelas, J. (2009) A numerical and experimental study of mass transfer in spacer-filled channels: Effects of spacer geometrical characteristics and Schmidt number. *Journal of Membrane Science*, 326, 234–251.

Krasner, S.W., Weinberg, H.S., Richardson, S.D., Pastor, S.J., Chinn, R., Sclimenti, M.J., On stad, G.D., Thruston, A.D. (2006) Occurrence of a New Generation of Disinfection Byprod ucts. *Environmental Science & Technology,* 40, 7175-7185.

Lackner, S., Gilbert, E.M., Vlaeminck, S.E., Joss, A., Horn, H., van Loosdrecht, M.C.M. (2014) Full-Scale Partial Nitritation/Anammox Experiences – An Application Survey. *Water Re search,* 55, 292–303.

Lahnsteiner, J., van Rensburg, P., Esterhuizen, J. (2017) Direct Potable Reuse – a Feasible Water Management Option. *Journal of Water Reuse and Desalination*, 8(1), 14–28.

Lamsal, R., Montreuil, K.R., Kent, F.C., Walsh, M.E., Gagnon, G.A. (2012) Characterization and removal of natural organic matter by an integrated membrane system. *Desalination,* 303, 12-16.

Lau, K.K., Abu Bakar, M.Z., Ahmad, A.L., Murugesan, T. (2009) Feed spacer mesh angle: 3D modeling, simulation and optimization based on unsteady hydrodynamic in spiral wound membrane channel. *Journal of Membrane Science*, 343, 16–33.

Laureni, M., Falås, P., Robin, O., Wick, A., Weissbrodt, D.G., Nielsen, J.L., Ternes, T.A., Mor genroth, E. Joss, A. (2016) Mainstream Partial Nitritation and Anammox: Long-Term Pro cess Stability and Effluent Quality at Low Temperatures. *Water Research,* 101, 628–39.

Lazarova, V., Choo, K.H., Cornel, P. (2012) *Water-Energy Interactions in Water Reuse*. Inter national Water Association, IWA, IWA Publishing, London, UK.

Le-Clech, P., Chen, V., Fane, T.A. (2006) Fouling in membrane bioreactors used in wastewater treatment. *Journal of Membrane Science*, 284(1-2), 17–53.

Lee, S., Ang, W.S., Elimelech, M. (2006) Fouling of reverse osmosis membranes by hydro philic organic matter: implications for water reuse. *Desalination,* 187, 313-321.

Lee, J.Y., Tan, W.S., An, J., Chua, C.K., Tang, C.Y., Fane, A.G., Chong, T.H. (2016) The potential to enhance membrane module design with 3D printing technology. *Journal of Membrane Science,* 499, 480–490.

Leverenz, H.L., Tchobanoglous, G., Asano, T. (2011) Direct potable reuse: a future imperative. Journal of Water Reuse and Desalination 1(1), 2-10.

Li, F., Meindersma, W., De Haan, B., Reith, T. (2002) Optimization of commercial net spacers in spiral wound membrane modules. *Journal of Membrane Science,* 208, 289–302.

Li, Q., Elimelech, M. (2006) Synergistic effects in combined fouling of a loose nanofiltration membrane by colloidal materials and natural organic matter. *Journal of Membrane Sci ence,* 278, 72-82.

Li, Y.L., Tung, K.L. (2008a) CFD simulation of fluid flow through spacer-filled membrane mod ule : selecting suitable cell types for periodic boundary conditions. *Desalination*, 233, 351–358.

Li,, Y.-L., Tung, K.L. (2008b) The effect of curvature of a spacer-filled channel on fluid flow in spiral-wound membrane modules. *Journal of Membrane Science*, 319, 286–297.

Li, T., Law, A.W.-K., Jiang, Y., Harijanto, A.K., FANE, A.G. (2016a) Fouling control of sub merged hollow fibre membrane bioreactor with transverse vibration. *Journal of Membrane Science,* 505, 216-24.

Li, H., Xia, H., Mei, Y. (2016b) Modeling organic fouling of reverse osmosis membrane: From adsorption to fouling layer formation. *Desalination,* 386, 25-31.

Lozán, J.L., Meyer, S., Karbe, L. (2007) Water as the basis of life. In: Lozán, J.L., Grassl, H., Hupfer, P., Menzel, L., Schönwiese, C.-D.: Global Change: Enough water for all?. Wissen schaftliche Auswertungen, Hamburg. Online: www.klima-warnsignale.uni-hamburg.de.

Lyster, E., Au, J., Rallo, R., Giralt, F., Cohen, Y. (2009) Coupled 3-D hydrodynamics and mass transfer analysis of mineral scaling-induced flux decline in a laboratory plate-and-frame reverse osmosis membrane module. *Journal of Membrane Science*, 339, 39–48.

Marcinek and Rosenkranz (1996) Das Wasser der Erde (in German). Gotha. 3. Auflage.

Martinez-Sosa, D., Helmreich, B., Netter, T., Paris, S., Bischof, F., Horn, H. (2011) Anaerobic Submerged Membrane Bioreactor (AnSMBR) for Municipal Wastewater Treatment under Mesophilic and Psychrophilic Temperature Conditions. *Bioresource Technology,* 102(22), 10377–85.

Mänttäri, M., Pekuri, T., Nyström, M. (2004) NF270, a new membrane having promising char acteristics and being suitable for treatment of dilute effluents from the paper industry. *Jour nal of Membrane Science,* 242, 107-116.

McCarty, P.L., Bae, J., Kim, J. (2011) Domestic wastewater treatment as a net energy producer – can this be achieved? *Environmental Science & Technology*, 45, 7100–7106.

McDonald, R.I., Weber, K., Padowski, J., Flörke, M., Schneider, C., Green, P.A., Gleeson, T., Eckman, S., Lehner, B., Balk, D., Boucher, T., Grill, G., Montgomery, M. (2014) Water on an urban planet: Urbanization and the reach of urban water infrastructure. *Global Environ mental Change*, 27, 96–105.

Metsämuuronen, S., Sillanpää, M., Bhatnagar, A. & Mänttäri, M. (2014) Natural Organic Matter Removal from Drinking Water by Membrane Technology. *Separation & Purification Re views,* 43, 1-61.

Mekonnen, M.M., Hoekstra, A.Y. (2016) Four billion people facing severe water scarcity. *Science Advances,* 2(2), 1-6.

Melin, T. (2007) Strategien zur Foulingkontrolle bei Membranbelebungsanlagen in der kommunalen Abwasserbehandlung (in German). Abschlussbericht für das Ministerium für Umwelt und Naturschutz, Landwirtschaft und Verbraucherschutz des Landes Nordrhein-Westfalen.

Melin, T., Rautenbach, R. (2007) Membranverfahren (in German), third ed., Springer-Verlag, Berlin Heidelberg, 2007.

Miyoshi, T., Yuasa, K., Iishigami, T., Rajabzadeh, S., Kamio, E., Ohmukai, Y., Saeki, D., Ni, J., Matsuyama, H. (2015) Effect of membrane polymeric materials on relationship between surface pore size and membrane fouling in membrane bioreactors. *Applied Surface Science,* 330, 351-7.

Mojab, S.M., Pollard, A., Pharoah, J.G., Beale, S.B., Hanff, E.S. (2014) Unsteady Laminar to Turbulent Flow in a Spacer-Filled Channel. *Flow, Turbulence and Combustion*, 92, 563–577.

Murphy, K.R., Hambly, A., Singh, S., Henderson, R.K., Baker, A., Stuetz, R., Khan, S.J. (2011) Organic Matter Fluorescence in Municipal Water Recycling Schemes: Toward a Unified PARAFAC Model. *Environmental Science & Technology,* 45, 2909-2916.

Mustafa, G., Wyns, K., Buekenhoudt, A., Meynen, V. (2016) New insights into the fouling mechanism of dissolved organic matter applying nanofiltration membranes with a variety of surface chemistries. *Water Research,* 93, 195-204.

Müller, J., Drewes, J.E., Hübner, U. (2017) Sequential biofiltration – A novel approach for enhanced biological removal of trace organic chemicals from wastewater treatment plant effluents. *Water Research*, 127, 127–138.

NASA (2018) https://www.nasa.gov/press-release/nasa-satellites-reveal-major-shifts-in-global-freshwater. National Aeronautics and Space Administration (NASA).

New Logic Research, Inc. (n.d.) New Logic Research, Inc. http://www.vsep.com (accessed 25 November 2018).

Nghiem, L.D., Coleman, P.J. (2008) NF/RO filtration of the hydrophobic ionogenic compound triclosan: Transport mechanisms and the influence of membrane fouling. *Separation and Purification Technology,* 62, 709-716.

Niero, M., Pizzol, M., Bruun, H.G., Thomsen, M. (2014) Comparative Life Cycle Assessment of Wastewater Treatment in Denmark Including Sensitivity and Uncertainty Analysis. *Journal of Cleaner Production,* 68, 25–35.

Noiva, K., Fernández, J.E., Wescoat Jr., J.L. (2016) Cluster analysis of urban water supply and demand: Toward large-scale comparative sustainability planning. *Sustainable Cities and Society*, 27, 484–496.

National Research Council (NRC) (2012) *Water Reuse – Potential for Expanding the Nation's Water Supply Through Reuse of Municipal Wastewater*. The National Academies Press, Washington, D.C.

National Water Research Institute (NWRI) (2013) *Final Report Examining the Criteria for Direct Potable Reuse Recommendations of an NWRI Independent Advisory Panel*. Prepared for WateReuse Research Foundation Project 11-02, Fountain Valley, CA.

Oki, T. (2005) Encyclopedia of Hydrological Sciences, vol 5. Part 1: Theory, Organization and Scale, Chapter 2 The Hydrologic Cycles and Global Circulation.

Oki, T., Kanae, S. (2006) Global Hydrological Cycles and World Water Resources. *Science*, 313, 1068–1072.

Olivieri, A.W., Crook, J., Anderson, M.A., Bull, R.J., Drewes, J.E., Haas, C.N., Jakubowski, W., McCarty, P.L., Nelson, K.L., Rose, J.B., Sedlak, D.L., Wade, T.J. (2016) Expert Panel Final Report: Evaluation of the Feasibility of Developing Uniform Water Recycling Criteria for Direct Potable Reuse. National Water Research Institute (NWRI). Sacramento, CA, USA.

Pánek, P., Kodým, R., Šnita, D., Bouzek, K. (2015) Spatially two-dimensional mathematical model of the flow hydrodynamics in a spacer-filled channel – The effect of inertial forces. *Journal of Membrane Science*, 492, 588–599.

Park, H., Choo, K.-H., Lee, C.-H. (1999) Flux Enhancement with Powdered Activated Carbon Addition in the Membrane Anaerobic Bioreactor. *Separation Science and Technology,* 34, 2781-92.

Pei, Q., Hu, W., McCoul, D., Biggs, S.J. (2016) Dielectric Elastomers as EAPs: Applications. In: *Electromechanically Active Polymers*, F. Carpi (ed.), Springer International Publishing, Cham, pp. 739–766Pei, Qibing; Hu, Wei; McCoul, David; Biggs, Silmon James.

Peinemann, K.-V., Nunes, S.P. (2010) *Membranes for Water Treatment*, Wiley-VCH Verlag GmbH & Co. KGaA.

Pelrine, R., Kornbluh, R. (2016) Dielectric Elastomers as Electroactive Polymers (EAPs): Fun damentals. In: *Electromechanically Active Polymers*, F. Carpi (ed.), Springer International Publishing, Cham, pp. 671–686Pelrine, Ron and Kornbluh, Roy.

Petropoulos, E., Dolfing, J., Davenport, R.J., Bowen, E.J., Curtis, T.P. (2017) Developing Cold-Adapted Biomass for the Anaerobic Treatment of Domestic Wastewater at Low Tempera tures (4, 8 and 15 °C) with Inocula from Cold Environments. *Water Research,* 112, 100–109.

Picioreanu, C., Vrouwenvelder, J.S., van Loosdrecht, M.C.M. (2009) Three-dimensional mod eling of biofouling and fluid dynamics in feed spacer channels of membrane devices. *Jour nal of Membrane Science*, 345, 340–354.

Puchongkawarin, C., Gomez-Mont, C., Stuckey, D.C., Chachuat, B. (2015) Optimization-Based Methodology for the Development of Wastewater Facilities for Energy and Nutrient Recovery. *Chemosphere,* 140, 150–58.

Radu, A.I., van Steen, M.S.H., Vrouwenvelder, J.S., van Loosdrecht, M.C.M, Picioreanu, C. (2014) Spacer geometry and particle deposition in spiral wound membrane feed channels. *Water Research*, 64, 160–176.

Rajabzadeh, A.R. (2010) Membrane Fouling During Hollow Fiber Ultrafiltration of Protein So lutions: Computational Fluid Modeling and Physicochemical Properties, Doctoral Thesis, University of Waterloo, Canada, 2010.

Rana, D., Matsuura, T. (2010) Surface Modifications for Antifouling Membranes. *Chemical Re views,* 110, 2448-71.

Ravishankara, A.R., Daniel, J.S., Portmann, R.W. (2009) Nitrous ocide (N_2O): The dominant ozone-depleting substance emitted in the 21st century. *Science*, 326(5949), 123–125.

Sedlak. D. (2014) Water 4.0. The Past, Present, and Future of the World's Most Vital Resource. Yale University Press.

Regnery, J., Lee, J., Kitanidis, P., Illangasekare, T., Sharp, J.O., Drewes, J.E. (2013) Integra tion of Managed Aquifer Recharge for Impaired Water Sources in Urban Settings – Over coming Current Limitations and Engineering Challenges. *Environmental Engineering Sci ence,* 30(8), 409-420.

Remy, C., Boulestreau, M., Lesjean, B. (2014) Proof of Concept for a New Energy-Positive Wastewater Treatment Scheme. *Water Science and Technology,* 70(10), 1709.

Remy, C., Boulestreau, M., Warneke, J., Jossa, P., Kabbe, C., Lesjean, B. (2016) Evaluating New Processes and Concepts for Energy and Resource Recovery from Municipal Wastewater with Life Cycle Assessment. *Water Science and Technology,* 73(5), 1074.

Rice, J., Wutich, A., Westerhoff, P. (2013) Assessment of de facto wastewater reuse across the U.S.: Trends between 1980 and 2008. *Environmental Science & Technology,* 47(16), 11099-11105.

Saeed, A., Vuthaluru, R., Yang, Y., Vuthaluru, H.P. (2012) Effect of feed spacer arrangement on flow dynamics through spacer filled membranes. *Desalination*, 285, 163–169.

Santos, J.L.C., Geraldes, V., Velizarov, S., Crespo, J.G. (2007) Investigation of flow patterns and mass transfer in membrane module channels filled with flow-aligned spacers using computational fluid dynamics (CFD). *Journal of Membrane Science,* 305, 103–117.

Schaum, C., Lensch, D., Cornel P. (2015) Water Reuse and Reclamation: A Contribution to Energy Efficiency in the Water Cycle. *Journal of Water Reuse and Desalination,* 5(2), 83.

Scherson, Y.D., Criddle, C.S. (2014). Recovery of Freshwater from Wastewater: Upgrading Process Configurations To Maximize Energy Recovery and Minimize Residuals. *Environ mental Science & Technology,* 48(15), 8420–32.

Scherson, Y.D., Wells, G.F., Woo, S.-G., Lee, J., Park, J., Cantwell, B.J., Criddle, C.S. (2013) Nitrogen removal with energy recovery through N_2O decomposition. *Energy Environmental Science,* 6(1), 241–248.

Scherson, Y.D., Woo, S.G., Criddle, C.S. (2014) Production of Nitrous Oxide From Anaerobic Digester Centrate and Its Use as a Co-Oxidant of Biogas to Enhance Energy Recovery. *Environmental Science & Technology,* 48(10), 5612–19.

Schimmoller, L., Kealy, M.J. (2014) *Fit for Purpose Water: The Cost of Overtreating Reclaimed Water*. WateReuse Research Foundation, WRRF, Alexandria, VA, USA.

Schimmoller, L.J., Kealy, M.J., Foster, S.K. (2015) Triple Bottom Line Costs for Multiple Pota ble Reuse Treatment Schemes. *Environmental Science: Water Research & Technology*, 1(5), 644–58.

Schmitz, J. (2017) Investigation of membrane fouling of NF/RO membrane applications to en hance efficiency of an integrated membrane system for potable water reuse. Master The sis. Technical University of Munich.

Schock, G., Miquel, A. (1987) Mass transfer and pressure loss in spiral wound modules. *De salination*, 64, 339–352.

Schwab, B.W., Hayes, E.P., Fiori, J.M., Mastrocco, F.J., Roden, N.M., Cragin, D., Meyerhoff, R.D., D'Aco, V.J., Anderson, P.D. (2005) Human pharmaceuticals in US surface waters: A human health risk assessment. *Regulatory Toxicology and Pharmacology,* 42(3), 296–312.

Seidel, A., Elimelech, M. (2002) Coupling between chemical and physical interactions in natu ral organic matter (NOM) fouling of nanofiltration membranes: implications for fouling con trol. *Journal of Membrane Science,* 203, 245-255.

Seredyńska-Sobecka, B., Stedmon, C.A., Boe-Hansen, R., Waul, C.K., Arvin, E. (2011) Mon itoring organic loading to swimming pools by fluorescence excitation–emission matrix with parallel factor analysis (PARAFAC). *Water Research,* 45, 2306-2314.

Sgroi, M., Vagliasindi, F.G.A., Snyder, S.A., Roccaro, P. (2018) N-Nitrosodimethylamine (NDMA) and its precursors in water and wastewater: A review on formation and removal. *Chemosphere*, 191, 685–703.

Shakaib, M., Hasani, S.M.F., Mahmood, M. (2007) Study on the effects of spacer geometry in membrane feed channels using three-dimensional computational flow modeling. *Journal of Membrane Science*, 297, 74–89.

Shiklomanov I. (1993) World fresh water resources. In: Water in Crisis: A Guide to the World´s Fresh Water Resources. Gleick, P.H. (editor). Oxford University Press. New York.

Shin, C., McCarty, P.L., Kim, J., Bae, J. (2014) Pilot-scale temperate-climate treatment of do mestic wastewater with a staged anaerobic fluidized membrane bioreactor (SAF-MBR). *Bioresource Technology,* 159, 95–103.

Shin, C., Kim, K., McCarty, P.L., KIM, J., Bae, J. (2016) Integrity of hollow-fiber membranes in a pilot-scale anaerobic fluidized membrane bioreactor (AFMBR) after two-years of opera tion. *Separation and Purification Technology,* 162, 101-5.

Siddiqui, A., Farhat, N., Bucs, Sz.S., Valladares, R., Picioreanu, C., Kruithof, J.C. (2016) De velopment and characterization of 3D-printed feed spacers for spiral wound membrane systems. *Water Research*, 91, 55–67.

Siddiqui, A., Lehmann, S., Haaksman, V., Ogier, J., Schellenberg, C., van Loosdrecht, M.C.M., Kruithof, J.C., Vrouwenvelder, J.S. (2017a) Porosity of spacer-filled channels in spiral-wound membrane systems: Quantification methods and impact on hydraulic characteriza tion. *Water Research*, 119, 304–311.

Siddiqui, A., Lehmann, S., Bucs, Sz.S., Fresquet, M., Fel, L., Prest, E.I.E.C., Ogier, J., Schel lenberg, C., van Loosdrecht, M.C.M., Kruithof, J.C., Vrouwenvelder, J.S. (2017b) Predict ing the impact of feed spacer modification on biofouling by hydraulic characterization and biofouling studies in membrane fouling simulators. *Water Research*, 110, 281–287.

Sillanpää, M. (2015) Chapter 1 - General Introduction. *Natural Organic Matter in Water.* But terworth-Heinemann.

Singh, R. (2015) Chapter 1 - Introduction to Membrane Technology. *Membrane Technology and Engineering for Water Purification (Second Edition).* Oxford: Butterworth-Heinemann.

Snyder, S.A., Trenholm, R., Snyder, E.M., Bruce, G.M., Pleus, R.C., Hemming, J.D. (2008) *Toxicological relevance of EDCs and Pharmaceuticals in Drinking Water.* Awwa Research Foundation Report. Denver, CO: Water Research Foundation.

Snyder, S.A., Benotti, M., Rosario-Ortiz, F., Vanderford, B., Drewes, J.E., Dickenson, E. (2014) Comparison of Chemical Composition of Reclaimed and Conventional Waters. Final Re port. WateReuse Research Foundation (WRRF-06-006). Alexandria, VA.

Sobieszuk, P., Szewczyk, K.W. (2006) Estimation of (C/N) Ratio for Microbial Denitrification. *Environmental Technology,* 27(1), 103–8.

Sperle, P. (2018) Development and Investigation of Vibration Based Membrane Fouling Miti gation and Cleaning Strategies. Master Thesis. Technical University of Munich.

Speth, T.F., Summers, R.S., Gusses, A.M. (1998) Nanofiltration Foulants from a Treated Sur face Water. *Environmental Science & Technology,* 32, 3612-3617.

State Water Resources Control Board (SWRCB) (2013) *Policy for Water Quality Control for Recycled Water (Recycled Water Policy).* Sacramento, CA, USA.

State Water Resources Control Board (SWRCB) (2018) Monitoring Strategies for Constituents of Emerging Concern (CECs) in Recycled Water. Sacramento, CA, USA.

Stokes, J.R., Horvath, A. (2009) Energy and Air Emission Effects of Water Supply. *Environ mental Science & Technology,* 43(8), 2680–87.

Tang, F., Hu, H.-Y., Sun, L.-J., Wu, Q.-Y., Jiang, Y.-M., Guan, Y.-T., Huang, J.-J. (2014) Foul ing of reverse osmosis membrane for municipal wastewater reclamation: Autopsy results from a full-scale plant. *Desalination,* 349, 73-79.

Tauseef, S.M., Abbasi, T., Abbasi, S.A. (2013) Energy Recovery from Wastewaters with High-Rate Anaerobic Digesters. *Renewable and Sustainable Energy Reviews,* 19, 704–41.

Tchobanoglous, G., Leverenz, H., Neller, M., Crook, J. (2011) *Direct Potable Reuse – A Path Forward*. WateReuse Research Foundation, Alexandria, VA.

Tchobanoglous, G., Stensel, H.D., Tsuchihashi, R., Burton, F.L., Bowden, G., Abu-Orf, M. Pfrang, W. (2014) *Wastewater engineering*: *Treatment and resource recovery,* 5th ed. McGraw-Hill Education, New York.

Tchobanoglous, G., Cotruvo, J., Crook, J., McDonald, E., Olivieri, A., Salveson, A, Trussell, S. (2015) Framework for Direct Potable Reuse. WateReuse Research Foundation, Alexan dria, VA.

Toray (2004) Romembra Toray Reverse Osmosis Elements, Model TMG-10. Available: http://www.toraywater.com/products/ro/pdf/TMG.pdf, Accessed 25.11.2018.

Trussel, R. (2014) Direct potable reuse – The equivalency of advanced treatment trains in the protection of public health. WateReuse Research Foundation Webcast Series, Feb. 20, 2014. Alexandria, VA.

Trussell, R.R., Trussell, R.S., Salveson, A., Steinle-Darling, E., He, Q., Snyder, S., Gerrity, D. (2017). *Equivalency of Advanced Treatment Trains for Potable Reuse*. WateReuse Re search Foundation, WRRF, Alexandria, VA, USA.

Thurman, E. M. (1985) *Organic Geochemistry of Natural Waters*, Springer Netherlands.

Umweltbundesamt (UBA) (German Environmental Protection Agency) (2011). Grenzwerte, Leitwerte, Orientierungswerte, Maßnahmenwerte – Aktuelle Definitionen und Höchstwerte. Umweltbundesamt, Dessau, Germany (in German).

United Nations (UN) (2017) *The United Nations World Water Development Report 2017: Wastewater - The Untapped Resource.* http://www.unwater.org/publications/world-water-development-report-2017/.

United Nations (UN) (2018) The Sustainable Development Goals Report 2018. United Nations (UN), New York.

UNESCO (2014) The United Nations World Water Development Report 2014. United Nations Educational, Scientific and Cultural Organization (UNESCO), Paris.

UNESCO (2018) The United Nations World Water Development Report 2018: Nature-Based Solutions for Water. United Nations Educational, Scientific and Cultural Organization (UNESCO), Paris.

U.S. Environmental Protection Agency (USEPA) (1992) Guidelines for Exposure Assessment. EPA/600/Z-92/001. Federal Register 57(104): 22888-22938. Washington, D.C.

U.S. Environmental Protection Agency (USEPA) (2012) Guidelines for Water Reuse. EPA/600/R-12/618. Washington, D.C.

van den Berg, M., Birnbaum, L.S., Denison, M., De Vito, M., Farland, W., Feeley, M., Fiedler, H., Hakansson, H., Hanberg, A., Haws, L., Rose, M., Safe, S., Schrenk, D., Tohyama, C., Tritscher, A., Tuomisto, J., Tysklind, M., Walker, N., Peterson, R.E. (2006) The 2005 World Health Organization reevaluation of human and mammalian toxic equivalency factors for dioxins and dioxin-like compounds. *Toxicological Sciences,* 93(2), 223-241.

van der Marel, P., Zwijnenburg, A., Kemperman, A., Wessling, M., Temmink, H., van der Meer, W. (2010) Influence of membrane properties on fouling in submerged membrane bioreac tors. *Journal of Membrane Science,* 348, 66-74.

Verstraete, W., Van de Caveye, P., Diamantis, V. (2009) Maximum Use of Resources Present in Domestic 'Used Water. *Bioresource Technology,* 100(23), 5537–45.

Vince, F., Aoustin, E., Bréant, P., Marechal, F. (2008) LCA Tool for the Environmental Evaluation of Potable Water Production. *Desalination,* 220(1), 37–56.

Vogel, D., Simon, A., Alturki, A.A., Bilitewski, B., Price, W.E., Nghiem, L.D. (2010) Effects of fouling and scaling on the retention of trace organic contaminants by a nanofiltration mem brane: The role of cake-enhanced concentration polarisation. *Separation and Purification Technology,* 73, 256-263.

Vrouwenvelder, J.S., van Paassen, J.A.M., Wessels, L.P., van Dam, A.F., Bakker, S.M. (2006) The membrane fouling simulator: a practical tool for fouling prediction and control. *Journal of Membrane Science*, 281, 316–324.

Vrouwenvelder, J.S., van Paassen, J.A.M., Kruithof, J.C., van Loosdrecht, M.C.M. (2009) Sensitive pressure drop measurement of individual lead membrane elements for accurate early biofouling detection. *Journal of Membrane Science,* 338, 92–99.

Vrouwenvelder, J.S., Picioreanu, C., Kruithof, J.C., van Loosdrecht, M.C.M. (2010) Biofouling in spiral wound membrane systems: Three-dimensional CFD model based evaluation of experimental data. *Journal of Membrane Science,* 346, 71–85.

Wada, Y., Flörke, M., Hanasaki, N., Eisner, S., Fischer, G., Tramberend, S., Satoh, Y., van Vliet, M.T.H., Yillia, P., Ringler, C., Burek, P., Wiberg, D. (2016) Modeling global water ue for the 21st century: the Water Futures and Solutions (WFaS) initiative and its approaches. *Geoscientific Model Development*, 9, 175–222.

Wang, Y.-N., Tang, C.Y. (2011) Protein fouling of nanofiltration, reverse osmosis, and ultrafiltration membranes—The role of hydrodynamic conditions, solution chemistry, and membrane properties. *Journal of Membrane Science,* 376, 275-282.

Wang, Z., Ma, J., Tang, C.Y., Kimura, K., Wang, Q., Han, X. (2014) Membrane cleaning in membrane bioreactors: A review. *Journal of Membrane Science*, 468, 276–307.

Wang, J., Zamani, F., Cahyadi, A., Toh, J.Y., Yang, S., Wu, B., Liu, Y., Fane, A.G., Chew, J.W. (2016) Correlating the hydrodynamics of fluidized granular activated carbon (GAC) with membrane-fouling mitigation. *Journal of Membrane Science,* 510, 38-49.

Wanner, O., Panagiotidis, V., Clavadetscher, P., Siegrist, H. (2005) Effect of Heat Recovery from Raw Wastewater on Nitrification and Nitrogen Removal in Activated Sludge Plants. *Water Research,* 39(19), 4725–34.

Water Corporation (2018) https://www.watercorporation.com.au/water-supply/ongoing-works/groundwater-replenishment-scheme. Access: 25.11.2018.

Weißbach, M. (2018) Technical implementation and development of control strategies for the integration of the Coupled Aerobic-anoxic Nitrous Decomposition Operation (CANDO) into wastewater treatment schemes for simultaneous nitrogen removal and energy recovery from nitrogen. Doctoral Thesis. Technical University of Munich.

Weißbach M., Thiel P., Drewes J.E., Koch K. (2018) Nitrogen removal and intentional nitrous oxide production from reject water in a coupled nitritation/nitrous denitritation system under real feed-stream conditions. *Bioresource Technology,* 255, 58–66.

Wert, E., Rosario-Ortiz, F., Snyder, S. (2009). Using UV absorbance and color to assess the oxidation of pharmaceuticals during the ozonation of wastewater. *Environmental Science & Technology,* 43(13), 4858–4863.

West, S., Wagner, M., Engelke, C., Horn, H. (2016) Optical coherence tomography for the *in situ* three-dimensional visualization and quantification of feed spacer channel fouling in reverse osmosis membrane modules. *Journal of Membrane Science,* 498, 345–352.

WHO (2017a) Potable reuse: Guidance for producing safe drinking-water. World Health Or ganization.

WHO (2017b) Guidelines for drinking-water quality, fourth edition, incorporating the 1st adden dum. World Health Organization.

Ying, Z., Ping, G. (2006) Effect of powdered activated carbon dosage on retarding membrane fouling in MBR. *Separation and Purification Technology,* 52, 154-60.

Ye, Y., Sim,L.N., Herulah,B., Chen, V., Fane, A.G. (2010) Effects of operating conditions on submerged hollow fibre membrane systems used as pre-treatment for seawater reverse osmosis. *Journal of Membrane Science*, 365(1-2), 78–88.

Zhao, Y., Song, L., Ong, S.L. (2010a) Fouling behavior and foulant characteristics of reverse osmosis membranes for treated secondary effluent reclamation. *Journal of Membrane Sci ence,* 349, 65-74.

Zhao, Y., Song, L., Ong, S.L. (2010b) Fouling of RO membranes by effluent organic matter (EfOM): Relating major components of EfOM to their characteristic fouling behaviors. *Jour nal of Membrane Science,* 349, 75-82.

Zularisam, A.W., Ismail, A.F., Salim, M.R., Sakinah, M., Ozaki, H. (2007) The effects of natural organic matter (NOM) fractions on fouling characteristics and flux recovery of ultrafiltration membranes. *Desalination,* 212, 191-208.

Appendix A – Additional achievements

Other topic related achievements:

Foundation of the Young Water Reuse Professionals (YWRP) within the Water Reuse Special Group (WRSG) of the International Water Association (IWA). The engagement includes regularly announcements in the quarterly WRSG newsletter, the Water-Wiki or IWA connect. Following presentations, meetings or session moderation are part of the YWRG engagement:

- Horstmeyer, N., Lefebvre, O. (2017) **YWRP Meeting – Current status, opportunities and future of the YWRP in the WRSG**. IWA 11th International Conference on Water Reclamation and Reuse, Long Beach, CA, USA, 23.-27.07.2017.
- Horstmeyer, N., Khan, S. (2015) **The Role of Young Water Reuse Professionals within the WRSG – Expectations, Opportunities, Networking**. IWA 10th International Conference on Water Reclamation and Reuse, Harbin, China, 05.-09.07.2015.
- Khan, S., Horstmeyer, N. (2015) **Young Water Reuse Professionals/Research Session**. IWA 10th International Conference on Water Reclamation and Reuse, Harbin, China, 05.-09.07.2015.

Proposals / Projects:

- Proposal to equip the Chair with 65 working places and 2 servers. Program "**Large equipments of the countries**", German Science Foundation (DFG) (GZ INST 95/1330-1 LAGG W), Funding amount 211,000 € (Proposal, Coordination, Tendering process, Procurement, Cost assessment)
- Project **Entwicklung und Untersuchungen alternativer energieeffizienter Verfahrenskonzepte zur Behandlung kommunalen Abwassers** (German). Oswald-Schulze-Foundation (AZ 1690/14). Project time: January 2015 – January 2016. Funding amount 22,000 € (Proposal, Project management, Project work, Final report)
- Project **Zustand der öffentlichen Kanalisation in Bayern** (German), Bayerisches Landesamt für Umwelt (AZ 66-0270-44552/2013). Project time: September 2013 – January 2015. Funding amount 94,000 € (Proposal, Project management, Final report)
- Project **Investitions- und Sanierungskosten bei kommunalen Abwasserentsorgungsanlagen**, Bayerisches Landesamt für Umwelt (AZ 66-44141-46076/2011). Project time: October 2011 – June 2013. Funding amount 143,000 € (Project work, Final report)

International Workshops / National Competitions:

- European Finalist, Climate Launchpad, European Institute of Innovation & Technology (EIT), vTech – good vibrations for water. Edingburgh, 01.11-02.11.2018.

- National Finalist Germany (2nd place), Climate Launchpad, European Institute of Innovation & Technology (EIT), vTech – good vibrations for water. Garching, Germany, 25.07.2018.
- National Finalist Germany (4th place), Climate Launchpad, European Institute of Innovation & Technology (EIT), greeNergy – Sustainable energy from nitrogen. Garching, Germany, 26.07.2017.
- Workshop: Status and Opportunities to Introducing Potable Water Reuse Practices in Europe and China, Tsinghua University, Peking, China (May 2016)
- Workshop: NeXus of Water, Food and Energy, Dar es Salaam, Tanzania (November 2014)
- 1st place Science Slam, Water reuse / Drinking water augmentation, 25th Kick-Off Seminar "Project Management" 08.-10.04.2014, Frauenchiemsee, TUM Graduate School, Technical University of Munich.
- Research stay at the School of Mines, Golden, Colorado, USA (April-July 2013)

Additional scientific engagement:

- Session moderator of Session C8: Water Reuse Planning – Costs and Economics. 23.-27.07.2017. IWA 11th International Conference on Water Reclamation and Reuse, Long Beach, CA, USA.
- Reviewer for Desalination, Journal of Membrane Science, Environmental Science: Water Research & Technology, Bioprocess and Biosystems Engineering and Journal of Water Reuse and Desalination.

Not topic related publications:

- Horstmeyer, N., Huber, M., Drewes, J.E., Helmreich, B. (2018) **Räumliche Verteilung der Schwermetallgehalte in den Oberböden von 35 Versickerungsmulden für Verkehrsflächenabflüsse** (German). *gwf - Wasser|Abwasser*.
- Horstmeyer, N., Huber, M., Drewes, J.E., Helmreich, B. (2016) **Evaluation of site-specific factors influencing heavy metal contents in the topsoil of vegetated infiltration swales**. *Science of the Total Environment*.
- Horstmeyer, N., Helmreich, B., Drewes, J.E. (2016) **Zustandsanalyse der bayerischen Kanalisation (Teil 1) – Vorgehensweise und allgemeine statistische Angaben zum Kanalnetz** (German). *Korrespondenz Abwasser, Abfall*.
- Horstmeyer, N., Helmreich, B., Drewes, J.E. (2016) **Zustandsanalyse der bayerischen Kanalisation (Teil 2) – Zustandserfassung, Sanierungsbedarf und Gesamtinvestitionsvolumen** (German). *Korrespondenz Abwasser, Abfall*.
- Horstmeyer, N., Rapp-Fiegle, S., Helmreich, B., Drewes, J.E. (2014) **Kosten der Abwasserbehandlung – Finanzierung, Kostenstrukturen und Kostenkenndaten der Bereiche Kanal, Sonderbauwerke und Kläranlagen** (German). Deutscher Industrie Verlag.

Not topic related scientific presentations / conference proceedings:

- Huber, M., Helmreich, B., Horstmeyer, N., Drewes, J.E. (2016) **Zustand des Kanalisationsnetzes in Bayern**. 22.11.2016. 4. Inspektions- und Sanierungstage DWA (IST), Dortmund.
- Huber, M., Horstmeyer, N., Drewes, J.E., Helmreich, B. (2015) **Bewachsener Oberboden nach DWA-A 138 und DWA-M 153 im Kontext des Entwurfs der Mantelverordnung und der Aktualisierung der Geringfügigkeitsschwellenwerte**. Tagung Straßenbauwerk - Umweltschutz - Kreislaufwirtschaft (StrUK), Bergisch Gladbach, Germany, 22.-23.06.2015.
- Horstmeyer, N. (2014) **Finanzierung und Kostenstrukturen der Abwasserbehandlung sowie Erhebung und Ermittlung spezifischer Investitions- und Sanierungskosten von kommunalen Kläranlagen- und Kanalbauteilen**. 47. ESSENER TAGUNG für Wasser- und Abfallwirtschaft; Essen, Germany, Kurzvorträge Forum „Young Scientists I“; 19.-21.03.2014.
- Horstmeyer, N., Helmreich, B. (2014) **Erfahrung mit Schwermetallbelastungen beim Betrieb von Versickerungsmulden**. 42. Abwassertechnisches Seminar (ATS) der Technischen Universität München und der Universität der Bundeswehr München, Zukunftsfähige Bewirtschaftungskonzepte für Niederschlagswasser. Garching, Germany, 10.07.2014.
- Horstmeyer, N. (2014) **Investitions- und Sanierungskosten bei kommunalen Abwasseranlagen**. Presentation at the Bavarian State Ministry for the Environment and Consumer Protection. 24.01.2014.

Supervised student projects / Internships:

Master Theses

- Philipp Sperle, Development and Investigation of Vibration Based Membrane Fouling Mitigation and Cleaning Strategies.
- Jonas Aniol, Investigation of Membrane Fouling Mitigation with Fluidized Granular Activated Carbon in Ultrafiltration Membrane Treatment of Municipal Wastewater.
- Jan Schmitz, Investigation of membrane fouling of NF/RO membrane applications to enhance efficiency of an integrated membrane system for potable water reuse.
- Cornelius Thies, Investigation of the Effect of Air Supported Cleaning for Ultrafiltration Membranes.
- Thomas Lippert, Hydrodynamics and Transport Phenomena within Osmotic Membrane Modules - A Modeling Approach by Use of COMSOL Multiphysics™.
- Maximilian Wunderle, Design, Construction and Implementation of an Automated Fluidized Bed Ultrafiltration Reactor for Treating Municipal Wastewater.
- Maximilian Stahlschmidt, 3D-Fluorescence Spectroscopy Coupled with Parallel Factor Analysis for Characterization of Natural Organic Matter During Managed Aquifer Recharge Operation.
- Philipp Michel, Evaluation of RO bench-scale application capabilities for inhibition effects for salt scaling caused by dissolved organic matter and salt scaling interactions with a SiO_2 preconditioned membrane.

- JinJin Guo, Improvement of Antifouling Polyvinylpyrrolidone (PVP) Modified Polyethersulfone (PES) Hollow Fiber Ultrafiltration (UF) Membrane with Different Spinning Parameters. inge GmbH (Co-Advisor).

Study Projects

- Philipp Sperle, 3D-Fluorescence Spectroscopy Coupled with Parallel Factor Analysis – Principles, Model Approaches and Application in Wastewater Treatment Schemes.
- Jonas Aniol, Membrane Fouling Mitigation in Municipal Wastewater Treatment Applications.
- David Schön, Impact of Feed Spacer Accuracy on Hydrodynamic Modeling of Pure Water Flow in Membrane Modules – A Modeling Approach by Using COMSOL Multiphysics™ and Geomagic Design™ X.
- Martin Larasser, Design, Construction and Commissioning of a Partially Automated Multi-Optional Membrane Test-Skid (NF/RO).
- Alicia Dery, Membrane Fouling of Nanofiltration Membrane (NF270): Fouling Potential and Cleaning Strategies.
- Cornelius Thies, Effects of different Operation Parameters on the Fouling Characteristics of an Ultrafiltration Membrane Reactor.
- Tim Fettback, Design of a Water Recycling Facility with the Purpose of Urban Farming. A Case Study in Dar es Salaam, Tanzania.
- Shamma Al-Riyami, Demonstration of Confocal Laser Scanning Microscopy in membrane biofilm analysis.
- Hooman Vatankhah, Evaluation of Alternative Treatment Design in Wastewater Treatment by Implementing a Toolbox.
- Thomas Lippert, Hydrodynamic Modelling of Pure Water Flow Within a Flatsheet Membrane Module By Use Of The Software Siemens NX 8.0™.
- Max Stahlschmidt, 3-D Fluorescence Spectroscopy - Fundamentals, measurement adjustement and analyses of selected water samples.
- Lin Zhuo, Fouling Test of NF-270 Nanofiltration Membrane by Organic Contaminants with Scaling Effect.

Bachelor Theses

- Andreas Hettmann, Design and Implementation of a LabVIEW™ Automation Control for an Ultrafiltration Membrane Reactor Test Skid.
- Martin Larasser, Literature study about scaling at membrane processes: Causes, influencing factors and mitigation strategies.
- Philipp Sperle, Development of a conception for using sewage water as nutrient for plants. Cradle to Cradle @ TUM (Co-Advisor).

Internships / Collaborations

- Rosiane Caetano (Internship) Investigation of membrane fouling, wetsus institute (Leeuwarden, Netherlands)
- Sarah G. Finder (Internship) Legislative, Energy, and Cost Consideration for Different Treatment Trains for Potable Water Reuse.

Appendix B – Curriculum vitae (Nils Horstmeyer)

Work history

Jan 2013 - current	**Research assistant / Doctoral candidate** Chair of Urban Water Systems Engineering, Technical University of Munich
May 2011 - Dec 2012	**Graduate assistant** (20h/Woche) Institute of Water Quality Control, Technical University of Munich
Jan 2011 - Apr 2011	**Project engineer** GFM Beratende Ingenieure GmbH, Munich
Mar 2008 - Aug 2009	**Student assistant** TÜV Nord Umweltschutz GmbH & Co. KG, Hamburg

Eduaction

Apr 2011 - Dec 2012	**Master studies Environmental Planning and Engineering Ecology (M.Sc.)** Technical University of Munich • Corefield modules: Waste Management / Water Quality Control (Overall average: 1.3) • Master thesis awarded with the Oswald-Schulze-Price 2014
Mar 2004 - Dec 2010	**Environmental Engineering studies** (Dipl.-Ing. FH) University of Applied Sciences, Hamburg • Main field of study: Environmental Rehabilitation /Environmental Evaluation (Overall average 1.9)
Mar 2003 - Feb 2004	Aircraft Construction studies for two terms at the University of Applied Sciences Hamburg
Dec 2001 - Sep 2002	Civil service (compulsory for all German men aged 18), “Leben mit Behinderung Hamburg” (Living with disability Hamburg)
1992 - 2001	“Allgemeine Hochschulreife” (equivalent to the A-Levels), Helene-Lange-Schule, Oldenburg

Appendix C – Supplementary material for chapter 4 / Publication #4

Table SM1. Raw wastewater characteristic and theoretical energy content of the WWTP Garching, Germany (average flowrate 4,644 ±724 m³/d) based on weekly measurements over a period of one year.

	Concentration (mg/L)	Theoretical energy potential (kWh/m³)
COD	496 ±129	1.91 ±0.50**
bCOD*	317 ±83	1.22 ±0.32**
nbCOD*	179 ±46	0.69 ±0.18**
TN	81 ±15	0.61 ±0.11***
TP	12 ±3	-
Total energy potential		**2.52 ±0.62**

*Based on a mean bCOD and nbCOD content of 64% and 36%, respectively (McCarty et al. 2011), **Based on complete COD oxidation and 3.86 kWh/kg COD, ***Based on (higher) heating value for ammonia-nitrogen. bCOD=biodegradable COD, nbCOD=non-biodegradable COD, TN=Total nitrogen, TP=Total phosphorus.

Table SM2. Annual sludge COD values from the WWTP Garching.

	Raw sludge	Digested sludge	Sludge utilized
COD [kg/d]	2310	714	1596*

*with 595 m³/d biogas with 60% methane content and a heating value of 9.97 kWh/m³ resulting in 2.25 kWh/kg COD.

Table SM3. Energetic comparison of benchmark (CAS+AWT) with scenario I, II and III.

	Benchmark	Scenario I	Scenario II	Scenario III	Source / Assumptions
Energy (waste)water treatment (INPUT) in kWh/m³					
Screening	0.01	-	0.02	0.02	Holloway et al. 2016, Fricke et al. 2015 (considering 496 mg/L COD), Arzbaecher et al. 2013
Settling / Buffer	0.04	-	-	-	Holloway et al. 2016, Fricke et al. 2015 (considering 496 mg/L COD), Arzbaecher et al. 2013
BNR	0.33	-	-	-	Holloway et al. 2016, Fricke et al. 2015 (considering 496 mg/L COD), Arzbaecher et al. 2013
Clarifier	0.04	-	-	-	Holloway et al. 2016, Fricke et al. 2015 (considering 496 mg/L COD), Arzbaecher et al. 2013
MF	0.23	-	-	-	Holloway et al. 2016
UF	-	0.23	-	-	same like MF
RO	0.46	0.46	0.46	0.46	Holloway et al. 2016
UV-H_2O_2	0.07	0.07	0.07	0.07	Holloway et al. 2016

Coagulation / Flocculation	-	0.06	-	-	Remy et al. 2014
Polymer	-	0.04	-	-	Remy et al. 2014
Microsieve (100 µm)	-	0.01	-	-	Remy et al. 2014
BAF	-	0.21	0.21	0.21	Remy et al. 2014
Disinfection (Cl_2)	-	0.02	0.02	0.02	Arzbaecher et al. 2013
AnMBR (UF)	-	-	0.06	0.06	Kim et al. 2011
Energy requirements (waste)water treatment (kWh/m³)	1.18	1.10	0.84	0.84	
Energy sludge treatment / Concentrate (INPUT) in kWh/m³					
Anaerobic digester	0.11	0.11	-	-	Arzbaecher et al. 2013
PN/A	-	-	-	0.07	Based on 0.90 kWh/kg N with N=0.081 kg/m³
CANDO	-	0.09	0.09	-	Based on 1.80 kWh/kg N with N=0.081 kg/m³ and 63% conversion efficiency of NH_4-N to N_2O-N (Weißbach et al. 2018)
Overall energy requirements	1.29	1.30	0.93	0.91	

INPUT (kWh/m³)					
		Energy recovery (OUTPUT) in kWh/m³			
Energy yield from CH_4 production	0.20*	0.36*	0.35**	0.35**	*Remy et al. 2014 (considering 496 mg/L), **Kim et al. 2011 (considering η_{el}=38%)
Additional CH_4 yield	-	0.22	0.22	0.34	Based on additional COD energy potential due to CANDO or PN/A nitrogen removal (7.20 and 10.9 kWh/kg N with N=0.081 kg/m³, 2.25 kWh/kg COD and η_{el}=38%
Energy yield from N_2O	-	0.04	0.04	-	Based on 0.53 kWh/ kg N with N=0.081 kg/m³ (Weißbach et al. 2018)
Overall energy recovery OUTPUT (kWh/m³)	0.20	0.62	0.61	0.69	
Energy net balance (kWh/m³)	1.09	0.68	0.32	0.22	

Appendix D – Supplementary material for chapter 6

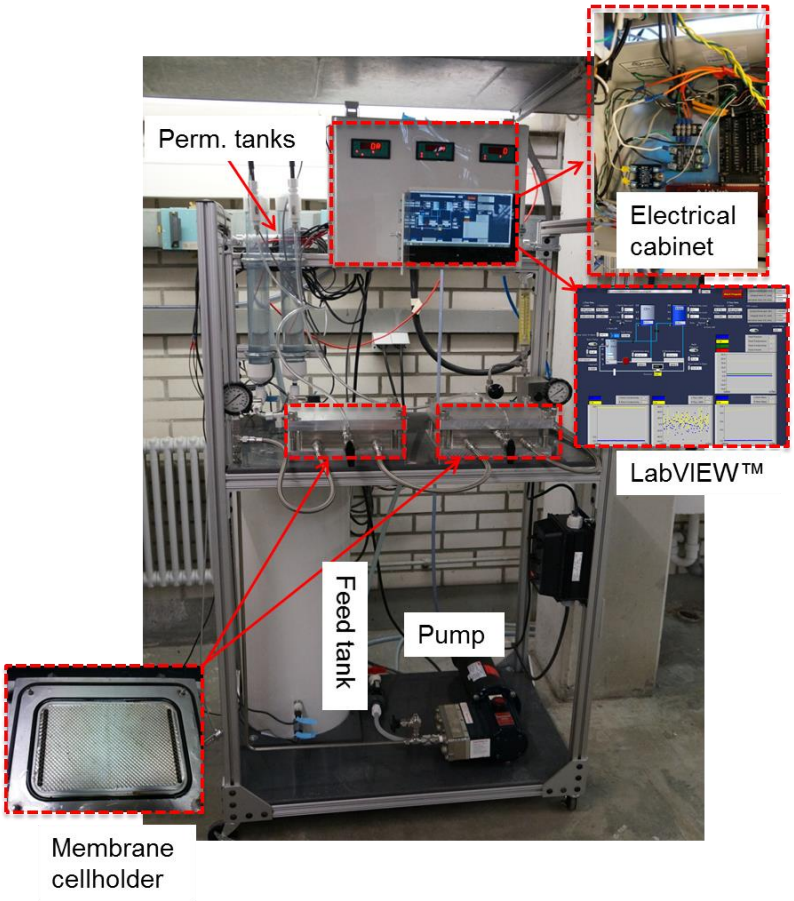

Figure SM1. Nanofiltration (NF) / Reverse osmosis (RO) flat-sheet test-skid.

Figure SM2. Ultrafiltration (UF) hollow-fibre laboratory-scale test-skid.

Appendix E – Supplementary material for chapter 7

Supplementary material chapter 7.1 (Publication #5)

Table SM4. Properties of the granular activated carbon (GAC) and modified granular activated carbon.

	Cyclecarb 401®	**Cyclecarb 401®, modified**
Bulk density [kg/m³]	450	594
Main particle diameter [mm]	1.1	1.1
Sieve Size [mm]	< 2.36 mm, > 0.425 mm	< 2.0 mm, > 1.0 mm
Cu [-]	1.823	not determined

Table SM5. Key parameters of the raw, settled and microsieved wastewater matrix (WWTP Munich).

		WWTP Munich (11/2016-12/2016)		
		Raw Wastewater	**Settled Wastewater**	**Microsieved Wastewater**
TOC	**[mg/L]**	71 ± 17 (4)	67 ± 16 (4)	64 ± 15 (4)
COD	**[mg/L]**	413 ± 72 (4)	370 ± 59 (4)	360 ± 54 (4)
EC	**[µS/cm]**	1322 ± 80 (4)	1317 ± 86 (4)	1315 ± 85 (4)
SUVA	**[L/(mg cm)]**	0.79 ± 0.16 (4)	0.80 ± 0.23 (4)	0.86 ± 0.30 (4)
NH_4-N	**[mg/L]**	32 ± 5 (4)	31 ± 4 (4)	30 ± 4 (4)

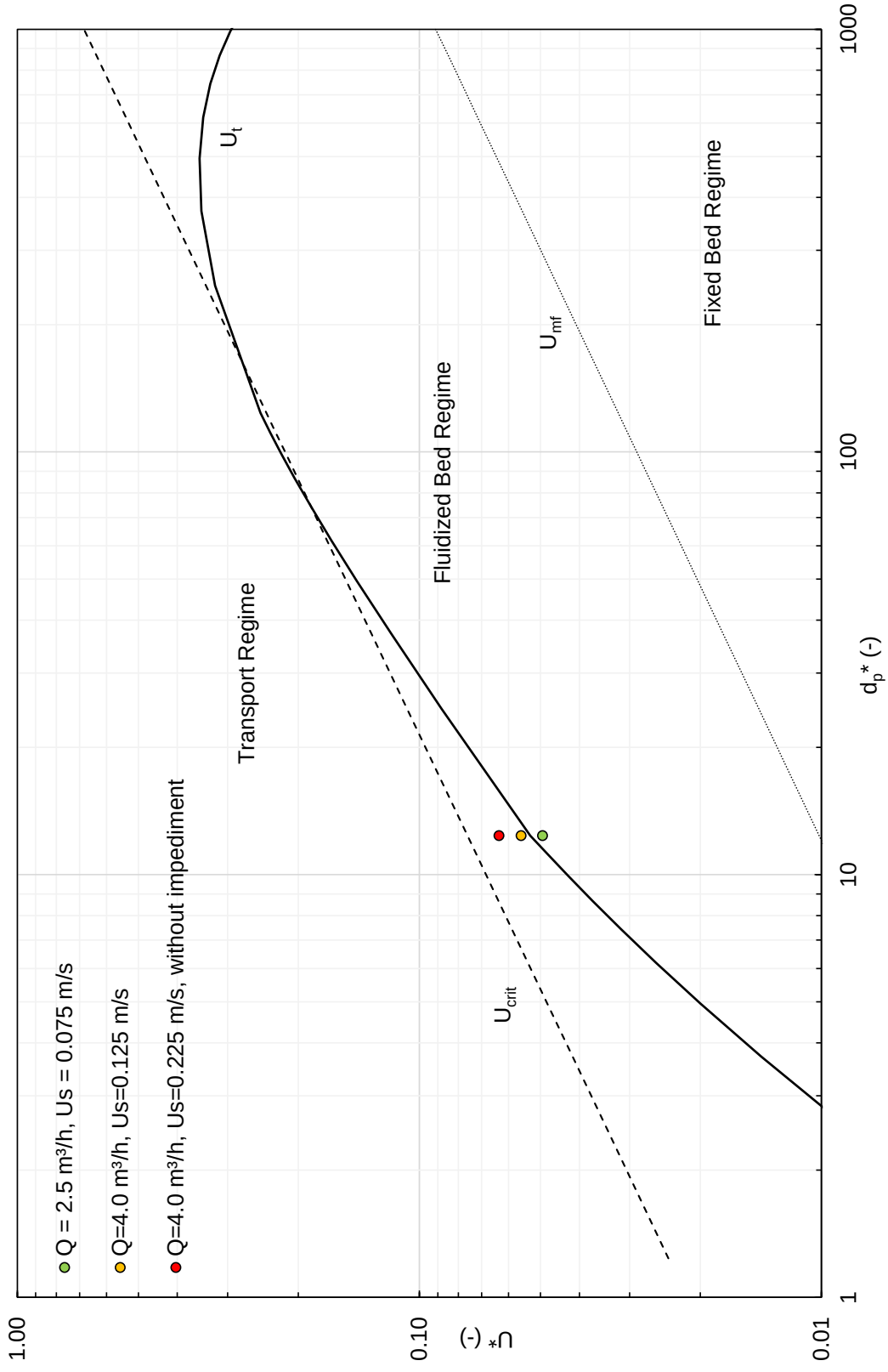

Figure SM3. Flow regime diagram of the liquid-solid fluidized bed regime.

Supplementary material for chapter 7.2

Feed matric characteristic

The pretreated wastewater was stored in a 300 L tank at 4 °C to alleviate biological degradation. An initial characterization of the matrix was made at the first batch test day of a test phase. Table SM6 summarizes the results of the analysis, showing that fluctuating weather conditions in summer 2017, dry weather flow followed by intense rain days, resulted in varying loadings of the feed water. The first (fluidized bed) and the last (best of) test phase had rather low loads regarding COD, TOC and TSS of 254 – 281 mg/L, 50.8 – 91.5 mg/L and 18.1 – 32.4 mg/L, respectively. Whereas, the second (packed bed) and third (adsorption test) falling in a higher range for COD, TOC and TSS of 420 – 451 ± mg/L, 126 – 139 mg/L and 57.4 – 71.5 mg/L, respectively. The UV_{254} absorption intensities were recorded together with 3D-EEM analysis, which showed less variations among the different test phases. The COD values listed in Table represent the COD content at the first and at the last batch test of a test phase. Only small differences between these figures indicate no significant degradation of the feed matrix during a test phase. The TOC and UV_{254} measurements that were made for each batch test (UV just for the last two test phases) also revealed no strong changes in contents or intensities, respectively, during test phases. Thus, the feed matrix could be kept stable for the period of a test phase, and no significant influence due to matrix degradation should be expected.

Table SM6. Feed matrix characteristics: COD, TOC, TSS, UV_{254}, pH, EC, O_2, and 3D-fluorescence excitation-emission matrix (3D-EEM).

Test Phase and Water Parameters			**3D-EEM Spectra**
<u>Fluidized Bed Test Phase (2017-05-30/06-02)</u>			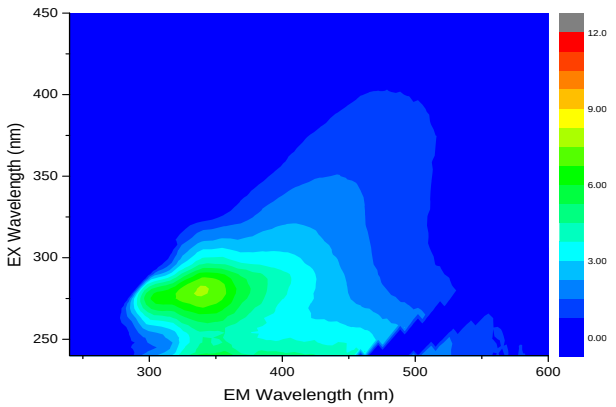
COD:	281 → 284 mg/L	(n = 2)	
TOC:	87.0 ± 3.7	mg/L (n = 5)	
TSS:	22.9 ± 3.8	mg/L (n = 5)	
UV_{254}:	34.124	1/m (n = 1)	
pH:	7.69 ± 0.05	(n = 5)	
EC:	1396 ± 3	µS/cm (n = 5)	
O_2:	1.43 ± 0.88 mg/L	(n = 5)	

Packed Bed Test Phase (2017-06-13/16)

COD:	423 → 420	mg/L	(n = 2)
TOC:	133.8 ± 4.6	mg/L	(n = 4)
TSS:	67.6 ± 3.0	mg/L	(n = 4)
UV_{254}:	34.836	1/m	(n = 1)
pH:	7.68 ± 0.03		(n = 4)
EC:	1286 ± 1	µS/cm	(n = 4)
O_2:	0.66 ± 0.41	mg/L	(n = 4)

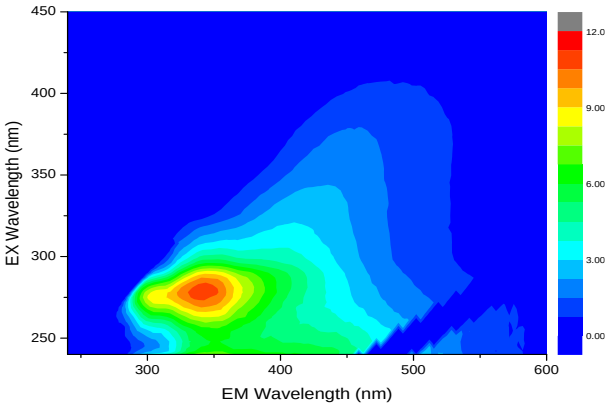

Adsorption Test Phase (2017-07-13)

COD:	451	mg/L	(n = 1)
TOC:	127.5 ± 2.1	mg/L	(n = 2)
TSS:	58.8 ± 1.9	mg/L	(n = 2)
UV_{254}:	39.52	1/m	(n = 1)

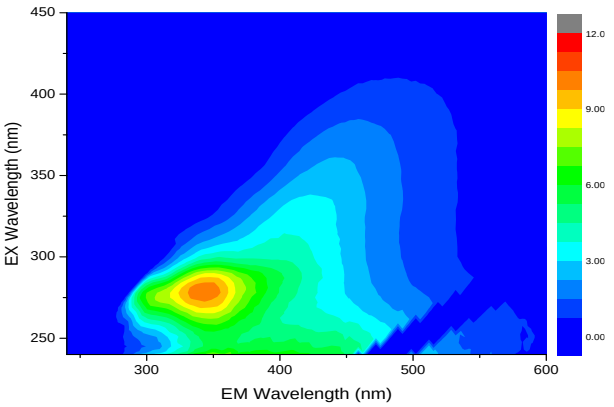

Best Of Test Phase (2017-07-26/27)

COD:	260 → 254	mg/L	(n = 2)
TOC:	55.4 ± 6.5	mg/L	(n = 2)
TSS:	25.3 ± 10.1	mg/L	(n = 2)
UV_{254}:	32.368	1/m	(n = 1)

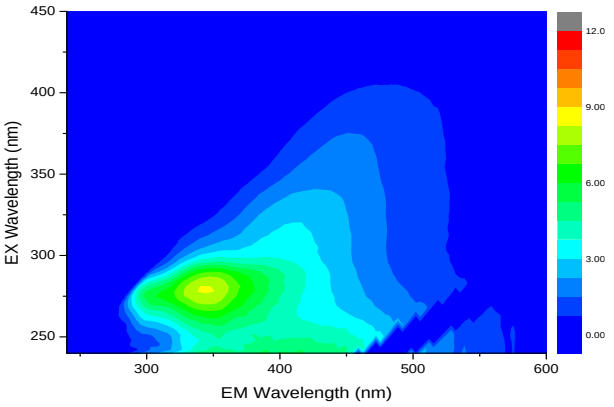

The 3D-EEM scans provide a qualitative impression of the DOM composition of the feed matrix. Here all samples show similar fluorescence distributions, just varying in their intensity due to higher or lower loadings (see COD, TOC concentrations). The triangular shaped area, at excitation wavelengths of (250 – 280 nm) and emission wavelengths < 380 nm, where emission due to excitation occurred for these wastewater samples, was declared as ‘soluble microbial byproduct-like material’ region (Chen et al. 2003). Collected from literature Chen et al. (2003) attributed to-biology-related substance as

- protein-like containing tryptophan,

- tyrosine- and protein-like,
- tryptophan and protein-like,
- tryptophan,

to that region. The similar 3D-EEM patterns further prove no serious differences in the composition characteristics of the used matrices.

Conductivity, pH, and oxygen were measured during each experiment in the test stand feed tank during the fluidized bed and the packed bed test phase (see Table SM6). No significant fluctuations were observed regarding these parameters within one test phase, and just marginal differences were noticed between the test phases for the conductivity and the oxygen content. The latter one was mainly influenced by the stirrer and the tank fill level that was mostly relative low at the end of the experiments when the measurements were carried out.

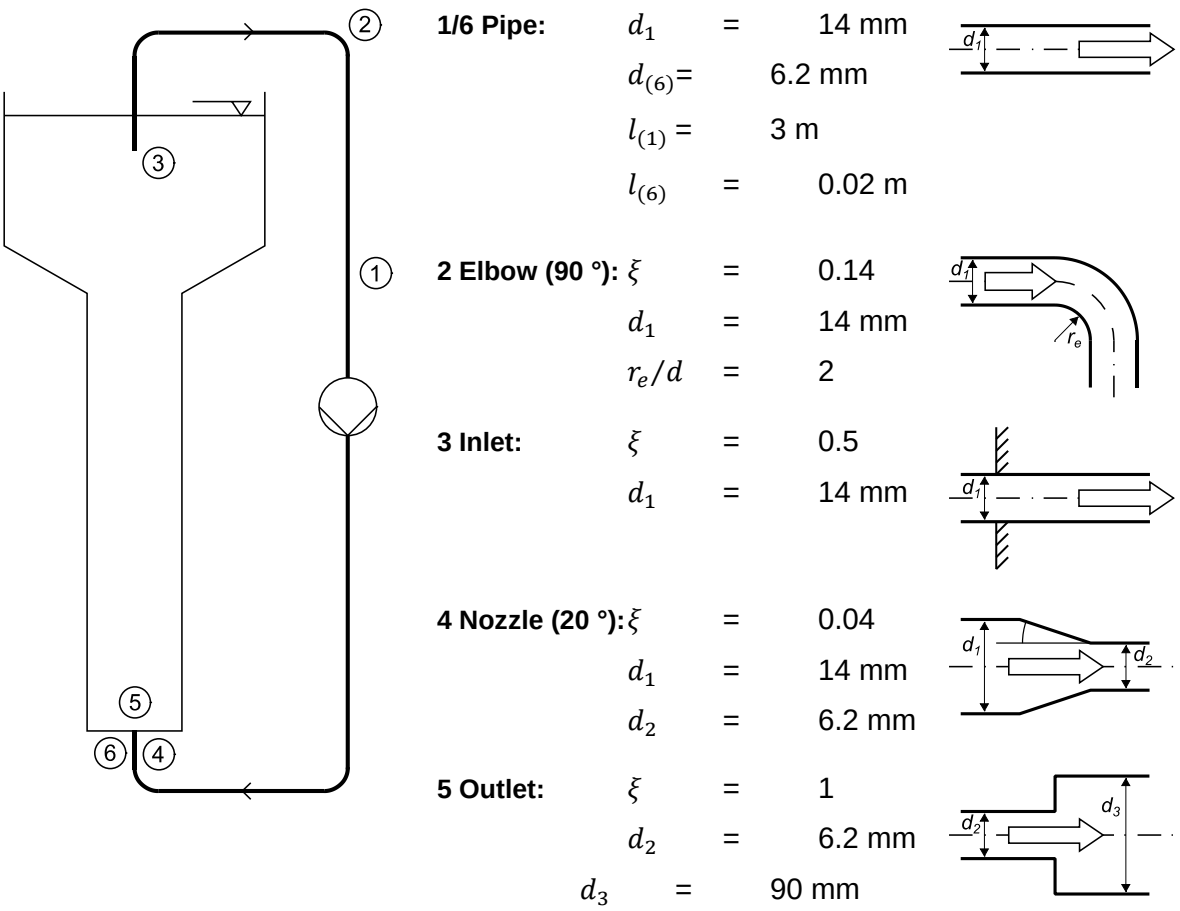

Figure SM4. Outline, geometry, and loss coefficients of the assumed recirculation pipe system.

Table SM7. Permeate quality and rejection rates for the fluidized as well as for the packed bed with granular activated carbon (GAC) (sampling during the end of the last flux step).

Fluidized bed (Feed: 87.0 ± 3.7 mg/L TOC)

	No GAC				*7.1 g/L*			*14.3 g/L*		
Reci. (L/min)	*0*	*2.2*	*2.9*	*3.6*	*2.2*	*2.9*	*3.6*	*2.2*	*2.9*	*3.6*
TOC (mg/L)	35.1	36.0	35.0	33.6	33.4	26.2	28.6	18.3	17.0	18.5
Rejection (%)	58.5	57.3	58.3	60.1	60.2	69.0	68.4	79.8	81.4	79.8

Packed bed (Feed: 133.8 ± 4.6 mg/L TOC)

	No GAC			*50 % bed*		*100 % bed*	
Reci. (L/min)	*0*	*1.5*	*3.0*	*1.5*	*3.0*	*1.5*	*3.0*
TOC (mg/L)	48.9	47.4	45.3	15.8	14.6	13.6	13.0
Rejection (%)	62.1	65.9	64.9	88.4	88.9	90.0	90.6

Appendix F – Supplementary material for chapter 8

Sample preparation / Feed matrix

For NF/RO feed sampling, UF permeate was collected in 40 L plastic cans throughout the day and stored in a fridge at 4 °C in the dark until it was used for further experiments in the NF/RO stage. For fouling experiments, care was taken to use UF permeate samples which were not older than 3 weeks. For later experiments the sampling procedure was changed so that only fresh UF permeate was used for fouling experiments. Now, the UF permeate was sampled overnight and the NF/RO fouling experiments were started directly on the next day without intermediate storage of the UF permeate.

Fouling experiments were usually conducted over 5 days which represents an operating time of 86-92 h each. Due to sampling reasons of really fresh UF permeate, experiments (since 08.11.2016) could be only started in the middle of each week since the UF feed matrix is renewed each Tuesday. To allow an operating time of the experiments of at least 80 h, the experiments were running until the following Monday for approximately 115-120 h. Since experiment 6 showed a high flux decline, experiment 7 was operated for 133 h to monitor long-term flux behavior during this batch operation. Table SM8 lists all performed fouling experiments in chronological order and the relevant operational conditions.

Table SM8. Performed fouling experiments and their relevant operational conditions.

			Operational parameters				
Exp. No./ Batch	**Membrane (Type/Model)**	**UF permeate from**	**Operating time (h)**	**Pressure (bar)**	**Flux (LMH)**	**CFV (m/s)**	**Initial DOC_{Feed} (mg/L)**
1/1	NF, DOW NF-270	22.07.2016	92	3.2	20	0.22	15.2
2/2	RO, Toray TMG10	08.08.2016	71	4.1	14	0.18	55.0
3/2	RO, Toray TMG10	08.08.2016	93	4.1	14	0.18	24.0
4/3	RO, Toray TMG10	24.08.2016	84	5.5	20	0.18	16.4
5/3	RO, Toray TMG10	24.08.2016	88	5.5	20	0.22	22.6
6/4	NF, DOW NF-270	09.09.2016	90	2.8	20	0.18	17.2
7/4	NF, DOW NF-270	09.09.2016	133	2.8	20	0.18	12.1
8/5	NF, DOW NF-270	07.10.2016	92	2.8	20	0.18	32.0
9/6	NF, DOW NF-270	12.10.2016	92	2.8	20	0.18	30.7
10/6	RO, Toray TMG10	12.10.2016	93	5.5	20	0.18	19.8
11/7	NF, DOW NF-270	07.11.2016	92	2.8	20	0.18	35.4

12/8	RO, Toray TMG10	07.11.2016	92	5.5	20	0.18	19.2
13/9	NF, DOW NF-270	23.11.2016	115	2.8	20	0.18	12.3
14/10	RO, Toray TMG10	30.11.2016	120	5.5	20	0.18	18.6
15/11	RO, Toray TMG10	07.12.2016	115	5.5	20	0.18	24.5
16/12	RO, Toray TMG10	14.12.2016	115	5.5	20	0.18	38.1
17/13	NF, DOW NF-270	13.01.2017	92	2.8	20	0.18	40.9
18/13	NF, DOW NF-270	13.01.2017	92	6.9	60	0.18	25.0

Table SM9. Spearman Rho correlation coefficients between protein and carbohydrate concentrations in the initial feed matrices and cake layers and extent of flux decline for the NF-270 and Toray TMG10 RO membrane.

		Feed (µg/mL)		**Cake layer (µg/cm²)[a]**	
Protein concentration		NF	RO	NF	RO
Flux decline (%)	Correlation coefficient	-0.541	0.042	0.396	0.452
	Significance (1-sided)	0.105	0.457	0.189	0.111
	Number of data, n	7	9	7	9
Carbohydrate concentration					
Flux decline (%)	Correlation coefficient	-0.691	-0.435	0.559	0.611
	Significance (1-sided)	0.086	0.242	0.096	0.040
	Number of data, n	7	9	7	9

[a]Total flux decline was considered. For the feed only the flux decline after 80 h of operation was considered.

Appendix G – Supplementary material for chapter 9 / Publication #6

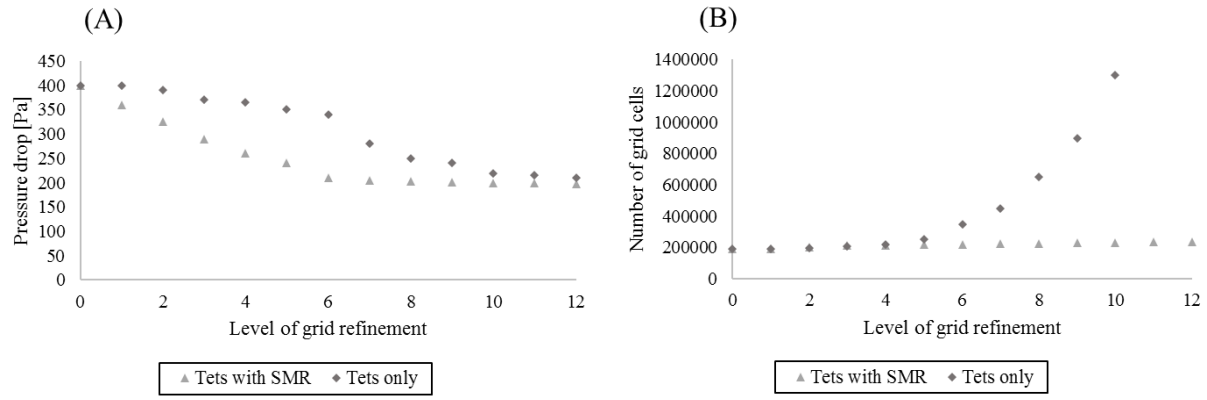

Figure SM5. Comparative grid convergence study of the pressure drop **(A)** and number of grid cells **(B)** in dependency of the level of grid refinement for tetrahedron (tet) cells only and hybrid meshes by use of tet-cells for the bulk volume and hexahedron cells for surface mesh refinements (SMR).

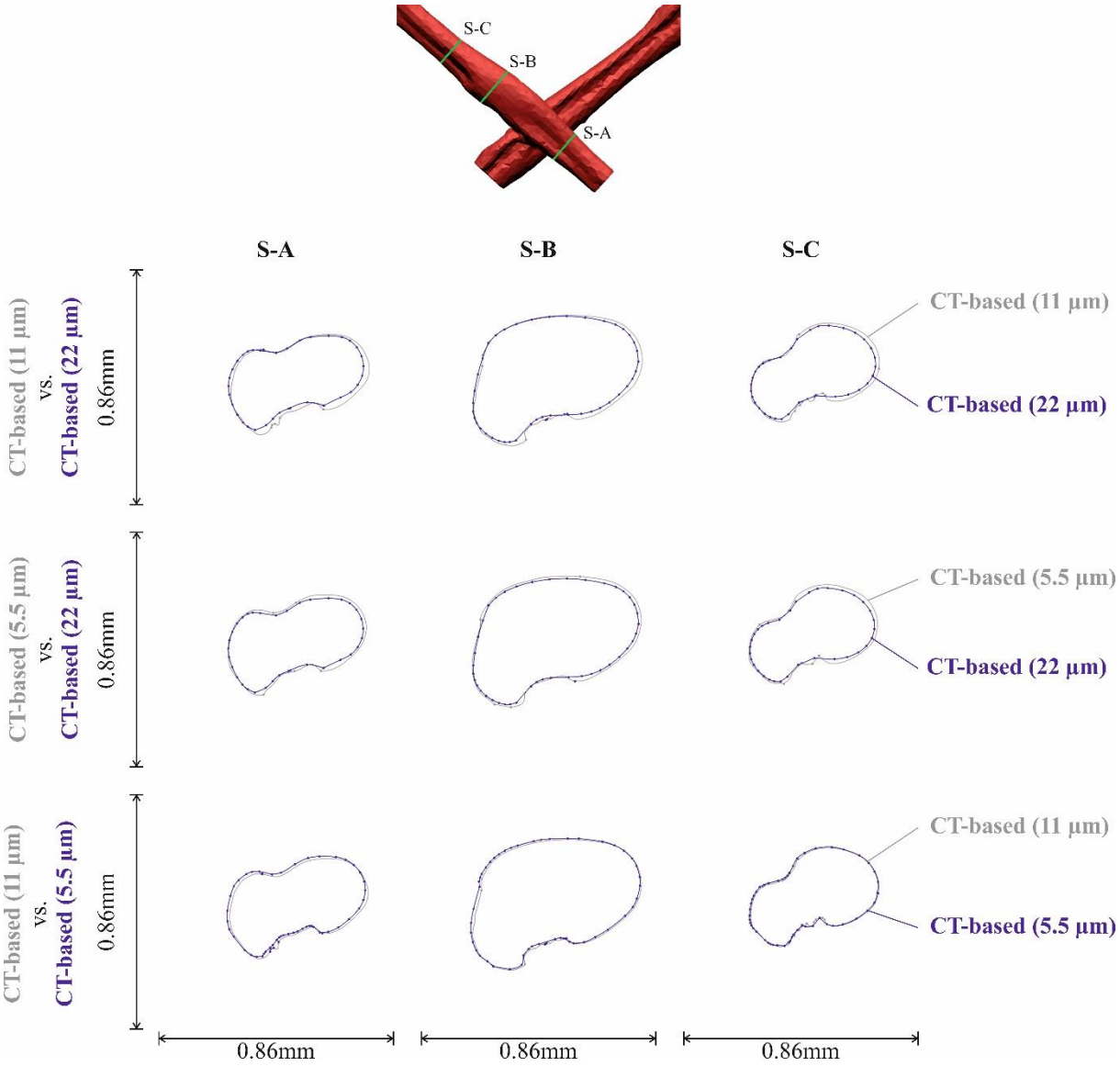

Figure SM6. Comparison of cross-sections of CT-based feed spacer models among each other (22 µm, 11 µm and 5.5 µm). Each row compares two cross-sections with a black and blue curve, labeled in the left column.

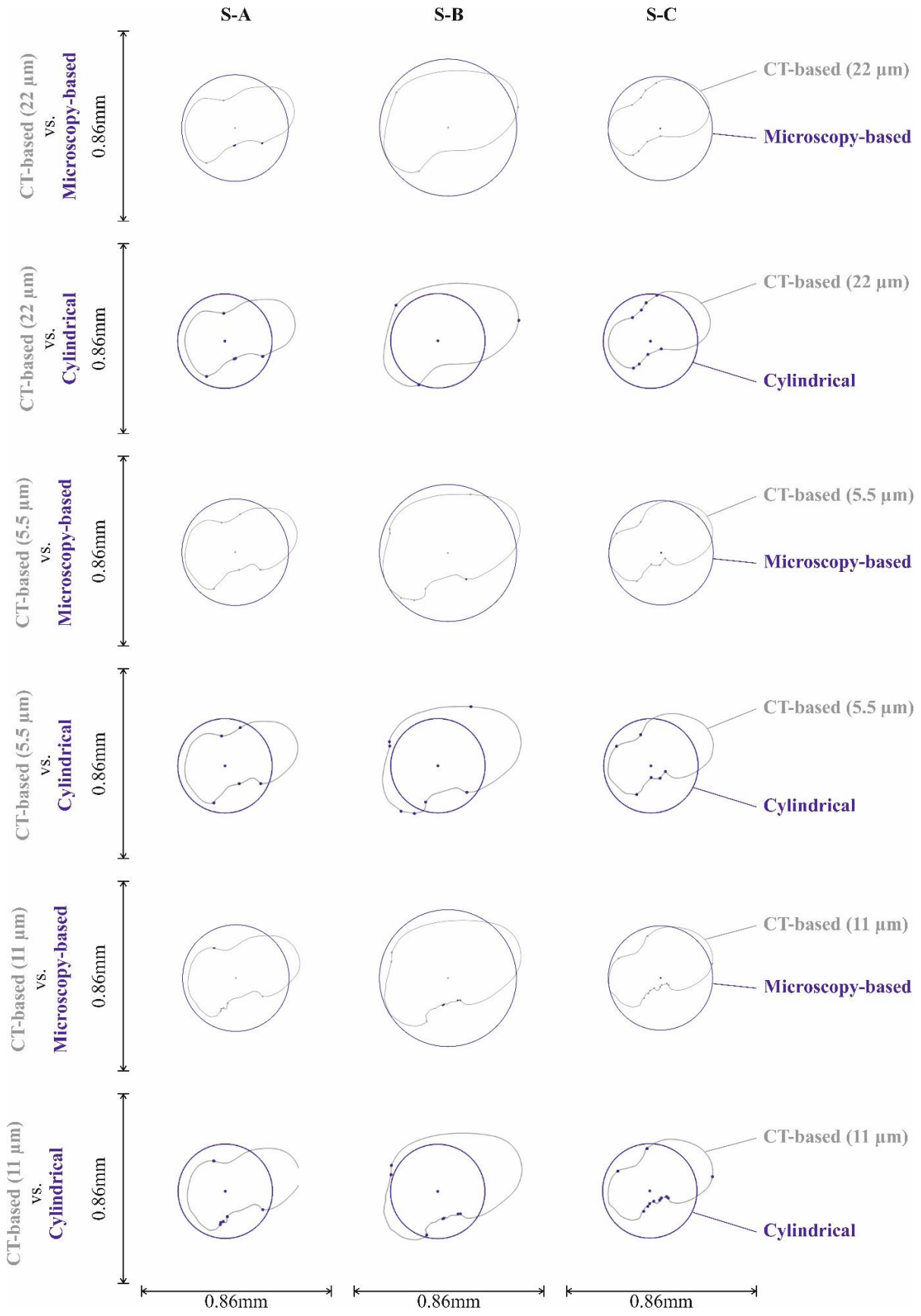
S-A
S-B
S-C
CT-based (22 µm) vs. Microscopy-based
0.86mm
CT-based (22 µm)
Microscopy-based
CT-based (22 µm) vs. Cylindrical
0.86mm
CT-based (22 µm)
Cylindrical
CT-based (5.5 µm) vs. Microscopy-based
0.86mm
CT-based (5.5 µm)
Microscopy-based
CT-based (5.5 µm) vs. Cylindrical
0.86mm
CT-based (5.5 µm)
Cylindrical
CT-based (11 µm) vs. Microscopy-based
0.86mm
CT-based (11 µm)
Microscopy-based
CT-based (11 µm) vs. Cylindrical
0.86mm
CT-based (11 µm)
Cylindrical
0.86mm
0.86mm
0.86mm

Figure SM7. Comparison of cross-sections of CT-based feed spacer models (22 µm, 11 µm, 5.5 µm) with microscopy-based and cylindrical feed spacer model. Position of cross-section see Figure SM5. Each row compares two cross-sections with a black and blue curve, labeled in the left column.

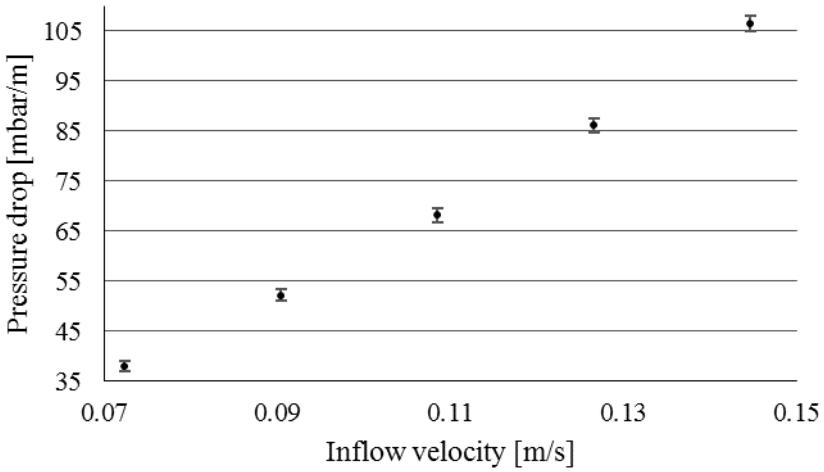

Figure SM8. Experimental measured mean pressure drop. Error bars are shown and represent the standard deviation between determination with n=3.

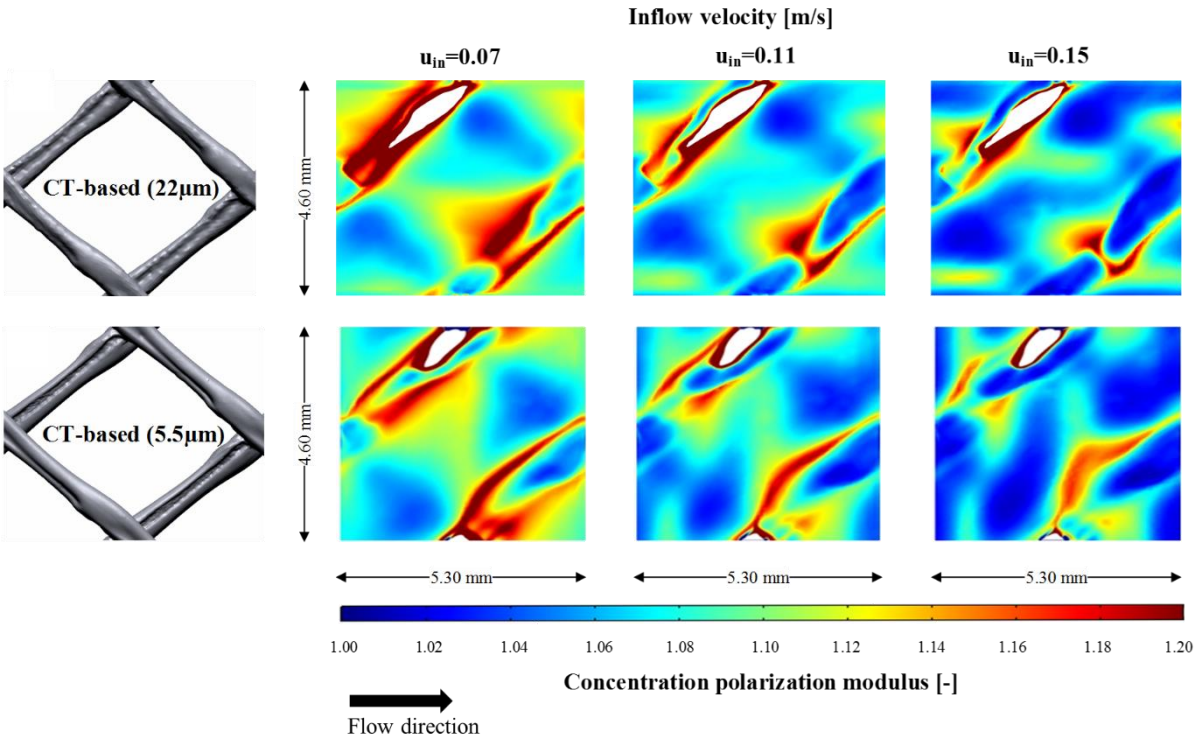

Figure SM9. Spatial distribution of concentration polarization modulus on the bottom membrane wall surface, for the highest (5.5 µm) and lowest (22 µm) CT scan accuracy of spacer representation and for

three inflow velocities (0.07, 0.11 and 0.15 $m \cdot s^{-1}$). For the ease of visual comparison, the color range was limited to a top value of CP 1.2.

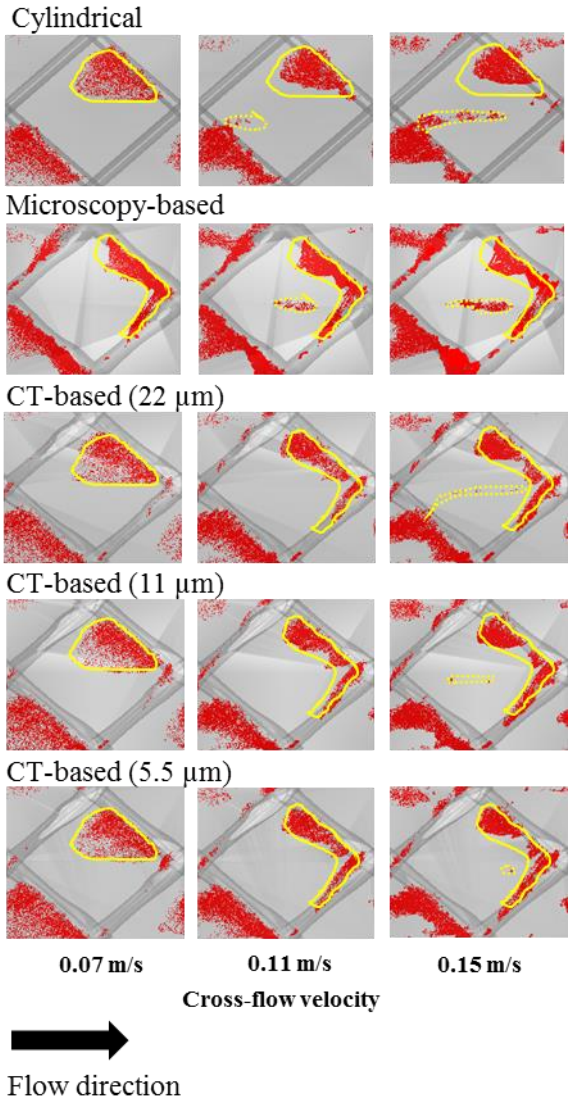

Figure SM10. Computed particle deposition patterns of the bottom membrane wall with spacer geometries based on cylindrical filaments, top-view microscopy and different CT scan accuracies (22 µm, 11 µm, 5.5 µm).